



# **Elucidating Mechanisms of Sulforaphane Induced Cell Stress and Death in the Human Lens**

---

**Ngoc Phuong Thao Huynh**

A thesis presented for the degree of Doctor of Philosophy (PhD)

University of East Anglia

School of Biological Sciences

United Kingdom

November 2021

© This copy of the thesis has been supplied on condition that anyone who consults it is understood to recognise that its copyright rests with the author and that use of any information derived there from must be in accordance with current UK Copyright Law. In addition, any quotation or extract must include full attribution.

# Acknowledgements

---

*“No one wins anything without help from mentors, family and friends who steer you away from bad ideas and toward good ones. Because every time anyone accomplishes anything, he or she achieves it with the help of a thousand silent heroes, the selfless team players who offer their support...”* - Modern Family, Season 6, Episode 21 (ABC, 2015).

First and foremost, I would like to express my deepest appreciation to my primary supervisor, Professor Michael Wormstone. His wisdom carried me through all the stages of my DPhil, while his encouragement as well as full support kept me sane. I would also like to thank my secondary supervisor, Professor Richard Bowater, and my independent academic supervisor, Dr Timothy Grocott, for their invaluable support and advice. This thesis would not have been possible without this fantastic supervisory team that I was blessed with. I would like to thank Mrs Yvette Wormstone and Dr Sarah Russell for technical assistance, and NHS Blood and Transplant for the provision of human tissue. I would also like to thank The Humane Research Trust for their generous financial support.

I am extremely grateful to all the former and current members of the Norwich Eye Research Group, who made the lab such an enjoyable place to be, including Mrs Yvette Wormstone, Dr Julie Eldred, Dr Sarah Russell, Dr Andrew Smith, and Dr Jeremy Rhodes.

I would like to acknowledge Dr Paul Thomas and Dr Philip Wilson for their training on how to use imaging facilities and their swift rescues. Their patience with me was also unbelievable.

I would also like to thank my two collaborators, Mr Federico Bernuzzi and Dr Shikha Saha at the Quadram Institute, for helping me run the liquid chromatography-mass spectrometry to analyse sulforaphane metabolites.

I would like to thank all previous research supervisors that I had prior to my DPhil degree, including Dr Naiara Beraza at the Quadram Institute, Professor Jacob Malone at the John Innes Centre, Dr Irina Mohorianu at the MRC Cambridge Stem Cell Institute, and Dr Nick Watmough at UEA. Without the research opportunities they had offered me and their guidance throughout those internships/projects, I would not have gained the essential skills and attitudes to finish this marathon.

My sincere thank you also goes to my wonderful friends, Ali Mohammed, Alice Godden, Annie Truc Truong, Hai Do, Katie Trinh Le, and Kavana Bywater-Brenna for always caring about me and checking up on me frequently.

Last but not least, my special thank you goes to my family: my extended families, my adopted brothers and sister, my closest cousin – Abby Uyen Nguyen, my fiancé’s family, my Vietnamese grandparents, my Brit-Kiwi grandmother – Elizabeth Whitehead, my adorable brother – Huy Huynh, my adorable sister – Thanh Huynh, my super Dad – Vinh Huynh, my super Mum – Trang Nguyen, and my beloved fiancé – Linh Nguyen. Without them, I could not have done this, especially during the Covid-19 pandemic. They all kept me going and believing in myself.

# Abstract

---

**Purpose:** Sulforaphane (SFN), derived from cruciferous vegetables, is an emerging therapeutic agent for many health conditions. Recently, SFN-induced cytotoxicity has been shown to have promise in preventing posterior capsule opacification (PCO) - a common lens disorder arising from undesirable cell proliferation and migration. However, no study in any models has elucidated the complete interplay and sequence of events contributing to the cytotoxicity. To address the gap in knowledge, this thesis, therefore, aimed to elucidate key processes and mechanisms linking SFN treatment to cell death in the human lens.

**Method:** The human lens epithelial cell line FHL124 and central anterior epithelium were used as experimental models. Cell death was assessed by microscopic observation and cell damage/viability assays. Gene or protein levels were assessed by qRT-PCR or Western blot. Mitochondrial networks and DNA damage were assessed by immunofluorescence. Mitochondrial membrane potential, ATF6 activity, GSH/GSSG ratio and glutathione reductase (GR) activity were measured using different light reporter assays. SFN metabolites were analysed by LC-MS/MS.

**Results:** High concentrations of SFN triggered mitochondrial dysfunction, endoplasmic reticulum stress, DNA damage, autophagy and cell death in both models. The treatment of a ROS scavenger prevented all of these stress responses. SFN also significantly depleted glutathione (GSH), the major antioxidant in the eye, via conjugation since SFN-GSH was detected as the most abundant intracellular SFN metabolite. SFN also reduced GR activity. The supplementation of GSH protected lens cells from all SFN-induced stress responses and death.

**Conclusions:** SFN depletes GSH levels in human lens epithelial cells through conjugation with GSH and inhibition of GR activity. This leads to ROS generation and oxidative stress that triggers mitochondrial dysfunction, ERS, autophagy and DNA damage leading to cell death. In summary, the work presented provides mechanistic understanding to support the therapeutic application of SFN for PCO and other conditions associated with GSH imbalance.

## **Access Condition and Agreement**

Each deposit in UEA Digital Repository is protected by copyright and other intellectual property rights, and duplication or sale of all or part of any of the Data Collections is not permitted, except that material may be duplicated by you for your research use or for educational purposes in electronic or print form. You must obtain permission from the copyright holder, usually the author, for any other use. Exceptions only apply where a deposit may be explicitly provided under a stated licence, such as a Creative Commons licence or Open Government licence.

Electronic or print copies may not be offered, whether for sale or otherwise to anyone, unless explicitly stated under a Creative Commons or Open Government license. Unauthorised reproduction, editing or reformatting for resale purposes is explicitly prohibited (except where approved by the copyright holder themselves) and UEA reserves the right to take immediate 'take down' action on behalf of the copyright and/or rights holder if this Access condition of the UEA Digital Repository is breached. Any material in this database has been supplied on the understanding that it is copyright material and that no quotation from the material may be published without proper acknowledgement.

## Conference Presentations

---

- **Huynh, TPN & Wormstone, IM.** (2019) “The mechanisms regulating sulforaphane induced cell death in PCO prevention”, at the **6<sup>th</sup> International Conference for the Lens**, Hawaii, US, oral presentation.
- **Huynh, TPN & Wormstone, IM.** (2019) “ROS play a critical role in sulforaphane induced events in human lens cells - implications for cataract study”, at **Redox Signalling in Physiology, Ageing and Disease**, Newcastle, UK, poster presentation.
- **Huynh, TPN & Wormstone, IM.** (2019) “Reactive oxidant species play a key role in endoplasmic reticulum stress triggered by sulforaphane in human lens epithelial cells”, at **ARVO Annual Meeting 2019**, Vancouver, Canada, poster presentation.
- **Huynh, TPN, Bowater, RB, Ball, S, Wormstone, IM.** (2018) “Reactive oxidant species play a key role in sulforaphane induced autophagy, and cell death in human lens epithelial cells”, at **ARVO Annual Meeting 2018**, Hawaii, US, poster presentation.

# Table of Contents

---

Acknowledgements .....	i
Abstract .....	ii
Conference Presentations .....	iii
Table of Contents .....	iv
Table of Figures .....	viii
Abbreviations.....	xii
Chapter 1 General Introduction .....	1
1.1 The eye and the lens .....	1
1.1.1 Lens development.....	2
1.1.2 The mature lens .....	4
1.1.3 Lens transparency .....	6
1.2 Cataract.....	7
1.2.1 Epidemiology .....	7
1.2.2 Risk factors and classification.....	8
1.2.3 Cataract surgery.....	11
1.3 Posterior capsular opacification .....	12
1.3.1 Pathogenesis and prevalence.....	12
1.3.2 Current treatments .....	14
1.3.3 Potential treatments .....	15
1.3.4 Experimental models .....	16
1.4 Sulforaphane .....	17
1.4.1 Origin of SFN.....	18
1.4.2 Metabolism and bioavailability of SFN.....	19
1.4.3 Functional roles of SFN.....	21
1.4.4 SFN in the human lens.....	27
1.5 Cellular stress and responses .....	28
1.5.1 Oxidative stress and mitochondrial dysfunction .....	29
1.5.2 Endoplasmic reticulum stress and unfolded protein response .....	32
1.5.3 DNA damage and DNA damage response.....	34
1.5.4 Autophagy .....	37
1.5.5 Cell death .....	41
1.5.5.1 Apoptosis.....	41
1.5.5.2 Necrosis.....	45
1.5.6 SFN and cellular responses .....	47
1.6 Background summary.....	47
1.7 Aims and objectives .....	49
Chapter 2 Materials and Methods.....	50

2.1 Experimental models.....	50
2.1.1 Cell culture.....	50
2.1.2 Human lens epithelium.....	51
2.2 Chemicals.....	51
2.3 Cell viability and death assays.....	52
2.3.1 Cytotoxicity Lactate dehydrogenase (LDH) assay.....	52
2.3.2 Cell Viability assay.....	53
2.3.3 Phase-contrast imaging.....	53
2.4 Gene expression analysis by quantitative real-time Polymerase Chain Reaction (qRT-PCR).....	54
2.4.1 Total RNA extraction.....	54
2.4.2 Total RNA quality and quantity assessment.....	54
2.4.3 cDNA synthesis.....	55
2.4.4 TaqMan qRT-PCR.....	55
2.5 Western blot analysis.....	56
2.5.1 Protein extraction.....	56
2.5.1.1 FHL124 cells.....	56
2.5.1.2 Human lens epithelium.....	56
2.5.2 Protein quantification.....	57
2.5.3 Sample preparation.....	58
2.5.4 SDS-PAGE gel electrophoresis.....	58
2.5.5 Protein transfer and immunoblotting.....	58
2.6 ATF6 reporter assay.....	60
2.7 $\gamma$ -H2AX Immunocytochemistry.....	61
2.8 Mitochondrial network analysis.....	62
2.8.1 MitoTracker Red staining.....	62
2.8.2 Mitochondrial network analysis.....	63
2.9 Mitochondria GFP tagged transfection – GFP labelling mitochondria.....	65
2.10 Live cell imaging of mitochondrial networks.....	66
2.11 Mitochondrial membrane potential.....	66
2.12 GSH/GSSG assay.....	67
2.12.1 FHL124 cells.....	67
2.12.2 Human lens epithelium.....	68
2.13 Glutathione reductase activity.....	69
2.14 SFN metabolites analysis.....	70
2.14.1 Metabolite extraction.....	70
2.14.2 Mass spectrometry analysis.....	70
2.15 Statistical analysis.....	71
2.15.1 Independent Student’s t-test.....	71
2.15.2 Paired Student’s t-test.....	72
2.15.3 One-way analysis of variance (ANOVA).....	72
Chapter 3 Cellular Responses to Sulforaphane.....	74
3.1 Introduction.....	74

3.2 Aims .....	77
3.3 Results .....	78
3.3.1 SFN decreases cell viability in FHL124 cells.....	78
3.3.2 SFN impairs the integrity of mitochondrial networks in FHL124 cells.....	79
3.3.3 SFN causes loss of mitochondrial membrane potential in FHL124 cells.....	83
3.3.4 SFN increases ATF6 transcriptional activity in FHL124 cells.....	84
3.3.5 SFN triggers DNA damage responses in FHL124 cells.....	85
3.4 Discussion.....	87
Chapter 4 ROS Have a Pivotal Role in SFN Induced Cellular Responses .....	93
4.1 Introduction.....	93
4.2 Aims .....	96
4.3 Results .....	96
4.3.1 Evaluating the effect of a ROS scavenger on cell viability following SFN treatment in FHL124 cells.....	96
4.3.2 NAC protects FHL124 from SFN-induced cytotoxicity.....	99
4.3.3 NAC protects against mitochondrial dysfunction caused by SFN in FHL124 cells.....	101
4.3.4 NAC prevents SFN-induced ERS responses in FHL124 cells.....	104
4.3.5 NAC prevents DNA damage induced by SFN in FHL124 cells.....	107
4.3.6 NAC prevents autophagy induced by SFN in FHL124 cells.....	109
4.3.7 NAC protects human lens epithelium from SFN-induced cytotoxicity.....	110
4.3.8 NAC prevents ERS induced by SFN in human lens epithelium.....	112
4.3.9 NAC prevents autophagy induced by SFN in human lens epithelium.....	114
4.4 Discussion.....	116
Chapter 5 Impacts of SFN on GSH Homeostasis.....	123
5.1 Introduction.....	123
5.2 Aims .....	126
5.3 Results .....	127
5.3.1 SFN depletes the intracellular GSH pool in FHL124 cells.....	127
5.3.2 Impacts of NAC treatment on SFN-induced GSH depletion.....	129
5.3.3 Analysis of intracellular SFN metabolites in FHL124 cells.....	131
5.3.4 SFN increases GR protein levels but decreases its activity in FHL124 cells.....	132
5.3.5 SFN depletes the intracellular GSH pool in human lens epithelium.....	133
5.4 Discussion.....	135
Chapter 6 SFN-Induced GSH Depletion Triggers Stress and Death.....	142
6.1 Introduction.....	142
6.2 Aims .....	145
6.3 Results .....	145
6.3.1 Evaluating the effect of GSH supplementation on cell viability following SFN treatment in FHL124 cells.....	145
6.3.2 GSH protects FHL124 cells from SFN-induced cytotoxicity.....	146
6.3.3 GSH protects against collapse of mitochondrial networks caused by SFN in FHL124 cells.....	148

6.3.4 GSH prevents SFN-induced ERS responses in FHL124 cells.....	151
6.3.5 GSH prevents DNA damage induced by SFN in FHL124 cells.....	153
6.3.6 GSH prevents autophagy induced by SFN in FHL124 cells.....	155
6.3.7 GSH protects human lens epithelium from SFN-induced cytotoxicity.....	156
6.3.8 GSH prevents autophagy induced by SFN in human lens epithelium.....	158
6.4 Discussion.....	160
Chapter 7 General Discussion.....	166
7.1 Summary of results and future work.....	166
7.2 Concluding remarks.....	179
Reference.....	180
Appendix.....	197

# Table of Figures

---

Figure 1. 1: The vertebrate eye.....	1
Figure 1. 2: Schematic diagrams of embryonic development with the lens.....	3
Figure 1. 3: The lens 3D structure.....	6
Figure 1. 4: Global prevalence of visual impairment due to cataract.....	8
Figure 1. 5: The Lens Opacity Classification System II (LOCS II).....	10
Figure 1. 6: PCO development following cataract surgery.....	14
Figure 1. 7: Myrosinase-catalysed reaction products and possible reaction products of glucosinolate hydrolysis.....	19
Figure 1. 8: Structure, intake and excretion of SFN.....	20
Figure 1. 9: Activation of the Nrf2 by SFN.....	23
Figure 1. 10: The role of ROS on the cell death induced by SFN.....	26
Figure 1. 11: The ROS formation and the antioxidant defence in a cell.....	31
Figure 1. 12: The molecular mechanisms of activation of ERS.....	33
Figure 1. 13: DNA damage and its consequences.....	35
Figure 1. 14: Overview of the mammalian autophagy pathway.....	38
Figure 1. 15: Molecular pathways of autophagy.....	40
Figure 1. 16: Signalling pathways of apoptosis.....	44
Figure 1. 17: Causal vs. accessory aspects of cell death from a therapeutic perspective.....	46
Figure 2. 1: The workflow of mitochondrial network quantification.....	64
Figure 2. 2: The representative preparation of an image.....	65
Figure 3. 1: SFN decreases cell viability in FHL124 cells over time.....	79
Figure 3. 2: SFN decreases the size of mitochondrial networks in FHL124 cells over time measured by widefield microscopy.....	81
Figure 3. 3: SFN decreases the size of mitochondrial networks in FHL124 cells over time measured by confocal microscopy.....	82
Figure 3. 4: SFN disrupts mitochondrial membrane potential ( $\Delta\psi_m$ ) in FHL124 cells over time.....	83
Figure 3. 5: SFN increases ATF6 transcriptional activity in FHL124 cells over time.....	84
Figure 3. 6: SFN triggers DNA double-strand breaks in FHL124 cells over time.....	86
Figure 3. 7: SFN induces a range of stress responses in human lens epithelial cells.....	92
Figure 4. 1: Effects of different concentrations of NAC and sodium pyruvate on cell viability following SFN treatment in FHL124 cells.....	98
Figure 4. 2: NAC protects cells from cytotoxicity induced by SFN in FHL124 cells.....	100
Figure 4. 3: NAC protects SFN-induced mitochondrial network shrinkage over time.....	102
Figure 4. 4: NAC protects against mitochondrial network shrinkage caused by SFN in FHL124 cells.....	103
Figure 4. 5: NAC protects cells from loss of mitochondrial membrane potential ( $\Delta\psi_m$ ) induced by SFN in FHL124 cells.....	104
Figure 4. 6: NAC prevents upregulation of ERS gene markers by SFN in FHL124 cells....	105
Figure 4. 7: NAC prevents elevation of ERS protein markers by SFN in FHL124 cells.....	106

Figure 4. 8: NAC prevents elevation in ATF6 transcriptional activity caused by SFN in FHL124 cells. ....	107
Figure 4. 9: NAC prevents DNA double-strand breaks induced by SFN in FHL124 cells. .	108
Figure 4. 10: NAC protects cells from autophagy induced by SFN in FHL124 cells. ....	109
Figure 4. 11: NAC protects cells from cell death induced by SFN in human lens epithelium. ....	111
Figure 4. 12: NAC prevents ERS induced by SFN in human lens epithelium.....	113
Figure 4. 13: NAC protects cells from autophagy induced by SFN in human lens epithelium. ....	115
Figure 4. 14: NAC displays antioxidant properties in different ways. ....	118
Figure 4. 15: ROS play a pivotal role in SFN-induced cytotoxicity in human lens epithelial cells. ....	122
Figure 5. 1: Maintenance of intracellular GSH levels. ....	126
Figure 5. 2: SFN impairs intracellular GSH/GSSG ratios in FHL124 cells.....	128
Figure 5. 3: Impacts of different concentrations of SFN on total glutathione, GSH and GSSG levels in FHL124 cells. ....	129
Figure 5. 4: NAC prevents the GSH depletion by SFN but fails to fully restore the GSH levels. ....	130
Figure 5. 5: Analysis of intracellular SFN metabolites in FHL124 cells.....	131
Figure 5. 6: SFN increases the GR protein level in FHL124 cells. ....	132
Figure 5. 7: SFN decreases GR activity. ....	133
Figure 5. 8: SFN impairs intracellular GSH levels in human lens epithelium.....	134
Figure 5. 9: Impacts of 50 $\mu$ M SFN on total glutathione, GSH and GSSG levels in human lens epithelium.....	135
Figure 5. 10: SFN causes GSH depletion via conjugation and inhibition of GSH regeneration in human lens epithelial cells.....	141
Figure 6. 1: Effects of different GSH concentrations on cell viability following SFN treatment in FHL124 cells.....	146
Figure 6. 2: GSH protects cells from cell death induced by SFN in FHL124 cells.....	147
Figure 6. 3: GSH protects against SFN-induced mitochondrial network shrinkage over time. ....	149
Figure 6. 4: GSH protects against mitochondrial network shrinkage caused by SFN in FHL124 cells. ....	150
Figure 6. 5: GSH prevents upregulation of ERS gene markers by SFN in FHL124 cells. ...	152
Figure 6. 6: GSH prevents elevation of ERS protein markers by SFN in FHL124 cells.....	153
Figure 6. 7: GSH prevents DNA double-strand breaks induced by SFN in FHL124 cells...	154
Figure 6. 8: GSH protects cells from autophagy induced by SFN in FHL124 cells. ....	155
Figure 6. 9: GSH protects cells from cell death induced by SFN in human lens epithelium.	157
Figure 6. 10: GSH protects cells from autophagy induced by SFN in human lens epithelium. ....	159
Figure 6. 11: GSH depletion mediates stress and death induced by SFN in human lens epithelial cells. ....	165
Figure 7. 1: Ca <sup>2+</sup> and ROS crosstalk between endoplasmic reticulum and mitochondria. ...	172
Figure 7. 2: A relationship between events mediated by SFN-induced ROS elevation in human lens epithelial cells.....	174
Figure 7. 3: A proposed mechanism of SFN-induced cytotoxicity in human lens epithelial cells. ....	178

Figure A. 1: The impacts of different concentrations of SFN on secreted LDH in FHL124 cells. .... 197

# Table of Tables

---

Table 1. 1: Morphological features and associated risk factors of different types of cataract.	10
Table 1. 2: Principles, mechanisms and exemplary molecules participating in cell repair mechanisms. ....	29
Table 2. 2: Details of primers used in the study. ....	56
Table 2. 3: Antibodies used in the experiment and corresponding % SDS-polyacrylamide gel. ....	60

# Abbreviations

---

•OH	Hydroxyl radical
8-Oxoguanine	8-oxo-7,8-dihydroguanine
AIF	Apoptosis-inducing factor
AMPK	AMP-activated protein kinase
ANOVA	One-way analysis of variance
Apaf-1	Apoptotic protease activating factor 1
APS	Ammonium persulphate
ARE	Antioxidant dependent element
ATF	Activating transcription factor
Atg	Autophagy-related protein homologue
ATM	Ataxia-telangiectasia mutated
ATP	Adenosine 5'-triphosphate
Bax	Bcl-2 associated X
BCA	Bicinchoninic acid
Bcl	B-cell lymphoma
Beclin 1	Bcl-2-interacting myosin-like coiled-coil protein 1
BiP	Binding immunoglobulin protein
BMP	Bone morphogenetic protein
BSA	Bovine serum albumin
BSO	Buthionine sulfoximine
Ca <sup>2+</sup>	Calcium
cGSH	Cytosolic GSH
CH <sub>3</sub>	Methyl group
CH <sub>3</sub> CO	Acetyl group
CHOP	C/EBP homologous protein
CLAHE	Contrast limited adaptive histogram equalization
Ct	Cycle threshold
Cys-S <sup>-</sup>	Catalytic cysteine
Cys-SOH	Cysteine sulfenic acid
DAPI	6-diamidino-2-phenylindole
DNMT	DNA methyltransferases
DPBS	Dulbecco's phosphate-buffered saline
Drp	Dynamin-related protein
EDTA	Ethylenediaminetetraacetic acid
eIF2 $\alpha$	Eukaryotic initiator of translation factor 2 $\alpha$
EMEM	Eagle's Minimum Essential Medium
ER	Endoplasmic reticulum
ER-GSH	Endoplasmic reticulum GSH
ERS	Endoplasmic reticulum stress
ERSE-I	Endoplasmic reticulum stress response elements
FBS	Foetal bovine serum
FHL124	Foetal human lens epithelial cell 124
FIP200	Focal adhesion kinase family interacting protein of 200kD
Fis1	Fission 1

GCL	Glutamate-cysteine ligase
GGC	$\gamma$ -glutamylcysteine
GGT	Gamma-glutamyl transpeptidase
GPx	Glutathione peroxidase
GR	Glutathione reductase
GSH	Reduced glutathione
GSL	Glucosinolate
GSSG	Oxidised glutathione
GST	Glutathione-S-transferase
H <sub>2</sub> O <sub>2</sub>	Hydrogen peroxide
H <sub>2</sub> S	Hydrogen sulfur
HDAC	Histone deacetylases
HIF-1 $\alpha$	Hypoxia-inducible factor
HO-1	Haem oxygenase-1
HR	Homologous recombination
IOL	Intraocular lens
IP <sub>3</sub> R	Inositol 1,4,5-trisphosphate receptor
IRE1 $\alpha$	Inositol requiring kinase 1 alpha
ITC	Isothiocyanate
JNK	c-Jun N-terminal kinase
Keap1	Kelch-like ECH associated protein
Klf9	Kruppel-like factor 9
LC-MS/MS	LC-MS mass spectrometer
LC3	Microtubule-associated protein 1A/1B-light chain 3
LC3-PE	LC3-phosphatidylethanolamine
LDH	Lactate dehydrogenase
M-PER	Mammalian protein extraction reagent
MAM	Mitochondria-associated membrane
MAPK	Mitogen-activated protein kinase
Mfn	Mitofusin
mGSH	Mitochondrial GSH
mTORC	Mammalian target of rapamycin complex
NAC	N-acetyl L cysteine
NADPH	Nicotinamide adenine dinucleotide phosphate dehydrogenase
NF- $\kappa$ B	Nuclear factor kappa-light-chain-enhancer of activated B cells
NHEJ	Non-homologous end-joining
NOX	NADPH oxidase
NQO1	NAD(P)H dehydrogenase quinone 1
Nrf2	Nuclear factor erythroid 2-related factor 2
O <sub>2</sub> <sup>-</sup>	Superoxide
ONOO <sup>-</sup>	Peroxynitrite
OPA1	Optic atrophy 1
P-eIF2 $\alpha$	Phosphorylated eukaryotic initiator of translation factor 2 $\alpha$
PAX6	Paired box protein-6
PCO	Posterior capsular opacification
PERK	Protein kinase R-like endoplasmic reticulum kinase
PHD	Prolyl hydroxylase
PITX3	Pituitary homeobox-3
Prdx6	Peroxiredoxin-6
Prx	Peroxiredoxin

PTEN	Phosphatase and tensin homolog deleted on chromosome 10
PTM	Post-translational modification
PVDF	Polyvinylidene fluoride
RNS	Reactive nitrogen species
ROS	Reactive oxygen species
SDS-PAGE	Sodium dodecyl-sulfate polyacrylamide gel electrophoresis
SFN	Sulforaphane
SFN-Cys-Gly	SFN-cysteine-glycine
SFN-cysteine	SFN-cysteine
SFN-GSH	SFN-glutathione
SFN-NAC	SFN-N-acetyl-cysteine
SIX	Homeobox protein
SO <sub>2</sub> H	Sulfinic
SO <sub>3</sub> H	Sulfonic
SOD	Superoxide dismutase
TEMED	Tetramethylethylenediamine
TERT	Telomerase reverse transcriptase
TGFβ	Transforming growth factor beta
TMRE	Tetramethylrhodamine ethyl ester
TNF-α	Tumour necrosis factor alpha
TNFR	Tumour necrosis factor receptor
TRAF2	TNF receptor-associated factor 2
TRAIL	TNF-related apoptosis-inducing ligand
Trx	Thioredoxin
ULK	UNC51-like kinase
UPR	Unfolded protein response
UV	Ultraviolet
Vps34	Vacuolar protein sorting
XBP1	Transcription factor X-box binding protein 1
Δψ <sub>m</sub>	Mitochondrial membrane potential

# Chapter 1 General Introduction

---

## 1.1 The eye and the lens

The human eye is a complex organ of approximately forty interconnected individual subsystems; with major structures that include sclera, cornea, iris, lens, retina and optic nerve (Cvekl & Ashery-Padan, 2014). The lens resides in the anterior part of the eye, positioned behind the cornea and the iris. This transparent organ is responsible for focusing light undistorted onto the retina in the posterior segment. Here light signals is converted to electrical signals and transmitted to the brain – the image-processing hub (Shi et al., 2009).

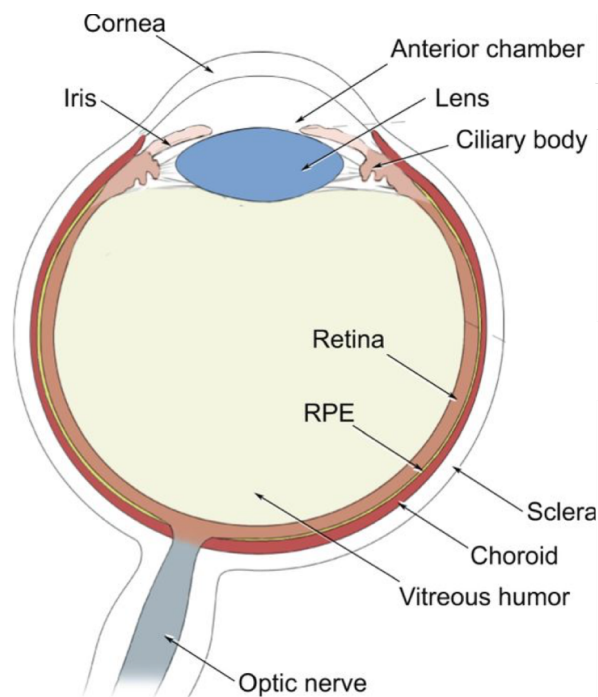


**Figure 1. 1: The vertebrate eye.**

Illustration of a transverse section of the vertebrate eye, showing the principal eye tissues and their arrangement within the eyeball. Reprinted from “The cellular and molecular mechanisms of vertebrate lens development” by A. Cvekl and R. Ashery-Padan, 2014, *Development*, 141, p.4433. Copyright 2014 by the Company of Biologists Ltd.

### **1.1.1 Lens development**

The eye is a sensory organ consisting of different tissues that contribute to optical, light-sensing and transmission functions. The lens, together with the cornea and the iris, which both reside directly in front of the lens, make up the ‘optical’ team. The lens differs from all other parts of the body in being avascular and non-innervated. Undergoing different stages of differentiation, one cell type, which is a group of ectoderm-derived lens precursor cells, eventually gives rise to the lens. The human lens begins to form when the embryo is approximately 4 mm long, at 3-4 weeks of gestation (Cvekl & Ashery-Padan, 2014; Francis, Berry, Moore, & Bhattacharya, 1999).

A diversity of transcription factors tightly regulates lens morphogenesis. Some examples are paired box protein-6 (PAX6), homeobox protein-3 (SIX3), SIX5 and pituitary homeobox-3 (PITX3) and growth factors, such as bone morphogenic protein (BMP), transforming growth factor-beta (TGF $\beta$ ), fibroblast growth factor (FGF) (Ales & Ruth, 2014). Among these names, PAX6 is considered as the eye “master gene” due to its pivotal role in eye development, although PAX6 alone is insufficient to drive the differentiation (Tsonis & Fuentes, 2006). The lens formation is initiated by the thickening of the head surface ectoderm to form the lens placodes of lens progenitor cells in a PAX6/SIX3-dependent gene regulatory network (Cvekl & Ashery-Padan, 2014). BMP and retinoic acid signalling also participate in this process. Then these progenitor cells invaginate to form the lens pit and the lens vesicle, which form the initial lens 3D structure. The gradients of growth factors, including FGFs and BMPs, polarise this 3D structure and consequently regulate the pattern of differentiation across the developing lens. The anterior lens vesicle cells become a sheet of cuboidal epithelium, while the posterior cells, following cell cycle exit, elongate and produce the primary lens fibres that will eventually construct the embryonic lens nucleus (Kallifatidis, Boros, Shin, McAvoy, & Lovicu, 2011; Y.

Li & Ding, 2017; Zhou, Leiberman, Xu, & Lavker, 2006) (**Figure 1. 2**). The final phase of the lens development is marked by several “engineering” processes. One process is the establishment of the correct mechanical stiffness of the lens, which is important for light focus and accommodation. The other process is the degradation of subcellular organelles to enable the lens to become transparent (Cvekl & Ashery-Padan, 2014).

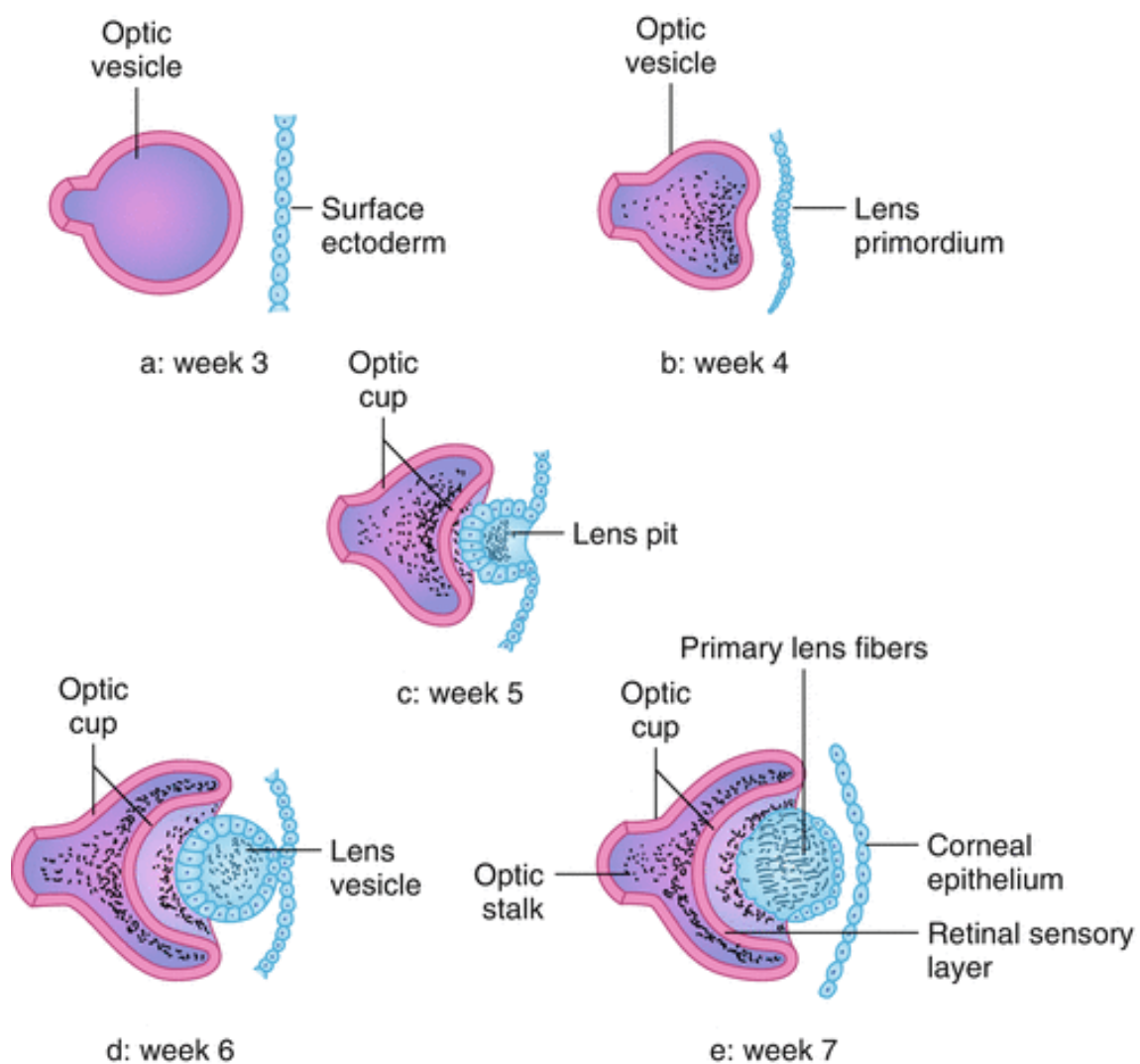


**Figure 1. 2: Schematic diagrams of embryonic development with the lens.**

A). The optic vesicle forms in the third week of gestation and begins to gradually make contact with the surface ectoderm. B) The lens placode forms in the fourth week of gestation. C) The lens placode and the optic vesicle invaginate in the fifth week of gestation. D) The lens vesicle forms completely in the sixth week of gestation. E) The primary lens fibre cells form in the seventh to eighth week of gestation. Reprinted from “Embryonic development of the human lens” by Y. Ling and Y. Ding, 2017, *Pediatric Lens Diseases*, p.2, Springer. Copyright 2017 by Springer Science+Business Media Singapore.

### 1.1.2 The mature lens

The final product of lens morphogenesis in vertebrate species is a biconvex lens suspended in the front of the eye by suspensory ligaments. The lens has three main structures, lens capsule, lens epithelium, and lens fibres (**Figure 1. 3**). With little to no cell loss and slow but persistent cell division, consequently, lens growth persists throughout life, accruing cells on its surface.

The lens is completely encapsulated by the lens capsule. The structure is a semi-elastic, amorphous, and transparent basement membrane (Abdelkader, Alany, & Pierscionek, 2014). It is secreted by lens cells and composed primarily of type IV collagen and laminin. As the lens grows during development and with age, new capsular lamellae are synthesised, deposited, and organised by constituents of lens epithelium and lens fibres (West-Mays & Korol, 2014). In a mature lens, the capsule varies from 2 – 28  $\mu\text{m}$  in thickness (Forrester, Dick, McMenamin, & Lee, 1995). The anterior capsule is thicker than the posterior one because of the more limited ability to secrete new basal lamina of the posterior fibre cells compared to the anterior lens epithelial cells (Krag & Andreassen, 2003). With certain physical and mechanical properties, the lens capsule is capable of shaping the lens and its surface curvature, allowing the lens accommodation. The capsule also acts as a growth factor reservoir and a vital epitope provider for lens cell surface receptors that collectively enhance lens cell survival and promote regional cell migration and differentiation.

Adhered to the anterior capsule is the lens epithelium. This structure of a continuous monolayer of cuboidal epithelial cells is believed to contain more than 400,000 cells in a human lens, and is often described as having a cobblestone appearance (Kuszak & Costello, 2004). Despite only representing a small fraction of the lens volume, the epithelium contains all the mitotically active cells in the tissue and can, therefore, be considered as the growth engine of the lens. The

mitotic index in the lens epithelium changes with latitudinal position, with lower values in the central region of the epithelium directly exposed to light and higher values in the protected-from-light peripheral region near the lens equator. These cells either divide to maintain the epithelial layer or terminally differentiate into fibre cells (Mallet & Rochette, 2011; Steven, 2014). Additionally, lens epithelial cells regulate the majority of the homeostatic functions of the lens. Those activities are, but are not limited to, the passage of nutrients, ions and antioxidants, and the biosynthesis of ultraviolet (UV) filters (Candia, 2004).

Lens fibre cells derived from lens epithelial cells are prismatic and very long, highly specialised cells. These fibres stretch from the equator towards two poles, but do not reach the poles; instead, they meet other fibres from the opposite equator and form a Y-shaped suture pattern with them, which may become visible during cataract. Throughout life, new fibres are laid down peripheral to the older fibres, and this phenomenon results in concentric layers of secondary lens fibres, making the structure of the lens similar to an onion: layer by layer, but each layer is made up of adjacent fibres. Regarding functions, lens fibre cells produce the predominant water-soluble proteins of the lens called crystallins. These crystallins proteins make up 90% of the dry weight of the lens and contribute to the refractive index required to focus light on the retina. Therefore, the transmission of light can become less efficient if the ordered packing of the crystallins is challenged. Moving towards the centre of the lens are elongated fibres, cortical fibres and nuclear fibres – the nucleus with a progressively increasing protein concentration and a gradual decrease in organelles to none (Ofri, 2008; L. A. Remington, 2012).

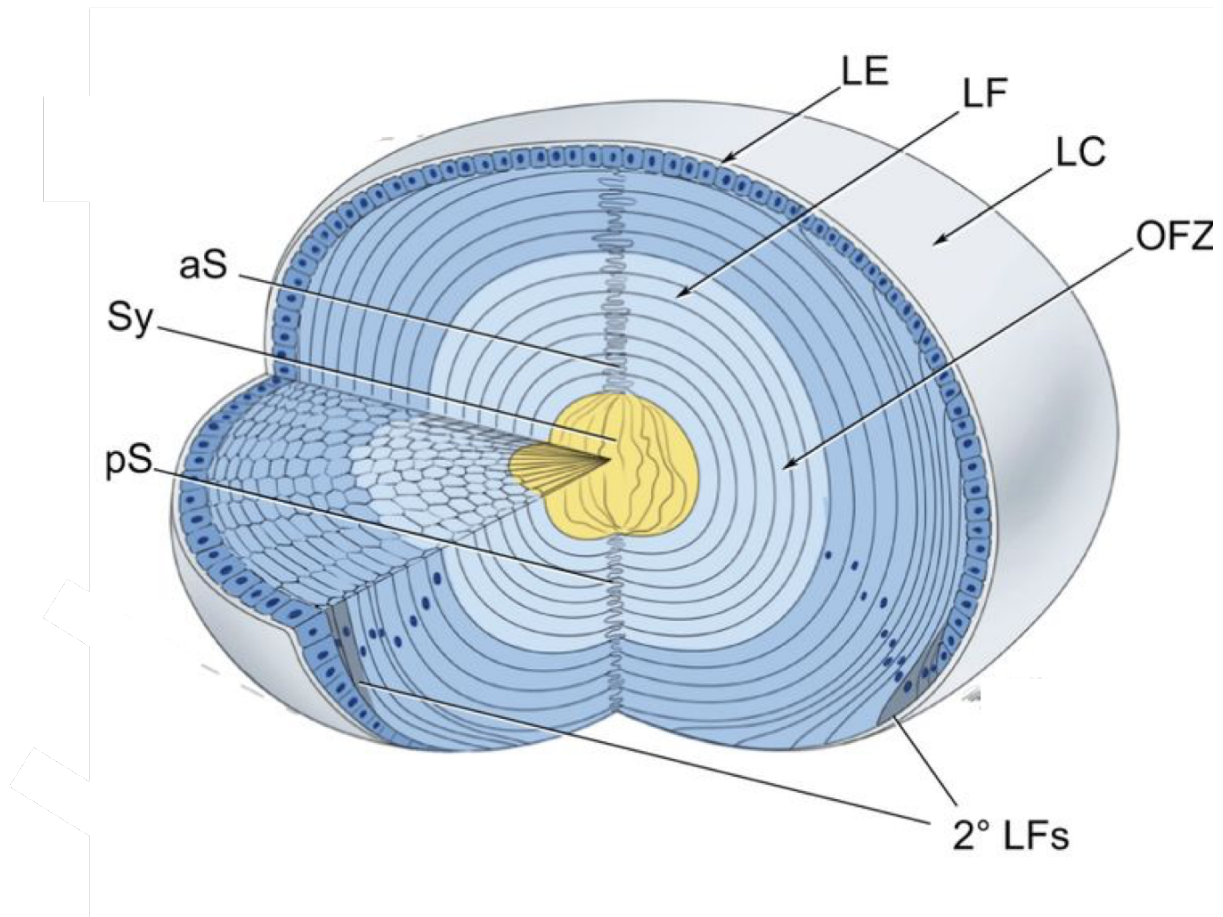


**Figure 1. 3: The lens 3D structure.**

The lens, which is part of the anterior segment within the eye, consists of the lens epithelium and lens fibre, which make up the bulk of the lens mass. Newly formed lens fibre cells are deposited on top of the ‘older’ central cells in the form of concentric shells of hexagonally packed and radially aligned fibre cells. aS, anterior suture; LE, lens epithelium; LF, lens fibre; LC, lens capsule; OFZ, organelle-free zone; pS, posterior suture; 2° LFs, secondary lens fibre; Sy, syncytium. Reprinted from “The cellular and molecular mechanisms of vertebrate lens development” by A. Cvekl and R. Ashery-Padan, 2014, *Development*, 141, p.4433. Copyright 2014 by the Company of Biologists Ltd.

### 1.1.3 Lens transparency

Despite the remarkable abundance of proteins, which is usually proportional to light scattering in protein solutions, the lens surprisingly serves as an effective ‘biological glass’ (Bassnett, Shi, & Vrensen, 2011). The transparency of a lens, as its most important characteristic, is primarily dependent on the structural integrity of the lens and the regular organisation of its cells. The lens is avascular without any innervation. Abundant adhesion junctions consisting of adherens and gap junctions help lens fibre cells be closely adhered to each other. The consequent close apposition minimises the dimensions of the extracellular space, hence, reducing the scattering

of the cell borders. Another factor is refractive index matching between lens membranes and cytosol as well as a uniform refractive index between the cytoplasm of adjacent cells. Other elements are pyknosis – the programmed elimination of nuclei – and loss of cell light-scattering organelles in cells residing within the pupillary space, the abundance and tight packing of the crystallins, and finally lamellar arrangements of the lens fibre cells in the cortex and nucleus (Abdelkader et al., 2014)

## **1.2 Cataract**

Lens disorders can be categorised based on shape, position and transparency. The first two groups are often related to injuries or rare congenital conditions, such as microphakia – a condition of a small lens, or lenticonus – a situation of anterior or posterior coning of the lens surface. Whereas the last one, loss of lens transparency, which is much more common, can be congenital or developed during adulthood due to numerous factors. The general terminology for this condition is cataract, which is accompanied by a progressive decrease in the field of vision and, eventually, total blindness.

### **1.2.1 Epidemiology**

According to the World Health Organisation, cataract remains one of the leading causes of blindness, especially in middle- and low-income countries. In Asian and African countries, the prevalence remains high (**Figure 1. 4**) (Lam et al., 2015). To put this into perspective, in 2017 cataract was estimated to globally cause moderate vision impairment to blindness to 65.2 million people, and contribute to more than 50% of vision loss worldwide (Bourne et al., 2017).

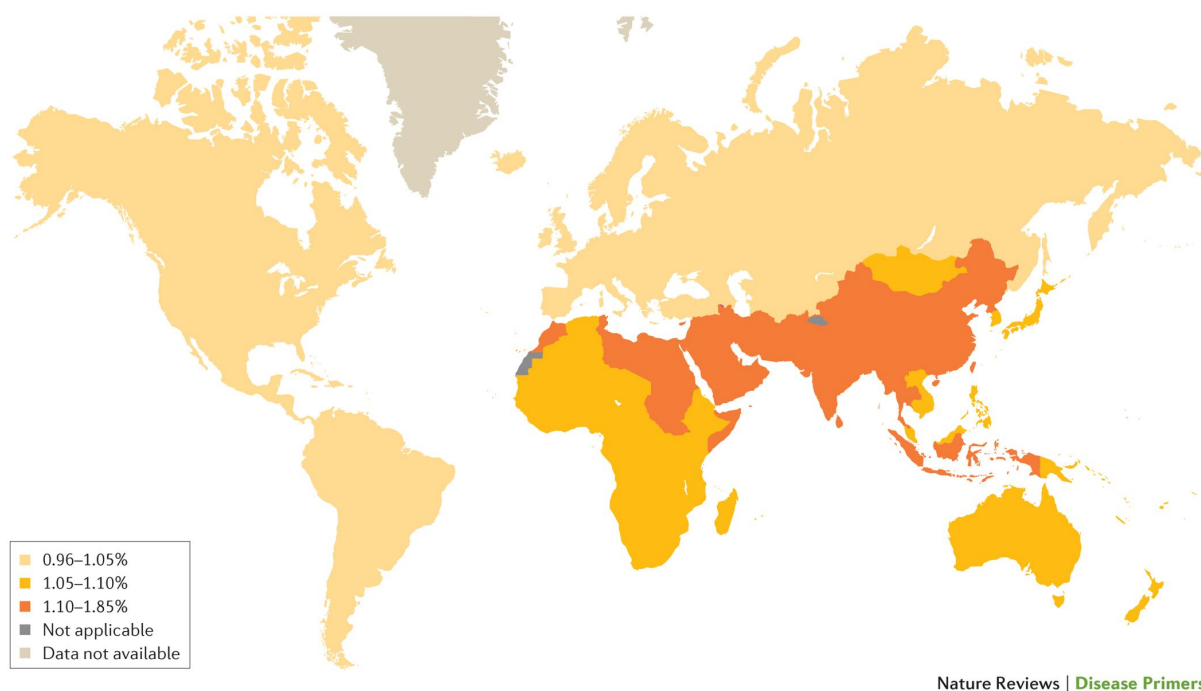


**Figure 1. 4: Global prevalence of visual impairment due to cataract.**

The lack of accessibility to health care and limited financial resources become prohibitive factors for patients with cataracts in developing countries, which results in more blindness due to cataract, especially in southeast Asia and Africa. (Lam et al., 2015). Reprinted from “Cataract” by D. Lam and co-authors, 2015, Nature Reviews Disease Primers, 1, p.2. Copyright 2015 by Springer Nature.

### 1.2.2 Risk factors and classification

Cataract prevalence increases with age in population-based studies. From the age of 40, the lens starts to lose its transparency while the risk of cataract increases with each decade of life (Keefe & Taylor, 1996; McCarty & Taylor, 2001). In Europe, the manifestation of cataract rose from 5% for the age group 52-62 and 30% for the group 60-69 to 64% for the population over 70 years (Das, Thompson, Patel, & Rosenthal, 1994; Moshetiva, 2008). In the UK, particularly, the majority of individuals aged 65 or older suffer from some degree of cataract-caused visual impairment. Fifty per cent of individuals over 80 years old have had or will have cataracts in their lifetime (Batliwala, Xavier, Liu, Wu, & Pang, 2017).

Cataract development is influenced by many factors. The biggest risk factor is age, making age-related cataract the most common type. Cataract can also manifest earlier in life due to

excessive exposure to UV radiation, cigarette smoke, air pollution, long-term usage of steroids, toxic or physical trauma. Systemic metabolic diseases, such as diabetes mellitus or galactosemia, can also cause cataract. Whereas, congenital cataract is due to genetic disorders or consequences of a noxious intrauterine event (for example, rubella) (Shiels & Hejtmancik, 2007).

Cataract can be classified via morphology. Depending on the location of opacity, the condition can be termed nuclear, cortical (both of which are strongly associated with ageing) or subcapsular cataract (posterior or anterior), as shown in **Figure 1. 5** (Chylack et al., 1989). Importantly, more than one type can be present in an eye. Along with various mechanisms, each type of cataract has different associated risk factors (**Table 1. 1**). Scientists have increasingly considered genetic predisposition to explain how individuals experience different onsets of age-related cataract given similar environmental factors. Hammond and collaborators showed that genetic factors versus environmental insults account for as much as 48% versus 14% in nuclear opacities, and 37-58% and 11-37% in cortical cataracts, respectively (Hammond, 2000, 2001).

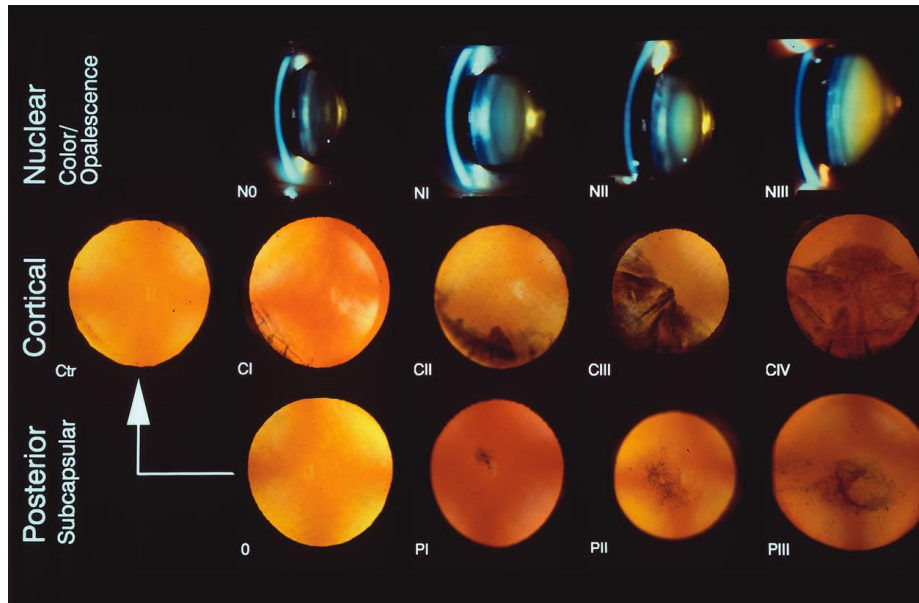


**Figure 1. 5: The Lens Opacity Classification System II (LOCS II).**

N = Nuclear photographs. Stage 0 = normal; I–III = various stages of nuclear cataract. For nuclear opalescence, the average opalescence across the entire nuclear region is used. An opalescence that is less than or equal to Photographic Standard 0 = grade 0; if the opalescence is less than or equal to Standard I, the grade is 1, and so on. For Colour Grading of the nucleus, only the N2 standard is used. (<N2 for colour=0, equal to N2 in colour=1, and N2 for colour = 2) C = Cortical photographs. 0-Trace (Tr) = normal; I–IV = various steps of cortical cataract (roughly CII  $\frac{1}{4}$ , CIII  $\frac{1}{2}$ , CIV  $\frac{3}{4}$ . CV  $> \frac{3}{4}$ ). P = Posterior subcapsular photographs. 0 = normal; I–III = various stages of posterior subcapsular cataracts. Reprinted from “Lens opacities classification system II (LOCS II)” by L.T. Chylack and M.C. Leske, 1989, JAMA Ophthalmology, 107, p.993. Copyright 1989 by American Medical Association.

**Table 1. 1: Morphological features and associated risk factors of different types of cataract.**

Type	Morphology	Risk factors
<b>Nuclear</b>	<ul style="list-style-type: none"> <li>The most common type of cataracts, involve the yellowing of the lens nucleus.</li> <li>An associated deposition of (pale and deep) yellow or brown pigment within the lens</li> </ul>	<ul style="list-style-type: none"> <li>Strongly age-relevant</li> <li>Smoking</li> <li>Increased ambient temperature → increased lens hardening</li> <li>Larger lens</li> <li>Hereditary (1/3)</li> <li>Poor diet</li> </ul>
<b>Cortical</b>	<ul style="list-style-type: none"> <li>Involving radial or wedge-like opacification, particularly in the cortex area</li> <li>Forming in the lens cortex, which is the outer shell of the lens.</li> <li>Extending its white spikes from the outside of the lens to the centre.</li> </ul>	<ul style="list-style-type: none"> <li>Diabetes</li> <li>High sunlight exposure</li> <li>Hereditary (50-60%)</li> <li>Age</li> <li>Smaller lens</li> </ul>
<b>Subcapsular</b>	<ul style="list-style-type: none"> <li>Usually involving the breakdown of lens fibres and the accumulation of granular or fibrillary material.</li> </ul>	<ul style="list-style-type: none"> <li>Diabetes</li> <li>Age</li> <li>High myopia</li> <li>Steroid consumption</li> <li>Ionising radiation</li> </ul>

### **1.2.3 Cataract surgery**

Cataract is the most common disease in clinical ophthalmologic practice, but also the most common curable cause of blindness in the world. Healthy and balanced dietary intake and behavioural traits can help protect the lens and delay cataract formation, but no one can escape cataract if that individual is blessed with longevity. Researchers have recently suggested disaggregation of crystallins as a method to treat nuclear cataract (Makley et al., 2015; Zhao et al., 2015), but this putative treatment still requires extensive development and evaluation before being considered as a reasonable therapeutic option (Wormstone, Wormstone, Smith, & Eldred, 2021). Therefore, cataract surgery remains the only effective treatment for cataract for now.

Cataract surgery has become one of the most performed surgical procedures in many economically developed countries, such as the United States and those in Europe, with millions of operations per year (W. Wang et al., 2016). During the procedure, a small incision in the sclera or cornea is made to pave a way for surgical tools to reach the eye with minimal physical disruption. Continuous curvilinear capsulorhexis (capsular tear) in the anterior capsule by capsulotomy or femtosecond laser creates an entry in the lens. This circular opening in the anterior capsule enables surgeons to access the central lens fibres, which are commonly removed by phacoemulsification. The femtosecond laser can sometimes be used to assist this process and, if necessary, traditional hydrodissection can also be used. Subsequently, residual fibre cells are removed by irrigation/aspiration techniques (Abouzeid & Ferrini, 2014; Wormstone & Eldred, 2016). A capsular bag that consists of a portion of the anterior and the entire posterior capsule is what remains of the lens after cataract surgery. The transparent intraocular lens (IOL) implanted in the bag permits a free passage of light along the visual axis to restore vision (Wormstone et al., 2021).

Society and individuals tremendously benefit from cataract surgery, which is considered the most cost-effective intervention with an approximate 4500% financial return on investment (Brown, Brown, Lieske, & Lieske, 2014). However, in light of the close association between the cataract surgical rate and the economic development, low-cost applications to treat cataract are utterly important to meet cataract surgical needs in low resource settings. With the growth of the ageing population and extended life expectancy, the number of people with cataract will continuously rise. Consequently, the condition is going to burden both the national health care system and the global economy (Yonova-Doing et al., 2016).

## **1.3 Posterior capsular opacification**

### **1.3.1 Pathogenesis and prevalence**

Despite the initial excellent results, the long-term success of cataract surgery is hindered by a secondary loss of vision caused by posterior capsule opacification (PCO) (Wormstone, 2020). However skilfully cataract surgery is performed, the procedure is inevitably a controlled trauma to the eye. A major consequence of this disruption to the integrity of the eye is a wound-healing response as an attempt to repair the damaged lens. Residual lens epithelial cells after cataract surgery repopulate all available surfaces in the bag, including the IOL surface and the previously cell-free posterior capsule, and eventually encroach on the visual axis. A homogenous thin layer of cells may negligibly affect the light path, but subsequent alterations to the matrix and cell organisation can cause light scattering (Eldred, Dawes, & Wormstone, 2011). The most common alterations bear some fibrotic features, such as matrix deposition, wrinkling/contraction of the posterior capsule, and increased presence of myofibroblasts. This is referred to as the fibrotic form of PCO (**Figure 1. 6**). In time, the second category of PCO, known as regenerative PCO, can also be observed in a portion of patients. Common features

of this type are Elschnig's pearls, arising from the formation of swollen globular cells, and Soemmerring's ring, arising from lens fibre differentiation in the peripheral capsular bag. These structures can cause significant visual disruption, hence placing the regenerative PCO above its fibrotic version on the severity scale (Wormstone et al., 2021).

Recent reports suggest that between 5 – 20% of patients post-cataract surgery require a PCO treatment in the form of laser ablation of the opacified central posterior capsule (Leydolt et al., 2020; Ursell, Dhariwal, O'Boyle, Khan, & Venerus, 2020). In contrast to age-related cataract, PCO has higher rates in young patients than in the aged group, approaching 100% in children (Binkhorst & Gobin, 1964; Khaja, Verma, Shoss, & Yen, 2011), which reflects an increased requirement for PCO treatment in young patients (Knight-Nanan, O'Keefe, & Bowell, 1996). This is likely due to the differences between young and older patients regarding the regeneration and growth capacity of their cells, which play a central role in wound healing response, hence causing PCO (H. Lin et al., 2016; Wormstone et al., 1997, 2021).

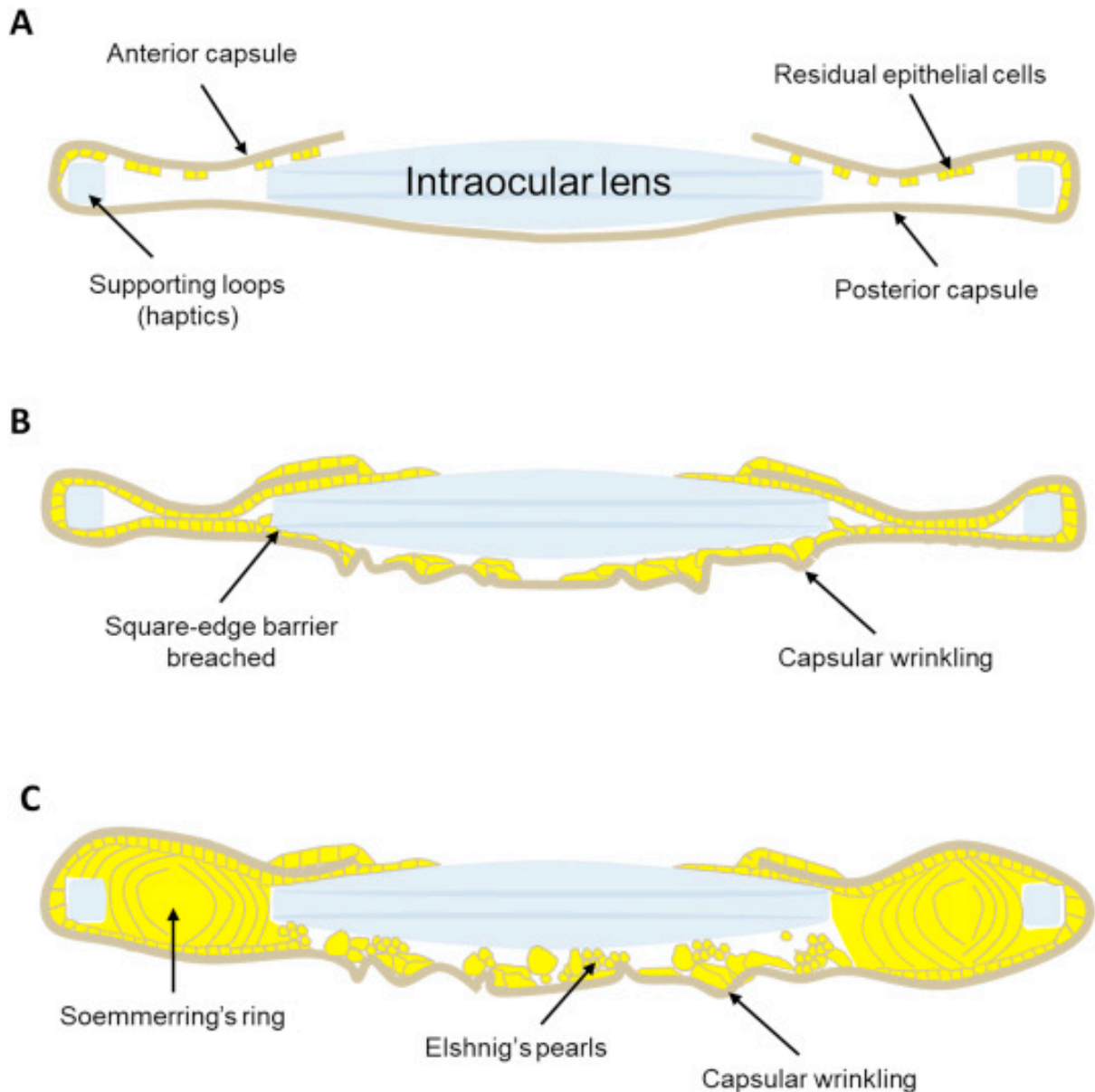


**Figure 1. 6: PCO development following cataract surgery.**

A Schematic diagram illustrating (A) the capsular bag immediately post-surgery, (B) development of fibrotic PCO showing invasion of the posterior capsule and matrix deformation/capsular wrinkling and (C) the changes that result from a combination of fibrotic and regenerative PCO with the formation of Elshnig's pearls and Soemmerring's ring. Reprinted from "Posterior capsule opacification: What's in the bag?" by I.M. Wormstone and co-authors, 2021, *Progress in Retinal and Eye Research*, 82, p.1. Copyright 2020 by Elsevier Ltd.

### 1.3.2 Current treatments

The current treatment for PCO is the corrective Nd:Yag laser treatment that ablates the central posterior capsule and associated cells (Wormstone, 2020). Nevertheless, this surgical intervention implies both high medical risks and economic costs. The medical risks include

retinal detachment, swelling in the retina (macular oedema), damage or replacement of the IOL, or corneal oedema. To address this, scientists have worked on non-surgical means to manage PCO. Targets for PCO prevention can be categorised as general measures, pharmacological measures, and non-pharmacological measures.

General measures work on the modification of IOLs regarding both materials and designs, and surgical techniques (Eldred, Zheng, Chen, & Wormstone, 2019; Leydolt et al., 2020; Perez-Vives, 2018; Slutzky & Kleinmann, 2018). There are certain improvements in this area, such as hydrophobic acrylic IOLs, open IOLs, and square-edged IOLs, which have helped lower the incidence of PCO worldwide, but unfortunately not its elimination (Linnola, Salonen, & Happonen, 1999; Oshika, Nagata, & Ishii, 1998).

### **1.3.3 Potential treatments**

IOL modification and Nd-Yag laser are currently the only ways to manage PCO, but alternative approaches have been proposed. Some non-pharmacological methods are gene therapy interfering with the TGF $\beta$  pathway (X. Yu, Zheng, Chan, & Wu, 2017), osmotic effective solutions (Duncan, Wang, Neilson, & Wormstone, 2007; Rekas, Klus, & Kosatka, 2013), or regeneration of the lens (H. Lin et al., 2016). In terms of drug delivery, the IOL itself can serve the purpose through its surface coating. Sealed drug delivery systems, such as the perfect capsule system, which allow localised drug exposure to lens cells within the capsular bag, have also been used (Duncan et al., 2007; Rabsilber, Limberger, Reuland, Holzer, & Auffarth, 2007). These approaches slowed the progression of PCO but failed to completely ablate all lens epithelial cells (Wormstone, 2020).

Postsurgical pharmacological measures focusing on inhibition of lens epithelial cell proliferation, migration, epithelial-mesenchymal transition, and matrix contraction or to kill residual lens epithelial cells have been extensively studied. A diversity of agents and drugs have been examined and shown potential. Several examples are resveratrol (Smith, Eldred, & Wormstone, 2019), aldose reductase inhibitors (Zukin et al., 2018), and CAT-152 (Wormstone et al., 2004). Nevertheless, no inhibitors have been approved to prevent the manifestation and progression of PCO at the cellular level. Therefore, the discovery of effective treatments is extremely important.

### **1.3.4 Experimental models**

To identify novel and promising targets, it is important to understand the basic biology of the condition and the mechanisms behind any putative therapies. To achieve these goals, appropriate experimental systems are required. Research on PCO can utilise a range of models. These are post-mortem analysis, cell culture, *in vivo* models, tissue culture models and stem cells (Wormstone et al., 2021). Post-mortem analysis of cadavers allows researchers to study PCO morphology and identify molecules present in the condition, but fails to provide definitive proof linking certain molecular suspects to PCO development. Cell culture, on the other hand, is the workhorse to enable elucidation of the mechanisms governing human lens cell biology for being amenable to molecular manipulation. While primary lens cells have limited longevity, lens cell lines can grow longer, hence allowing long-term experiments and substantial data acquisition. However, in addition to typical shortcomings of *in vitro* models, lens cell lines exhibit some degrees of transdifferentiation to myofibroblasts, which can limit the understanding of changes directly associated with surgery/injury. Appropriate stimuli should be carefully considered to establish working models to study certain features of PCO.

The use of *in vivo* models will help eliminate the disadvantages of cell culture models. Rodents and rabbits can offer full replication of post-surgical events and complete inflammatory responses. However, caution has to be taken when drawing the link between findings in animal studies and possible phenomena in humans in light of disparities in protein profiles between species. For tissue cultures, researchers can work on lens epithelium explant cultures from animals or capsular bags, even from human donors. The *in vitro* human capsular bag model, which is prepared following steps performed in standard cataract surgery, has been shown to reflect the clinical scenario post-cataract surgery; hence making it a valuable tool to understand the biological mechanisms governing PCO and to evaluate surgical methods, designs of IOLs and putative therapeutic agents (Wormstone, 2020). Last but not least, similarly to how stem cells have innovated the study of other disorders, recent innovations in the field have listed stem cells as the newest model to investigate PCO too.

Each of these models has certain inherent advantages and disadvantages, so researchers need to consider them to select suitable models for their studies. The value of the research can also be increased by comparative studies between different models.

## **1.4 Sulforaphane**

Recently, a novel compound called sulforaphane (SFN) has been proposed to manage PCO. Liu and co-authors demonstrated that high concentrations of SFN started to cause various stress responses and, notably, cell death in human lens cells (H. Liu et al., 2017). When applied to human capsular bags, a model for PCO, SFN decreased lens cell growth and viability, making the compound a promising agent to prevent PCO. To realise this potential of SFN, it is important to understand better the pharmacological actions of SFN.

### 1.4.1 Origin of SFN

SFN is mostly known as a potent chemopreventive agent (Fahey, Talalay, & Kensler, 2012). It comes from glucosinolates (GSLs) found in cruciferous vegetables, such as broccoli and kale (Dinkova-Kostova & Kostov, 2012; Yagishita, Fahey, Dinkova-Kostova, & Kensler, 2019). Under hydrolytic reactions, GSLs produce isothiocyanates (ITCs). SFN [R-1-isothiocyanato-4-methylsulfinylbutane] is an ITC variant.

GSLs, an important group of phytochemicals, are  $\beta$ -D-thioglucosides that differ from each other by their organic side chains (the R group) and can be classified as either aliphatic, aromatic or indole forms. Since its discovery in 1831 by Robiquet and Boutron, more than 120 distinct GSLs have been described, and most of them are isolated from the cruciferous (*Brassicaceae*) vegetable family. They are chemically stable and biologically inert. In plants, GSLs are accompanied by, yet physically separated from, the  $\beta$ -D-thioglucosidase enzymes called myrosinases; and only upon plant tissue injury, such as cutting or chewing, will they come into contact with each other and will rapid hydrolysis take place. The hydrolytic reaction yields glucose and unstable aglycone that spontaneously rearranges into different possible products, the most reactive of which are ITCs (**Figure 1. 7**). Noticeably, mammalian cells do not possess myrosinases, but the conversion can still happen owing to the bacterial microflora of the gastrointestinal tract. ITCs are amino acid derivatives that contain a monovalent group. They contain a very electrophilic carbon atom, which makes them highly reactive with nucleophiles, such as hydroxyl, amino or thiol groups to form *O*-thiocarbamates, thioureas or dithiocarbamates. ITCs react with thiol groups 1,000 times faster than amine or hydroxyl groups (Podhradsky, Drobica, & Kristian, 1979). Therefore, in humans, ITCs quickly react with GSH, the most abundant thiol in animal cells, with the assistance of glutathione

transferases (Dinkova-Kostova & Kostov, 2012; Holst & Williamson, 2004; Yagishita et al., 2019).

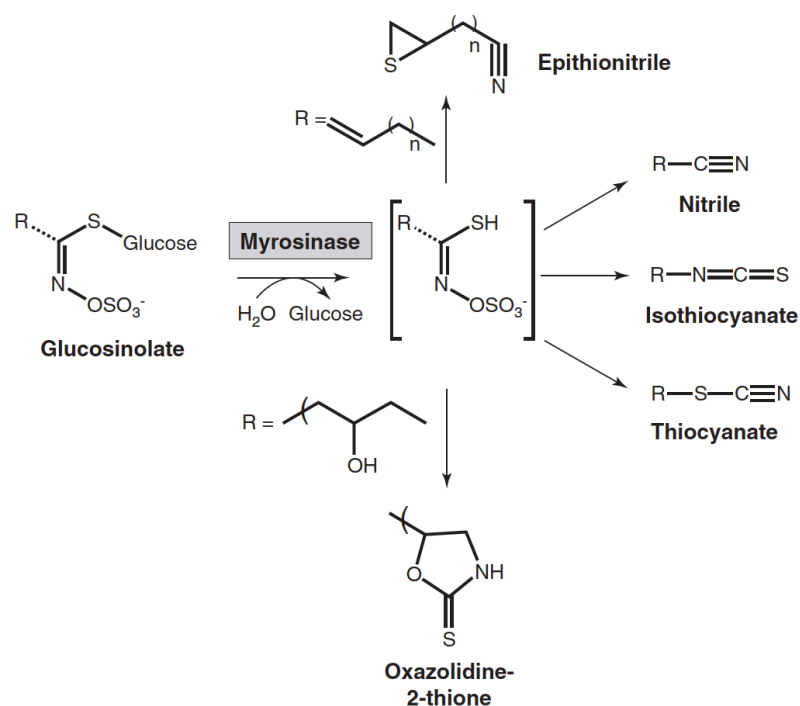


**Figure 1. 7: Myrosinase-catalysed reaction products and possible reaction products of glucosinolate hydrolysis.**

The hydrolysis of glucosinolates is catalysed by myrosinase to give unstable aglycones and liberate glucose. Depending on the reaction conditions and the structure of the glucosinolate side chain (R), a series of products can be formed, including nitriles, thiocyanates, epithionitriles, oxazolidine-2-thiones, and isothiocyanates (Dinkova-Kostova & Kostov, 2012). Reprinted from “Glucosinolates and isothiocyanates in health and disease” by A.T. Dinkova-Kostova and R.V. Kostov, 2012, Trends in Molecular Medicine, 18, p.338. Copyright 2012 by Elsevier Ltd.

### 1.4.2 Metabolism and bioavailability of SFN

SFN is an ITC derived from its precursor 4-methylsulfinylbutyl glucosinolate, or commonly known as glucoraphanin. Broccoli (*Brassica oleracea var. italica*) has the most glucoraphanin among *Brassica* species, and glucoraphanin is found in all parts of this plant, although its amount varies in each tissue. The seeds have the highest abundance of glucoraphanin and this rapidly declines as the seeds develop. In certain cruciferous vegetables, their 3-day-old sprouts were shown to have 10 – 100 times higher concentrations of glucoraphanin than the

corresponding mature plants (Fahey, Zhang, & Talalay, 1997). Depending on the genotype and growing conditions, cultivars of broccoli can accumulate from less than 1 to 10  $\mu\text{mol}$  per gram of glucoraphanin in their florets (Yagishita et al., 2019). Mild cooking can preserve myrosinase activity and result in nearly 100% conversion of glucoraphanin into SFN (Juge, Mithen, & Traka, 2007). Upon entry into mammalian cells, SFN reacts with GSH to form SFN-GSH conjugates (dithiocarbamates), then these dithiocarbamates get metabolised through the mercapturic pathway and excreted in the urine as a mercapturic acid (**Figure 1. 8**) (Briones-Herrera, Eugenio-Perez, Reyes-Ocampo, Rivrea-Mancia, & Pedraza-Chaverri, 2018). Additionally, SFN can be converted to erucin, which is then similarly metabolised.

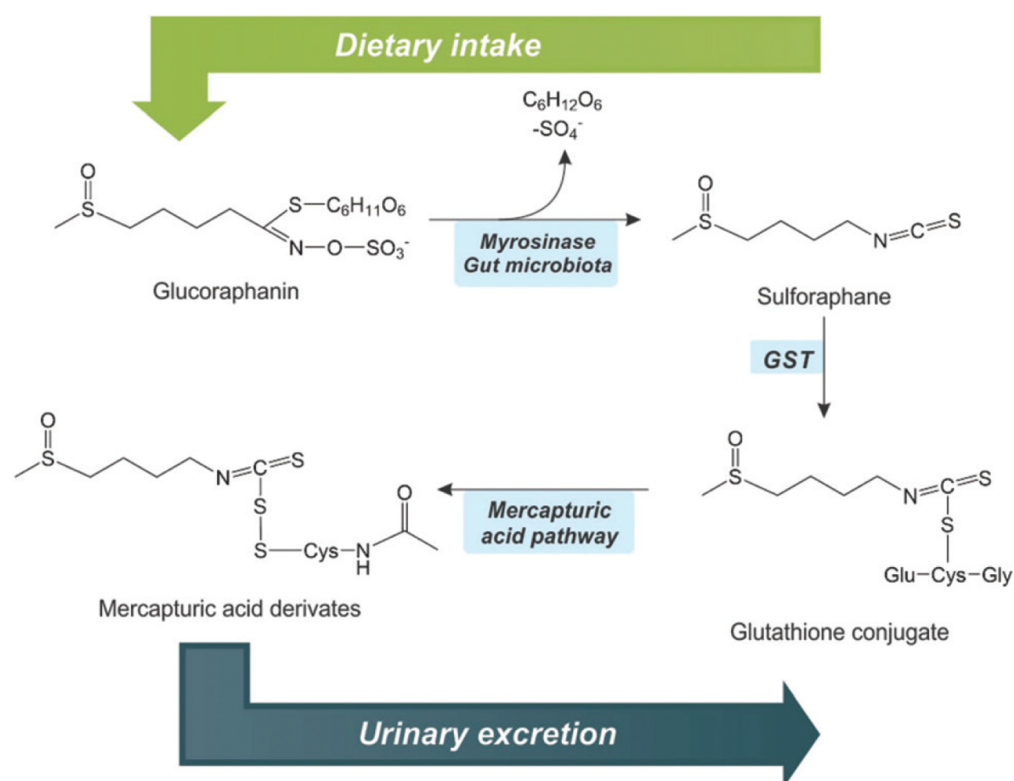


**Figure 1. 8: Structure, intake and excretion of SFN.**

SFN equivalents can be obtained from the dietary intake of Brassica vegetables, which contain high amounts of GLs and glucoraphanin. Glucoraphanin is hydrolysed by myrosinase or by gut microbiota, obtaining a moiety of sulforaphane, glucose and sulfuric acid. Sulforaphane can be later metabolised by glutathione-S-transferase (GST), producing glutathione conjugates, and then processed by the mercapturic acid pathway, producing mercapturic acid derivatives which are excreted in the urine. Reprinted from “New highlights on the health-improving effects of sulforaphane” by A. Briones-Herrera and co-authors, 2018, Food & Function, 9, p.2590. Copyright 2018 by Royal Society of Chemistry.

In terms of bioavailability, SFN is rapidly absorbed and eliminated with small inter-individual variations and typical urinary excretion of 60% to 90% of the dose. Also, the level of SFN metabolites found in plasma is usually low. In a study of 20 participants, only 0.7 +/- 0.2 µM was found in plasma after 3 hours of administration of 200 µmol SFN (Atwell et al., 2015). Another study of 10 participants showed a peak plasma value of 0.61 +/- 0.50 µM after being given broccoli soup containing 452 µmol of glucoraphanin (Sivapalan et al., 2018). Together with other studies, these two examples show that oral uptake of SFN results in more bioavailability, quicker elimination, and less inter-individual variation in excretion than glucoraphanin. These properties collectively make the use of SFN more appealing to pharmaceutical companies. However, SFN is unstable, as opposed to its inert precursor. Therefore, pharmaceutical companies have been developing stabilised versions of SFN, for example, Prostaphane®, or glucoraphanin samples enriched with active myrosinase, for example, Avmacol® (Dinkova-Kostova & Kostov, 2012; Yagishita et al., 2019).

### **1.4.3 Functional roles of SFN**

SFN is a hormetic agent, meaning that its concentration determines its mode of action, cytoprotection or cytotoxicity. At low concentrations, which can be achieved via dietary consumption or supplementary intake, SFN appears to trigger many protective effects; whereas at high, supranutritional concentrations, which are impossible to achieve via those means listed above, SFN can cause cell death. Following numerous studies done on SFN, Liu and co-authors showed that SFN could be both cytoprotective and cytotoxic to human lens cells in a dose-dependent manner (H. Liu et al., 2013).

#### 1.4.3.1 Antioxidant and cytoprotection

SFN is most known for its strong potency in inducing the redox-sensitive transcription factor Nrf2 pathway (**Figure 1. 9**). This pathway is the major regulator of cytoprotective responses to endogenous and exogenous caused by reactive oxygen species (ROS) and electrophiles (Kansanen, Jyrkkanen, & Levonen, 2012). Nrf2 is constitutively synthesised in a cell, but negatively regulated by a cytosolic protein called Kelch-like ECH associated protein (Keap1): two Keap1 molecules bind to Nrf2 and direct Nrf2 to ubiquitylation degradation. In basal conditions, some Nrf2 molecules escape this fate and translocate into the nucleus to orchestrate antioxidant dependent element (ARE)-dependent gene expression to maintain cellular homeostasis. Under stress conditions, inducers inhibit the Keap1-dependent control check, Nrf2 levels quickly increase in the nucleus and upregulate a battery of cytoprotective ARE genes, such as nicotinamide adenine dinucleotide phosphate dehydrogenase quinone 1 (NADPH quinone 1 or NQO1), haeme oxygenase 1 (HO-1), glutamate-cysteine ligase (GCL) and glutathione-S-transferase (GST), collectively known as phase II antioxidant enzymes. Additionally, Nrf2 can also raise reduced glutathione (GSH) levels by inducing the rate-limiting enzyme, glutamate-cysteine ligase, for GSH synthesis (Batliwala et al., 2017; Nguyen, Nioi, & Pickett, 2009).

As a potent inducer of phase 2 antioxidant enzymes, SFN can indirectly upregulate and increase the activity of many cytoprotective antioxidants through the Nrf2-ARE pathway (Y. Zhang, Talalay, Cho, & Posner, 1992). A study in humans has shown that daily consumption for 2 weeks of broccoli sprouts containing 100  $\mu$ mol SFN increased the expression of NQO1 and HO-1 in alveolar macrophages to aid bacterial clearance (Harvey et al., 2011). The redox modulation of SFN also extends to non-enzymatic antioxidants, with GSH being one of the

major beneficiaries. GSH levels are reported to be increased by SFN in a clinical pilot study (100  $\mu$ mol encapsulated SFN over 7 days) (Sedlak et al., 2018).

In addition to antioxidant properties, SFN can be anti-inflammatory in an Nrf2 dependent manner (Juge et al., 2007), which makes SFN a promising agent to treat inflammatory conditions, such as arthritis (R. Davidson et al., 2017; R. K. Davidson et al., 2013) and inflammatory bowel dysfunction (Y. Zhang et al., 2020). Other beneficial effects of SFN are alleviating mitochondrial dysfunction, increasing mitochondrial biogenesis, and enhancing autophagy. These cytoprotective properties make SFN a popular agent in studies of various disorders, including, but not limited to, cancers, cardiovascular diseases and central nervous system diseases (Dinkova-Kostova & Kostov, 2012; Houghton, 2019).

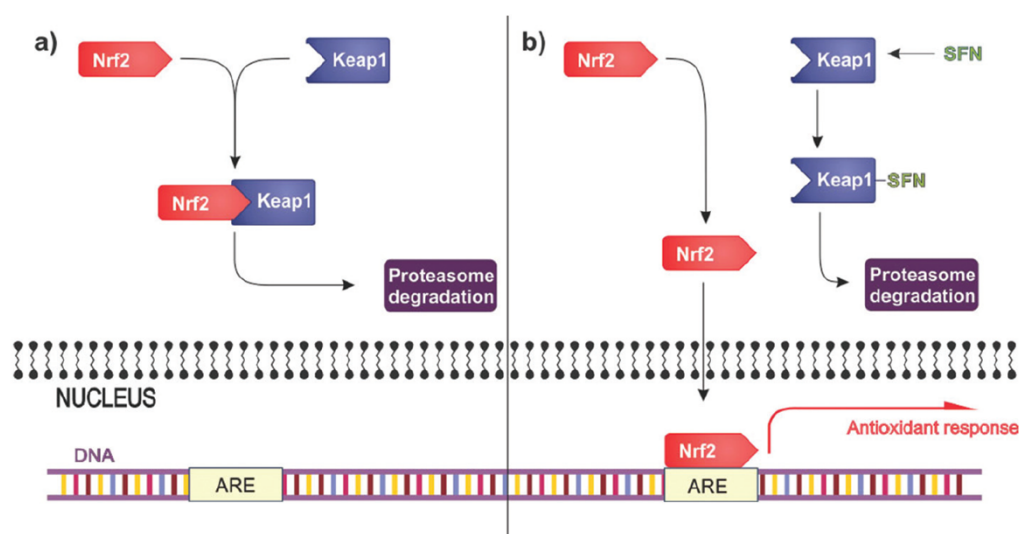


**Figure 1. 9: Activation of the Nrf2 by SFN.**

A) Under normal conditions, Nrf2 is constitutively present on cells, as well as its repressor the Kelch-like ECH-associated protein 1 (Keap1); thus, Keap 1 is constantly interacting with Nrf2 and carrying it to its degradation by the proteasome, maintaining basal levels of Nrf2. B) SFN can react with some cysteine residues of Keap1, obtaining some adducts and inhibiting its union to Nrf2. Thus, the nuclear translocation of Nrf2 and its union to deoxyribonucleic acid in the antioxidant responsive elements (ARE) can activate cytoprotective genes. Reprinted from “New highlights on the health-improving effects of sulforaphane” by A. Briones-Herrera and co-authors, 2018, Food & Function, 9, p.2590. Copyright 2018 by Royal Society of Chemistry.

#### 1.4.3.2 Anti-proliferation and cytotoxicity

In contrast to its cytoprotective properties described above, SFN can also elicit cell cycle arrest and cell death. Regarding cell cycle arrest, SFN can induce epigenetic modifications in several studies (Atwell et al., 2016; Bassett & Garnett, 2014; Parnaud et al., 2004). Epigenetic modifications are reversible changes that affect the genomic structure and regulate gene expression without influencing the DNA sequence itself. Common mechanisms are DNA methylation (adding methyl (CH<sub>3</sub>) groups to DNA to repress gene expression), histone acetylation (adding acetyl groups (CH<sub>3</sub>CO) to lysine residues on histone proteins to relax chromatin to enable transcription), or histone phosphorylation (similar to acetylation, but phosphate groups onto serine, threonine or tyrosine instead of acetyl groups on to lysine). In cancer cells, from molecular docking analyses, SFN appeared to bind to the substrate pockets of histone deacetylases (HDAC, enzymes removing acetyl groups) and of DNA methyltransferases (DNMT, enzymes adding methyl groups) to suppress HDAC and DNMT activity. Consequently, tumour suppressor genes and cell cycle arrest genes escape the inhibitory regulation of HDAC and DNMT, undergo transcription and translation, and arrest the cell cycle at different stages of its progression. SFN also upregulates histone phosphatases to decrease H1 phosphorylation, which is known to play a role in cell cycle progression (Abbaoui et al., 2017). Another mechanism for SFN to halt the cell cycle is methylating the promoter of telomerase reverse transcriptase (TERT), which protects chromosome edges, to prevent its expression (Kaiser et al., 2021).

SFN-mediated cell death is propagated via various pathways (Briones-Herrera et al., 2018; Juge et al., 2007). SFN has been shown to activate programmed cell death – apoptosis – to cause cell death in different cancer cell models. SFN at concentrations of 10 – 40 μM caused

a release of cytochrome c from the mitochondria to the cytosol, which binds to apoptotic protease activating factor 1 (Apaf-1) to activate the caspase-9 cascade, leading to cell death. Similar concentrations of SFN were also shown to imitate the downstream intracellular apoptotic machinery upon the binding of death ligands, such as Fas-L and TNF-related apoptosis-inducing ligand (TRAIL) onto their cell surface receptors (Sestili & Fimognari, 2015).

The tumour suppressor protein p53 helps regulate apoptosis and progression through the cell cycle. The activation of p53 was found to be essential for SFN induced cytotoxicity (K. Rudolf, Cervinka, & Rudolf, 2014; Y. Wang et al., 2021), but dispensable in colon cancer cells and osteosarcoma (Oliveira *et al.*, 2014). The mitogen-activated protein kinase (MAPK) signalling pathway is another route that SFN activates to induce cell death in cancer cells (Geng et al., 2017; Hsu, Chang, Wang, Chen, & Huang, 2013; Lan, Yuan, & Lin, 2017). SFN was also reported to induce cell death by increasing intracellular calcium ( $\text{Ca}^{2+}$ ) levels. In three different cancer cell lines and transgenic mice with developed tumours, SFN-induced apoptosis was shown to be mediated by SFN-induced depletion of reticular  $\text{Ca}^{2+}$  and modulation of transcription factors through nuclear  $\text{Ca}^{2+}$  upregulation (Hudecova et al., 2016).

Another mechanism to induce cytotoxicity upon SFN treatment is an increase in ROS levels (**Figure 1. 10**) (Briones-Herrera et al., 2018; Sestili & Fimognari, 2015). As little as 10  $\mu\text{M}$  of SFN is already able to augment ROS levels, decrease GSH content and glutathione reductase (GR) activity, and consequently induce apoptosis via both intrinsic and extrinsic mechanisms. GR is the enzyme that converts one oxidised glutathione (GSSG) molecule to two GSH molecules. Decline in GSH amount might increase ROS levels, while decreases in GR activity might worsen the reduced GSH levels. Ferreira de Oliveira and co-authors suggested that

oxidative stress arising from ROS accumulation and impaired GSH recycling triggered cell death in osteosarcoma cells in a p53-independent manner (de Oliveira, Costa, Pedrosa, Pinto, Remedios, et al., 2014), while Lan and co-authors linked ROS and MAPK pathways together via the mechanisms of SFN cytotoxicity in p53-deficient colon cancer cells (Lan et al., 2017). Nrf2 induced by SFN can protect cells from oxidative stress via upregulation of antioxidant genes, but a study in NIH3T3 cells shows that excessive ROS can lead to Nrf2 dependent activation of Kruppel-like factor 9 (Klf9), which can amplify the ROS production cascade and trigger oxidative-stress induced cell death (Zucker et al., 2014). Other mechanisms associated with SFN-induced apoptosis are the JNK signalling pathway (E. Rudolf & Cervinka, 2011) and ERS (Doudican, Wen, Mazumder, & Orlow, 2012). Importantly, all of these mechanisms are not mutually exclusive and can be triggered simultaneously or subsequently to lead to cell death.

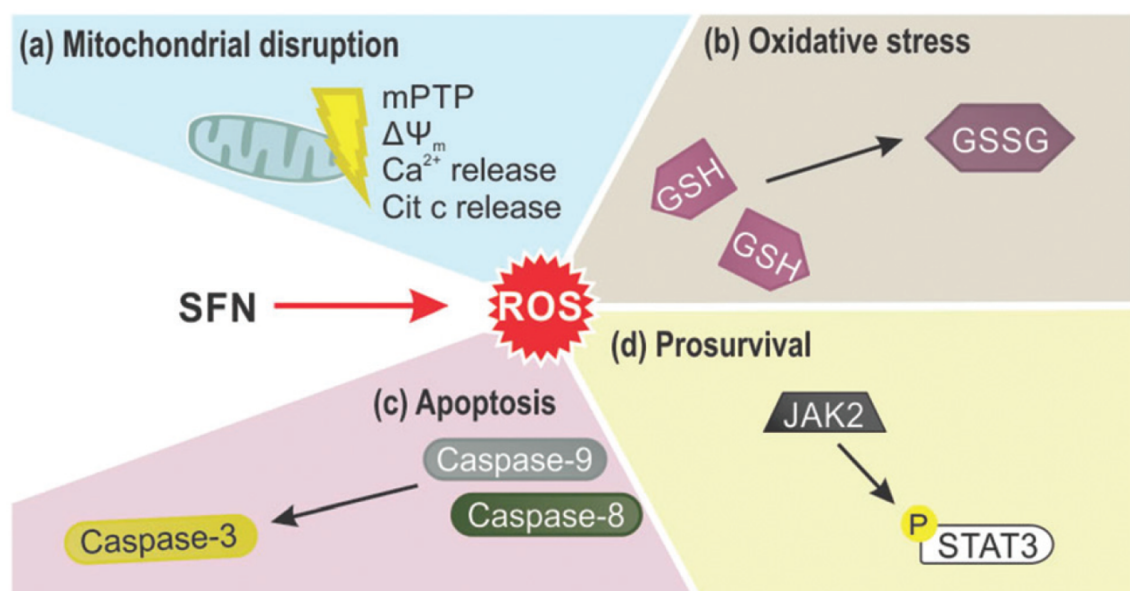


**Figure 1. 10: The role of ROS on the cell death induced by SFN.**

At first, ROS can induce (a) mitochondrial disruption characterised by the opening of the mitochondrial permeability transition pore (mPTP), dissipating the mitochondrial membrane potential ( $\Delta\Psi_m$ ), and augmenting Ca<sup>2+</sup> and cytochrome c (Cyt c) release. (b) High ROS levels lead to oxidative stress by the depletion of glutathione (GSH), obtaining its oxidised form, glutathione disulfide (GSSG). (c) Then, ROS and further oxidative stress can lead to apoptosis by the activation of caspases 8 and 9 and then

activating caspase-3. (d) ROS can also oxidise some other proteins, Janus kinase 2 (JAK2) among them, disrupting the phosphorylation of its target STAT3 (signal transducer and activator of transcription 3) and diminishing cell viability. Reprinted from “New highlights on the health-improving effects of sulforaphane” by A. Briones-Herrera and co-authors, 2018, Food & Function, 9, p.2598. Copyright 2018 by Royal Society of Chemistry.

#### **1.4.4 SFN in the human lens**

The diverse effects of SFN have shown potential to manage or prevent major lens disorders. It was reported that at low micromolar concentrations (less than 10  $\mu\text{M}$ ), SFN could restore transparency in cultured whole lenses exhibiting opacity due to oxidative stress. This represents SFN as a non-surgical alternative to treat cataract (H. Liu et al., 2013). On the other hand, the cytotoxicity of SFN achieved at high concentrations can be used in a positive way to prevent PCO (H. Liu et al., 2017). In that study, the authors reported the application of SFN at high concentrations increased reactive oxygen species (ROS), and induced several cellular stress events, such as endoplasmic reticulum stress and autophagy, and cell death in FHL124 cells (H. Liu et al., 2017). However, there is no knowledge of how cell death was triggered in this study. On the other hand, using a different human lens epithelial cell model, Chhunchha and collaborators linked cell death induced by SFN to the activation of a non-canonical Nrf2 redox signalling pathway (Chhunchha, Kubo, & Singh, 2019). As discussed above, upon cellular entry, SFN can bind to Keap1, allowing Nrf2 to translocate into the nucleus to influence gene expression patterns. The Chhunchha et al study showed that excessive nuclear Nrf2, resulting from high concentrations ( $> 15 \mu\text{M}$ ) of SFN, also bound to the regulation region of the *Klf9* gene promoter and activated its expression, in addition to those ARE-related antioxidant genes. Importantly, *Klf9* acted as a repressor of peroxiredoxin-6 (Prdx6), which is abundantly expressed in the eye, localised in almost all ROS-producing organelles, and responsible for regulating ROS levels. Consequently, the aberrant activation of *Klf9* led to suppression of Prdx6, elevation of ROS, and cell death, which were significantly reduced by *Klf9* deletion. However, *Klf9* deletion failed to restore the ROS levels and cell viability to the baseline levels,

suggesting that Klf9 is not the key player in SFN-induced cell death. Those three studies together illustrate the diverse cytotoxic impacts of SFN on human lens cell lines. Nevertheless, to demonstrate SFN as an excellent candidate to manage PCO, a complete interplay between these stress responses (and more) and cell death is pivotal.

## 1.5 Cellular stress and responses

Cells growing *in vivo* or *in vitro* are constantly subjected to various forms of internal and external stimuli, some of which may induce stress (Milisav, 2011). These can cause damage to intracellular macromolecules, such as proteins, DNA, RNAs and lipids. Several cellular stress stimuli include, but are not limited to, chemotherapeutic agents, irradiation, heat shock, oxidative stress and endoplasmic reticulum stress (ERS). Stressors can also be metabolic or therapeutic, such as shortage or overload of certain nutrients, growth factor deprivation or inhibition of certain signalling pathways. In general, a stressor is one causing any deviation from the normal environment of a cell.

In non-immune cells, such as lens epithelial cells, stressors can cause intrinsic stresses, such as DNA damage, hypoxia, and disturbances in mitochondria. Following stress stimuli, especially at low levels, cells initially elicit adaptive responses to allow them to fight against and recover from the insult. In contrast, following prolonged or overwhelming stress, cells tend to succumb to death, which is common in age-related disorders or cancer treatments. The nature and duration of the stress and the type of cells, therefore, largely determine the fate of stressed cells: survival and growth or death (Fulda, Gorman, Hori, & Samali, 2010; Poljšak & Milisav, 2012).

Cellular responses can be categorised into four groups: 1) cell repair mechanisms (**Table 1. 2**), (Fulda, Gorman, et al., 2010), responses to achieve temporary adaptation, 3) autophagy, or 4)

cell death. Adaptation responses to stress circumscribe acclimation and physiological adjustments to sublethal stress, which lead to greater stress tolerance. The phenomenon has been observed in both prokaryotes and eukaryotes, including humans, such as malignant transformation in cancer. Autophagy is a self-degradative process featured by the formation of double-membrane vesicles called autophagosomes to sequester cytoplasm. This process plays a role in the elimination of misfolded or aggregated proteins and damaged organelles, namely mitochondria, ER and peroxisomes. Autophagy can also be involved in cell death in cultured mammalian cells, and can occur before, alongside, or during the final stages of apoptosis. The interplay between autophagy and apoptosis is, in fact, dynamic, and can be inhibitory or stimulatory.

**Table 1. 2: Principles, mechanisms and exemplary molecules participating in cell repair mechanisms.**

<b>Principles</b>	<b>Mechanisms</b>
Altered gene expression	Modulation of transcription
	Translational regulation of gene expression
Protein quality control and repair	Ubiquitin proteasome system
	Chaperons
	Unfolded protein responses in ER
Signalling pathways	Nuclear receptor signalling
	Mitogen-activated protein kinase (MAPK) signalling
	Autophagy signalling
	Hypoxia signalling

### **1.5.1 Oxidative stress and mitochondrial dysfunction**

ROS are any free radicals involving oxygen, including hydroxyl radical ( $\bullet\text{OH}$ ), superoxide ( $\text{O}_2^-$ ), hydrogen peroxide ( $\text{H}_2\text{O}_2$ ), and peroxynitrite ( $\text{ONOO}^-$ ) with  $\bullet\text{OH}$  as the most reactive (Berthoud & Beyer, 2009). The source of ROS in the lens can come from exogenous or endogenous sources. Exogenous sources encompass UV light (UVC and UVB particularly), chemotherapeutics, inflammatory cytokines and environmental toxins. Since the lens is constantly exposed to sunlight, so UV light is the major source in this category. Whereas

endogenous ROS come as by-products of cellular metabolic activities in peroxisomes, lipoxygenases, cytochrome P450 and mitochondria, the fundamental source of endogenous ROS in the lens (Andley, Song, Wawrousek, Fleming, & Bassnett, 2000). The lens is avascular, so it receives oxygen from the surrounding aqueous and vitreous humour pools (Brennan, McGreal, & Kantorow, 2012). Approximately 90% of oxygen consumption is due to mitochondrial respiration in mitotically active lens epithelial cells and newly differentiated fibre cells near the equator. Under normal respiratory conditions, as much as 2% of oxygen is then converted to  $O_2^-$ , which can further lead to the formation of multiple damaging ROS (Grosswiler, 1984; Zoric et al., 2008).

To keep a balanced redox state and maintain transparency, the lens is equipped with a well-designed defence system with both non-enzymatic and enzymatic against oxidative damage, as shown in **Figure 1. 11** (Lou, 2003; Mironczuk-Chodakowska, Witkowska, & Zujko, 2018; Yoon, Kim, & Shin, 2015). The non-enzymatic antioxidants are GSH, ascorbic acid or vitamin C, vitamin E, and carotenoids to neutralise or scavenge ROS. These ROS scavengers act as chain breakers to directly prevent ROS formation via direct binding. By contrast, the antioxidant enzymes catalytically remove ROS by generating either less toxic ROS or non-oxidative molecules. Some examples are superoxide dismutase (SOD), catalase, and peroxiredoxins. Oxidative stress arises from the excessive production of ROS in the face of insufficient or defective antioxidant defence systems. Excessive ROS generation or deficiency of the antioxidant defence systems is strongly associated with ageing, but there are other external factors, such as toxins, xenobiotics, UV or pollutants, and internal factors, such as genetic defects or mitochondrial dysfunction.

Mitochondria, the powerhouses of the cell, are responsible for numerous essential functions and events, including intracellular calcium  $\text{Ca}^{2+}$  regulation, ROS production and scavenging, and regulation of cell death. Emerging evidence has showcased mitochondria as integral players in molecular signalling and cell fate determination through ROS (Peoples, Saraf, Ghazal, Pham, & Kwong, 2019). There is also a strong association between mitochondrial dysfunction and oxidative stress in ageing, cancer, degenerative conditions, and metabolic disorders. In response to the accumulation of ROS, mitochondria undergo numerous alterations in biogenesis, membrane potential, network dynamics, and number (Bhatti, Bhatti, & Reddy, 2017). The ability of mitochondria to withstand oxidative damage is extremely important for cell survival because its collapse can open mitochondrial pores and release not only ROS but also other contents requiring containment, such as pro-apoptotic proteins and enzymes.

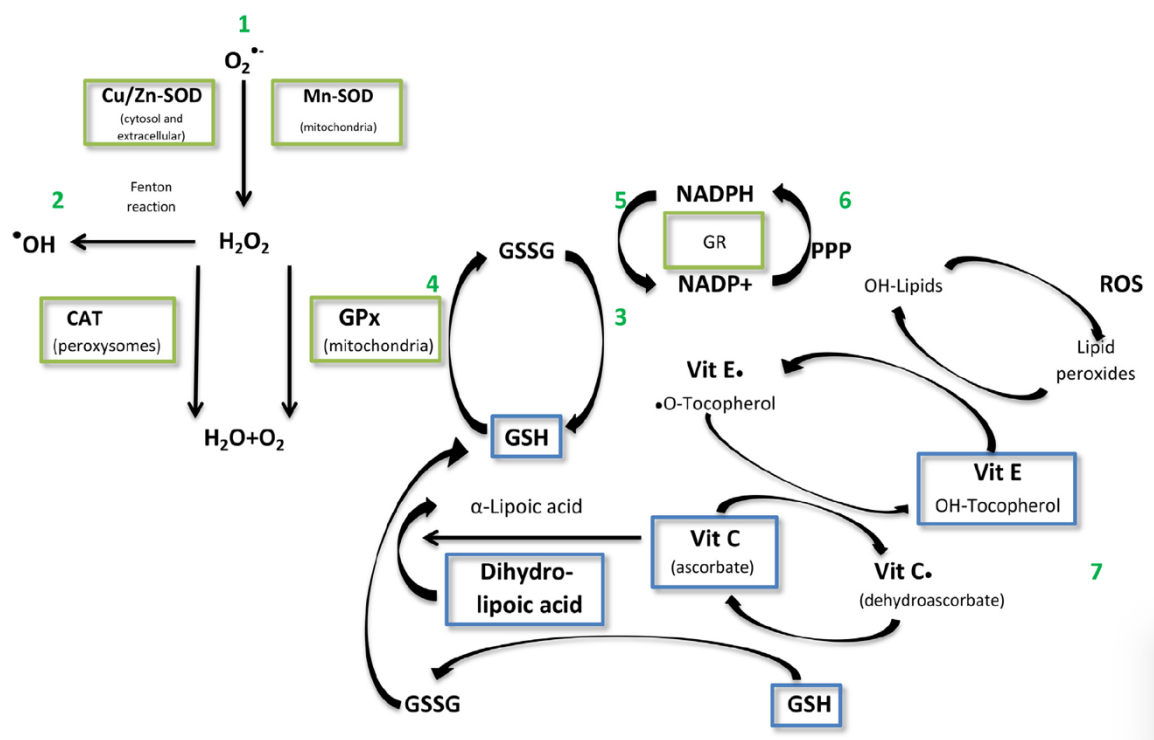


**Figure 1. 11: The ROS formation and the antioxidant defence in a cell.**

1) Superoxide radical ( $\text{O}_2^{\bullet-}$ ) is formed by a single-electron reduction of oxygen. In a reaction catalysed by superoxide dismutase (Cu/Zn-SOD or Mn-SOD), superoxide radical binds an electron, which leads to the formation of hydrogen peroxide ( $\text{H}_2\text{O}_2$ ). In the further reduction of  $\text{H}_2\text{O}_2$  to water and oxygen are involved two enzymes catalase (CAT) and glutathione peroxidase (GPx). 2) In the Fenton's reaction, which is catalysed by transition metals,  $\text{H}_2\text{O}_2$  is transformed to hydroxyl radical ( $\bullet\text{HO}$ ), which further participates in the free radical chain reactions. 3) Reduced glutathione (GSH), due to the presence of the thiol group of cysteine reacts with free radicals of proteins or other macromolecules, restoring them

to the reduced form. **4)**  $\text{H}_2\text{O}_2$  is reduced by reduced glutathione in the reaction catalysed by glutathione peroxidase. The resulting oxidised glutathione oxidises thiols of proteins. **5)** Glutathione disulfide is reduced by glutathione reductase (GR) using hydrogen of Reduced nicotinamide adenine dinucleotide phosphate (NADPH), which is oxidised to  $\text{NADP}^+$ . **6)** NADPH is generated in the first oxidative phase of the pentose phosphate pathway. In this phase, glucose-6-phosphate is dehydrogenated by glucose-6-phosphate dehydrogenase to ribulose 5-phosphate, and at the same time, two molecules of  $\text{NADP}^+$  are reduced to NADPH. Vitamin C and  $\alpha$ -lipoic acid support the regeneration of GSSG back into GSH. A hydrogen donor Vitamin E scavenges lipid peroxides and terminates oxidative chain reactions. Unoxidised form of vitamin E can be recycled back by vitamin C and glutathione (Mironczuk-Chodakowska et al., 2018). Reprinted from “Endogenous non-enzymatic antioxidants in the human body” by I. Mironczuk-Chodakowska and co-authors, 2018, *Advances in Medical Sciences*, 69, p.2598. Copyright 2017 by Medical University of Bialystok.

### 1.5.2 Endoplasmic reticulum stress and unfolded protein response

Endoplasmic reticulum (ER) is the site of synthesising and folding of proteins, synthesising lipids, and storing free  $\text{Ca}^{2+}$ . Its usual functions are easily affected by hypoxia, nutrient deprivation, viral infection, and ROS overload (J. H. Lin, Walter, & Yen, 2013). These perturbations in ER impairs the folding and degradation machineries, and accumulate misfolded and unfolded proteins in the ER lumen, thereby causing ERS. In response to ERS, a group of signal transduction pathways (collectively termed the unfolded protein response – UPR) is activated to resolve imbalanced protein folding and restore ER homeostasis. The UPR consists of three intertwined pathways, initiated by three distinct internal ER proteins: inositol requiring kinase 1 alpha ( $\text{IRE1}\alpha$ ), protein kinase R-like endoplasmic reticulum kinase (PERK), and activating transcription factor 6 (ATF6), as shown in **Figure 1. 12** (Periyasamy & Shinohara, 2017). Under resting states, the ER-resident chaperone binding immunoglobulin protein (BiP/GRP78) binds to these three ERS sensors to keep them idle; upon sensing disrupted equilibrium, BiP dissociates, allowing them to exercise their power (Bhattarai, Riaz, Kim, & Chae, 2021). These are canonical ERS pathways, and other noncanonical ERS pathways independent of the classical UPR exist too, but are not a focus of this study.

Depending on the activation mode with different intensity and duration, the three UPR branches may act differentially or synergistically. The  $\text{IRE1}\alpha$  pathway is the most conserved

ERS branch. Following UPR, IRE1 $\alpha$  dimerises and trans-autophosphorylates to ultimately activate the transcription factor X-box binding protein 1 (XBP1), which upregulates multiple pro-survival target genes and increases protein secretion rate in ER. In the PERK pathway, PERK phosphorylates eukaryotic initiator of translation factor 2 $\alpha$  (eIF2 $\alpha$ ) to halt protein synthesis in the ER lumen. Simultaneously, phosphorylated-eIF2 $\alpha$  (P-eIF2 $\alpha$ ) also increases the translation of specific mRNAs, including the ATF4 mRNA, which can upregulate many downstream genes to alleviate ERS. In the last branch, upon activation, ATF6 translocates to the nucleus and associates with endoplasmic reticulum stress response elements (ERSE-I) to induce expression of UPR target genes, such as XBP1 and BiP. Despite initiated as an adaptive response, prolonged UPR signals are eventually converted to alternative signals called terminal UPR signals that promote apoptosis.

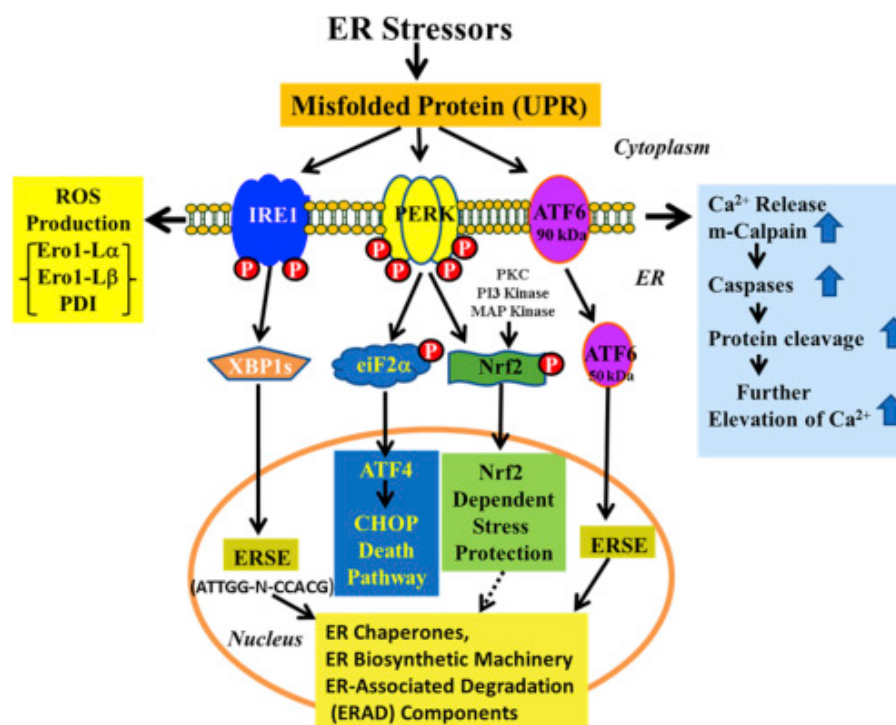


**Figure 1. 12: The molecular mechanisms of activation of ERS.**

The UPR can be activated by three intertwined pathways comprising the UPR which are initiated by the phosphorylation of PERK and IRE1 and cleavage of ATF6. Via a series of downstream mechanisms (transcriptional induction of endogenous proteins, increased activity of chaperones, ER biosynthetic machinery, and ER-associated degradation components), the misfolded protein load is reduced for cell survival. Upon chronic ER stress, the apoptotic UPR genes and death pathways are activated, while

calcium ions are released into the cytoplasm instead, which results in senescence or cell death. Reprinted from “Age-related cataracts: Role of unfolded protein response, Ca<sup>2+</sup> mobilization, epigenetic DNA modifications, and loss of Nrf2/Keap1 dependent cytoprotection” by P. Periyasamy and co-authors, 2017, Progress in retinal and eye research, 60, p.8. Copyright 2017 by Elsevier Ltd.

### **1.5.3 DNA damage and DNA damage response**

Every cell in the human body experiences tens of thousands of DNA lesions daily from a wide spectrum of exogenous and endogenous agents (Lindahl, 1993; Lindahl & Barnes, 2000). The most pervasive exogenous stimulus is UV light, which can induce approximately 100,000 lesions per affected cell every hour, whereas the most prominent endogenous DNA-damaging inducer is ROS generated during cellular metabolism, such as H<sub>2</sub>O<sub>2</sub> (Jackson & Bartek, 2009). The majority of DNA damage can be repaired; however, DNA repair systems are not 100% efficient, leaving unrepaired DNA prone to mutations following replication. Mutations in certain genes can give rise to cancer and a variety of pathological conditions. On the other hand, the accumulation of unrepaired DNA damage can lead to a variety of molecular consequences, such as genome instability, telomere dysfunction, epigenetic alterations, ERS and compromised mitochondrial function. Accumulating evidence has shown that DNA damage affects most, if not all, aspects of the ageing phenotype, making it a potentially unifying cause of ageing and several health conditions (Schumacher, Pothof, Vijg, & Hoeijmakers, 2021; Shimada, Crother, & Arditi, 2014). Causes of DNA damage and consequences at different levels of DNA damage are summarized in **Figure 1. 13**.

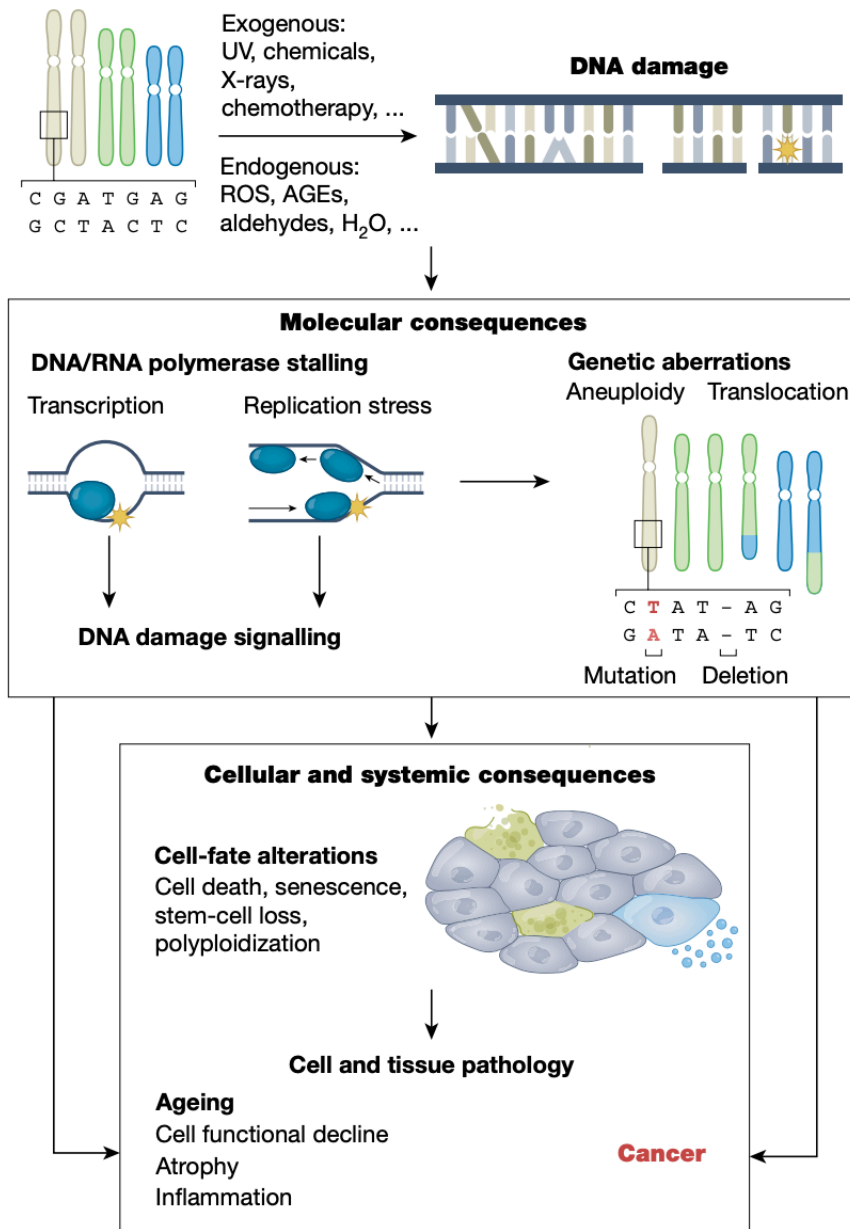


**Figure 1. 13: DNA damage and its consequences.**

The nuclear and mitochondrial genomes are continuously damaged by exogenous agents (such as UV, X-rays, chemical compounds in food, water and air), endogenous sources such as reactive oxygen species (ROS), aldehydes and advanced glycation end products (AGEs) and spontaneous reactions (hydrolysis). Molecular consequences of time-dependent accumulating DNA damage are: (1) genetic aberrations, such as mutations and chromosomal instability, and (2) stalling of RNA and DNA polymerases by DNA lesions, which provokes DNA damage signalling and interferes with primary DNA functions. Cellular and tissue consequences of DNA damage include cell fate decisions such as cell death and senescence, leading to functional loss of cells and organs, cancer, atrophy and inflammation. Reprinted from “The central role of DNA damage in the ageing process” by B. Schumacher and co-authors, 2021, *Nature*, 592, p.696. Copyright 2021 by Springer Nature Limited.

DNA lesions can be sorted into 6 types: oxidative processes, alkylation of bases, base loss caused by the hydrolysis of bases, bulky adduct formation, DNA cross-linking, and DNA

strand breaks (single and double-strand breaks). Among these types, a DNA double-strand break is arguably the most significant, since small numbers of un-repaired or mis-repaired double-strand breaks can cause cell death or chromosomal translocations, an early step in the aetiology of carcinogenesis. (Jeggo & Lobrich, 2007).

The cellular mechanisms countering DNA damage are collectively termed the DNA-damage response. The DNA damage response is responsible for detecting DNA damage and promoting repair. There are multiple, largely distinct DNA damage response mechanisms to efficiently repair different types of DNA lesions. Some examples include direct DNA-lesion reversal, mismatch repair, base excision repair, nucleotide excision repair, homologous recombination, and non-homologous end-joining. Excluding the direct protein-mediated reversal route, the rest of DNA damage responses rely on a sequence of catalytic events mediated by multiple proteins to restore DNA integrity.

In eukaryotic cells, two major pathways that have evolved to repair double-strand breaks are homologous recombination (HR) and non-homologous end-joining (NHEJ). The balance between HR and NHEJ is essential for genome stability. The mechanism of HR relies on the genetic information from a corresponding undamaged region present on sister chromatids or homologous chromosomes; re-synthesis of the damaged DNA sequence is accomplished using the undamaged molecule as a template. Consequently, HR leads to accurate repair and the preservation of the genetic material. However, the use of other homologous regions rather than sister chromatids can cause gross chromosomal rearrangements, such as deletions, inversions or loss of heterozygosity. In contrast, there is no need for a template in NHEJ because this mechanism works by directly ligating the two ends of damaged DNA molecules with little or no processing. While HR is mainly active during the S and G2 phases of the cell cycle, NHEJ

is always active (Podhorecka, Skladanowski, & Bozko, 2010) and is also the only double-strand break repair pathway activated in post-mitotic cells (Wells & El-Khamisy, 2014). The efficiency of NHEJ is high and mammals mainly rely on NHEJ, but this also makes the repair pathway prone to mutations at the joining sites and gross chromosomal rearrangements, such as inversions and translocations (Aguilera & Gómez-González, 2008; Huertas, 2010). To sum up, the balance between the two systems is heavily regulated and it appears that NHEJ generally acts as the first line of repair for double-strand breaks, with any failed-to-repair lesions necessitating the activation of HR. However, the wiring and the hierarchy governing this network remain incompletely understood (Brandsma & van Gent, 2012; Schumacher et al., 2021).

#### **1.5.4 Autophagy**

In response to damaged organelles, accumulation of misfolded or unfolded proteins, or ROS and DNA damage, a major catabolic pathway known as autophagy is activated. The process is highly conserved and necessary for cell survival and homeostasis maintenance in eukaryotic living systems (Galati, Boni, Gerra, Lazzaretti, & Buschini, 2019; Kang, Zeh, Lotze, & Tang, 2011). Under normal conditions, autophagy is kept at low basal levels and serves as the major intracellular degradation system that produces new building blocks for renovation by degrading long-lived or damaged proteins and organelles. On the other hand, prolonged or extreme stress stimuli may trigger autophagy-dependent cell death. The balance of autophagy-related stress adaptation and cell death is related to several physiological processes, such as ageing and neurodegeneration, and health conditions, such as cardiovascular diseases and cancers.

Autophagy is an umbrella term for all lysosome-dependent degradation pathways and is divided into three main types: macroautophagy, microautophagy, and chaperone-mediated

autophagy (Mizushima & Komatsu, 2011). These types differ at the initiation point where materials are targeted, but eventually all three converge at the lysosome (**Figure 1. 14**). Macroautophagy is the major type. Thus, when autophagy is mentioned, it usually means macroautophagy.

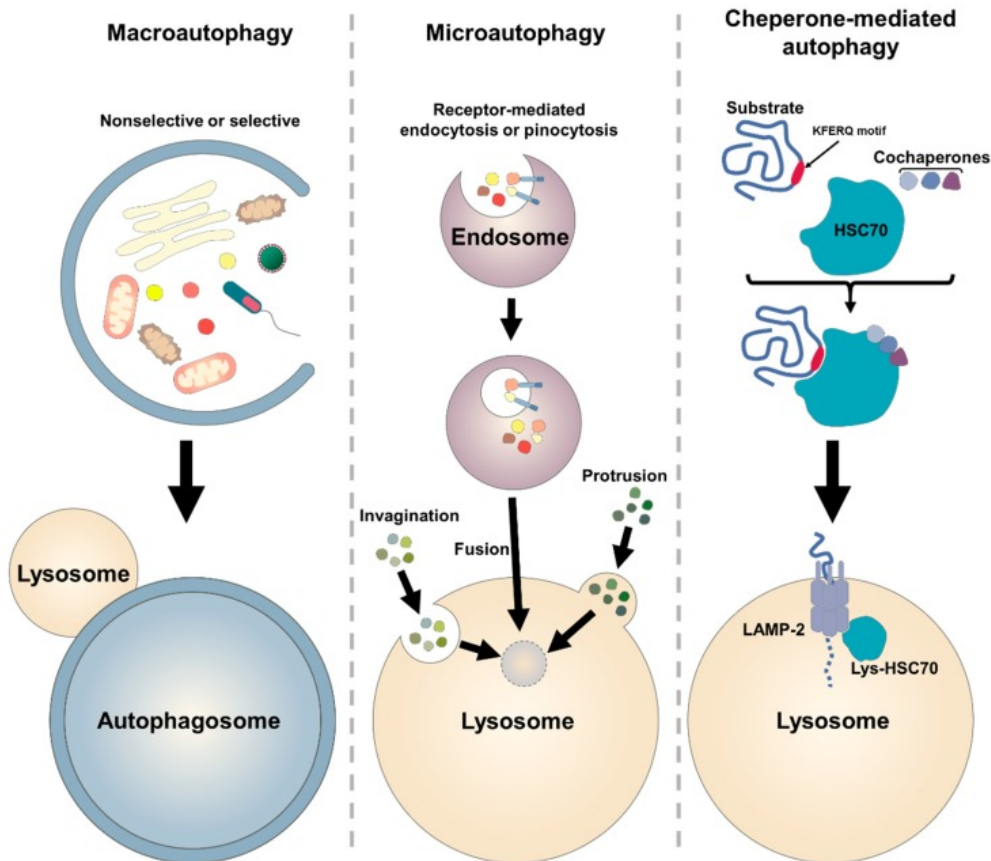


**Figure 1. 14: Overview of the mammalian autophagy pathway.**

Macro-autophagy encapsulates the cytoplasmic cargo by a delimiting membrane, which forms an autophagosome, which finally fuses with lysosome for degradation of the substrates. Micro-autophagy involves invagination or protrusion of the vacuole, which is formed by a lysosomal membrane. It also degrades extracellular molecules encapsulated by endocytosis (receptor-mediated pathway) or pinocytosis, following fusion with the lysosome. The pinocytotic vesicles fuse with endosomes to hydrolyse the substrates. Chaperone-mediated autophagy is a selective degradation pathway, in which the protein substrates containing KFERQ-like motifs are recognised by chaperone HSC70 and cochaperones, such as carboxyl terminus of HSC70-interacting protein (CHIP), heat shock protein 40 (HSP40) and HSP70-HSP90 organizing protein (HOP), and are transferred into the lysosome via a lysosomal receptor complex, LAMP-2. Reprinted from “Roles in Autophagy in Oxidative Stress” by H.R. Yun and co-authors, 2020, International Journal of Molecular Sciences, 21, p.3291. Copyright 2020 by MDPI.

The molecular machinery of autophagy consists of three major steps: 1) initiation/nucleation, 2) expansion/completion, and 3) degradation/retrieval as shown in **Figure 1. 15** (Kang et al.,

2011; Y. Lee, Kim, Park, & Lee, 2019; Morishita & Mizushima, 2016; Yun et al., 2020). The first step is driven by two protein complexes, the UNC51-like kinase 1 (ULK1) and the Bcl-2-interacting myosin-like coiled-coil protein (Beclin 1). In normal conditions, mammalian target of rapamycin complex 1 (mTORC1) interacts with a complex containing ULK1/2, autophagy-related protein homologue 13 (Atg13), focal adhesion kinase family interacting protein of 200kD (FIP200) and Atg101, and keeps this complex inactive via phosphorylation. Following autophagy inducers, such as nutrient starvation, oxidative stress or rapamycin, mTORC1 disassociates from the ULK complex, and ULK1 is liberated from the complex to initiate autophagy (**initiation**). ULK1 subsequently frees Beclin 1 from its interacting protein and Beclin 1 starts to form its complex with vacuolar protein sorting 34 (Vps34), Vps15 and Atg14, which results in the generation of isolation double membranes called phagophores around materials targeted for degradation (**nucleation**). The Golgi complex, endosomes, ER, mitochondria and the plasma membrane are potential providers of membrane for the phagophore (Tooze & Yoshimori, 2010).

In the following step, the nascent membranes elongate thanks to two ubiquitin-like conjugation systems, Atg16L and microtubule-associated protein 1A/1B-light chain 3 (LC3)-Atg3 which lead to the formation of LC3-phosphatidylethanolamine (LC3-PE or LC3-II) (**expansion**). The two edges of the membranes eventually fuse to form double-membrane vesicles called autophagosomes that engulf the waste materials (**completion**). The final step of autophagy involves the formation of autophagolysosomes, which arise from the fusion of mature autophagosomes with lysosomes. In autophagolysosomes, sequestered materials are degraded by lysosomal hydrolases (**degradation**). Following the cue coming from the degradation of autolysosomal products, mTOR signalling is reactivated. Increased mTOR activity suppresses autophagy and produces proto-lysosomal tubules and vesicles, which extrude from

autolysosomes and develop into functional lysosomes, effectively replenishing the portion of lysosomes in the cell (**retrieval**) (L. Yu et al., 2010). In brief, autophagy is characterised by the creation of autophagosomes that enclose cytoplasmic materials and organelles and eventually merge with lysosomes, resulting in the degradation of the vesicle's contents (Lee *et al.*, 2019).

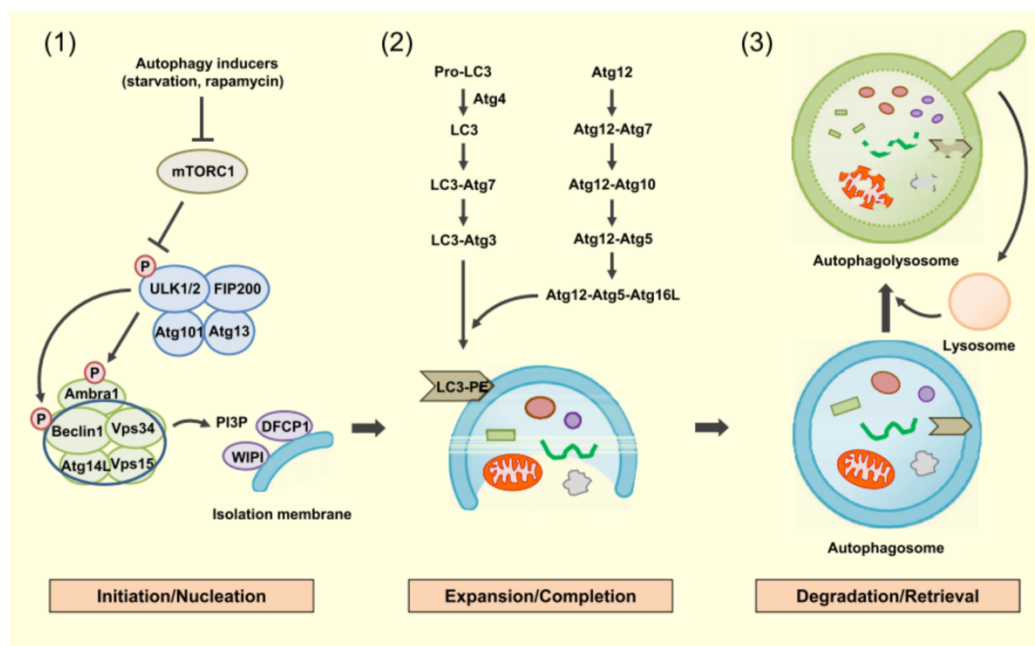


**Figure 1. 15: Molecular pathways of autophagy.**

(1) Initiation/Nucleation: Autophagy inducers, such as nutrient deprivation or rapamycin reduce mTORC1 phosphorylation, which liberates the ULK1/2 complex. The ULK1/2 complex increases the activity of the Beclin1/Vps34 complex through phosphorylation of Ambra1 and Beclin 1. PI3P, produced by Vps34, recruits effector proteins, such as DFCP1 and WIPI2 to promote the formation of the isolation membrane and to constitute the nucleation step. (2) Expansion/Completion: Expansion of autophagosome is mediated by two conjugated systems comprising Atg12-Atg5-Atg16L and LC3-Atg3 which lead to the formation of LC3-PE (LC3-II). (3) Degradation/Retrieval: After completion, mature autophagosome fuses with lysosome forming autophagolysosome, wherein the sequestered materials or organelles are degraded by lysosomal enzymes. After digestion of entrapped materials, nutrients become available and mTORC1 is reactivated. Proto-lysosomal tubules are then formed that mature into functional lysosomes, constituting the retrieval process. Reprinted from “ $\beta$ -cell autophagy: Mechanism and role in  $\beta$ -cell dysfunction” by Y.H. Lee and co-authors, 2019, *Molecular Metabolism*, 27, p.S93. Copyright 2019 Elsevier GmbH.

### **1.5.5 Cell death**

To offset stress stimuli, varying cellular responses are triggered to restore cellular homeostasis. When these adaptive attempts lose the battle to prolonged or intense stressors and the point of no return is reached, a cell's foregoing of its life is important. The elimination of useless or potentially dangerous cells and the ability of dying cells to alert their surroundings about a potential threat help preserve organismal homeostasis. However, cell death is not always a necessary evil; in fact, a fine balance between cell proliferation and death is crucial. Cell death is required in many stages of development, including neural development, reduction in egg cells at birth, as well as the construction of fingers and vestigial organs in humans. It is estimated that in a human body 60 - 86.4 billion cells die every day in a multitude of ways (X. Liu et al., 2018). At the pinnacle of countless pathological conditions and ageing is dysregulated cell death, either too much or too little. Insight into the mechanisms of cell death both sheds light on basic cellular biology and accelerates novel therapeutic strategies against proliferative, degenerative, infectious and autoimmune diseases (Nirmala & Lopus, 2020). Cell death typically follows two main mechanisms, apoptosis and necrosis, although under great scrutiny derived from them are at least 34 ad-hoc variants (Lemasters, 2019; X. Liu et al., 2018).

#### 1.5.5.1 Apoptosis

Apoptosis, also known as programmed cell death, is a carefully regulated, complex adenosine 5'-triphosphate (ATP)-dependent process of cell death. The process is important in normal physiology and pathobiology; it is apoptosis that sculpts and remodels tissues and organs in development. Apoptotic cells undergo membrane blebbing, shrinkage, orderly DNA and cellular fragmentation without cellular membrane rupture to minimise systemic or localised damage and maximise immune tolerance. Generally, apoptosis can be executed via two different pathways, extrinsic and intrinsic, which can converge or influence each other to bring

forth the culminating face of cellular demise (Igney & Krammer, 2002; Nirmala & Lopus, 2020) (**Figure 1. 16**). The common element between these routes is the activation of a proteolytic caspase cascade, in which downstream effector caspases can directly generate the apoptotic phenotype and inhibit anti-apoptotic signals. Some may argue the dispensability of caspases in light of ‘caspase-independent apoptosis’, but this phenomenon is not ubiquitous in all animals (Tait & Green, 2008).

The extrinsic pathway is initiated by perturbations of the extracellular microenvironment. The process is mostly driven by either of two types of plasma membrane receptors, death receptors that are activated by the binding of death ligands, or dependence receptors that are activated when the levels of their specific ligand drop below a specific threshold (Galluzzi, Vitale, & Aaronson, 2018). Some common death receptors are the Fas receptor and those belonging to the tumour necrosis factor receptor family (TNFR). Upon binding to death ligands, such as TNF- $\alpha$  and Fas, cytoplasmic domains of death receptors cluster to provide a docking site for adaptor proteins, which subsequently activate different upstream (initiator) procaspases, such as caspase-8 and -10. These activated initiators then activate downstream (executioner) caspases, such as caspase-3, -6 and -7, to execute cell death.

On the other hand, the initiators of the intrinsic pathway come from intracellular microenvironments. Several prominent causes are growth factor withdrawal, radiation, hypoxia, DNA damage, ROS overload, ERS, and replication stress. Most chemotherapeutic and targeted cancer therapies promote cell death via this pathway, and defects and mutations in this machinery contribute to failed chemotherapy. Apoptosis in the intrinsic pathway is regulated by members of the B-cell lymphoma 2 (Bcl-2) family situated on the mitochondrial membrane, such as Bcl-2 associated X (Bax) and Bcl-2, act as pro- or anti-apoptotic regulator

proteins, respectively. Hence, it is also called the mitochondrial pathway. The functional consequences of pro-apoptotic signalling from the aforementioned stimuli are mitochondrial outer membrane permeabilisation, loss of mitochondrial membrane potential and subsequent releases of pro-apoptotic proteins from the intermembrane space into the cytosol. The key molecule of the first released batch is cytochrome c. Cytochrome c and Apaf1 together activate the initiator caspase 9. Similar to caspase 8 in the extrinsic pathway, activated caspase 9 will then activate executioner caspases-3/6/7. Later in the process, when the cell has committed to dying, mitochondrial proteins, such as apoptosis-inducing factor (AIF) and endonuclease G, are released from the mitochondria to initiate DNA fragmentation. ERS discussed in **Section 1.5.2** can also trigger intrinsic apoptosis by influencing the Bcl family proteins via c-Jun N-terminal kinase (JNK)/p38 MAPK signalling pathways (Galluzzi et al., 2018; Nirmala & Lopus, 2020). The IRE1 $\alpha$  pathway can interact with TNF receptor-associated factor 2 (TRAF2) to induce inflammatory and apoptotic signals, while PERK can upregulate the expression of C/EBP homologous protein (CHOP), a transcription factor that regulates genes encoding apoptosis components.

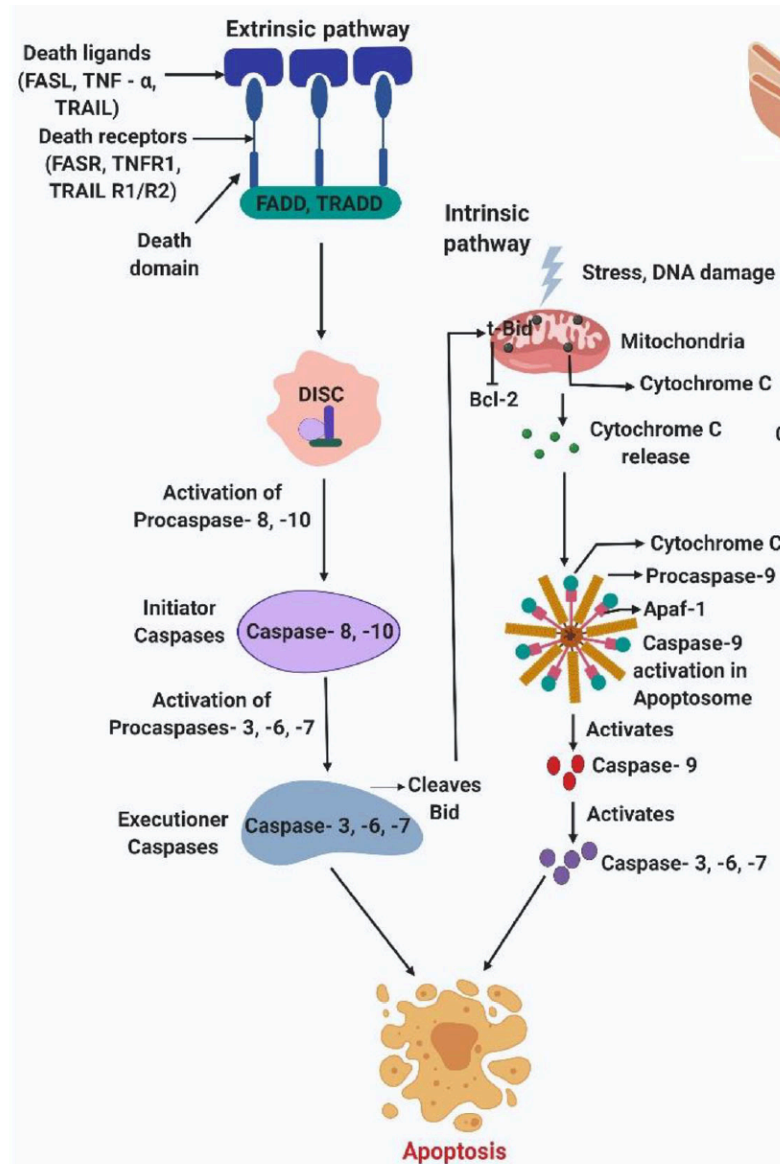


**Figure 1. 16: Signalling pathways of apoptosis.**

The extrinsic pathway of apoptosis is mediated by the binding of death-inducing ligands to death receptors, such as TNFR1, FASR, and TRAIL R1/R2. The binding recruits adapter proteins and initiator procaspases (procaspase-8, procaspase-10) to the death domains of the receptors, TRADD and FADD, leading to the formation of death-inducing signalling complex (DISC). The induced proximity thus achieved by the procaspases activates them. The initiator caspases then activate executioner procaspases (procaspase-3, procaspase-6, and procaspase-7) leading to cell death. The intrinsic pathway of apoptosis is mediated by cellular stress results in the permeabilisation of mitochondrial membranes by the proapoptotic family of Bcl-2 proteins. Following apoptotic stimulation, cytochrome c, and subsequently, other apoptosis-promoting factors are released from the mitochondria. In the cytosol, cytochrome c associates with Apaf-1 to form apoptosome, activating thus caspase-9, leading to the activation of downstream caspases resulting in apoptosis. Reprinted from “Cell death mechanisms in eukaryotes” by J.G. Nirmala and M. Lopus, 2020, *Cell Biology and Toxicology*, 36, p.150. Copyright 2019 Springer.

#### 1.5.5.2 Necrosis

If apoptosis is cell suicide, necrosis is cell homicide. Necrosis, a type of unprogrammed cell death, is caused by severe stress stimuli that can kill cells instantly, usually exogenous stressors, such as infection, high-dose radiation, shock or high pressure, and ATP-depletion. Additionally, in contrast to calculated, caspase-mediated apoptosis, abrupt necrosis does not follow the ordered signal transduction pathway, despite being able to be transduced through both extrinsic and intrinsic routes (Nirmala & Lopus, 2020). Morphologically, necrotic cells exhibit membrane blebbing, mitochondrial swelling, dilation of ER, cellular swelling, and eventually the rupture of cell membrane followed by the cytoplasmic constituents oozing out into the extracellular space. This messy process inevitably evokes inflammatory responses, which are minimised in apoptosis, and can cause tissue damage, which can deposit scars in organs with little regenerative capacity, like the heart or brain. Chronic necrosis can even overwhelm robust regeneration in organs like the liver and lead to cirrhosis (Lemasters, 2019).

Cell death, manifested as apoptosis, necrosis or their variants, plays a major role in multiple pathophysiological conditions, making it a major therapeutic target to manage numerous human disorders (**Figure 1. 17**). Many drugs promoting cell death have already been successfully marketed and used, whereas the development of cytoprotective strategies targeting cell death signalling is much more challenging. To some degree, this discrepancy reflects the high interconnectivity of the signalling molecules involved in cell death. Therefore, while it is easy to tilt the balance toward cell death, the simultaneous inhibition of several signal transduction models may be required to reverse the tilted balance. This is undoubtedly tricky, since points of no return are hitherto poorly defined. Nonetheless, targeting cell death is and will be a powerful tool to treat and prevent many diseases, but much work is needed to devise the most efficient strategies (Galluzzi et al., 2018).

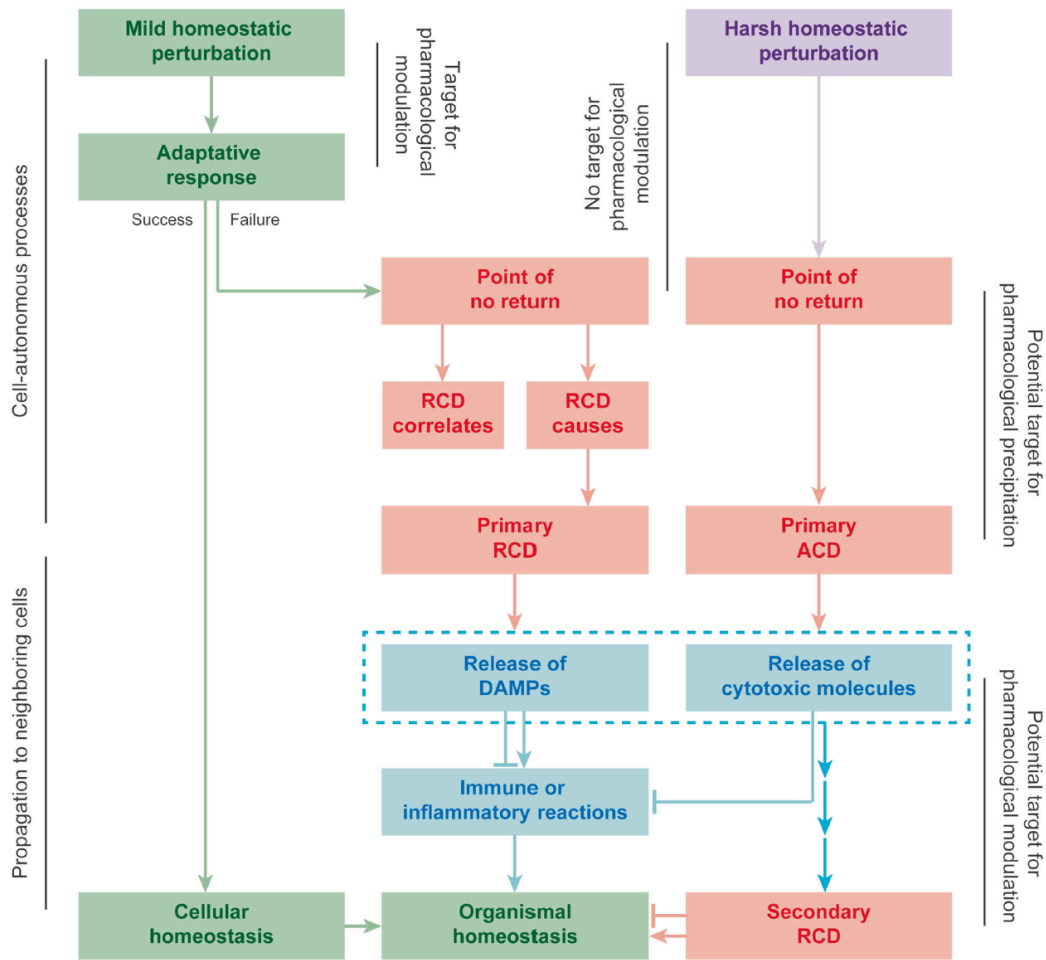


**Figure 1. 17: Causal vs. accessory aspects of cell death from a therapeutic perspective.**

Cells exposed to very harsh environmental conditions disassemble in a virtually instantaneous and uncontrollable manner, a process that is referred to as accidental cell death (ACD). Conversely, relatively mild perturbations of exogenous or endogenous origin promote adaptive stress responses aimed at the restoration of cellular homeostasis. If such responses fail, cells generally activate one or more of multiple, highly interconnected signal transduction modules that precipitate regulated cell death (RCD). ACD cannot be retarded by pharmacological or genetic interventions, and most (if not all) strategies conceived so far to block RCD in mammalian organisms fail to efficiently do so, at least in part owing to the elevated interconnectivity of the process. Conversely, some agents that de facto promote RCD by primarily targeting the underlying molecular machinery (rather than by targeting normal cellular functions) are already available for use in the clinic. The events that follow primary cell death—including a secondary wave of RCD in neighbouring cells established (directly or indirectly) by molecules released from the cells succumbing to the primary insult, as well as danger-associated molecular pattern (DAMP) signalling—may also be targets for pharmacological interventions. Finally, although altering quantitatively the percentage of cells succumbing to primary RCD remains challenging (especially when a hitherto poorly defined point-of-no-return of the process has been trespassed), favouring the use of specific signalling modules over others may have prominent effects on long-term disease outcomes. Reprinted from “Molecular mechanisms of cell death: recommendations of the Nomenclature Committee on Cell Death 2018” by L. Galluzzi and co-authors, 2020, *Cell Death & Differentiation*, 25, p.512. Copyright 2018 ADMC Associazione Differenziamento e Morte Cellulare.

### **1.5.6 SFN and cellular responses**

SFN can provoke a wide range of cellular responses, including all that have been mentioned and discussed in this section. SFN can increase ROS generation, cause mitochondrial dysfunction, activate ERS, damage DNA integrity, elevate autophagy, and trigger cell death. (Geng et al., 2017; Hac et al., 2019; H. Liu et al., 2017; Naumann et al., 2011, 2017; Negrette-Guzman, Huerta-Yepe, Tapia, & Pedraza-Chaverri, 2013; Sestili et al., 2010; D. Xiao, Powolny, Antosiewicz, Hahm, & Bommarreddy, 2009; Zou, Qu, Fang, Shi, & Ji, 2017). These have also been proposed to govern SFN-induced cytotoxicity, and oxidative stress appears to be the key mediator (Sestili & Fimognari, 2015). However, the information comes from diverse studies using different models, mostly cancer, and different SFN concentrations. No study has reported that one concentration of SFN can trigger all these events, or has elucidated a complete interplay and sequence of events. For example, in the lens, SFN was reported to induce ERS, autophagy and cell death in one study using human lens capsular bags and a human lens epithelial cell line (H. Liu et al., 2017), and found to trigger cell death via oxidative stress in a different study using mouse models and another human lens epithelial cell line (Chhunchha et al., 2019). Therefore, a study linking multiple processes is needed to provide important information to understand the pharmacological actions of SFN.

### **1.6 Background summary**

Cataract, a clouding of the lens, is a leading cause of blindness in the world; surgery is currently the only effective treatment. Unfortunately, a post-surgery complication known as PCO can cause approximately 5-20% of patients to lose their vision again (Wormstone et al., 2021). In this condition, remaining lens cells proliferate, invade the previously cell-free regions, and eventually disrupt the visual axis. An Nd:Yag laser can treat it but it is costly and has associated risks. It is accepted that prevention of PCO is preferable and, to this end, efforts have been

guided towards improving the design of IOLs (Eldred et al., 2019; Leydolt et al., 2020; Perez-Vives, 2018), routinely implanted during cataract surgery, to suppress PCO progression. Pharmacological approaches may also yield benefits, but currently, none are in clinical use (Nibourg et al., 2015; Wormstone et al., 2021). It is thus important and valuable to find an effective way to manage this condition.

The use of phytochemicals for therapeutic purposes is a growing area of medicine (Budisan et al., 2017; Houghton, 2019; Yoo, Kim, Nam, & Lee, 2018). SFN is one such molecule. SFN is an isothiocyanate derived from glucosinolates in cruciferous vegetables, such as broccoli and kale (Juge et al., 2007). This hormetic chemical displays contrasting properties depending upon concentration and induces a plethora of cellular events (H. Liu et al., 2013; Sestili & Fimognari, 2015). At low doses, SFN can trigger the activation of phase-II detoxification enzymes, increase antioxidant defence, decrease inflammatory responses and promote cell survival via the Nrf2-ARE pathway. High levels of SFN block cell proliferation and induce cell death. Owing to its multifaceted *in vivo* and *in vitro* effects, SFN has selectively been studied to treat cancer, metabolic disorders or inflammatory conditions (R. K. Davidson et al., 2013; Dinkova-Kostova & Kostov, 2012; Kyung et al., 2018; Vanduchova, Anzenbacher, & Anzenbacherova, 2019).

Recently, SFN has shown potential in preventing PCO (H. Liu et al., 2017). The authors demonstrated that when applied to human capsular bags, a model for PCO, high supranutritional SFN concentrations caused cell death to remaining cells and prevented opacification, making SFN a potential agent to manage PCO (H. Liu et al., 2017). To utilise all therapeutic potential of SFN for PCO and other disorders, first and foremost, it is important to understand the mechanisms that mediate SFN-induced cytotoxicity. Several studies have

shown the potential contribution of multiple mechanisms to SFN-induced cytotoxicity (Sestili & Fimognari, 2015), but none has offered a complete interplay and sequence of events. A study linking multiple cellular stress responses is necessary to address gaps in our knowledge and provide important mechanistic information to understand the pharmacological actions of SFN.

## **1.7 Aims and objectives**

This PhD thesis aimed to elucidate the mechanisms of SFN induced stress responses and death in non-cancer human experimental models using a human lens cell line and human lens epithelium. The lens affords a model system that is well placed to tease out key processes and mechanisms linking SFN treatment to cell death. The lens epithelium is a distinct population of cells that naturally grow in isolation and in the absence of vasculature. These traits, along with defined molecular characteristics, render lens cell and tissue cultures a tractable experimental system for the study of SFN. Previously, Liu et al (2017) reported that SFN increased ROS levels, therefore the hypothesis to be tested was that **ROS played a critical role in SFN-induced cytotoxicity**. To address the hypothesis, the study aimed to achieve the following objectives.

- 1) To expand the knowledge of SFN induced cytotoxicity in the human lens – **Chapter 3**.
- 2) To assess cellular benefits of ROS scavengers against cytotoxicity caused by SFN – **Chapter 4**.
- 3) To investigate the impacts of SFN on antioxidant defence systems – **Chapter 5**.
- 4) To evaluate cellular benefits of antioxidant enhancement against cytotoxicity caused by SFN – **Chapter 6**.
- 5) To construct a possible model illustrating the interplay between cellular responses induced by SFN that ultimately leads to death – **Chapter 7**.

# Chapter 2 Materials and Methods

---

## 2.1 Experimental models

### 2.1.1 Cell culture

Foetal human lens-124, FHL124, is a non-virally transformed cell line generated from human capsule-epithelial explants, and shares a 99.5% homology with the native lens epithelium in transcript profile (Wormstone et al 2004). FHL124 cells were routinely cultured at 35°C with 5% CO<sub>2</sub>, 95% air in Eagle's Minimum Essential Medium (EMEM) (Gibco, Paisley, UK) supplemented with 5% vol/vol foetal bovine serum – (FBS; Gibco, Paisley, UK) and 50 µg/mL gentamicin (Sigma-Aldrich, Dorset, UK).

Upon reaching 85 – 95% confluency, cells were passaged. The culture medium was aspirated and cells were washed once with warmed-up Dulbecco's phosphate-buffered saline (DPBS) (Sigma-Aldrich, Dorset, UK). Cells were then trypsinised with 0.05% trypsin in EMEM at room temperature for 2 minutes or until cells were detached from the base of the culture flask. The trypsin solution was neutralised with a double amount of EMEM supplemented with 5% FBS and a cell suspension was formed through several pipetting cycles. Cell number was counted using a haemocytometer while the cell suspension was centrifuged at 13 rpm for 5 minutes to obtain a cell pellet. The supernatant was removed and discarded while the cell pellet was re-suspended in a desired amount of EMEM supplemented with 5% FBS to be transferred to a new flask or to be seeded for specific experiments.

FHL124 cells were seeded onto 35 mm tissue-culture treated dishes (Corning, Corning, New York, USA) for protein and RNA extraction, 18 mm x 18 mm 0.08 mm glass coverslips (VWR, Leicestershire, UK) contained in 35 mm non-treated culture dishes (Corning, Corning, New York, USA) for immunocytochemistry or 96-well plates for several cell behavioural assays (Nunc, Rochester, New York, USA). Cells were maintained in EMEM with 5% FBS and 50 µg/mL gentamicin for 48 hours then replaced with serum-free EMEM with 50 µg/mL gentamicin 24 hours before the start of experimental conditions.

### **2.1.2 Human lens epithelium**

Donor human eye globes were obtained with informed consent and used following the tenets of the Declaration of Helsinki. Approval for the study and experimental protocols (NREC 04/Q0102/57 – IRAS D 293806) was granted by a national research ethics committee under the Health Research Authority (UK). The centre of the anterior capsule was punctured using an insulin needle, then an approximately 2.5 mm radial incision was made from the centre to the periphery to create a capsular flap. The flap was then pulled and lifted at its edge. A continuous curvilinear capsulorhexis was created by tugging the flap with surgical forceps. The entire capsulorhexis was then secured onto a non-treated 30 mm triple vent petri dish (Thermo Scientific, Basingstoke, UK) entomological pins and maintained in EMEM supplemented with 5% FBS and 50 µg/mL gentamicin.

## **2.2 Chemicals**

R-Sulforaphane (Enzo Life Sciences, Exeter, UK) was dissolved in sterile DMSO to achieve a stock concentration of 50 mM. N-acetyl L cysteine (Sigma-Aldrich, Dorset, UK) was dissolved in either normal EMEM or EMEM without phenol red (Sigma-Aldrich, Dorset, UK), depending on experimental requirements and filtered to reach a stock concentration of 100

mM. Sodium pyruvate (Sigma-Aldrich, Dorset, UK) was dissolved in sterile double distilled water to achieve a stock concentration of 1 M. L-Glutathione reduced (Sigma-Aldrich, Dorset, UK) was dissolved in PBS pH 6.5 and filtered to achieve a stock concentration of 100 mM.

## **2.3 Cell viability and death assays**

### **2.3.1 Cytotoxicity Lactate dehydrogenase (LDH) assay**

The Cytotoxicity Detection LDH kit (Roche, Mannheim, Germany) is a colourimetric assay for the quantification of cytotoxicity, based on the measurement of LDH activity. For FHL124 cells, cells were seeded at a density of 50,000 cells per culture dish. At the endpoint, 50 µl out of 1,500 µl cultured medium was sampled and transferred to a clear 96-well microtitre plate containing 150 µl EMEM medium per well. For lens epithelium, whole capsulorhexis samples were secured on dishes by entomological pins as described before. At the endpoint, 100 µl out of 1,000 µl cultured medium was sampled and transferred to a clear 96-well microtitre plate containing 100 µl EMEM medium per well.

A working solution was made by mixing the catalyst and the dye using a 1:45 ratio, then 100 µl of the working solution was added to each well. The whole plate was then covered in foil and incubated on a microtitre plate shaker at room temperature for 15 minutes, and absorbance at 490 nm was measured with a microplate reader FLUO star Omega (BMG LabTech, Bucks, UK) at 490 nm. Wells containing only 200 µl EMEM medium and the working solution served as background controls. For experiments involving N-acetyl L cysteine (NAC), 200 µl EMEM medium containing 1 mM NAC and the working solution was used to serve as background controls for samples containing NAC because the presence of NAC created a higher background value. Data were represented as a percentage change in absorbance at 490 nm from untreated cells.

### **2.3.2 Cell Viability assay**

FHL124 cells were seeded onto clear 96-well microtitre plates (Nunc, Rochester, New York, USA) at a density of 2,500 cells/well and cell viability was measured using the CellTiter-Glo Luminescent Assay (Promega, Southampton, UK). The kit determines the number of viable cells in culture based on quantitation of the ATP present, which is an indicator of metabolically active cells. CellTiter-Glo Buffer and Substrate were mixed 1:1 to make CellTiter-Glo reagent in advance and stored at -20°C. Upon the endpoint of experimental treatments, the cultured medium was aspirated and 100 µl of CellTiter-Glo reagent was added to each well. The whole plate was incubated at room temperature for 10 minutes. An amount of 70 µL of the cellular solution was transferred to a white opaque 96-well plate compatible with luminescence reading and the plate was immediately analysed for luminescence on a microplate reader FLUO star Omega (BMG LabTech, Bucks, UK). The number of viable cells in the culture is directly proportional to the absorbance intensity measured. Data were represented as a percentage change in luminescence reading from untreated cells.

### **2.3.3 Phase-contrast imaging**

FHL124 cells grown on 35 mm tissue-culture treated dishes (Corning, Corning, New York, USA) or human lens epithelium grown on non-treated 30 mm triple vent petri dishes (Thermo Scientific, Basingstoke, UK) were observed using a Nikon Ti2 inverted light microscope and phase-contrast images were obtained using a camera (DS-Qi2 Mono Digital Microscope Camera, Nikon)

## **2.4 Gene expression analysis by quantitative real-time Polymerase Chain Reaction (qRT-PCR)**

### **2.4.1 Total RNA extraction**

Total RNA was extracted from FHL124 cells (seeded at a density of 50,000 cells per culture dish) following the protocol of the ReliaPrep RNA Cell Miniprep System (Promega, Southampton, UK). All centrifuge steps were at 13,000 x g. In summary, cells were first washed with ice-cold, sterile DPBS (Thermo Fisher Scientific, Basingstoke, UK) then 250  $\mu$ L of Lysis buffer was added to cells. After several pipetting, cell lysates were collected into microcentrifuge tubes. An amount of 35  $\mu$ L of 100% Isopropanol was added to cells, followed by 5-second vortexing. The lysate was transferred to ReliaPrep™ Minicolumn and centrifuged for 30 seconds at room temperature. The Minicolumns were further added with 500  $\mu$ L of RNA Wash Solution and centrifuged for 30 seconds. After this, 30  $\mu$ L of DNase I incubation mix was added to each column, and the columns were incubated for 15 min at room temperature. Then 200  $\mu$ L of Column Wash Solution was added and the columns were centrifuged for 15 seconds. This was followed by two wash steps with 500  $\mu$ L and 300  $\mu$ L of RNA Wash Solution for 30 seconds and 2 minutes, respectively. RNA was finally eluted in 50  $\mu$ L Nuclease-Free Water after the columns were centrifuged for 1 minute and stored at -20°C or -80°C for short- or long-term storage, respectively.

### **2.4.2 Total RNA quality and quantity assessment**

RNA was quantified using a NanoDrop ND-1000 spectrophotometer (NanoDrop, Wilmington, Delaware, USA). An amount of 1  $\mu$ L sterile double distilled water was used to calibrate and also served as a blank. For each round of RNA extracted, a ratio of absorbance at 260/280 nm

ranged from 1.9 – 2.2 was accepted, which was used for quality control purposes. Any samples with lower ratios were discarded.

### **2.4.3 cDNA synthesis**

cDNA was generated using the PCR Biosystems Kit (PCR Biosystems, London, UK). Each 10  $\mu$ L reaction had 2  $\mu$ L 5X mix, 0.5  $\mu$ L RTase (20X), 200ng RNA with corresponding volume and RNase-free H<sub>2</sub>O. PCR conditions were 42°C for 30 minutes followed by 85°C for 10 minutes using a PTC-200 Gradient Thermal Cycler (Marshall Scientific, Hampton, New Hampshire, USA). The obtained cDNA was diluted in RNase-free H<sub>2</sub>O to achieve a concentration of 0.5 ng/ $\mu$ L and stored at -20°C ready for further applications.

### **2.4.4 TaqMan qRT-PCR**

qRT-PCR reactions were carried out using an RT-PCR machine (ABI7700, Applied Biosystems, Thermo Fisher Scientific, Basingstoke, UK). Assuming 100% efficiency in the RT reactions, either 1 or 5 ng cDNA was used to detect the expression of 18S gene and other genes, respectively. Reagent-based assays (TaqMan Universal PCR Master Mix, PCR Biosystem) containing all PCR reagents were employed according to the manufacturer's instructions and reaction solutions were added to MicroAmp Fast Optical 96 well (Applied Biosystems, Thermo Fisher Scientific, Basingstoke, UK). Each reaction was performed in 25  $\mu$ L and contained cDNA, primers (**Table 2. 1**) and predesigned Taqman probes (Life Technologies, Carlsbad, California, USA). The conditions for the PCR reaction were; 2 minutes at 50°C, 10 minutes at 95°C and then 40 cycles, each of which consists of 15 seconds at 95°C and 1 minute at 60°C. The cycle number at which amplification entered the exponential phase (raw data cycle threshold [Ct]) was determined and this number was used as an indicator

for the amount of target RNA in each sample. Relative quantification is expressed as  $2^{-\Delta Ct}$  where  $\Delta Ct$  is  $Ct(\text{gene of interest}) - Ct(18S\ rRNA)$ .

**Table 2. 1: Details of primers used in the study.**

Gene	Encoded protein	Ref seq	Taqman primer
<i>DDIT3</i>	CHOP	NM_001195053	Hs00358796_g1
<i>ERN1</i>	IRE1	NM_001433	Hs00980095_m1
<i>HSPA5</i>	BiP	NM_004836.3	Hs99999174_m1

## 2.5 Western blot analysis

### 2.5.1 Protein extraction

#### 2.5.1.1 FHL124 cells

Cells were seeded at a density of 100,000 cells per 35 mm culture dish (Corning, Corning, New York, USA). At the end of the experiment, the medium was aspirated and cells were washed once with ice-cold DPBS (Thermo Fisher Scientific, Basingstoke, UK). The lysis buffer is made of mammalian protein extraction reagent (M-PER™) buffer (Thermo Fisher Scientific, Basingstoke, UK) supplemented with phosphatase and protease inhibitors and 0.5 M Ethylenediaminetetraacetic acid (EDTA) (Thermo Fisher Scientific, Basingstoke, UK) at 10  $\mu$ l/mL immediately before use. DPBS was aspirated and cells were lysed in a desired amount of lysis buffer by 10 – 15 pipetting cycles. Cell lysates were then collected and centrifuged at 13,000 rpm for 10 minutes at 4°C. The soluble fractions were transferred to new tubes and stored at -20°C while pellets of cell debris were discarded.

#### 2.5.1.2 Human lens epithelium

Match-paired whole capsulorhexis samples were used. Before extraction, the working M-PER™ lysis buffer was prepared in a similar way as for FHL124 cells and 70  $\mu$ l of it was added into different 0.5 mL Eppendorf tubes. These tubes were left on ice. At the end of the

experiment, the culture medium of capsulorhexis was aspirated and capsulorhexis was washed once with ice-cold DPBS (Thermo Fisher Scientific, Basingstoke, UK). Pins were removed using forceps and capsulorhexis was transferred to 0.5 mL Eppendorf tubes containing the working M-PER<sup>TM</sup> lysis buffer. Capsulorhexis samples were briefly vortexed and centrifuged at 13,000 rpm for 15 seconds at 4°C. Samples were left on ice for 10 minutes with a brief vortex every 5 minutes. Then samples were centrifuged at 13,000 rpm for 10 minutes at 4°C. The soluble fractions were transferred to new tubes and stored at -20°C while remaining capsulorhexis samples were discarded.

### **2.5.2 Protein quantification**

The bicinchoninic acid BCA assay (Pierce, Thermo Fisher Scientific, Basingstoke, UK) was used to determine the total protein concentration. Bovine serum albumin (BSA) (Sigma-Aldrich, Dorset, UK) was dissolved in MPER lysis to create a range of protein standards (0 – 1,000 µg/mL). A working solution in each well of a 96 well plate consisted of a constant volume of protein standard and lysate samples (10 µL for FHL124 cell experiments and 5 µL for capsulorhexis experiments), 40 µL of distilled water and 200 µL of the two supplied BCA reagents in a 50:1 ratio. All standards were done in triplicate, and all samples were done in duplicate. The plate was protected from light, placed on a microtitre plate shaker for 1 minute before a 1-hour incubation at 37°C. The absorbance at 550 nm was measured by a microplate reader FLUO star Omega (BMG LabTech, Bucks, UK). Values of protein standards were used to construct a standard curve to determine the concentration of the samples.

### **2.5.3 Sample preparation**

A loading buffer was made of sample buffer and  $\beta$ -mercaptoethanol at the ratio of 7:1. A sample buffer (pH 6.8) consisted of 7.6% (wt/vol) Tris, 2% (wt/vol) Sodium dodecyl sulphate SDS, 0.01% (wt/vol) bromophenol blue and 10% (wt/vol) glycerol. Based on the concentrations obtained from the BCA assay, samples were diluted further in M-PER™ lysis to achieve equal amounts across all samples. Then loading buffer was added to each sample at the ratio of 1:4 (vol/vol), and the whole solution was heated at 100°C for 5 minutes to allow complete protein denaturation before Sodium dodecyl-sulfate polyacrylamide gel electrophoresis (SDS-PAGE).

### **2.5.4 SDS-PAGE gel electrophoresis**

SDS-PAGE gels were prepared as follows. The running gel layer was prepared at 10% or 12% acrylamide by mixing distilled water, 30% acrylamide (Bio-Rad Laboratories, Hempstead, UK), 1.5 Tris (pH 8.8), 10% SDS (Thermo Fisher Scientific, Basingstoke, UK), 10% ammonium persulphate (APS Sigma-Aldrich, Dorset, UK), and tetramethylethylenediamine (TEMED; Sigma-Aldrich, Dorset, UK). The stacking gel was prepared at 5% acrylamide by mixing distilled water, 30% acrylamide, 1.5 Tris (pH 6.8), 10% SDS, 10% APS, and TEMED. Bio-Rad Precision Plus protein Dual Colour Standards (Bio-Rad Laboratories, Hempstead, UK) and denatured protein samples were then loaded onto SDS-PAGE gels for electrophoresis and the gel was run in a running buffer (3% wt/vol Tris, 15% wt/vol glycine, and 1.2% vol/vol 10% SDS).

### **2.5.5 Protein transfer and immunoblotting**

Proteins were transferred to a mini 0.2  $\mu$ m polyvinylidene fluoride (PVDF) membrane using a Transblot Turbo transfer cell (Bio-Rad Laboratories, Hempstead, UK). In detail, after gel

electrophoresis, all components were assembled as shown in the image below. The whole cassette was then placed into the instrument and the transfer ran at the default “MIXED MW” function (7 minutes at a constant voltage up to 25 V).

After transfer, blotting membranes were blocked with PBS containing 3% wt/vol BSA and 0.1% vol/vol Tween-20 for 1 hour at room temperature with gentle agitation. After that, the blocking solution was removed and blotting membranes were hybridised with the primary antibody diluted in the blocking solution (details provided in **Table 2. 2**) at 4°C overnight. Membranes were washed 4 times in 0.1% vol/vol Tween/PBS (PBST) at 7 minutes intervals with gentle agitation before a 1-hour incubation at room temperature with secondary antibody conjugated with horseradish peroxidase (GE Healthcare, Little Chalfont, UK). Membranes were then washed 5 times in PBST at 7 minutes intervals as before.

Proteins were detected using the Clarity Western ECL Substrate (Bio-Rad Laboratories, Hempstead, UK) and developed by Chemidoc XRS+ (Bio-Rad Laboratories, Hempstead, UK). Membranes were drained of excess PBST before loading onto the Chemidoc chamber. Clarity Peroxide Reagent and Clarity Enhancer Reagent were mixed at the ratio of 1:1 and evenly applied onto the membrane and images of the membranes were captured and analysed by Image-J.  $\beta$ -Actin was used as a loading control and for band intensity normalisation because this protein is ubiquitously expressed in eukaryotic cell and is mostly not affected by cellular treatments, except for samples from *Schistosoma japonicum* infection (B. Zhang et al., 2019).

**Table 2. 2: Antibodies used in the experiment and corresponding % SDS-polyacrylamide gel.**

Primary Ab (Species)	Manufacturer (Code)	% SDS-polyacrylamide gel
LC3 (Rabbit)	Sigma-Aldrich, Dorset, UK (L8918)	12%
Phosphor-eIF2 $\alpha$ (P-eIF2 $\alpha$ ) (Rabbit)	Cell Signalling Technology, Massachusetts, US (3398)	10%
XBP-1 (Rabbit)	Abcam, Cambridge, UK (ab220783)	10%
Glutathione reductase (Rabbit)	Abcam, Cambridge, UK (ab124995)	10%
$\beta$ -Actin (Rabbit)	Cell Signalling Technology, Massachusetts, US (4970)	12% or 10%

## 2.6 ATF6 reporter assay

FHL124 cells were seeded onto clear 96-well microtitre plates (Corning, Corning, New York, USA) at a density of 5,000 cells/well. The ATF6 reporter assay was modified based on the method described by Wang and co-authors (L. Wang et al., 2012). Before transfection, cells were washed with 100  $\mu$ L Opti-MEM<sup>TM</sup> I reduced serum medium (Gibco, Paisley, UK) and supplemented with 80  $\mu$ L Opti-MEM. Signal ATF6 Reporter (Qiagen, Crawley, UK) and Oligofectamine<sup>TM</sup>-transfection reagent (Invitrogen, Paisley, Scotland, UK) were used for the transfection. For each well, 1  $\mu$ L of the construct at 100 ng/ $\mu$ L (Reporter, Negative control or Positive control) was diluted in 16  $\mu$ L of Opti-MEM<sup>TM</sup> I reduced serum medium (Gibco, Paisley, UK), while the transfection solution was made up of 0.5  $\mu$ L Oligofectamin and 2.5  $\mu$ L Opti-MEM. These two solutions were left at room temperature for 5 minutes before being mixed together to achieve a total volume of 20  $\mu$ L for each well, which was incubated at room temperature for 20 minutes before being added to cells. Each well by then had a total volume of 100  $\mu$ L. After a 4-hour incubation, a further 50  $\mu$ L of Opti-MEM was added to each well and the microtitre plates were maintained for another 20 hours at 35°C in a 5% CO<sub>2</sub> incubator before experimental conditions. At the end of the treatment, the culture medium was gently

aspirated and briefly rinsed with 100  $\mu$ l DPBS (Thermo Fisher Scientific, Basingstoke, UK). DPBS was removed and cells were lysed using 25  $\mu$ L 1 $\times$  passive lysis buffer, part of the Dual-Luciferase reporter assay kit (Promega, Southampton, UK), for 15 minutes at room temperature on a microtitre plate shaker. An amount of 20  $\mu$ L of lysed cells was transferred to a white opaque 96-well plate and 100  $\mu$ L of firefly luciferase assay substrate solution (Promega, Southampton, UK) was added to each well and the plate was immediately analysed for luminescence on a Fluostar Omega plate reader (BMG LabTech, Bucks, UK). After quantifying the firefly luminescence, this reaction was quenched, and the *Renilla* luciferase reaction was simultaneously initiated by adding 100  $\mu$ l Stop & GloR Reagent. *Renilla* luciferase luminescence was detected using a Fluostar Omega microplate reader (BMG LabTech, Bucks, UK) spectrophotometer plate reader and the Stop & GloR reagent served as a transfection control. The data were normalised by dividing the firefly (*Photinus pyralis*) luciferase result by the *Renilla* (*Renilla reniformis*) luciferase data.

## 2.7 $\gamma$ -H2AX Immunocytochemistry

FHL124 cells were seeded onto coverslips at a density of 5,000 cells. After the end of experimental conditions, coverslips were fixed with 4% vol/vol formaldehyde (Sigma-Aldrich, Dorset, UK) in PBS for 20 minutes. Three 5-minute washes in PBS were performed before blocking for nonspecific binding sites with 3% normal donkey serum in 1% vol/vol BSA/PBS for 1 hour at 37°C.  $\gamma$ -H2AX (Cell Signalling Technology, Massachusetts, US) was diluted 1:200 in 1% wt/vol BSA/PBS and applied to cells for 2 hours at 37°C. The incubation was followed by another three PBS washes. Then cells were added with secondary antibody AlexaFluor 488-conjugated donkey anti-rabbit (Invitrogen, Paisley, Scotland, UK) at 1:200 dilution in 1% BSA/PBS for 1 hour, protected from light at 37°C in a humidified atmosphere. Coverslips were then counterstained with 6-diamidino-2-phenylindole (DAPI; Sigma-Aldrich,

Dorset, UK) for nucleus staining at 1:200 in 1% vol/vol BSA/PBS for 10 minutes at room temperature. After three washes, samples were mounted on 0.8 – 1.0 mm glass microscope slides (Thermo Fisher Scientific, Basingstoke, UK) with Hydro mount (National Diagnostics, Scientific Laboratories Supplies, Nottingham, UK). Samples were viewed with fluorescence microscopy, widefield microscope Zeiss Axipolar 2ie. Image quantification was performed using ImageJ 1.45 image analysis software (<http://imagej.nih.gov/ij/>; provided in the public domain by the National Institutes of Health, Bethesda, MD, USA).

## **2.8 Mitochondrial network analysis**

### **2.8.1 MitoTracker Red staining**

FHL124 cells were seeded onto coverslips at 2,000 cells. On the day of the experiment, cells were treated with appropriate conditions. At the endpoint, the culture medium was aspirated and cells were stained with MitoTracker Red CMXRos (Invitrogen, Paisley, Scotland, UK). This was achieved by incubating the cells with the serum-free EMEM without phenol red containing 100 nM MitoTracker Red, which had been dissolved in DMSO, for 15 minutes in the incubator. After that, cells were washed three times using pre-warmed EMEM medium without phenol red. Cells were then fixed with 4% vol/vol formaldehyde (Sigma-Aldrich, Dorset, UK) in PBS for 20 minutes, followed by three 5-minute washes in PBS. If the confocal microscope Zeiss LMS510 was going to be used, cells did not undergo DAPI staining because the machine could not capture the DAPI signal. If the confocal microscope Zeiss LMS980 with Airyscan 2 was going to be used, cells underwent DAPI staining as follows. Cells on coverslips were stained with DAPI (Sigma-Aldrich, Dorset, UK) at 1:200 in 1% vol/vol BSA/PBS for 10 minutes at room temperature, followed by three 5-minute washes in PBS. Samples were subsequently mounted on 0.8 – 1.0 mm glass microscope slides (Thermo Fisher Scientific, Basingstoke, UK) with Hydro mount (National Diagnostics, Scientific Laboratories Supplies,

Nottingham, UK). Cells were individually imaged with confocal microscopes Zeiss LMS980 with Airyscan 2 or Zeiss LSM510 META with a 63x with oil objective. For each experimental condition, 10-20 cells were captured and analysed.

## **2.8.2 Mitochondrial network analysis**

After image acquisition, the size of mitochondrial networks was analysed using ImageJ 1.45 image analysis software (<http://imagej.nih.gov/ij/>; provided in the public domain by the National Institutes of Health, Bethesda, MD, USA). The analysis procedure was modified based on a paper by the Stuart group (Valente, Maddelena, Robb, Moradi, & Stuart, 2017).

The analysis of mitochondrial networks requires sharp, high contrast images exhibiting minimal noise; however, images obtained confocal microscopy are often not sharp enough due to the diffraction effects of the system, especially considering the small size of mitochondria. To enhance the image quality prior to analysis, image pre-processing was essential. Unsharp masking helped enhance the sharpness of an image, while contrast limited adaptive histogram equalization (CLAHE) helped adjust the pixel intensities and inhibit over-amplification of noise at the same time. The setting for CLAHE was 127 pixel block size, 256 histogram bins, and a maximum slope of 3 by default. Unsharp masking and CLAHE, however, could greatly amplify salt and pepper noise that is usually found in fluorescent images. The last step of pre-processing, median filtering, helped reduce or eliminate this type of noise. The filter was applied to a specified radius of three pixels.

For analysis, the pre-processed image was converted to binary, and then skeletonised. The skeletonised networks represented the features in the original image using a wireframe of lines one pixel wide. The skeletonised networks were then analysed using Analyze Skeleton, which

would measure the length of each branch and the number of branches in each skeletonised feature. The mitochondrial network size was calculated as follows:

*Mitochondrial network size* =  $\sum \text{Branches} \times \text{Averaged branch length}$ . The

workflow is summarized below in and the representative preparation of an image is shown in

**Figure 2. 2.**

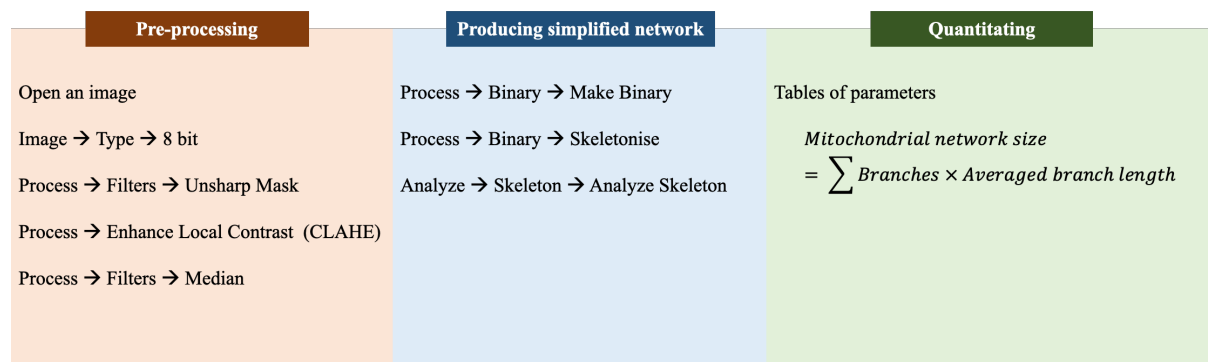


**Figure 2. 1: The workflow of mitochondrial network quantification.**

Images are pre-processed to improve quality prior to binarizing and skeletonizing. Descriptive parameters are calculated from the skeletonized image.

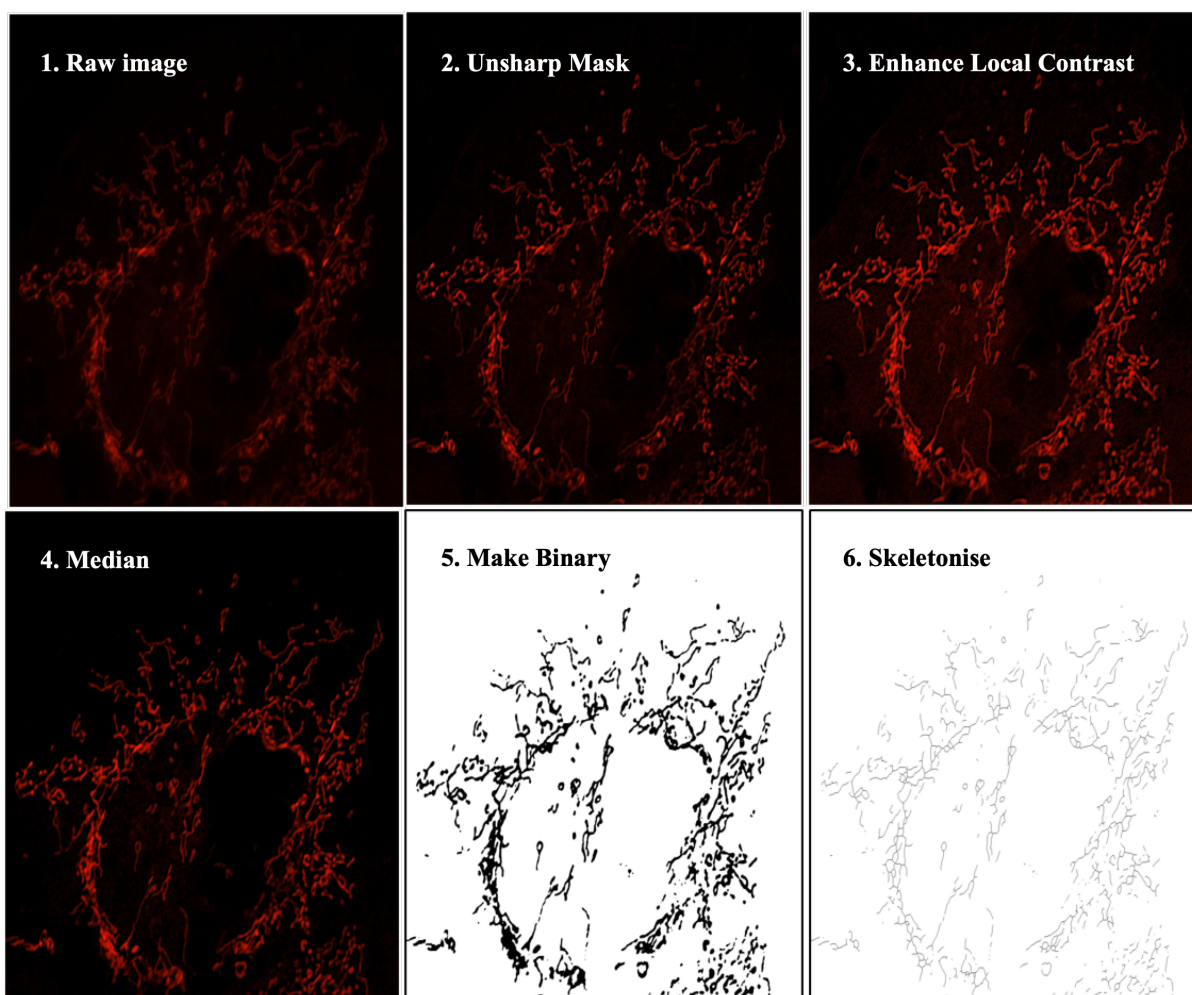


**Figure 2. 2: The representative preparation of an image.**

The image was pre-processed from step 2 – 4, and then made binary in step 5 and skeletonised in step 6. The skeleton was ready for quantitation.

## **2.9 Mitochondria GFP tagged transfection – GFP labelling**

### **mitochondria**

FHL124 cells were seeded onto 35 mm tissue-culture treated culture dishes (Corning, Corning, New York, USA) until 50% confluency in 5% FBS EMEM medium. Before the transfection, cells were washed once with pre-warmed DPBS and then maintained in 900 µl Opti-MEM (Gibco, Paisley, UK). Transient transfection was performed by using Viafect™ transfection reagent (Promega, Southampton, UK), and pAcGFP-Mito plasmid DNA (Takara Bio, Saint-Germain-en-Laye, France) at a 6:1 reagent to DNA ratio following the manufacturer's

instructions. Opti-MEM was used to achieve a transfection mix of a volume of 100  $\mu$ L. After mixing, the transfection mix was incubated at room temperature for 10 minutes before being added to cells. The culture dishes were gently shaken for mixing and cells were incubated as usual. After 24 hours, the transfected cells were placed into 5% vol/vol FBS EMEM with 50  $\mu$ g/mL gentamicin and maintained as normal FHL124 cells. When cells reached confluency, routine cell splitting and cultures were conducted to transfer cells from 35 mm culture dishes to T25 flasks and then T75 flasks for higher yield and downstream applications.

## **2.10 Live cell imaging of mitochondrial networks**

Transfected FHL124 cells with pAcGFP-Mito were seeded onto each chamber of a 4-chamber 35 mm glass-bottom dish with 20 mm microwell (Cellvis, Mountain View, California, USA) at a density of 2,000 cells/chamber. On the day of the experiment, cells were stained with MitoTracker Red CMXRos (Invitrogen, Paisley, Scotland, UK) following the protocol above. After MitoTracker Red was removed, cells were maintained in a serum-free EMEM medium without phenol red and transported to the imaging room. The Zeiss Observer 7 microscope was used for live imaging. The microscope stage was maintained at 35°C with 5% CO<sub>2</sub>, 95% air during imaging. Cells were viewed with a 63x with oil objective. After several locations were chosen and saved, experimental conditions were applied to appropriate chambers of the dish. The imaging procedure started immediately and images were taken every 7.5 minutes. The focus was manually adjusted if the focus shifted when the microscope moved across different chambers.

## **2.11 Mitochondrial membrane potential**

FHL124 cells were seeded onto black plate clear bottom 96-well microtitre plates (Perkin Elmer, Beaconsfield, UK) at a density of 5,000 cells/well. Mitochondrial membrane potential

was assessed using the tetramethylrhodamine ethyl ester (TMRE) Mitochondrial Membrane Potential Assay kit (Abcam, Cambridge, UK). TMRE is a cell-permeant, positively-charged, red-orange dye that readily accumulates in active mitochondria because of their relative negative charge. The accumulation of TMRE in mitochondria depends on the mitochondrial membrane potential. Depolarised or inactive mitochondria have decreased mitochondrial membrane potential and fail to sequester TMRE, hence, high TMRE fluorescent signals mean high potentials. FCCP was used as a positive control, following the manufacturer's instructions. At the end of the experiments, the medium was aspirated and incubated with 100  $\mu$ L 400 nM TMRE in serum-free EMEM for 25 minutes in the culture incubator. Then TMRE solution was aspirated, cells were washed once with 100  $\mu$ L 0.2% wt/vol BSA/PBS and left in 100  $\mu$ L new 0.2% wt/vol BSA/PBS ready for measurement. The signal was measured with a microplate reader BMG Labtech Fluostar Omega (BMG LabTech, Bucks, UK), with excitation at 549 nm and emission at 5757 nm for every 3 minutes for 15 minutes. Peak signals were chosen for analysis.

## **2.12 GSH/GSSG assay**

### **2.12.1 FHL124 cells**

FHL124 cells were seeded onto clear 96-well microtitre plates (Corning, Corning, New York, USA) at a density of 5,000 cells/well. Cell lysates were analysed for glutathione using the GSH/GSSG-Glo<sup>TM</sup> assay (Promega, Southampton, UK). Before exposure to the experimental conditions, cells were placed into EMEM without phenol red (Sigma-Aldrich, Dorset, UK) as instructed by the manufacturer to eliminate background signals. At the end of the experiment, the cell medium was removed and 50  $\mu$ L of Total Glutathione Lysis or Oxidised Glutathione Lysis was added to appropriate wells and the plate was left at room temperature for 5 minutes on a plate shaker. Then 50  $\mu$ L Luciferin Generation reagent was added to each well and the

plate was further incubated for 30 minutes. This was followed by the addition of 100  $\mu$ L of Luciferin Detection reagent per well and a further 15-minute incubation. In the end, 180  $\mu$ L of the total volume in each well was transferred to a white opaque luminometer-compatible 96-well plate. The luminescent signal was measured by a BMG Labtech Fluostar Omega (BMG LabTech, Bucks, UK) and the ratio of GSH/GSSG was calculated as:

$$\frac{(\text{Net total glutathione RLU} - \text{Net GSSG RLU})}{(\text{Net GSSG RLU})} \times 2.$$

### **2.12.2 Human lens epithelium**

Match-paired halves of capsulorhexis samples were used. Before exposure to the experimental conditions, capsulorhexis samples were placed into EMEM without phenol red (Sigma-Aldrich, Dorset, UK). Two halves of capsulorhexis from the same eye would have the same treatment, and would have a different treatment from the other two halves from the other eye. At the end of the experiment, the cell medium was removed, and capsulorhexis samples were transferred to 0.5 mL Eppendorf tubes. For each pair of capsulorhexis from the same eye, one half would be treated with 50  $\mu$ L of Total Glutathione Lysis and the other with Oxidised Glutathione Lysis. The tubes containing capsulorhexis in lysis buffer were briefly vortex and centrifuged at 13,000 rpm for 30 seconds at room temperature. Tubes were then placed on the rack and other solutions were subsequently added in the same order as for FHL124 cells. At the end of the final incubation, the tubes were centrifuged at 13,000 rpm for 1 minute at room temperature and 180  $\mu$ L of the total volume in each tube was transferred to a white opaque luminometer-compatible 96-well plate. The signal was measured and analysed in the same way as for FHL124 cells.

## 2.13 Glutathione reductase activity

FHL124 cells were seeded onto 35 mm treated culture dishes (Corning, Corning, New York, USA) until 95% confluency. Glutathione reductase (GR) activity was measured using the GR assay kit (Abcam, Cambridge, UK). At the end of the experiment, cells were washed once with cold DPBS, and 300  $\mu$ L of assay buffer was added. Cells were scraped using rubber policemen (Thermo Fisher Scientific, Basingstoke, UK) and the mix was collected into 1.5 mL Eppendorf tubes (Thermo Fisher Scientific, Basingstoke, UK). The mix was then homogenised on ice using a 2 mL Dounce homogeniser (Abcam, Cambridge, UK) with 50 strokes for each sample. Efficient lysis was confirmed by viewing a drop of the lysate on a haemocytometer: no whole cells was the indicator. The lysate was transferred to a new 1.5 mL Eppendorf tube and centrifuged at 13,000 rpm for 15 minutes at 4°C. The supernatant was collected and stored at -80°C. The BCA assay was used to measure the concentration of the supernatant, and the same protein amount (20  $\mu$ g) was used for all the samples. The GR activity was measured following the manufacturer's instructions. Standard samples were created by mixing TNB with assay buffer to get 0, 5, 10, 20, 30 and 40 nmol TNB/well, and 100  $\mu$ L of each standard was added to a well of a clear 96-well plate in duplicate. The standards were measured by a microplate reader at 405 nm and the values were obtained to create a standard curve for calculation. On the other hand, the supernatant was treated and mixed with 5  $\mu$ L 3% H<sub>2</sub>O<sub>2</sub>, and incubated at 25°C for 5 minutes. An amount of 5  $\mu$ L catalase was added to the mix and the whole solution was incubated at 25°C for further 5 minutes. An amount of 50  $\mu$ L of each sample was transferred into a well of the same 96-well plate. The positive control well consisted of 10  $\mu$ L GR and 40  $\mu$ L assay buffer. Then 50  $\mu$ L reaction mix was added to each well; each reaction mix contained 40  $\mu$ L assay buffer, 2  $\mu$ L DTNB solution, 2  $\mu$ L NADPH-GNERAT<sup>TM</sup> solution and 6  $\mu$ L GSSG solution. The whole plate was briefly placed on a shaker and the OD<sub>405nm</sub> was quickly measured as T<sub>1</sub> in a microplate reader BMG Labtech Fluostar Omega (BMG LabTech,

Bucks, UK). After a 30-minute incubation at 25°C, the second reading of the OD<sub>405nm</sub> was taken as T<sub>2</sub>. The data analysis was conducted following the manufacturer's instructions.

## **2.14 SFN metabolites analysis**

### **2.14.1 Metabolite extraction**

FHL124 cells were seeded onto 100 mm culture dishes until 95% confluency in 10 mL medium. At the end of the experiment, 1 mL of the cultured media was transferred into a 1.5 mL Eppendorf tube containing 100 µL 3 mM perchloric acid (Sigma-Aldrich, Dorset, UK), and the mixture was kept on ice for 10 minutes and then centrifuged at 13,000 x g at 4°C for 10 minutes; the supernatant was collected and stored at -80°C. The remaining cultured medium was aspirated and cells were washed twice with cold 0.9 % sodium chloride (Sigma-Aldrich, Dorset, UK). Cells were then trypsinised with 0.05 % Trypsin/EDTA following the laboratory's standard procedure and counted using a haemocytometer. Next, the solutions were collected into 25 mL Sterilin tubes (Thermo Scientific, Basingstoke, UK) and were centrifuged at 1,200 x g at room temperature for 10 minutes. The supernatant was removed and the pellets were resuspended in pre-warmed 10 mL 0.9 % sodium chloride, and the solutions were centrifuged again at 1,200 x g at room temperature for another 10 minutes. The supernatant was removed and the pellets were resuspended in cold 0.5 mL 0.3 mM perchloric acid. The solutions were kept on ice for 10 minutes. After that, the solutions were transferred to 1.5 mL microcentrifuge tubes and centrifuged at 13,000 x g at 4°C for 10 minutes. The supernatant was collected and stored at -80°C for further analysis.

### **2.14.2 Mass spectrometry analysis**

SFN and its conjugates SFN-cysteine (SFN-Cys), SFN-glutathione (SFN-GSH), SFN-cysteine-glycine (SFN-Cys-Gly) and SFN-N-acetyl-cysteine (SFN-NAC) were measured in

cells using a validated LC-MS mass spectrometer (LC-MS/MS) method (Janobi et al., 2006). A 5-point, a calibration curve was generated by twofold serial dilution of standards (SFN, SFN-Cys, SFN-GSH, SFN-NAC and SFN-Cys-Gly) in MilliQ pore water for cells and EMEM media for media. The starting concentration of the SFN stock was 50  $\mu$ M and the starting concentration of the isothiocyanate standards is also 50  $\mu$ M. SFN and its metabolites were quantified using an Agilent 6490 triple-quad LC-MS/MS (Agilent technologies) with a HPLC PhenomenexR Luna 3u C18 (2) (100A, 100 x 2.1 mm) column with a PhenomenexR C18 100A column guard. The system comprised a degasser, binary pump, column oven, cooled autosampler, diode array detector and a 6490 MS. The LC-MS/MS was set on a flow rate of 0.3 mL/minute. The column temperature and autosampler were maintained at 40°C and 4°C respectively. Samples were injected at 5  $\mu$ l, 'system suitability' was injected at 1  $\mu$ l, and a blank was injected at 20  $\mu$ l. Separation of metabolites was carried out with 0.1% ammonium acetate in Milli Q water plus 0.1 % acetic acid (mobile phase A, pH=4) and 0.1% acetic acid in acetonitrile (mobile phase B). The LC eluent flow was sprayed into the mass spectrometer interface without splitting. Sulforaphane and conjugates were monitored using mass spectrometry Multiple Reaction Monitoring mode in positive polarity with an electrospray ionisation source. The source parameters were: gas temperature of 200°C with a gas flow of 12 L/minute, a sheath gas temperature of 400°C with a sheath gas flow of 12 L/minute, a nebuliser pressure of 60 psi and a capillary voltage of 4000 V. Microsoft Excel was used for further data processing.

## **2.15 Statistical analysis**

### **2.15.1 Independent Student's *t*-test**

An independent Student's *t*-test analysis compares the means of two independent groups to determine whether there is statistical evidence that the associated means are significantly

different (Kent State University Libraries, 2017b). Therefore, it was performed using Microsoft Excel software (Excel, Microsoft, Redmond, WA, USA) to determine any statistical difference between two experimental conditions between two cell populations treated with two different conditions. A  $P$  value  $\leq 0.05$  was considered significant.

### **2.15.2 Paired Student's *t*-test**

A paired Student's *t*-test analysis compares the means of two measurements taken from the same individual, object or related units (Kent State University Libraries, 2017a). Therefore, it was performed using Microsoft Excel software (Excel, Microsoft, Redmond, WA, USA) to determine any statistical difference between two experimental conditions on epithelium tissues derived from the same donor. A  $P$  value  $\leq 0.05$  was considered significant.

### **2.15.3 One-way analysis of variance (ANOVA)**

One-way ANOVA compares the means of two or more independent groups to determine whether there is statistical evidence that the associated population means are significantly different (Kent State University Libraries, 2017c). As a parametric test, ANOVA usually has more statistical power than its equivalent nonparametric test, the Kruskal-Wallis test by ranks, meaning that it is more likely to detect a significant effect when one truly exists (Bremer & Doerge, 2010). Therefore, ANOVA tests were preferred to assess statistical differences of various experimental conditions, which were all  $\geq 3$ , in this work. All experimental groups also met the requirements of a parametric test, such as homogeneity of variances – same sample size, no outliers, random sample of data, independence of observation, although no test for the normality (a requirement for a parametric test) was conducted.

To assess multiple groups when all or many pairwise comparisons were of interest, one-way ANOVA with Tukey's post hoc analysis was used (SPSS 16.0, SPSS Inc., Chicago, IL, USA), for example, in experiments involving different combinations of chemical treatments. On the other hand, to assess all groups compared against the control group, One-way ANOVA with Dunnett's post hoc analysis (SPSS 16.0) was used, for example, in time-response or dose-response experiments. A  $P$  value  $\leq 0.05$  was considered significant.

# Chapter 3 Cellular Responses to Sulforaphane

---

## 3.1 Introduction

Cataract remains the leading cause of blindness around the world, and currently the only effective treatment for cataract is surgical removal. However, patients may experience loss of vision again due to a secondary cataract known as PCO. This condition manifests when residual lens epithelial cells proliferate, differentiate, and migrate after surgery. These cells invade previously cell-free areas and obstruct the visual axis. The Nd-Yag laser treatment can be used to ablate these cell populations, but it is expensive and has associated risks, such as retinal detachment, macular oedema, or corneal oedema. Consequently, there is a strong demand for effective preventative measures and therapies. SFN is a dietary ICT derived from a precursor – glucoraphanin, which is found in cruciferous vegetables of the genus *Brassica*. Some vegetables belonging to this genus are cauliflower, kale and broccoli, with broccoli being the major source of glucoraphanin, hence SFN. Liu and co-authors demonstrated SFN as a potential agent to manage PCO by showing that when applied to an *in vitro* model for PCO using human capsular bags, high supranutritional SFN concentrations caused cell death to remaining cells and prevented opacification (H. Liu et al., 2017). The authors further illustrated that SFN increased gene and protein levels of ERS markers, triggered MAPK-dependent autophagy and increased ROS levels. Additionally, other authors have also reported the effects of SFN on other cellular compartments, such as mitochondria and the genome.

Mitochondria are widely known as a ‘powerhouse’ for cells, but these double-membrane organelles do more than that (Lane & Martin, 2010). Over the past two decades, researchers

have unveiled the surprising complexity of mitochondrial activities and linked mitochondrial energetics to various cellular aspects, such as protein biogenesis, metabolic pathways, cellular signalling circuitry, stress responses and apoptosis (Pfanner, Warscheid, & Wiedemann, 2019). It may be unsurprising that mitochondrial dysfunction is the cause of severe, often maternally inherited diseases, and also plays a key role in ageing and complex diseases (Kühlbrandt, 2015), such as neurodegenerative diseases and metabolic disorders.

Mitochondria display complex patterns including oscillatory dynamics, phase transitions and fractality to complement their multifaceted roles. The majority of mitochondria are tube-like structures or ovoid bodies of 0.5 – 1.0  $\mu\text{m}$  in diameter, but in most cell types, mitochondria exist as a network called syncytium that contains multiple copies of mitochondrial DNA (Alberts et al., 2014). Active, growing or migrating cells typically have increased numbers of mitochondria to meet the high ATP demand, while quiescent cells have the opposite scenario (Zamponi, Zamponi, & Cannas, 2018). This dynamic and plastic morphology is balanced by two contrasting processes: fission and fusion, and depending on their relative dominance, the overall connectivity and structural properties of the mitochondrial network are established to suit the cellular status. The dysregulated networks are implicated in several inherited and age-related diseases. Another element essential to mitochondrial functions is the mitochondrial membrane potential ( $\Delta\psi_m$ ).  $\Delta\psi_m$  and the mitochondrial pH gradient are two components of the electrochemical proton motive force across the mitochondrial intermembrane. While the proton motive force monitors the production of ATP,  $\Delta\psi_m$  provides the essential charge gradient for mitochondrial  $\text{Ca}^{2+}$  homeostasis and ROS generation. Therefore,  $\Delta\psi_m$  is a key indicator of both mitochondrial and cellular health.

There are two genomic types of DNA, one located in the nucleus whilst the other is found in the mitochondria, only nuclear DNA will be discussed further in this chapter. Every moment, DNA encounters a variety of damaging stimuli, both exogenously, such as UV light and ionising radiation, and endogenously, such as ROS from metabolic processes. The human cell is estimated to have approximately 10,000 DNA lesions daily (Lindahl, 1993). The DNA damage that ensues can be base damage, sugar damage, single-strand breaks or double-strand breaks, with the latter being the most harmful DNA lesions. If left unrepaired, even one double-strand break is sufficient to trigger cell death (Jackson, 2002; Sonoda, Hohegger, Saberi, Taniguchi, & Takeda, 2006). A single-strand break happens when only one strand is affected, whereas a double-strand break affects both strands of the double helix DNA. Accumulation of unchecked DNA damage is associated with embryonic lethality, developmental disorders, cell ageing and cancer (Tanaka, Huang, & Halicka, 2007). Fortunately, cells are also equipped with several DNA repair mechanisms to provide defence and ensure cell survival.

In human cells, DNA is wrapped around histone octamers, consisting of core histones H2A, H2B, H3 and H4. H2AX, one of the four variants of H2A, accounts for around 10% of the total H2A protein and is randomly located in histones throughout the genome (Rogakou, Pilch, Ivanova, & Bonner, 1998). This molecule is critical in the repair process of double-strand breaks (Dickey et al., 2009; Weyemi et al., 2018). When a double-strand break occurs, H2AX proteins in the proximity of a few megabases of the damage site are phosphorylated on the 139<sup>th</sup> serine residue to become  $\gamma$ -H2AX by several kinase enzymes. Hundreds to thousands of  $\gamma$ -H2AX can be found per double-strand break (Pilch et al., 2003). One function of  $\gamma$ -H2AX is to accumulate DNA damage signalling and repair proteins for double-strand breaks.  $\gamma$ -H2AX also amplifies signals, remodels chromatin to prevent dissociation of break ends, and recruits cohesins necessary for DNA repair (Podhorecka et al., 2010).

SFN has dual effects on mitochondria and genome integrity. In dietary studies, SFN is associated with various benefits for mitochondria. SFN preserves mitochondrial respiratory capacity, prevents pro-apoptotic events, such as  $\Delta\psi_m$  disruption and mitochondrial permeability transition, improves mitochondrial bioenergetics, and reinforces mitochondrial defence against ROS via increasing intramitochondrial GSH level and phase II enzyme activity (Negrette-Guzman et al., 2013). Contrarily, SFN can cause  $\Delta\psi_m$  disruption in human cardiomyocytes, and leukaemia cells (W. Y. Choi, Choi, Lee, & Choi, 2008; Rhoden et al., 2021). Regarding mitochondrial networks, SFN inhibition of mitochondrial fission is also found to be both cytoprotective (O’Mealey, Berry, & Plafker, 2017) and cytotoxic (Geng et al., 2017). In consideration of genomic integrity, SFN can protect DNA from damage and reduce mutation rates by acting as a histone deacetylase inhibitor and a phase II enzyme inducer (Bansal, Singh, Pal, Dev, & Ansari, 2018). However, SFN can also cause DNA damage by acetylating DNA repair proteins (Rajendran et al., 2013) and generating ROS (Sestili et al., 2010). Therefore, it was important to find out the impacts of SFN on mitochondria and DNA in human lens cells.

### **3.2 Aims**

This chapter aims to confirm previous work performed by Liu and co-authors in FHL124 and expand the range of cellular events that are triggered by SFN in human lens epithelial cells. Cell viability and ERS will be measured using different approaches from those performed by Liu and co-authors. Two new aspects of interest are mitochondrial integrity and genome integrity. Mitochondrial integrity will be determined by evaluating mitochondrial networks and mitochondrial membrane potential. The genome integrity will be assessed based on the number

of  $\gamma$ -H2AX foci, which are points where  $\gamma$ -H2AX accumulates with hundreds of other proteins around double-strand breaks (Mah, El-Osta, & Karagiannis, 2010).

### **3.3 Results**

#### **3.3.1 SFN decreases cell viability in FHL124 cells.**

Previously, 100  $\mu$ M SFN was used to examine cell death and other stress responses in FHL124 cells (H. Liu et al., 2017). Using an LDH-based cytotoxicity assay, a concentration of 50  $\mu$ M SFN was reported to yield similar cytotoxic effects as 100  $\mu$ M (**Figure A. 1** in Appendix), therefore, 50  $\mu$ M SFN was used in this current study to investigate cellular events of interest. To test the effect of SFN on lens cell viability, the Cell-TitreGlo luminescent assay was used. FHL124 cells were treated with 50  $\mu$ M SFN over 18 hours, and the level of ATP, an indicator of viable cells, was measured. Cell viability increased steadily and peaked after 5 hours with a  $142.4 \pm 15.0\%$  improvement over the baseline level. Afterwards, cell viability significantly plummeted to  $29.8 \pm 20.5\%$  in the next 3 hours and reached  $15.6 \pm 8.0\%$ , relative to the control value at 18 hours post treatment (**Figure 3. 1**).

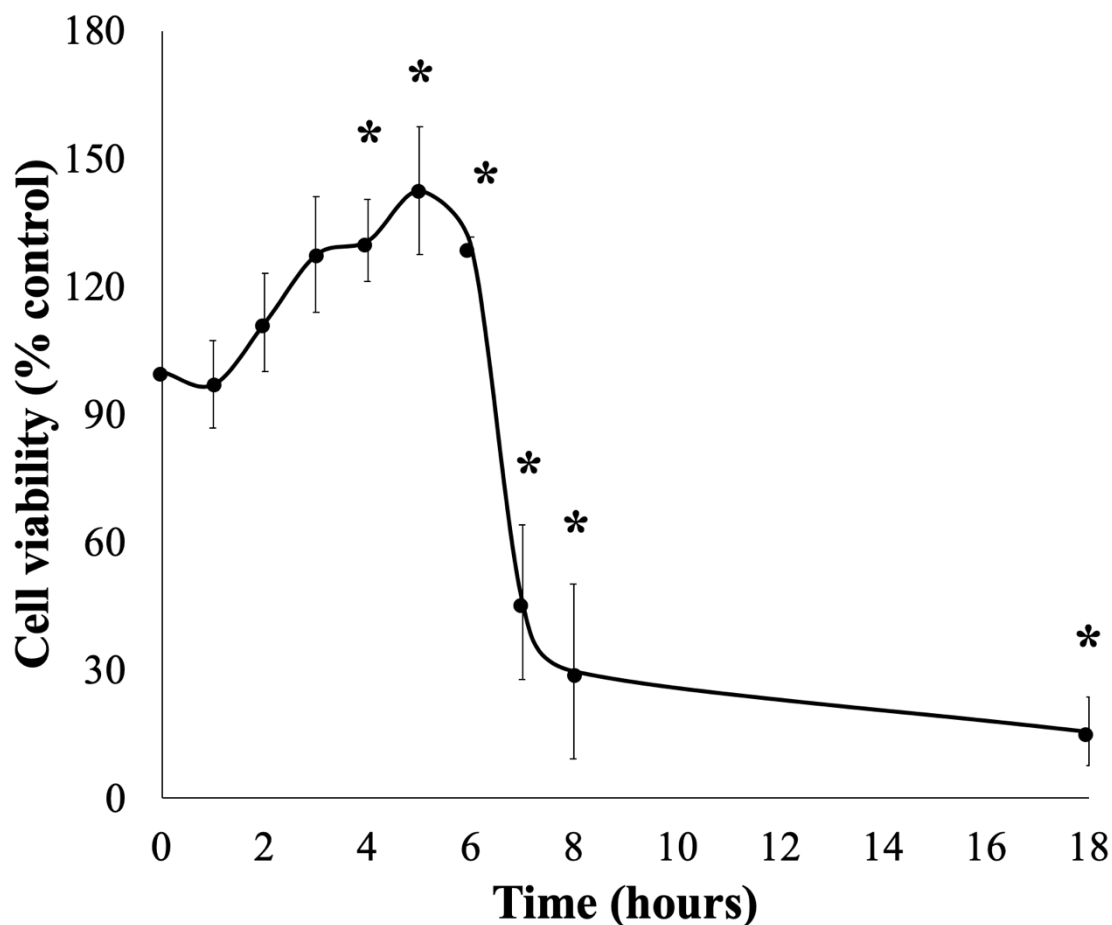


**Figure 3. 1: SFN decreases cell viability in FHL124 cells over time.**

FHL124 cells were treated with 50  $\mu$ M SFN for different durations over 18 hours and the cell viability was assessed using the Cell-TitreGlo Luminescent assay. Quantitative data are shown as mean  $\pm$  SEM (n = 4). An asterisk indicates a significant difference between the treated group and the untreated control at t=0 ( $p \leq 0.05$ ; ANOVA with Dunnett's post hoc test).

### 3.3.2 SFN impairs the integrity of mitochondrial networks in FHL124 cells.

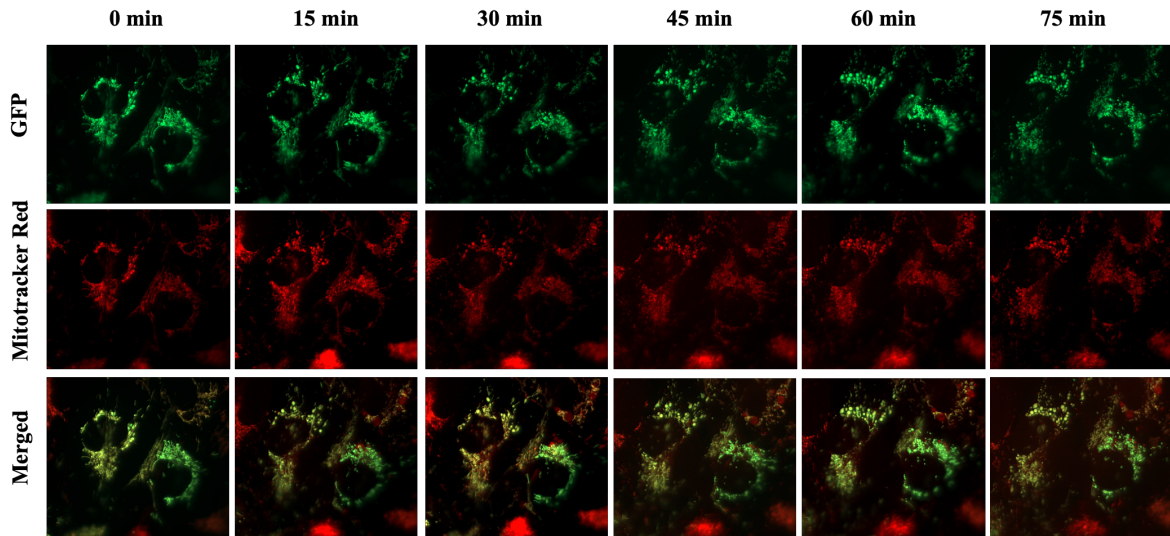
To assess impacts of SFN on mitochondria in FHL 124 cells, two methods of observing mitochondrial networks were utilised. In the first approach, FHL124 cells transfected with pAcGFP-Mito were labelled with 100 nM MitoTracker Red and live cells were imaged using Zeiss Axio Observer every 15 minutes for a total duration of 75 minutes. Changes in the mitochondrial networks in cells treated with SFN were noticeable after 15 minutes: the networks were much smaller and consisted of saturated green dots, instead of tubules of varying sizes (**Figure 3. 2**). At the end of the imaging process, the mitochondrial networks of

SFN-treated cells lost all their dynamic features, such as long branches, a mixture of long and short mitochondria; in some cases, cells had already detached and floated away, indicating cell death. In contrast, the mitochondrial networks of the control maintained their shapes and sizes. Despite having fewer long branches after 75 minutes, mitochondrial networks in the control still had a mixture of puncta and branches, and distinguished networks.

Importantly, the red MitoTracker signal aligned with the green GFP signal, indicating that the MitoTracker Red signal was not affected by mitochondrial membrane potential in this system, and MitoTracker Red alone would be a reliable tool for evaluating the morphology of mitochondrial networks using confocal microscopy.

In the second approach, mitochondrial networks in fixed FHL124 cells that were only labelled with MitoTracker Red were visualised using a confocal microscope. This method allowed the acquisition of images with higher resolution and definition (**Figure 3. 3A**). In fixed cells, SFN appeared to take much longer to cause changes to mitochondrial networks. After 2 hours of the treatment: the networks began to hyperfuse and lose individual puncta, and have longer, more connected branches. After 4 hours, the pattern became more noticeable, but diminished after 6 hours, when the mitochondrial networks appeared condensed, lost the dynamic features observed in the control groups, and had increasing numbers of puncta. To quantify the observed networks, the acquired image was converted and analysed by ImageJ. SFN reduced the size of mitochondrial networks in FHL124 cells over time and the size of the endpoint was less than  $29.0 \pm 4.5\%$  of the control values (**Figure 3. 3B**).

## Control



## 50 $\mu$ M SFN

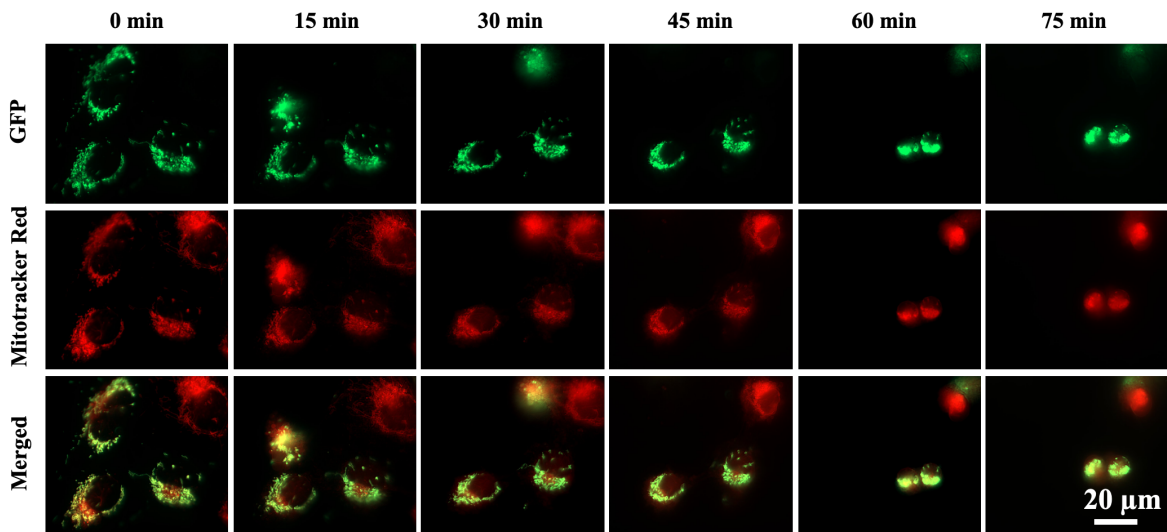


**Figure 3. 2: SFN decreases the size of mitochondrial networks in FHL124 cells over time measured by widefield microscopy.**

Mitochondria in FHL124 cells were labelled with GFP (green) by transfection and MitoTracker Red CMXROS (red) by direct staining. Cells were then treated with 50  $\mu$ M SFN and their mitochondria were visualised by a widefield microscope for a total duration of 75 minutes.

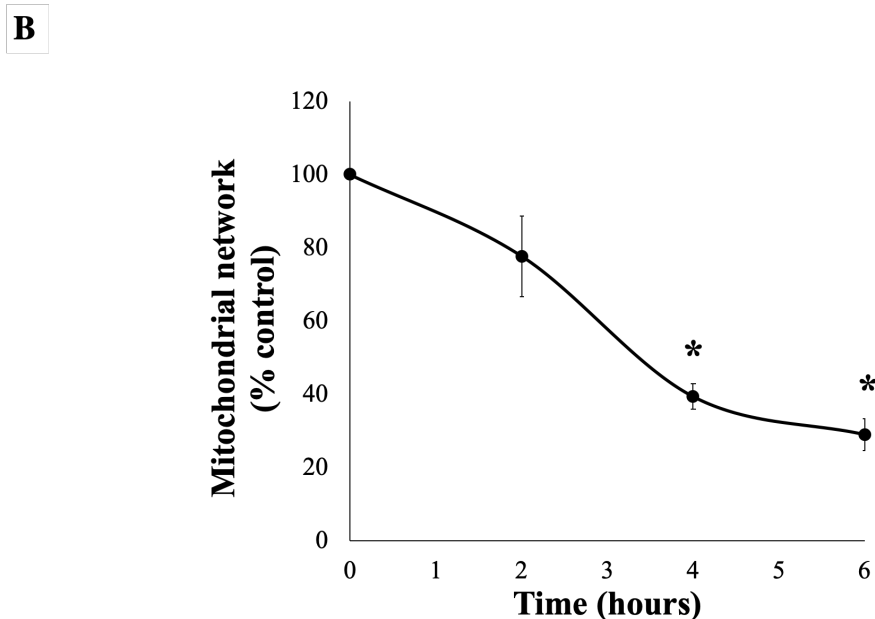
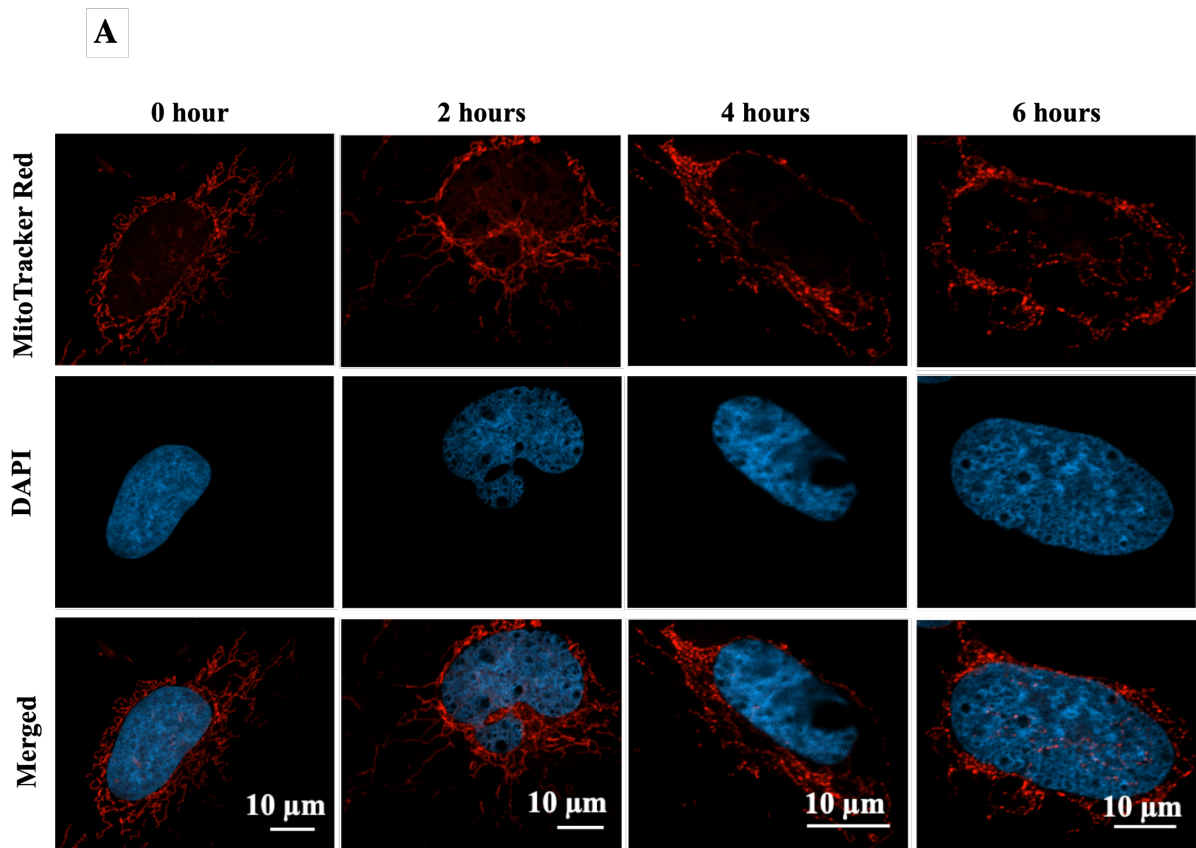


**Figure 3. 3: SFN decreases the size of mitochondrial networks in FHL124 cells over time measured by confocal microscopy.**

FHL124 cells were treated with 50  $\mu$ M SFN for different durations over 6 hours. Mitochondria were labelled with 100nM MitoTracker Red CMXRos and fixed. Images were observed by confocal microscopy and 10 cells of each time point were captured and analysed by Image J. A) Representative images (red – MitoTracker, blue – DAPI, merged – MitoTracker and DAPI), and B) quantitative data are shown as mean  $\pm$  SEM (n = 4). An asterisk indicates a significant difference between the treated group and the untreated control at t=0 ( $p \leq 0.05$ ; ANOVA with Dunnett’s post hoc test).

### 3.3.3 SFN causes loss of mitochondrial membrane potential in FHL124 cells.

Mitochondrial membrane potential –  $\Delta\psi_m$  in FHL124 cells was measured after 50  $\mu\text{M}$  SFN treatment using the fluorescent TMRE dye. The  $\Delta\psi_m$  increased by  $107.3 \pm 6.0\%$  in the first hour of the SFN treatment, then gradually decreased towards the end of the experiment, suggesting sustained depolarisation of the  $\Delta\psi_m$ . After 8 hours, the  $\Delta\psi_m$  significantly decreased by more than half ( $44.7 \pm 9.5\%$ ) against the baseline level (**Figure 3. 4**).

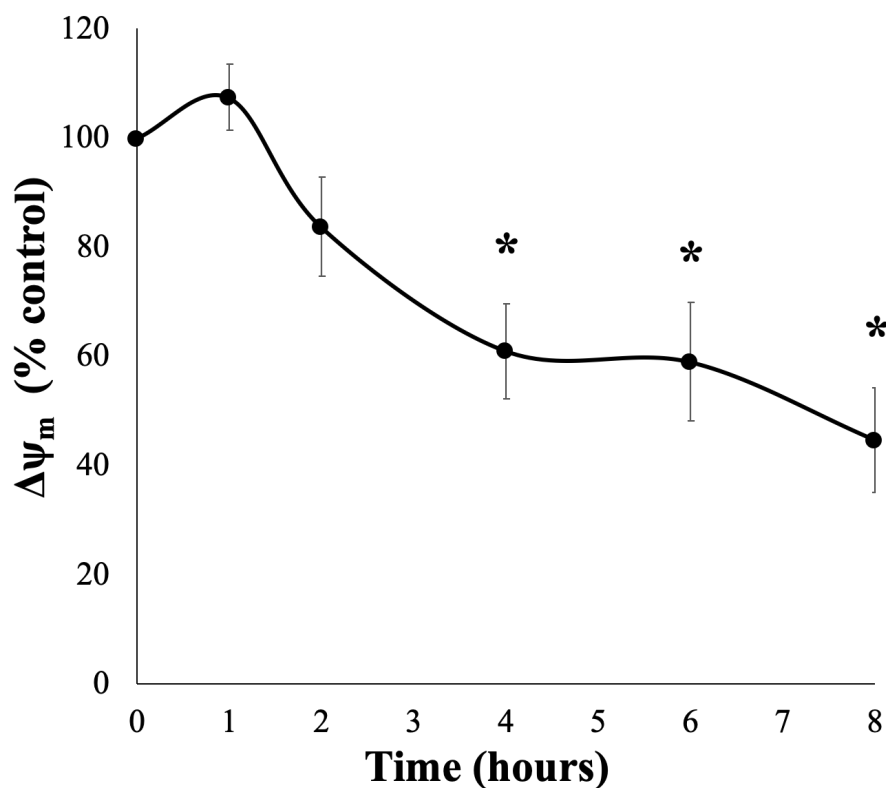


**Figure 3. 4: SFN disrupts mitochondrial membrane potential ( $\Delta\psi_m$ ) in FHL124 cells over time.** FHL124 cells were treated with 50  $\mu\text{M}$  SFN for different durations over 8 hours, then incubated with 400 nM tetramethylrhodamine ethyl ester – TMRE. The peak TMRE signal was measured using a microplate reader at Excitation/Emission = 549/575 nm. Quantitative data are shown as mean  $\pm$  SEM (n = 5). An asterisk indicates a significant difference between the treated group and the untreated control at t=0 ( $p \leq 0.05$ ; ANOVA with Dunnett's post hoc test).

### 3.3.4 SFN increases ATF6 transcriptional activity in FHL124 cells.

Activating transcription factor 6 (ATF6) is a member of the leucine zipper family of transcription factors that is found in the ER. Following the accumulation of unfolded proteins, ATF6 is cleaved to release its cytoplasmic domain and the 50 kDa activated form of ATF6 enters the nucleus to induce transcription of genes necessary for the ERS (Hillary & FitzGerald, 2018). A dual renilla-luciferase luminescent assay was used to evaluate ATF6 transcriptional activity. The ATF6 reporter was transfected into the FHL124 cells, and the luminescent signal was measured using a microplate reader. Transfected FHL 124 cells were treated with 50  $\mu$ M SFN over 6 hours. After 45 minutes of SFN treatment, ATF6 transcriptional activity almost doubled ( $183.5 \pm 44.3\%$ ) relative to the control. The next two hours witnessed the steepest rise, with the activity significantly rising to  $458.5 \pm 27.0\%$  at 3 hours post treatment. Subsequently, the activity appeared to plateau out and settled at  $490.1 \pm 101.0\%$ , reflecting a fivefold increase over the baseline level (Figure 3. 5).

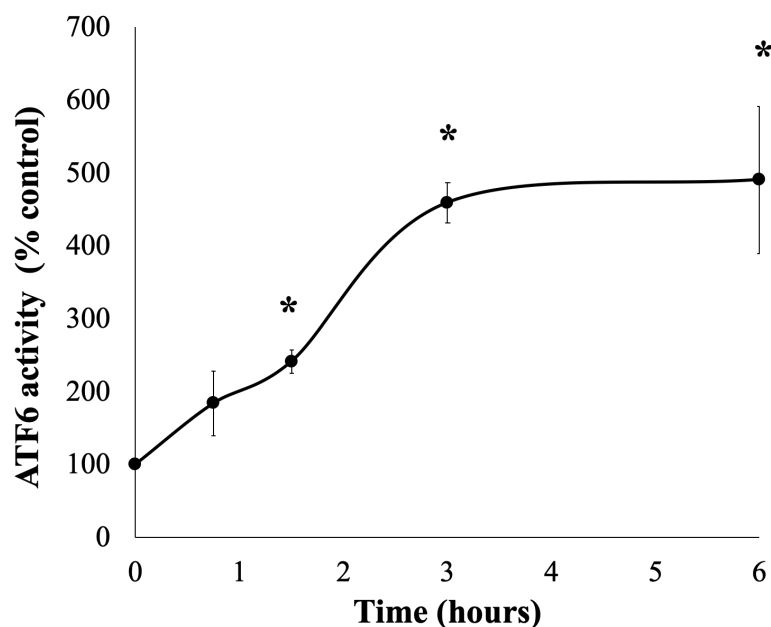


**Figure 3. 5: SFN increases ATF6 transcriptional activity in FHL124 cells over time.**

FHL124 cells were treated with 50  $\mu$ M SFN for different durations over 6 hours. ATF6 transcriptional activity was measured using the dual-luciferase reporter assay. Quantitative data are shown as mean  $\pm$  SEM (n = 4). An asterisk indicates a significant difference between the treated group and the untreated control at t=0 ( $p \leq 0.05$ ; ANOVA with Dunnett's post hoc test).

### **3.3.5 SFN triggers DNA damage responses in FHL124 cells.**

DNA damage in the form of double-strand breaks was assessed by determining  $\gamma$ -H2AX foci in FHL 124 cells upon a treatment with 50  $\mu$ M SFN (**Figure 3. 6A**). SFN increased the number of  $\gamma$ -H2AX foci, hence double-strand breaks, over time but the increase was not significant until 6 hours post treatment when the number of foci was  $875.6 \pm 230.3\%$  higher than control values (**Figure 3. 6B**). There were also more nuclei distinct with green foci, signifying an extreme abundance of double-strand breaks.

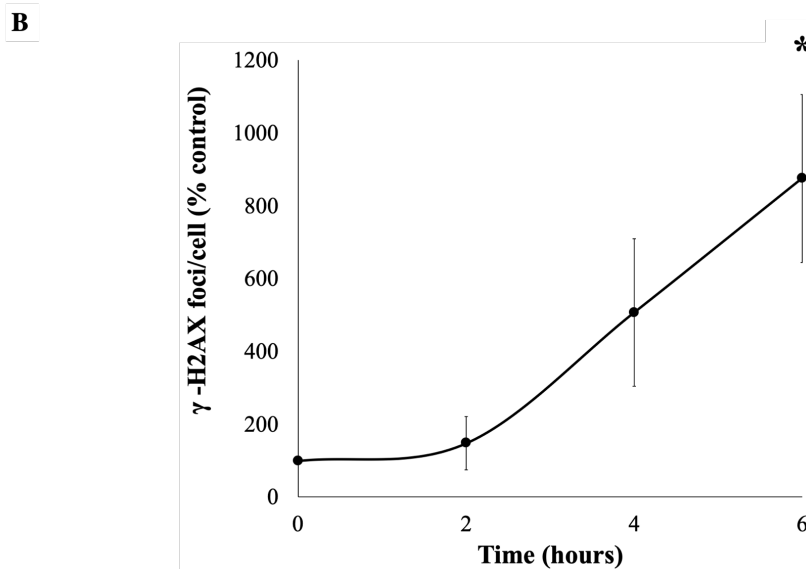
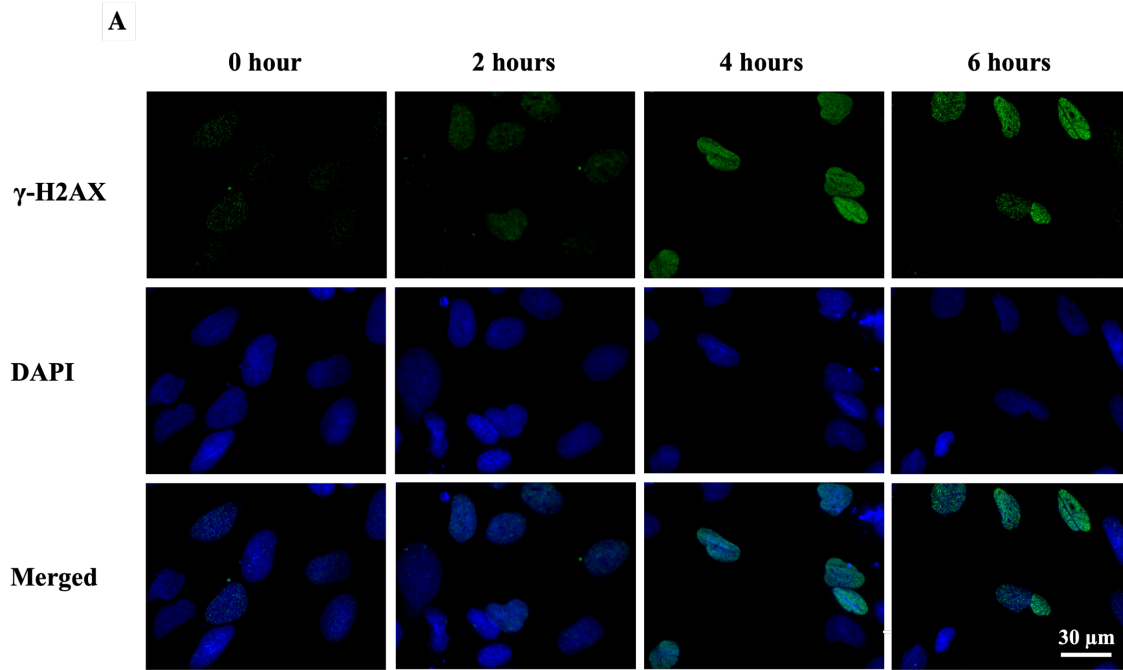


**Figure 3. 6: SFN triggers DNA double-strand breaks in FHL124 cells over time.**

FHL124 cells were treated with 50  $\mu$ M SFN for different durations over 6 hours.  $\gamma$ -H2AX was used as a measure of DNA double-strand breaks by immunocytochemistry, such that foci per cell nucleus were determined by a widefield microscope. A) Representative images (green –  $\gamma$ -H2AX, blue – DAPI, merged –  $\gamma$ -H2AX and DAPI), and B) quantitative data are shown as mean  $\pm$  SEM (n = 4). An asterisk indicates a significant difference between the treated group and the untreated control at t=0 ( $p \leq 0.05$ ; ANOVA with Dunnett's post hoc test).

### 3.4 Discussion

SFN is a phytochemical derived from cruciferous vegetables, such as broccoli. SFN can target many organelles and trigger varying cellular responses. Previously, SFN at high concentrations has been shown to cause ERS, autophagy and cell death in human lens epithelial cells (H. Liu et al., 2017). The present work further investigated the impacts of SFN on mitochondria and the nucleus. SFN at 50  $\mu$ M damaged mitochondrial networks, impaired  $\Delta\psi_m$ , elevated ATF6 transcriptional activity, induced double-strand breaks, and ultimately triggered cell death.

SFN is reported to influence mitochondrial function and structure in various ways in many cell lines, both positively and negatively (W. Y. Choi et al., 2008; Guerrero-Beltran et al., 2010; Napoli, Flores, Mansuri, Hagerman, & Giulivi, 2021; Rhoden et al., 2021). The current study is the first to report on SFN-induced effects in human lens cells, where SFN damaged mitochondrial networks and impaired  $\Delta\psi_m$ . Mitochondrial networks were severely damaged by SFN. Despite some degree of network elongation observed in the first two hours, the mitochondrial morphology at the endpoint exhibited network shrinkage and concentrated around the nucleus.

The initial fusion of mitochondrial networks suggests two possible impacts of SFN on mitochondria: 1) increased stress load, possibly due to ROS, and 2) electron transport chain impairment. Derived from several studies in various models, by fusing into bigger networks and spreading the insulting effects across them, mitochondria can alleviate the stress load on affected mitochondria and maintain energy production. However, as cellular stress continues, this coping mechanism can only last for a short time before the collapse of the mitochondrial networks. As described by Willems and co-authors, the loss of tubularity and the shift towards

fragmentation and condensation in the mitochondrial networks over time confirmed escalating stress levels (Willems, Rossignol, Dieteren, Murphy, & Koopman, 2015).

There has been little research on the effects of SFN on mitochondrial networks, and variations in experimental parameters make it difficult to gain a full understanding. In human retinal pigment epithelial cells, 50  $\mu\text{M}$  SFN has been reported to promote mitochondrial fusion by interfering with the fission machinery (O'Mealey et al., 2017). The appearance of the hyperfused networks in this analysis was comparable to the first 2 hours of the current study. That experiment, however, was neither longer than 4 hours nor a time-response study. Therefore, it is difficult to predict whether mitochondrial fission or fragmentation will occur later. On the other hand, a 24-hour treatment with 15  $\mu\text{M}$  SFN was confirmed to induce mitochondrial fusion, which contributed to apoptosis in human non-small cell lung cancer. (Geng et al., 2017). However, based on their description of hyperfused mitochondria, it seems that their mitochondrial fusion resembles the giant spherical morphology that occurs after severe fragmentation due to irreversible stress, and therefore is not mitochondrial fusion by characterisation (Willems et al., 2015). Nevertheless, the Geng *et al* (2017) study agrees with the present work that mitochondria become smaller following SFN treatment.

$\Delta\psi_m$  is an essential component to produce ATP and a driving force for the transport of ions and proteins necessary for healthy mitochondrial functioning (Zorova et al., 2018). Mitochondria have a highly negative  $\Delta\psi_m$ , approximately -180 mV and it is important to avoid prolonged changes in  $\Delta\psi_m$ . TMRE is a positively charged dye and would readily accumulate in active mitochondria. Therefore, the gradual drops in TMRE signals over time following SFN indicate prolonged depolarisation of the  $\Delta\psi_m$ , suggesting the gradual impairment of mitochondrial functions. In agreement, SFN has also been reported to similarly disrupt  $\Delta\psi_m$  in various human

cell lines, such as cardiomyocytes, leukaemia cells and prostate cancer cells (W. Y. Choi et al., 2008; Rhoden et al., 2021; D. Xiao et al., 2009). Depolarised mitochondria not only produce less ATP but also open more mitochondrial permeability transition pores, release more  $\text{Ca}^{2+}$  and produce more ROS. Therefore, via investigating  $\Delta\psi_m$ , this finding provides convincing evidence of the negative impacts of SFN on mitochondrial functions in FHL124 cells.

The UPR is comprised of three pathways: IRE1, PERK and ATF6. ATF6 is a 90 kDa transmembrane protein that is ubiquitously expressed and located in the ER. Upon ERS, ATF6 is released from BiP, and traffics to the Golgi apparatus, where it is cleaved to release the 50 kDa transcriptionally active N-terminus cytosolic portion. Active ATF6 subsequently translocates to the nucleus and upregulates the expression of chaperones and protein degradation enzymes. There are three phases of UPR: adapt, alarm, and apoptosis. The initial intent of the UPR is to adapt to the changing environment and to restore cellular homeostasis. However, prolonged ER dysfunction and UPR will trigger cell death. Among the three branches of UPR, the ATF6 pathway is more inclined towards the adaptation role (Xu, Bailly-Maitre, & Reed, 2005).

The data from this study demonstrates that 50  $\mu\text{M}$  SFN significantly increased ATF6 transcriptional activity relative to the control at 75 minutes post treatment. Concurrently, Liu and co-authors reported that 100  $\mu\text{M}$  SFN induced ERS after a 24-hour treatment, as evidenced by the induction of ERS gene and protein expression (H. Liu et al., 2017). Zou and co-authors also observed a similar trend after a 48-hour treatment with 20  $\mu\text{M}$  SFN in human hepatocellular carcinoma cells (Zou et al., 2017). The current time response experiment further provides evidence that indicates ERS as an early event. The early induction of the ATF6

pathway could be interpreted as an initial adaptive response to curb the overload of misfolded and unfolded proteins.

SFN also caused double-strand breaks, as demonstrated by increased  $\gamma$ -H2AX foci in FHL124 cells over time. This result is in line with previous research. At 1-hour post treatment, 40  $\mu$ M SFN caused a substantial accumulation of  $\gamma$ -H2AX in human pancreatic cancer cells (Naumann et al., 2017), and at 2-hour post treatment in prostate cancer cells (Hac et al., 2019). Whereas, in human leukaemia cells, after 3 hours of SFN treatments (10 – 30  $\mu$ M), only single-strand breaks were detected by the fast-halo assay (Sestili et al., 2010). This difference could be due to variations in the detection method. Future studies should aim to use various techniques to examine DNA damage and assess mitochondrial DNA integrity in response to SFN. Compared to cellular responses in mitochondria and endoplasmic reticulum, DNA damage was detected much later. This observation could imply that SFN induced accumulative effects reached the alarm threshold faster in mitochondria and ER than in nucleus, or that SFN induced stress signals from two former organelles spread to the latter. The precise sequence of these events is beyond the scope of this current study.

Regarding cell death, similar to previous findings, SFN at 50  $\mu$ M, a supranutritional dose, was lethal to human lens cells. Interestingly, cell viability increased by 150% in the first 5 hours rather than decreasing monotonously over 18 hours. The CellTitre-Glo assay determines the number of viable cells in culture based on the quantitation of ATP. The length of a cell cycle in a fast-dividing mammalian cell on average takes approximately 24 hours (Harper & Brooks, 2005). Therefore, the increase in recorded signals during the first 5 hours of the SFN treatment may be interpreted as an increase in ATP production of the existing population, rather than an increase in the cell population. Apoptosis is an ATP-dependent process, and the elevation of

cytosolic ATP levels has been documented to be a requisite for this death mode (Zamaraeva et al., 2005). The present work did not rule out necrosis, therefore the observed elevated ATP levels could not be explained by the mode of cell death. Given the number of energy-consuming cellular events and responses activated before cell death, such as dysregulated  $\Delta\psi_m$ , ATF6 signalling pathway, and DNA damage repair, this short-term rise in ATP may be due to increases in cellular demands to evoke these stress responses.

The study illustrates the wide spectrum of SFN-induced cytotoxicity in FHL124 cells. In agreement with the previous work performed by Liu and co-authors (H. Liu et al., 2017), SFN induced cell death and ERS. SFN was further shown to impair mitochondria and genome integrity. These cellular events individually may not suffice to induce cell death and some can also be anti-apoptotic at some point (Horwacik et al., 2015; Nishikawa et al., 2010; Xu et al., 2005). Nevertheless, considering their chronicity and intensity, it is likely that they collectively contribute to SFN induced cell death (**Figure 3. 7**). Overall, the work presented demonstrates further knowledge of SFN-induced events in human lens cells and expands the repertoire of assays to be employed. Consequently, this creates a robust platform to investigate the mechanisms by which SFN regulates these events leading to cell death. The next question is to examine whether all of these cellular responses share an upstream mediator.

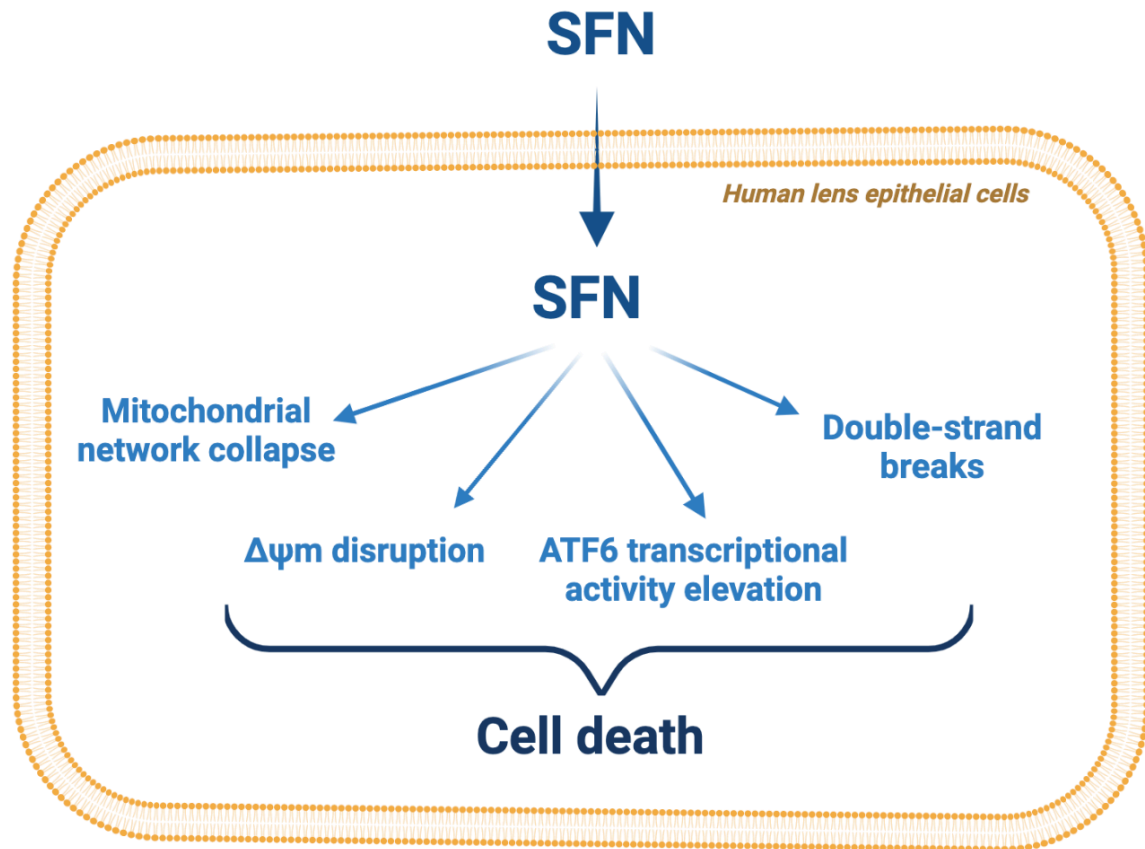


**Figure 3. 7: SFN induces a range of stress responses in human lens epithelial cells.**

Upon cellular entry, high concentrations of SFN induce mitochondrial network collapse and loss of mitochondrial membrane potential ( $\psi_m$ ), increase ERS via upregulating ATF6 transcriptional activity and trigger DNA damage response to double-strand breaks. The intensity and chronicity of these events eventually lead to death in human lens epithelial cells.

# Chapter 4 ROS Have a Pivotal Role in SFN Induced Cellular Responses

---

## 4.1 Introduction

ROS are oxygen-containing intracellular chemical species that are reactive towards lipids, proteins and DNA. Different ROS have different intrinsic chemical properties and preferred biological targets (Schieber & Chandel, 2014). Mitochondria and the family of NADPH oxidases (NOXs) located on plasma membranes are major endogenous sources of ROS. There are at least eight known ROS-generating sites in mitochondria, for example, complex I and complex III from the electron transport chain (Brand, 2016). Due to unpaired electrons, oxygen is susceptible to free radical formation. The immediate product of the reduction of oxygen is  $O_2^-$ . Subsequently,  $O_2^-$  is converted to peroxide  $\bullet O_2^{-2}$  then  $H_2O_2$ . The molecule  $H_2O_2$  has three fates: 1) being converted to harmless water, 2) contributing to cell signalling, or 3) being transformed into the most deleterious form of intracellular ROS,  $\bullet OH$ , in iron-dependent Haber-Weiss Fenton reactions. Due to its ability to readily diffuse through membranes,  $H_2O_2$  serves as a better intracellular signalling molecule than other ROS, and its levels dictate different cellular outcomes. There is evidence supporting the presence of  $O_2^-$ -mediated signalling pathways but these have yet to be elucidated (Shadel & Horvath, 2015).

Post-translational modifications (PTMs) are a well-known mechanism of redox signalling. ROS can interact with cysteine in proteins involved in cell proliferation and apoptotic pathways and consequently influence their activities.  $H_2O_2$  is believed to act by oxidising catalytic cysteines  $Cys-S^-$  present in phosphatase enzymes, which then becomes cysteine sulfenic acid

(Cys-SOH) (Finkel, 2012; Rhee, 2006). This results in allosteric changes within targeted proteins that alter their function. For example, redox-sensitive anti-proliferative phosphatase and tensin homolog deleted on chromosome 10 (PTEN) and MAPK phosphatases can be deactivated due to thiol oxidation, and consequently, cells are more likely to survive and grow. The oxidation of Cys-S<sup>-</sup> is H<sub>2</sub>O<sub>2</sub> level-dependent: nanomolar ranges of H<sub>2</sub>O<sub>2</sub> allow reversible conversions between Cys-S<sup>-</sup> and Cys-SOH, whereas higher levels lead to further oxidation to sulfinic (SO<sub>2</sub>H) or sulfonic (SO<sub>3</sub>H) and these modifications are permanent, resulting in irreversible alterations to macromolecules.

ROS were once thought to be harmful to cells due to their association with ageing and other pathological conditions (Bhatti et al., 2017; Nita & Grzybowski, 2016). However, studies over the last two decades have demonstrated the imperative role of ROS in redox homeostasis and cellular functions. For example, a lack of ROS in the immune system can impair its ability to fight pathogens (Schieber & Chandel, 2014). Both innate immunity and acquired immunity employ ROS as signal cues for proper activation. Another beneficial effect of ROS is its function in angiogenesis. Angiogenesis is essential for growth and wound healing, and angiogenesis is orchestrated by several transcription factors, one of which is hypoxia-inducible factor (HIF-1 $\alpha$ ). Under normal conditions, HIF-1 $\alpha$  is targeted for degradation by prolyl hydroxylases (PHDs). When hypoxia occurs, PHDs become inactivated, potentially due to the formation of a disulfide bond between critical cysteine residues in a ROS-dependent manner (G. Lee et al., 2016). Consequently, HIF-1 $\alpha$  is free to induce pro-angiogenic signals and promote angiogenesis-driven wound healing responses.

On the other hand, the detrimental effects of ROS are more extensively studied. The pathogenesis of various health conditions is aided by abnormal intracellular ROS levels and

impaired redox status (Sies & Jones, 2020). Regarding the ability of H<sub>2</sub>O<sub>2</sub> to block anti-proliferative phosphatases, unchecked cell proliferation can promote tumorigenesis, while ROS-driven HIF-1 $\alpha$  activation can contribute to pathologic angiogenesis involved in metastasis. Uncontrolled levels of ROS also appear to cause inflammatory diseases, such as rheumatoid arthritis and multiple sclerosis (Q. Li & Verma, 2002). Furthermore, the excessive production of ROS can ultimately lead to apoptosis. As discussed in **Chapter 1**, accumulative damage caused by ROS over years can accelerate the opacity of the eye lens. ROS are also associated with ageing as suggested by the “free radical theory” of ageing proposed by Harman in 1956 (Harman, 1956). Since then, the hypothesis has been experimentally solidified but not proven. Even though aerobic metabolism and ROS generation are the most widely accepted causes of ageing, there are still many gaps and unknowns. Cells continuously make free radicals, yet whether that ROS are a cause, a consequence of or a correlation with ageing is unknown (Balaban, Nemoto, & Finkel, 2005; Ziada, Smith, & Côté, 2020).

SFN increases ROS levels in many cell lines and the generated ROS have been shown to play a critical role in SFN-induced cell death through varying mechanisms (Chhunchha et al., 2019; Lan et al., 2017; Shen, Xu, Chen, Hebbar, & Kong, 2006; Singh et al., 2005; D. Xiao et al., 2009). SFN is a potent inducer of the Nrf2 pathway, which regulates detoxification and antioxidant defence processes. Nonetheless, the elevation of Nrf2 activity beyond physiological levels can be detrimental to cells. As previously mentioned in **Chapter 1**, high levels of SFN-induced ROS were reported to cause Nrf2 dependent activation of Klf9, which further fuelled ROS production and promoted oxidative-stress induced death in a human lens cell line, (Chhunchha et al., 2019). ROS is also shown to activate AMP-activated protein kinase (AMPK) and MAPK to induce apoptosis in several cancer cell lines (Y. H. Choi, 2018; Lan et al., 2017). On the other hand, SFN-induced ROS did not kill untransformed primary human T-

cells but induced immunosuppressive effects by inhibiting their activation and subsequent proliferation (Liang et al., 2018). In FHL124 cells, Liu and co-authors reported a 130% increase in ROS levels following 2 hours of 100  $\mu$ M SFN treatment (H. Liu et al., 2017).

## 4.2 Aims

The data in the previous chapter provide evidence that SFN can cause a wide range of cellular responses. Since SFN has been reported to induce ROS in FHL124 cells (H. Liu et al., 2017), it is of great interest to understand the role of ROS in the cellular responses to SFN in human lens cells. The hypothesis tested is that **ROS play a critical role in SFN-mediated cellular responses**. To address the hypothesis, the current work aims to assess the protection of a ROS scavenger against a range of cellular events induced by SFN, including cell death, mitochondrial dysfunction, ERS, DNA damage and autophagy. The experimental models are FHL124 cells and human lens epithelial tissues.

## 4.3 Results

### 4.3.1 Evaluating the effect of a ROS scavenger on cell viability following SFN treatment in FHL124 cells.

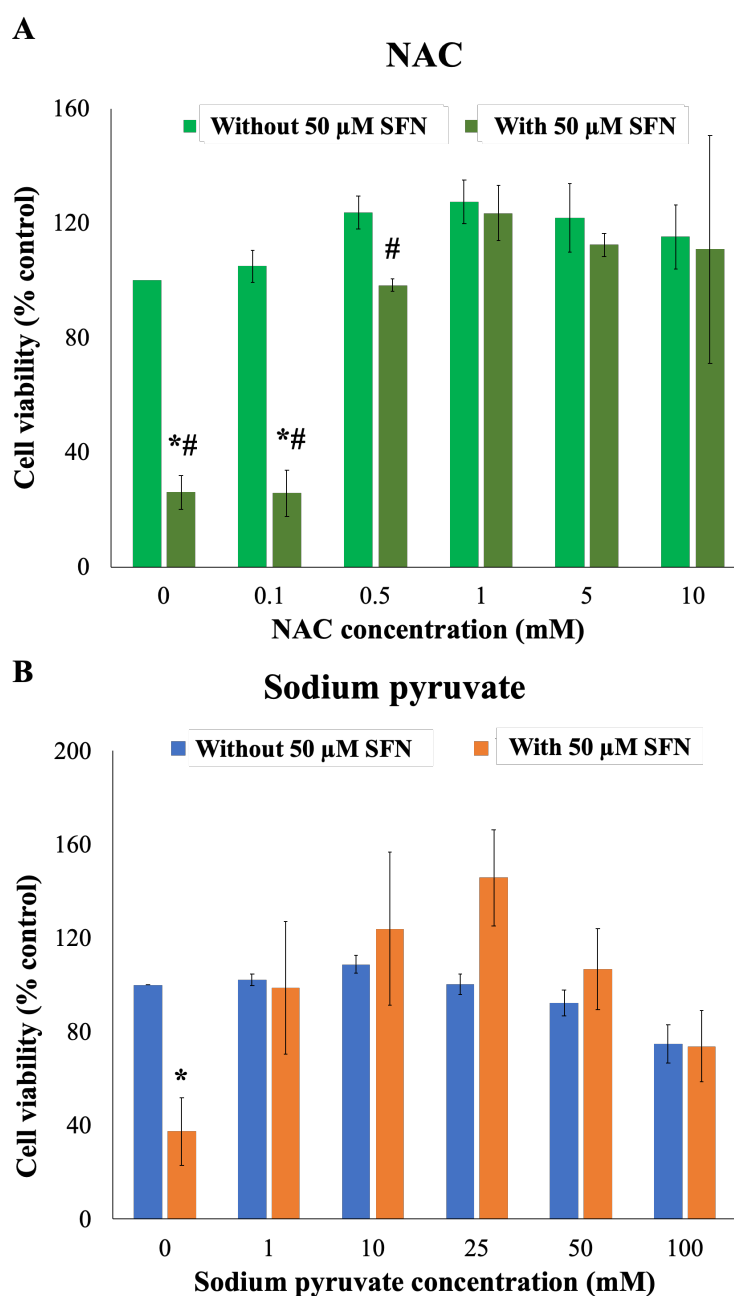
Two ROS scavengers, N-acetyl-L-cysteine (NAC) and sodium pyruvate, were used to assess their protection against the loss of cell viability induced by SFN. NAC is a thiol antioxidant and is commonly used in diverse studies (Ezerina, Takano, Hanaoka, Urano, & Dick, 2018; S. C. Kim, Choi, & Kwon, 2017; Sun, 2010; Zheng, Ma, Wang, He, & Deng, 2020). It can scavenge a range of ROS directly via its thiol groups, or via increasing levels of glutathione, a major intracellular antioxidant, or via generating anti-electrophilic stress hydrogen sulfur ( $H_2S$ ) and sulfane sulfur. Previously, in the laboratory, 1 mM NAC was shown to completely

obliterate ROS in FHL124 cells treated with or without 100  $\mu$ M SFN (unpublished data). This demonstrates the powerful antioxidant properties of NAC. On the other hand, pyruvate is an  $\alpha$ -ketoacid and an end product of glycolysis. While the physiological levels of pyruvate have little role in H<sub>2</sub>O<sub>2</sub> clearance, an increased extracellular concentration of pyruvate can remarkably eliminate H<sub>2</sub>O<sub>2</sub> (Guarino, Oldham, Loscalzo, & Zhang, 2019). As a result, pyruvate has been used as a ROS scavenger in different cell lines (Varma & Hegde, 2004; X. Wang et al., 2007).

In the current study, FHL124 cells were either maintained in serum-free (control) EMEM or EMEM supplemented with different concentrations (0.1 – 10 mM) of NAC or different concentrations (1 – 100 mM) of sodium pyruvate. Following a period of 1 hour, half the preparations were treated with SFN (final concentration 50  $\mu$ M) while the other half did not receive SFN treatment. Cells were incubated in experimental conditions for 18 hours. The effect of ROS scavengers on cell viability following SFN treatment was assessed using the Cell-TitreGlo assay. NAC did not have any impact on the SFN- induced loss of cell viability at 0.1 mM but yielded complete protection against SFN starting from 0.5 mM to 10 mM (**Figure 4. 1A**). Sodium pyruvate significantly protected cells from reduced viability from 1 mM (**Figure 4. 1B**). These findings strongly suggest that the deleterious impact of SFN on cell viability was mediated by ROS.

Between the two ROS scavengers, NAC was more commonly used, hence, NAC was chosen as the main ROS scavenger for the rest of the investigation. Within two experimental conditions containing 0.5 mM NAC with and without SFN, there was a significant difference. Therefore, 1 mM NAC was chosen for having an insignificant difference between the two

treatment groups, with and without SFN. This concentration is also similar to the one used in several previous studies (S. C. Kim et al., 2017; Shen et al., 2006).

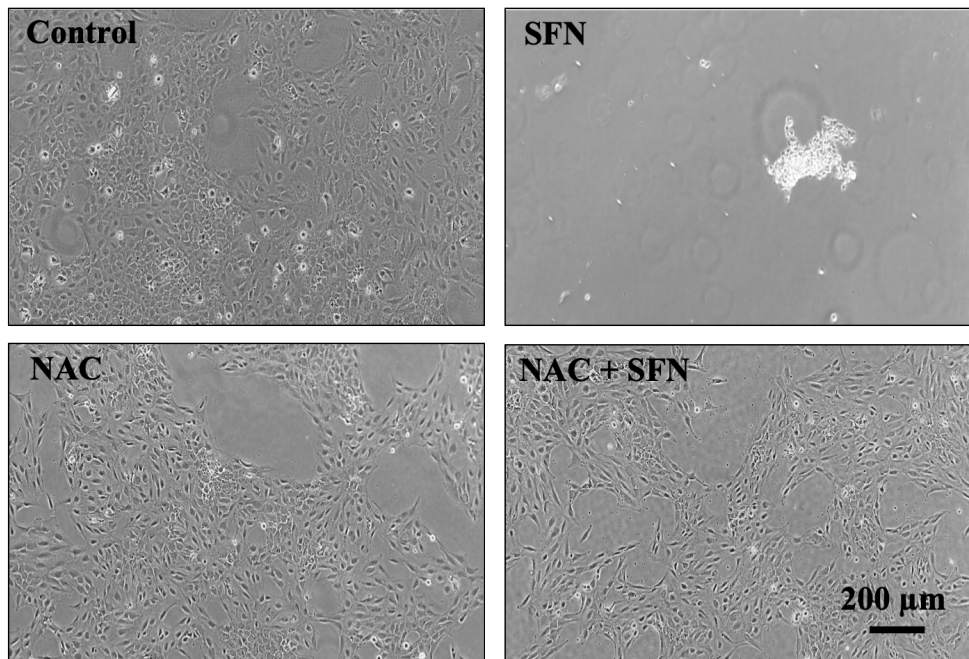
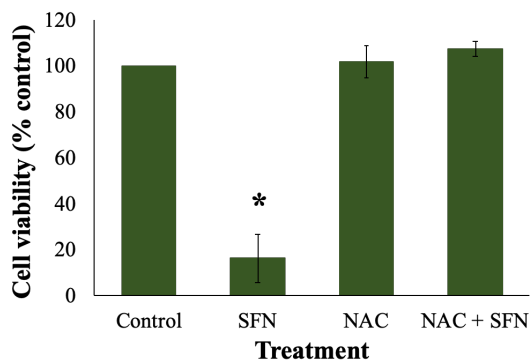
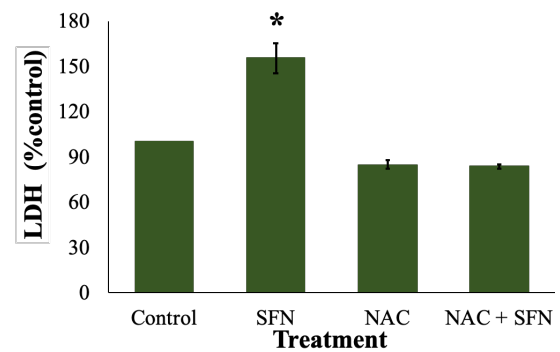


**Figure 4. 1: Effects of different concentrations of NAC and sodium pyruvate on cell viability following SFN treatment in FHL124 cells.**

FHL124 cells were either maintained in serum-free (control) EMEM or EMEM supplemented with different concentrations (0.1 – 10 mM) of NAC or different concentrations (1 – 100 mM) of sodium pyruvate. Following a period of 1 hour, half the preparations were treated with SFN (final concentration 50  $\mu$ M) while the other half did not receive SFN treatment. Cell viability was measured after 18 hours treated with SFN using a Cell-TitreGlo Luminescent assay. A) NAC and B) Sodium pyruvate. Quantitative data are shown as mean  $\pm$  SEM (n=3 for NAC, n=4 for sodium pyruvate). An asterisk indicates a significant difference between the treated group and the untreated group ( $p \leq 0.05$ ; ANOVA with Dunnett's post hoc test), a hashtag indicates a significant difference between with and without SFN groups of the same concentration of a particular ROS scavenger ( $p \leq 0.05$ ; independent Student's *t-test*).

### **4.3.2 NAC protects FHL124 from SFN-induced cytotoxicity.**

FHL124 cells were either maintained in serum-free (control) EMEM or EMEM supplemented with 1 mM NAC. Following a period of 1 hour, half the preparations were treated with SFN (final concentration 50  $\mu$ M) while the other half did not receive SFN treatment. After 18 hours treated with 50  $\mu$ M SFN, FHL124 cells showed morphological alterations, such as cell detachment, cytoplasmic shrinkage, nuclear condensation and filament formation, relative to the control showing a normal healthy phenotype, as visualised using phase-contrast microscopy (**Figure 4. 2A**). Biological assays showed that 50  $\mu$ M SFN decreased cell viability to  $29.4 \pm 5.9\%$  relative to the control and increased LDH secretion to  $155.6 \pm 10.0\%$  compared to the baseline (**Figure 4. 2B & C**). The treatment with NAC successfully prevented the morphological effects and cell damage induced by SFN (**Figure 4. 2**)

**A****B****C**

**Figure 4. 2: NAC protects cells from cytotoxicity induced by SFN in FHL124 cells.**

FHL124 cells were either maintained in serum-free (control) EMEM or EMEM supplemented with 1 mM NAC. Following a period of 1 hour, half the preparations were treated with SFN (final concentration 50  $\mu\text{M}$ ) while the other half did not receive SFN treatment. Cells were treated for 18 hours after the addition of SFN. A) Cell morphology was observed using phase-contrast microscopy; B) Cell viability was assessed using a CellTiter-Glo assay; C) Cytotoxicity was assessed using an LDH assay. Data are shown as mean  $\pm$  SEM (n=4). An asterisk indicates a significant difference between the treated group and all other groups ( $p \leq 0.05$ ; ANOVA with Tukey's post hoc test).

### **4.3.3 NAC protects against mitochondrial dysfunction caused by SFN in FHL124 cells.**

The data presented in **Chapter 3** showed that SFN disrupted mitochondrial networks, so it was important to assess whether NAC could prevent this phenomenon. Mitochondrial networks in both live cells and fixed cells were observed. Mito-GFP cells were co-labelled with MitoTracker Red and the live cells were observed using a Zeiss Observer 7 microscope. SFN disrupted the mitochondrial networks over a duration of 75 minutes, and NAC treatment prevented that. It was noticed that the mitochondrial networks in the control, NAC alone, and NAC + SFN samples shrank over time too, however, the extent of shrinkage was negligible compared to the SFN sample (**Figure 4. 3**).

In the fixed cell experiment, mitochondria in FHL124 cells were stained with MitoTracker CMXRos red and treated with 50  $\mu$ M SFN for 4 hours. Control groups showed a clear distribution of mitochondria comprising punctae and branched networks of different sizes, they positioned themselves both near the nucleus and sparse in the cytoplasm. In agreement with the previous finding, under the treatment with SFN, most mitochondria were observed to be smaller, more condensed and positioned perinuclearly; a small number of cells displayed mitochondrial networks with a hyperfused phenotype (**Figure 4. 4A**). From ImageJ analysis, SFN reduced the network size to less than a third of the control ( $30.6 \pm 1.8\%$ ). The presence of NAC restored the morphology and the mitochondrial network size to baseline levels (**Figure 4. 4B**).

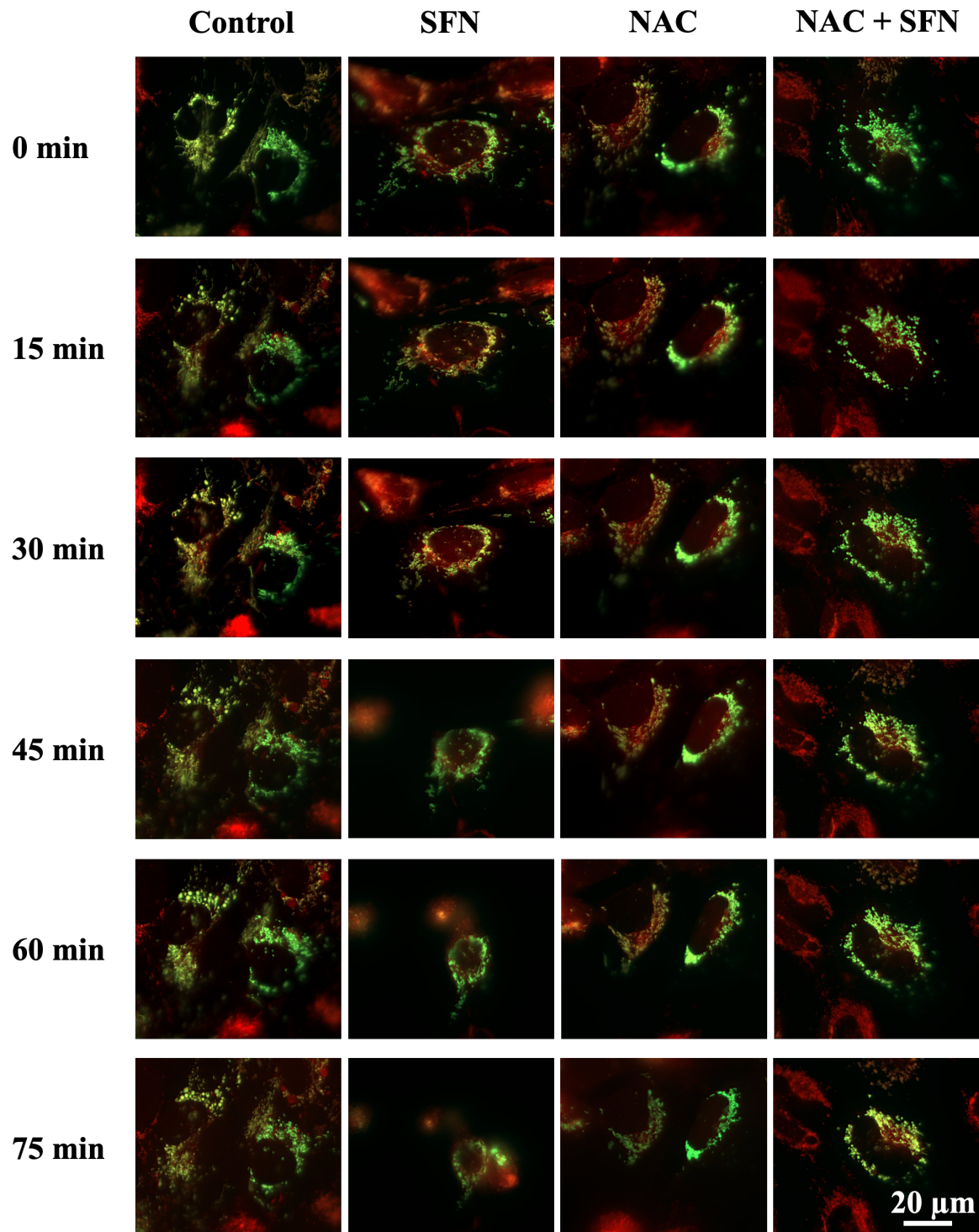
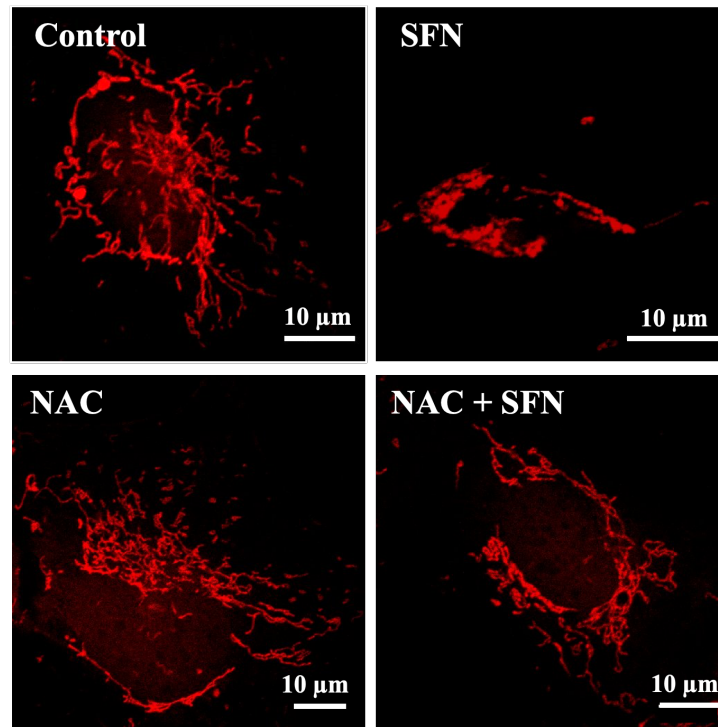


**Figure 4. 3: NAC protects SFN-induced mitochondrial network shrinkage over time.**

Mitochondria in FHL124 cells were labelled with GFP (green) by transfection and MitoTracker Red CMXRos (red) by direct staining. FHL124 cells were either maintained in serum-free (control) EMEM or EMEM supplemented with 1 mM NAC. Following a period of 1 hour, half the preparations were treated with SFN (final concentration 50  $\mu$ M) while the other half did not receive SFN treatment. Their mitochondria were visualised using widefield microscopy over a duration of 75 minutes after the addition of SFN.

A



B

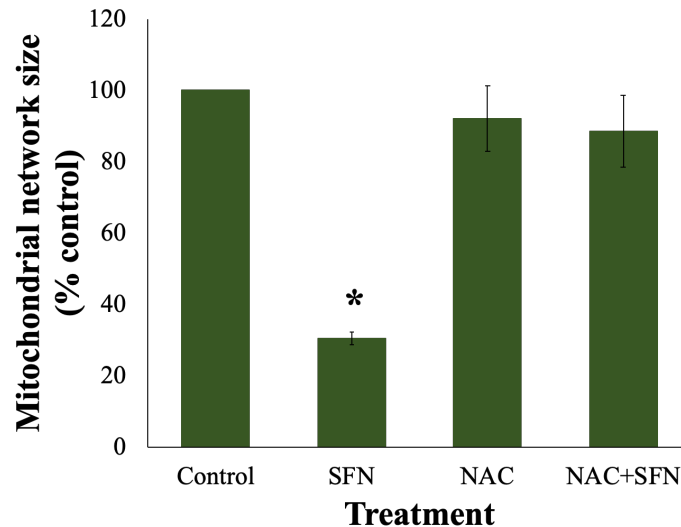


**Figure 4. 4: NAC protects against mitochondrial network shrinkage caused by SFN in FHL124 cells.**

FHL124 cells were either maintained in serum-free (control) EMEM or EMEM supplemented with 1 mM NAC. Following a period of 1 hour, half the preparations were treated with SFN (final concentration 50  $\mu$ M) while the other half did not receive SFN treatment. Cells were treated for 4 hours after the addition of SFN. A) Representative images of mitochondria labelled with 100 nM MitoTracker CMXRos RED using confocal microscopy and B) quantitative data pooled from four separate experiments shown as mean  $\pm$  SEM (10 cells/experiment). An asterisk indicates a significant difference between the treated group and all other groups ( $p \leq 0.05$ ; ANOVA with Tukey's post hoc test).

The next feature under investigation was  $\Delta\psi_m$ . After 4 hours, 50  $\mu\text{M}$  SFN decreased the TMRE signal by approximately 20% ( $78.8 \pm 5.9\%$ ) in FHL124 cells, and NAC treatment completely protected cells from this effect induced by SFN ( $102.4 \pm 5.4\%$ ) (**Figure 4. 5**).

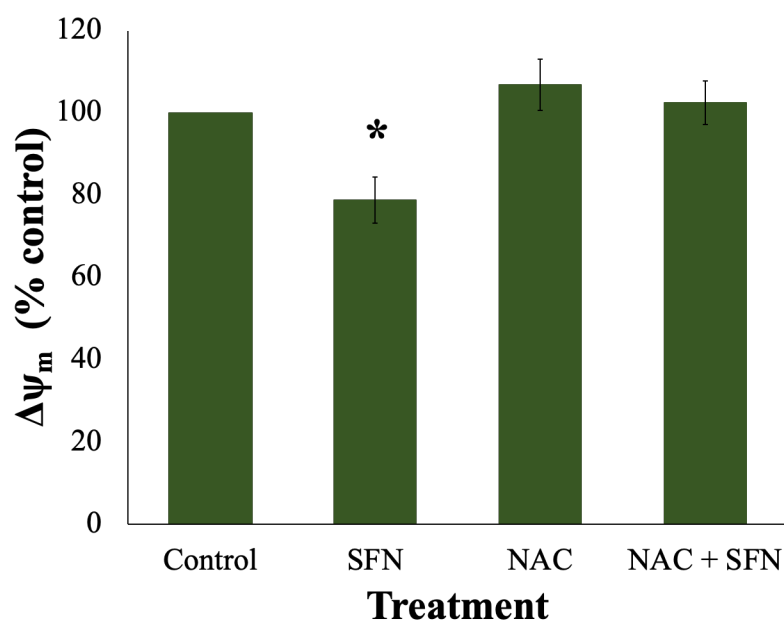


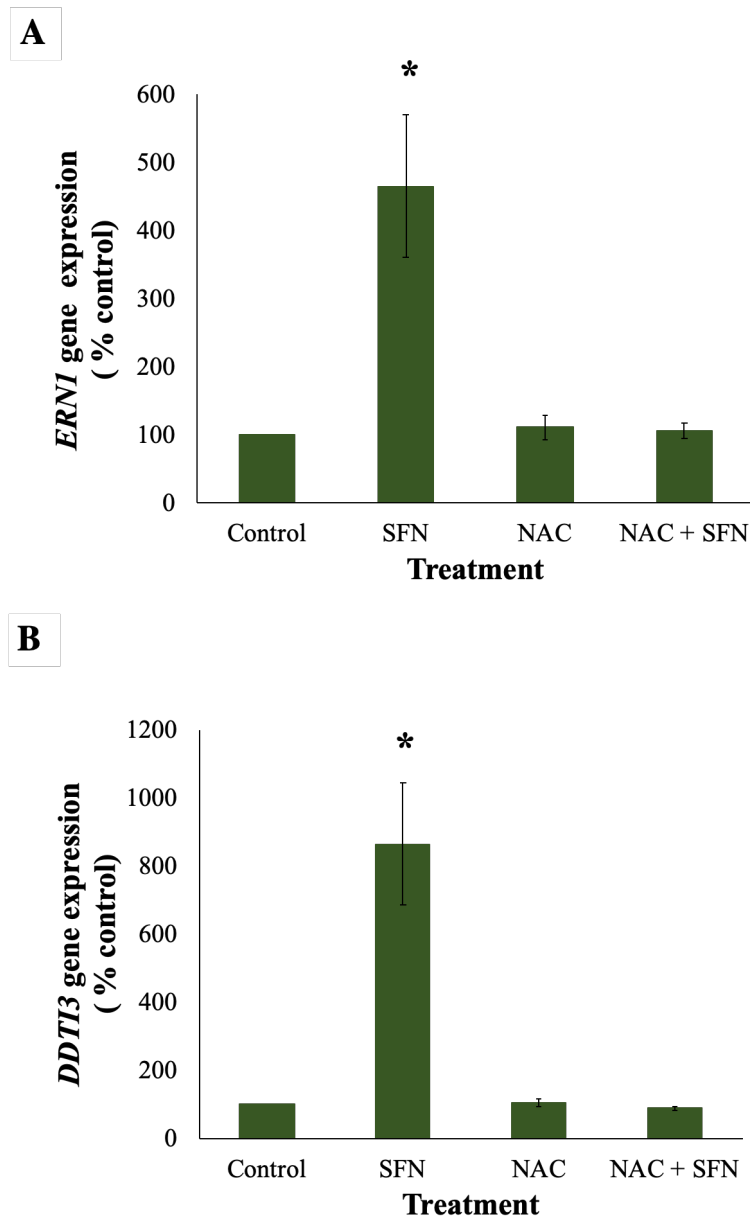
**Figure 4. 5: NAC protects cells from loss of mitochondrial membrane potential ( $\Delta\psi_m$ ) induced by SFN in FHL124 cells.**

FHL124 cells were either maintained in serum-free (control) EMEM or EMEM supplemented with 1 mM NAC. Following a period of 1 hour, half the preparations were treated with SFN (final concentration 50  $\mu\text{M}$ ) while the other half did not receive SFN treatment. After 4 hours, mitochondrial membrane potential was measured using TMRE signal at fluorescence excitation/emission wavelengths of 549/575 nm. Quantitative data are shown as mean  $\pm$  SEM (n=4). An asterisk indicates a significant difference between the treated group and all other groups ( $p \leq 0.05$ ; ANOVA with Tukey's post hoc test).

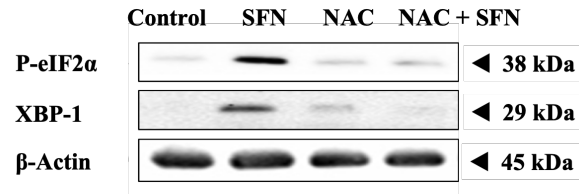
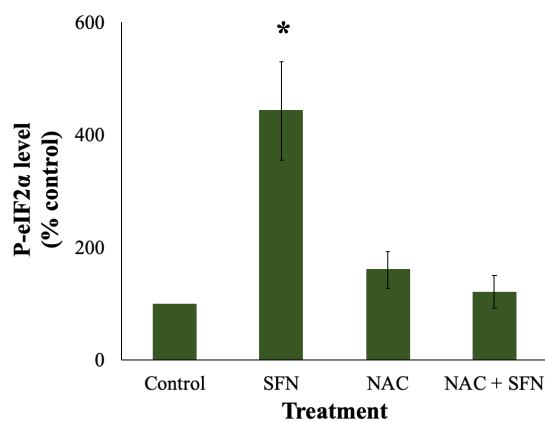
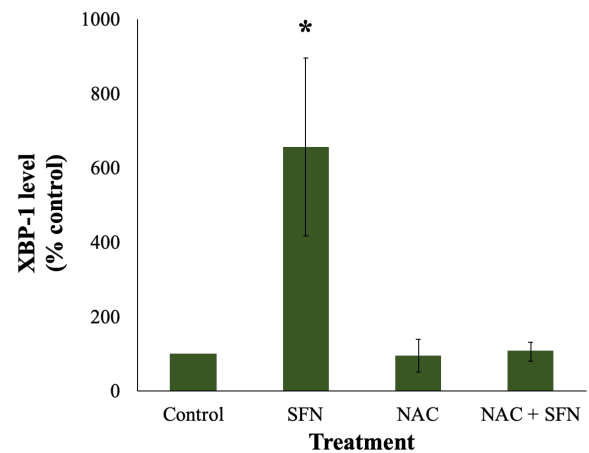
#### 4.3.4 NAC prevents SFN-induced ERS responses in FHL124 cells.

ERS is mediated by three signalling pathways: IRE1, PERK and ATF6. In FHL124 cells, after 18 hours, there was increased expression of ERS genes *ERN1*, encoding IRE1, and *DDIT3*, encoding CHOP – a downstream signal of PERK, by approximately  $465.1 \pm 105.1\%$  and  $863.8 \pm 179.1\%$ , respectively (**Figure 4. 6**) The protein levels of two ERS markers: P-eiF2 $\alpha$  and XBP-1 were also elevated by  $175.3\% \pm 87.6\%$  and  $657.2\% \pm 416.5\%$ , respectively, relative to the control group, (**Figure 4. 7**). The level of ATF6 transcriptional activity increased by 890.9

$\pm 347.7\%$  at 6-hour post treatment (**Figure 4. 8**). Induced gene expression, elevated protein levels associated with the IRE1 and PERK pathways and increased ATF6 activity by SFN were significantly inhibited by NAC treatment in FHL124 cells.



**Figure 4. 6: NAC prevents upregulation of ERS gene markers by SFN in FHL124 cells.** FHL124 cells were either maintained in serum-free (control) EMEM or EMEM supplemented with 1 mM NAC. Following a period of 1 hour, half the preparations were treated with SFN (final concentration 50  $\mu$ M) while the other half did not receive SFN treatment. After 18 hours, gene expression was measured using Taqman qRT-PCR. A) Gene expression of *ERN1*, encoding IRE1; B) Gene expression of *DDTI3*, encoding CHOP. Quantitative data are shown as mean  $\pm$  SEM (n=4). An asterisk indicates a significant difference between the treated group and all other groups ( $p \leq 0.05$ ; ANOVA with Tukey's post hoc test).

**A****B****C**

**Figure 4. 7: NAC prevents elevation of ERS protein markers by SFN in FHL124 cells.**

FHL124 cells were either maintained in serum-free (control) EMEM or EMEM supplemented with 1 mM NAC. Following a period of 1 hour, half the preparations were treated with SFN (final concentration 50  $\mu$ M) while the other half did not receive SFN treatment. After 18 hours, protein level was measured using Western blot. A) Protein levels of P-eIF2 $\alpha$  and XBP-1 were assessed via Western blot; B) Quantification of Western blot data of P-eIF2 $\alpha$  normalised against  $\beta$ -Actin using ImageJ; C) Quantification of Western blot data of XBP-1 normalised against  $\beta$ -Actin using ImageJ. Quantitative data are shown as mean  $\pm$  SEM (n=3). An asterisk indicates a significant difference between the treated group and all other groups ( $p \leq 0.05$ ; ANOVA with Tukey's post hoc test).

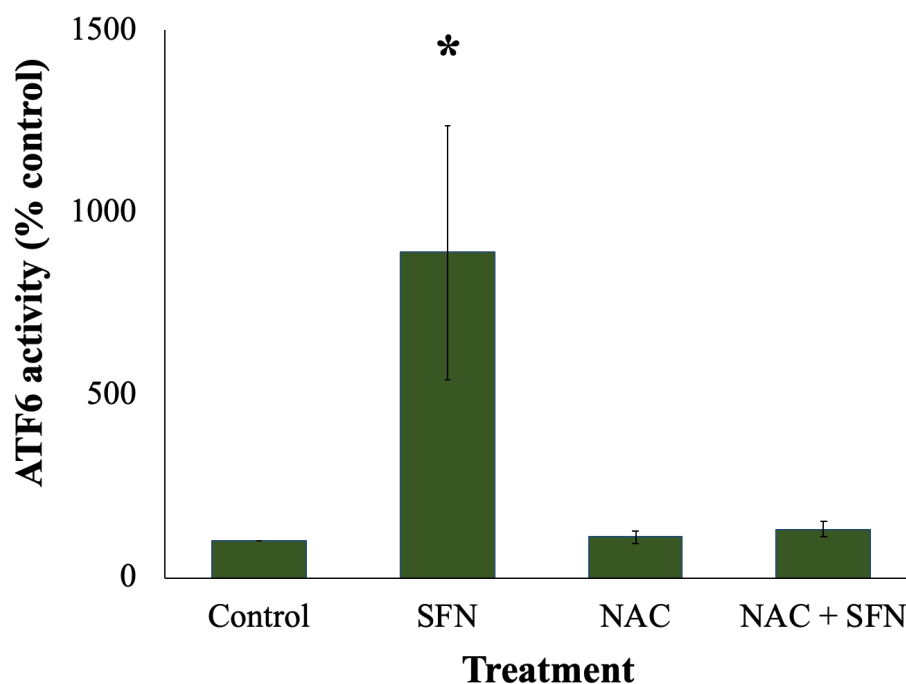


**Figure 4. 8: NAC prevents elevation in ATF6 transcriptional activity caused by SFN in FHL124 cells.**

FHL124 cells were either maintained in serum-free (control) EMEM or EMEM supplemented with 1 mM NAC. Following a period of 1 hour, half the preparations were treated with SFN (final concentration 50  $\mu$ M) while the other half did not receive SFN treatment. After 6 hours, the transcriptional activity of ATF6 was measured using a dual-luciferase reporter assay. Data are shown as mean  $\pm$  SEM (n=4). An asterisk indicates a significant difference between the treated group and all other groups ( $p \leq 0.05$ ; ANOVA with Tukey's post hoc test).

#### **4.3.5 NAC prevents DNA damage induced by SFN in FHL124 cells.**

FHL124 cells were treated with 50  $\mu$ M SFN for 6 hours and were stained for  $\gamma$ -H2AX foci and DAPI (**Figure 4. 9**).  $\gamma$ -H2AX foci were increased by  $440.4 \pm 78.7\%$  relative to control. Treatment of 1 mM NAC significantly lowered this but did not completely bring the number of foci to the baseline levels,  $201.7 \pm 33.5\%$  relative to the baseline. There was no significant difference between the control and NAC + SFN groups.

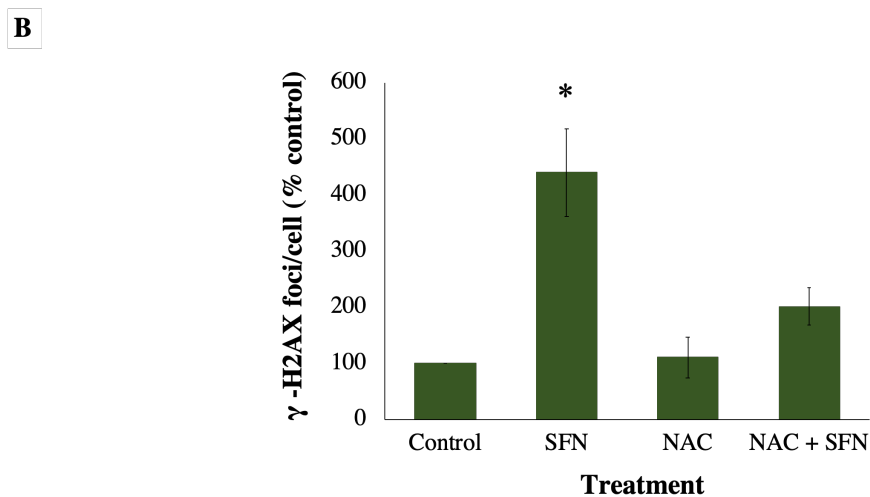
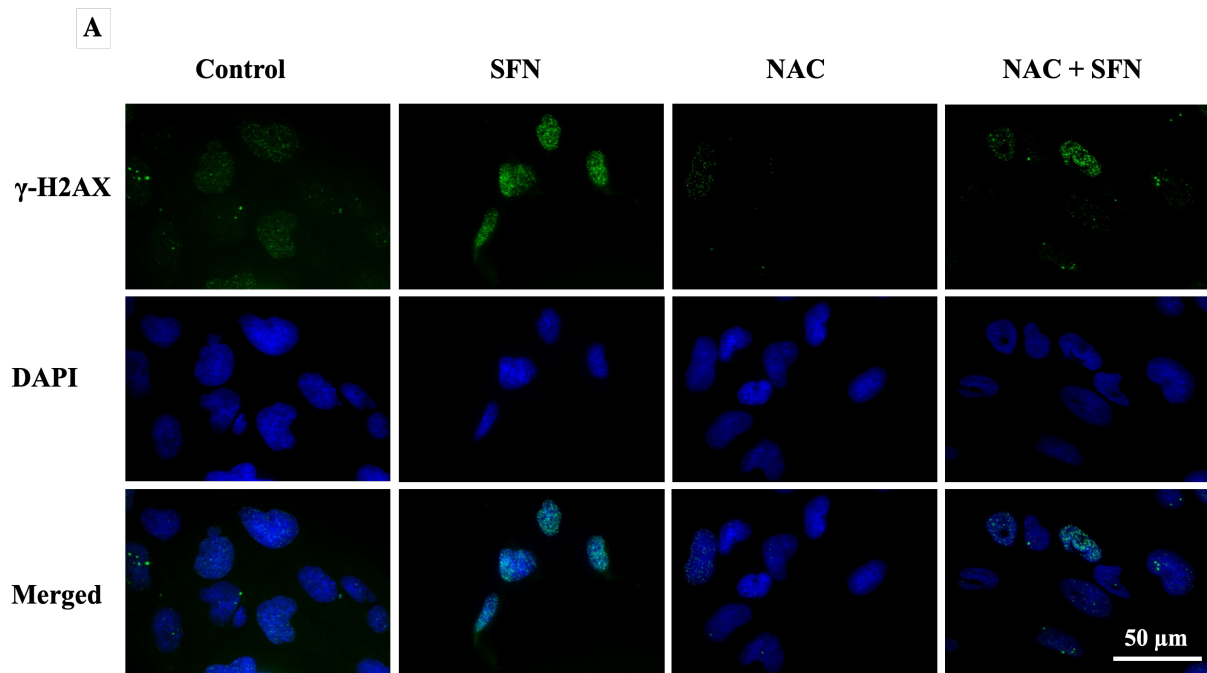


**Figure 4. 9: NAC prevents DNA double-strand breaks induced by SFN in FHL124 cells.**

FHL124 cells were either maintained in serum-free (control) EMEM or EMEM supplemented with 1 mM NAC. Following a period of 1 hour, half the preparations were treated with SFN (final concentration 50  $\mu$ M) while the other half did not receive SFN treatment. After 6 hour,  $\gamma$ -H2AX foci were measured using wide-field microscopy. (A) Representative images (green –  $\gamma$ -H2AX, blue – DAPI, merged –  $\gamma$ -H2AX and DAPI) and (B) quantitative data are shown as mean  $\pm$  SEM (n=3). An asterisk indicates a significant difference between the treated group and all other groups ( $p \leq 0.05$ ; ANOVA with Tukey’s post hoc test).

### 4.3.6 NAC prevents autophagy induced by SFN in FHL124 cells.

Upon autophagy, a cytosolic form of LC3 – LC3-I, is conjugated to phosphatidylethanolamine to form LC3-phosphatidylethanolamine conjugate or LC3-II, which is then recruited to autophagosomal membranes. In FHL124 cells, to examine autophagy, immunoblotting of microtubule-associated protein light chain LC3 was used (**Figure 4. 10A**). No change in LC3-I was detected, but at 18 hours post treatment with 50  $\mu$ M SFN the level of LC3-II significantly increased by  $219.9 \pm 8.8\%$  in FHL124 cells, indicating elevated autophagy. This increase was completely prevented in the presence of 1 mM NAC ( $81.3 \pm 5.2\%$ ) (**Figure 4. 10B**).

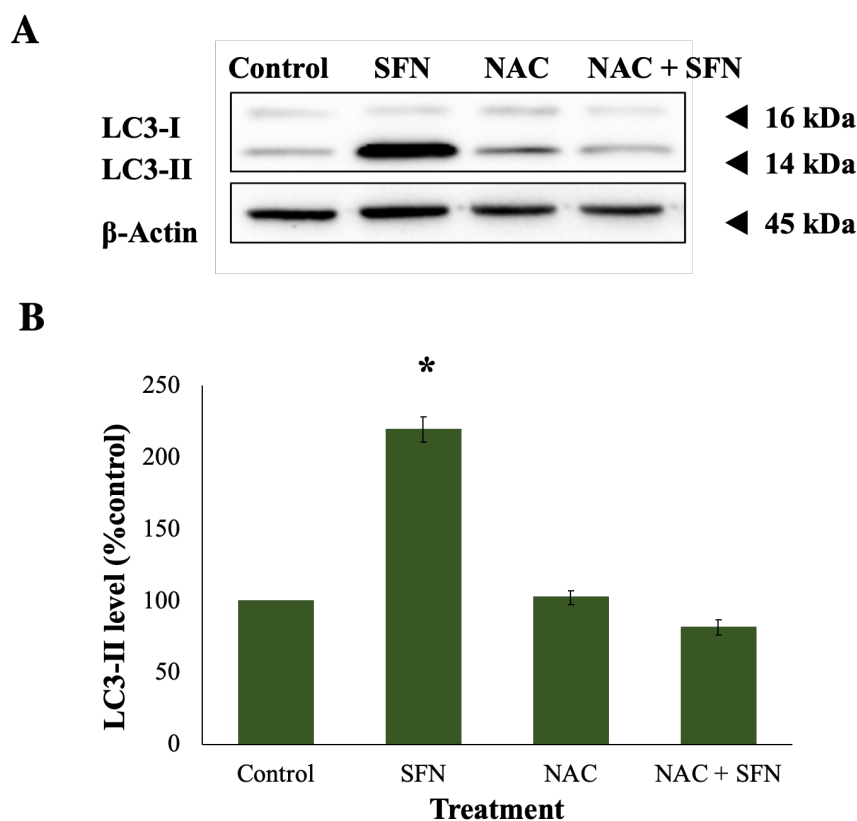


**Figure 4. 10: NAC protects cells from autophagy induced by SFN in FHL124 cells.**

FHL124 cells were either maintained in serum-free (control) EMEM or EMEM supplemented with 1 mM NAC. Following a period of 1 hour, half the preparations were treated with SFN (final concentration 50  $\mu$ M) while the other half did not receive SFN treatment. After 18 hours, LC3-I and LC3-II protein levels were measured using Western blot. A) Representative blot and B) Quantitative data of LC3-II normalised against  $\beta$ -Actin using ImageJ. Quantitative data are pooled from four separate experiments for FHL124 cells. Data are presented as mean  $\pm$  SEM (n = 4). An asterisk indicates a significant difference between the treated group and all other groups ( $p \leq 0.05$ ; ANOVA with Tukey's post hoc test).

#### **4.3.7 NAC protects human lens epithelium from SFN-induced cytotoxicity.**

Whole capsulorhexis samples were either maintained in serum-free (control) EMEM or EMEM supplemented with 1 mM NAC. Following a period of 1 hour, half the preparations were treated with SFN (final concentration 50  $\mu$ M) while the other half did not receive SFN treatment. Tissue samples were then incubated for 24 hours. Human lens epithelium tissues also presented similar damaged features induced by 50  $\mu$ M SFN: from a single layer of cuboidal epithelial cells positioned next to each other to separated, swollen, round cells (**Figure 4. 11A**). SFN also increased LDH secretion nearly twofold in the human lens epithelium (**Figure 4. 11B**). The use of NAC averted all these detrimental effects induced by SFN on the human lens epithelium.

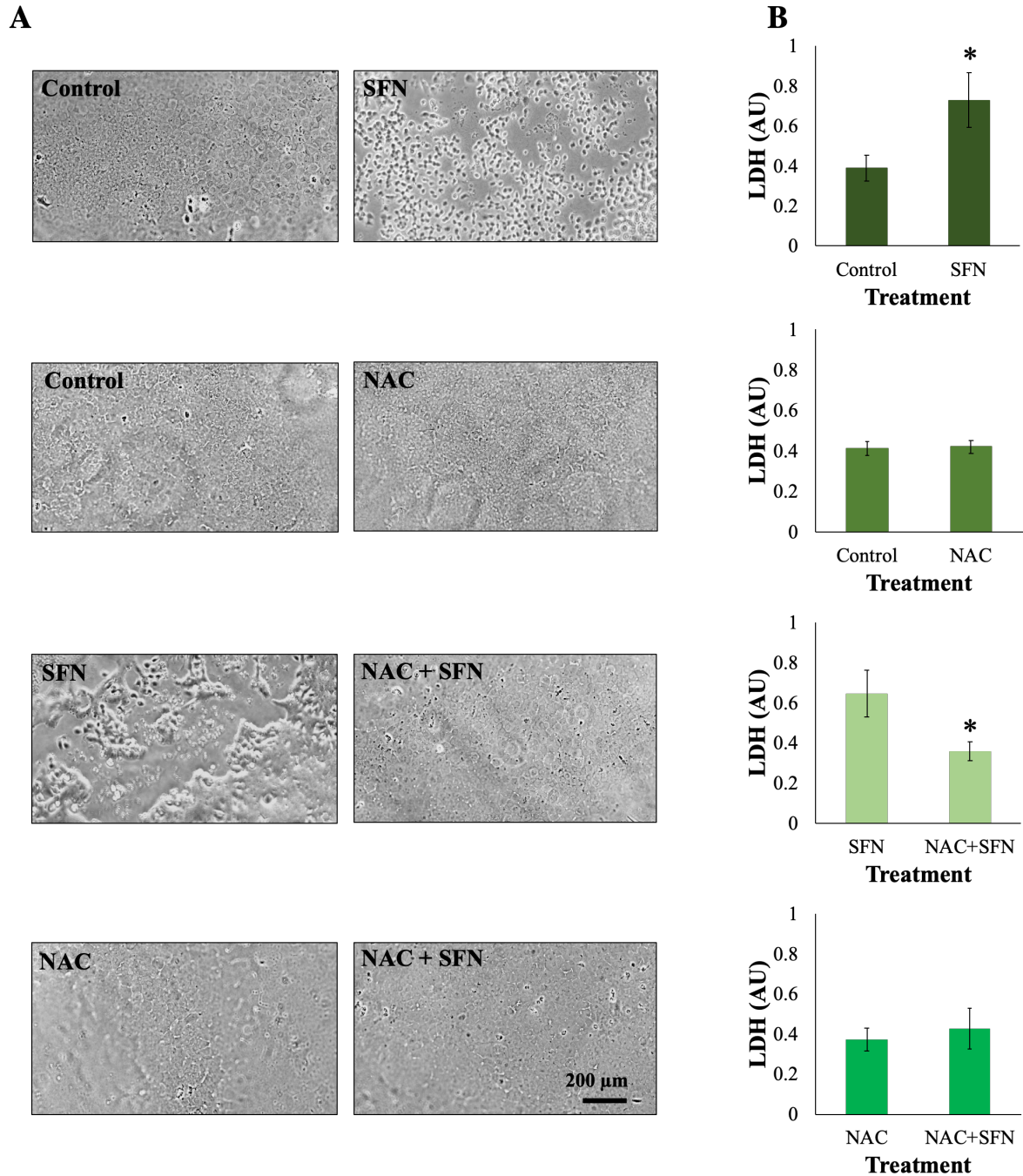


**Figure 4. 11: NAC protects cells from cell death induced by SFN in human lens epithelium.**

Whole capsulorhexis samples were either maintained in serum-free (control) EMEM or EMEM supplemented with 1 mM NAC. Following a period of 1 hour, half the preparations were treated with SFN (final concentration 50  $\mu$ M) while the other half did not receive SFN treatment. Tissue samples were treated for 24 hours after the addition of SFN. A) Cell morphology was observed using phase-contrast microscopy; B) Cytotoxicity was assessed using an LDH assay. Quantitative data are pooled from four match-paired human epithelium tissues. Data are shown as mean  $\pm$  SEM. An asterisk indicates a significant difference between the second group and the first group for each pair of treatments ( $p \leq 0.05$ ; paired Student's *t*-test).

#### **4.3.8 NAC prevents ERS induced by SFN in human lens epithelium.**

In human lens epithelium tissues, protein levels of P-eiF2 $\alpha$  were assessed in matched pair experiments. After 24 hours, SFN increased levels of P-eiF2 $\alpha$  by more than fivefold relative to the control and the use of 1 mM NAC prevented the elevation (**Figure 4. 12**).

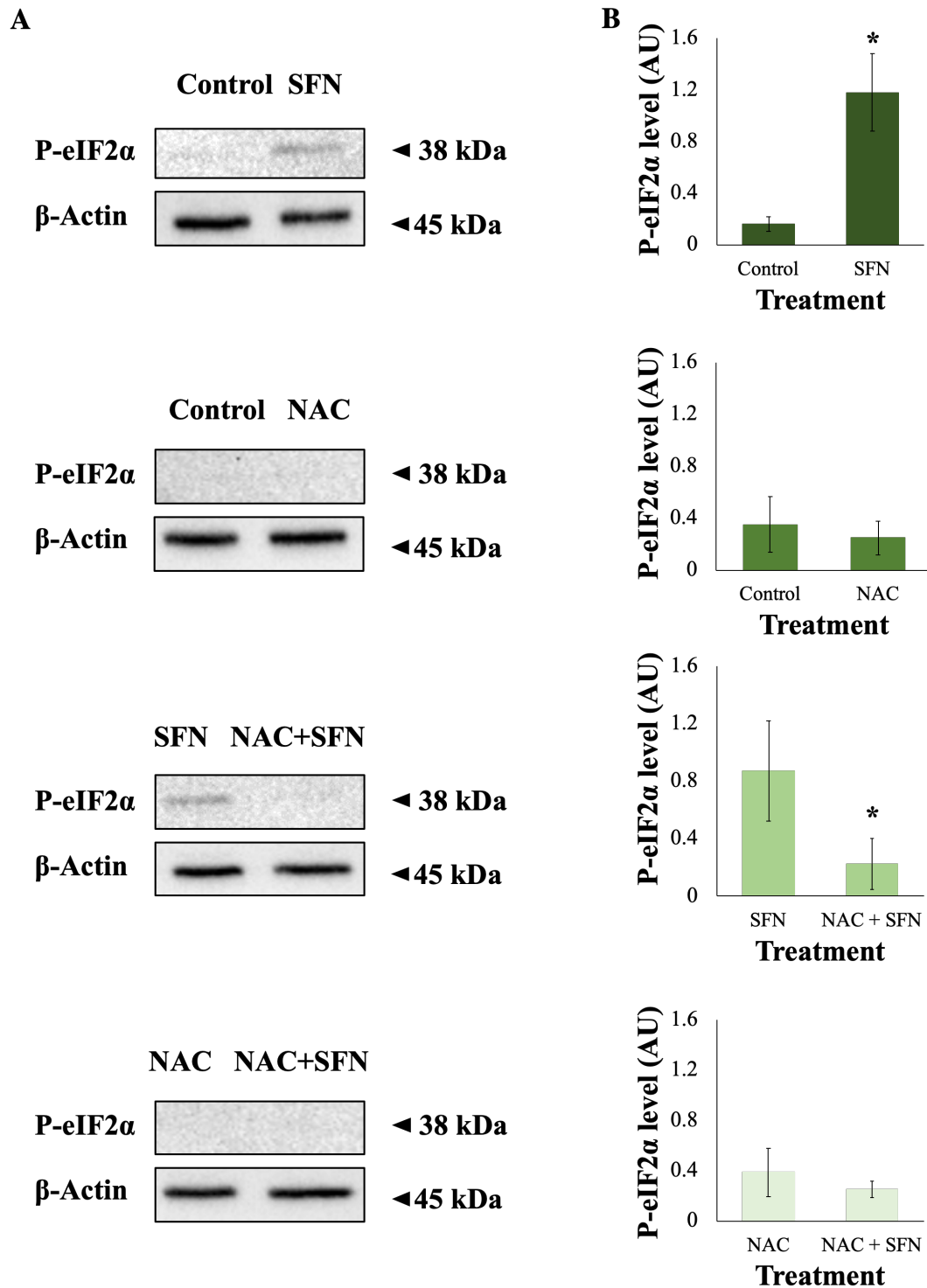


**Figure 4. 12: NAC prevents ERS induced by SFN in human lens epithelium.**

Whole capsulorhexis samples were either maintained in serum-free (control) EMEM or EMEM supplemented with 1 mM NAC. Following a period of 1 hour, half the preparations were treated with SFN (final concentration 50  $\mu$ M) while the other half did not receive SFN treatment. After 24 hours, the protein level of P-eIF2 $\alpha$  was assessed using Western blot. A) Representative blot and B) quantification of Western blot data normalised against  $\beta$ -Actin. Quantitative data are pooled from four match-paired human epithelium tissues. Data are shown as mean  $\pm$  SEM. An asterisk indicates a significant difference between the second group and the first group for each pair of treatments ( $p \leq 0.05$ ; paired Student's *t*-test).

#### **4.3.9 NAC prevents autophagy induced by SFN in human lens epithelium.**

In human lens epithelium, immunoblotting of LC3 was also used to assess autophagy (**Figure 4. 13A**). 100  $\mu$ M SFN significantly induced LC3 elevation after 24 hours (lower concentrations of SFN and shorter treatments did not raise the level of LC3 – data not shown). The treatment of 1 mM NAC also prevented the elevation of LC3 protein levels in human lens epithelium (**Figure 4. 13B**).

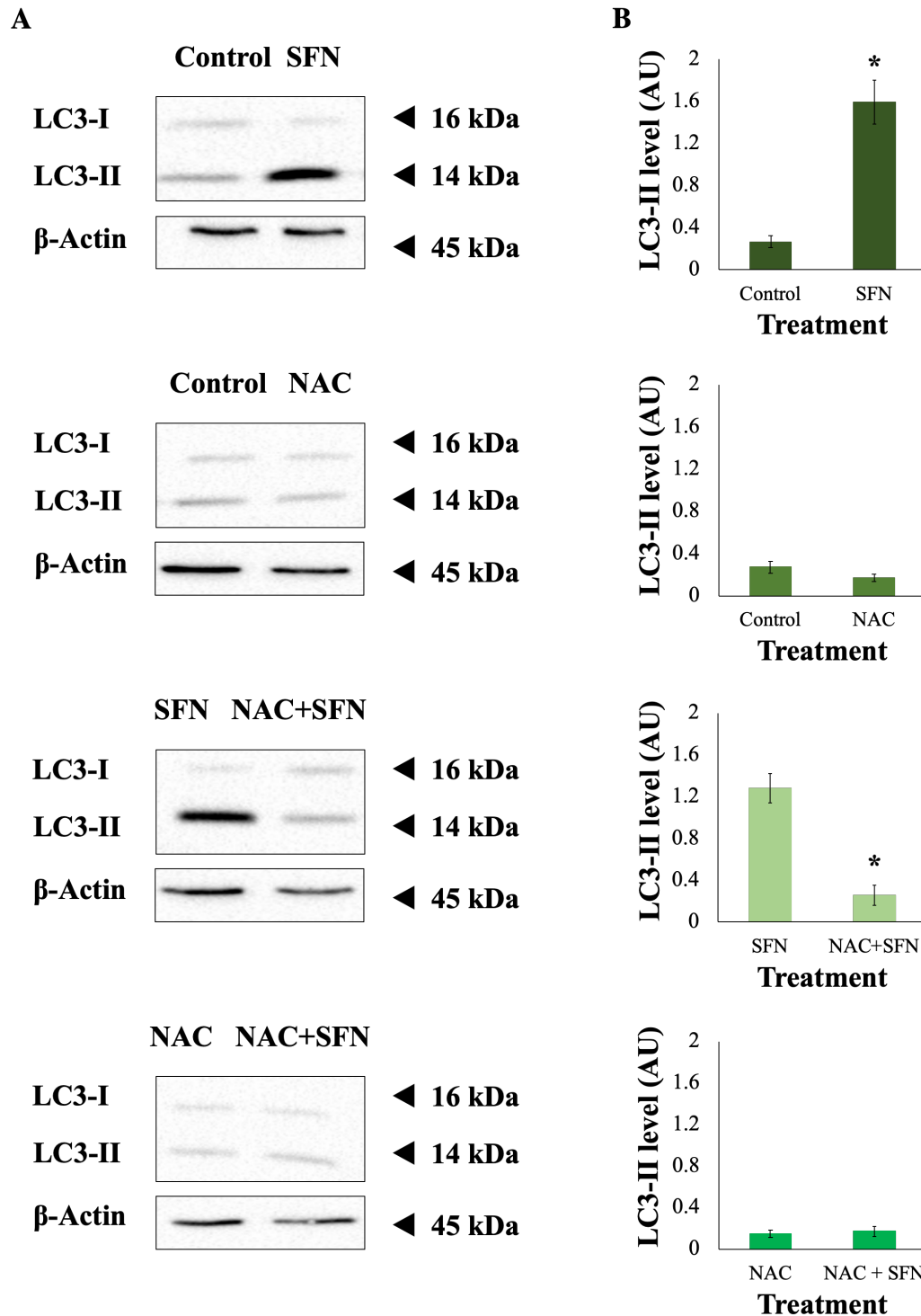


**Figure 4.13: NAC protects cells from autophagy induced by SFN in human lens epithelium.**

Whole capsulorhexis samples were maintained under the control condition (serum-free EMEM), treated with 1mM NAC, 100  $\mu$ M SFN or NAC + SFN. For the co-treatment condition (NAC + SFN), NAC was added into the culture medium 1 hour before the addition of SFN into the same culture medium. After 24 hours, LC3-I and LC3-II levels were detected using Western blot. A) Representative blots and B) Quantitative data of LC3-II normalised against  $\beta$ -Actin using ImageJ. Quantitative data are pooled from five match-paired human epithelium tissues. Data are presented as mean  $\pm$  SEM. An asterisk indicates a significant difference between the second group and the first group for each pair of treatments ( $p \leq 0.05$ ; paired Student's *t*-test).

## 4.4 Discussion

SFN is an agent that can elicit a wide spectrum of effects on cells and tissues. Therefore, it has been selectively studied in various health conditions. Previously, SFN has been reported to have therapeutic potential to manage PCO, a vision-threatening condition in the lens, via its cytotoxic mode of action. Multiple mechanisms have been discussed to mediate SFN cytotoxicity. In various cancer cells and tumour types, ROS were reported to orchestrate the process (Sestili & Fimognari, 2015). Despite the exhaustive knowledge of SFN cytotoxicity in cancer models, its understanding in non-cancer models is significantly lacking. In this current study, ROS elevation following SFN treatment was reported to be responsible for mitochondrial dysfunction, ERS, DNA damage, and autophagy, which collectively led to cell death. Therefore, the findings demonstrated here support the hypothesis that ROS plays a key role in SFN-mediated stress and death in human lens cells.

Both NAC and sodium pyruvate protected human lens epithelial cells from cell loss induced by SFN. The protection afforded by sodium pyruvate is convincingly owing to its ability to directly alleviate ROS levels (Guarino et al., 2019; X. Wang et al., 2007), whereas that afforded by NAC could be argued due to 1) GSH replenishment, rather than due to direct ROS scavenging, and 2) direct conjugation of NAC with SFN in the medium. To address the first point, NAC is known to exhibit its protection against ROS and oxidative stress in a GSH-independent manner on many occasions (**Figure 4. 14**), as extensively reviewed by Pedre and co-authors. (Pedre, Barayeu, Ezerina, & Dick, 2021). The *de novo* synthesis of GSH is limited by the availability of cysteine (Meister, 1995). As a membrane-permeable cysteine precursor, NAC can rapidly release cysteine for GSH synthesis upon cellular entry. NAC-derived cysteine can subsequently contribute to GSH synthesis. Nevertheless, NAC-derived cysteine can also

promote the intracellular production of H<sub>2</sub>S and sulfane sulfur species that all have ROS scavenging and antioxidant properties (Ezerina et al., 2018; Q. Xiao, Ying, Xiang, & Zhang, 2018). Moreover, in GSH synthesis-arrested glial cells, NAC at concentrations similar to that used in the current study still sufficiently protected against glutamate-induced cytotoxicity, suggesting that the protective effects of NAC at these concentrations can be independent of its pro-GSH properties (Han et al., 1997). Hence, the antioxidant properties of NAC are multifaceted and not solely GSH-related.

Regarding the second point on the conjugation of NAC with SFN in the medium, as a reactive nucleophile, NAC, can react non-enzymatically with SFN, an electrophile, in the medium. However, the presence of NAC at low millimolar concentrations used in this study should not affect the uptake of SFN. Mi and co-authors reported that at the molar ratio of NAC:SFN as 500:1 (5 mM vs 10  $\mu$ M) NAC treatment inhibited the uptake of SFN by 8-fold (Mi, Sirajuddin, Gan, & Wang, 2010). In the current study, if 1 mM of NAC is considered, the molar ratio of NAC:SFN is only 20:1, suggesting that 1 mM NAC treatment will have negligible or no impact on SFN uptake. Moreover, 1 mM NAC is not even the lowest concentration that can provide complete protection from SFN-induced loss of cell viability. Therefore, extracellular conjugation should be negligible and should not interfere with the cellular uptake of SFN. Taken together, mounting evidence from previous studies consolidates the subsequent application of NAC for the rest of this current study to investigate the role of ROS in SFN-induced cytotoxicity.

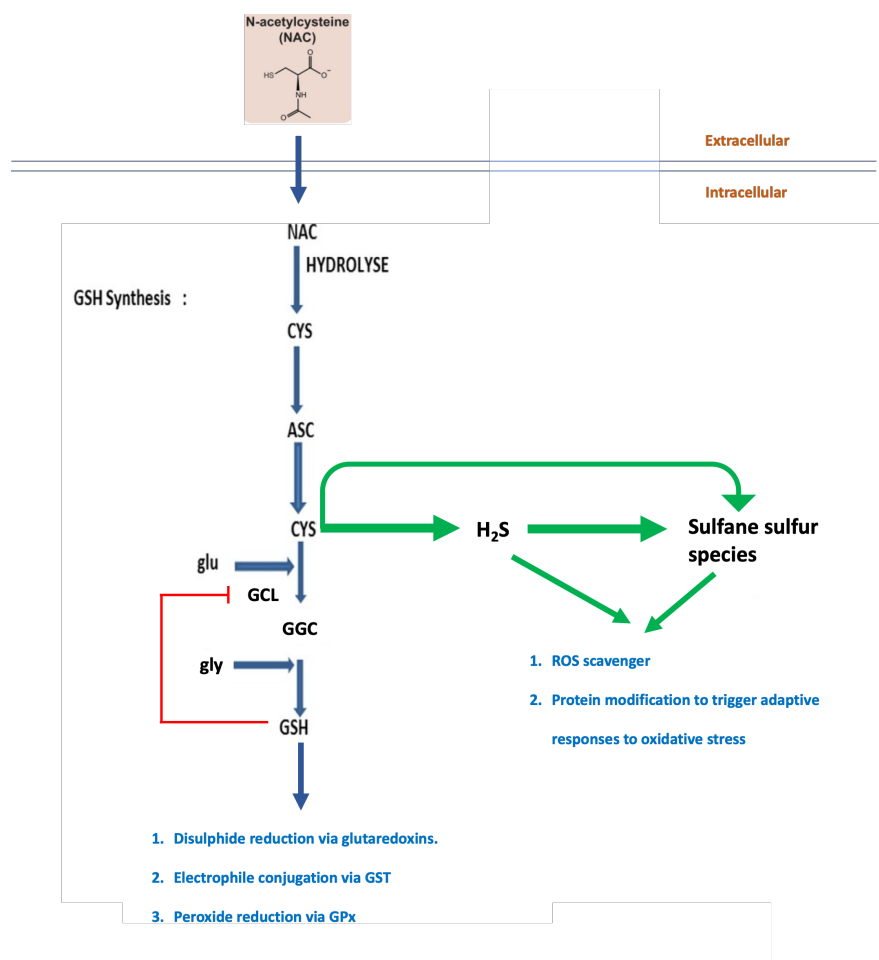


**Figure 4. 14: NAC displays antioxidant properties in different ways.**

NAC acts as a GSH precursor and replenishes GSH levels, supports enzymatic disulfide reduction by glutaredoxins, electrophile detoxification by GST, peroxide scavenger by GPx. NAC also contributes to the production of H<sub>2</sub>S and sulfane sulfur species, which can act as direct radical scavengers and modify proteins to induce stress-adaptive cellular responses. Adapted and modified from “The mechanism of action of N-acetylcysteine (NAC): The emerging role of H<sub>2</sub>S and sulfane sulfur species” by B. Pedre and co-authors, 2021, *Pharmacology & Therapeutics*, 228, 107930. Copyright 2021 by Elsevier Inc.

SFN reduced cell viability and increased cellular damage in both FHL124 cells and human lens epithelium tissues. The treatment with 1 mM NAC completely prevented the deleterious effects of SFN. The present results broadly support the work of other studies in several cancer cell lines. The overexpression of catalase, an endogenous antioxidant, or the addition of NAC or another ROS inhibitor – (2R, 4R)-4-aminopyrrolidine-2,4-dicarboxylate (ADPC) – was shown to prevent SFN-induced cell cycle arrest or cell death (Singh *et al.*, 2005; Shen *et al.*, 2006; Xiao, *et al.*, 2009). These results indicate that ROS mediates SFN-induced cell death.

Before cell death, 50  $\mu$ M SFN was also found to elicit a range of cellular events, including disrupting the mitochondrial network and mitochondrial membrane potential, damaging DNA integrity, promoting ERS, and increasing autophagy flux in FHL124 cells. Some of the cellular responses, such as cell death, ERS and autophagy, were also mirrored in human epithelium tissues. The treatment with 1 mM NAC, a ROS scavenger, completely protected FHL124 cells and human lens epithelium against SFN-induced cytotoxicity in both FHL124 cells and human lens epithelium.

Prolonged oxidative stress has been shown in different cell lines to induce irreversible changes in mitochondrial networks, whereby interconnected tubular mitochondrial networks are reorganised as small puncta and rods due to widespread fission, resulting in mitochondrial fragmentation (Hung et al., 2018). In fibroblasts, H<sub>2</sub>O<sub>2</sub> treatments impaired the mitochondrial fusion machinery and induced mitochondrial fragmentation, and similar to the current study, impaired mitochondrial networks induced by ROS was prevented by the addition of an antioxidant (Rakovic et al., 2011). Combined together, these *in vitro* findings from the current and Rakovic et al studies reflect what Breckwoldt and co-authors found in their *in vivo* study. The authors discovered a link between oxidation of the mitochondrial matrix environment and mitochondrial tubule shortening using a novel optical approach to measure fast redox signals in transgenic mice (Breckwoldt et al., 2014).

The impacts of SFN-induced ROS on mitochondrial dynamics could be linked to ROS-induced PTMs (Willems et al., 2015). Mitochondrial fusion is usually associated with mitofusin 1/2 (Mfn 1/2) and optic atrophy 1 (Opa1) proteins, whereas mitochondrial fission is with dynamin-related proteins (Drp) and fission 1 (Fis1) proteins. The fusion/fission machinery, however,

employs many more molecules. Mounting evidence has reported that free radicals can induce redox-sensitive PTMs on Drp, Fis1, Opa1, Mfn1/2 and other associated proteins, which consequently promote or demote their activity. It also appears that ROS-associated PTMs favour mitochondrial fission, which may explain the observed mitochondrial fragmentation and shrinkage in the current study.

In terms of ROS-dependent SFN impacts on  $\Delta\psi_m$  in FHL124 cells, a similar finding was reported in human leukaemia cells. In that study, SFN caused mitochondria-dependent cell death through a mechanism associated with increased  $\Delta\psi_m$ ; the addition of NAC also prevented disrupted  $\Delta\psi_m$  and subsequent cell death (W. Y. Choi et al., 2008). Perturbations in  $\Delta\psi_m$  have also been linked with ROS. Mitochondrial permeability transition pores are considered the major ROS target inside mitochondria. Following increases in ROS levels and ROS-induced PTMs on constituent proteins, the mitochondrial permeability transition pores enter a high-conductance state that immediately leads to depolarisation (loss) of  $\Delta\psi_m$  and osmotic swelling of the mitochondrial matrix (Fulda, Galluzzi, & Kroemer, 2010; Zoratti & Szabo, 1995). Using fine kinetics analysis, Zorov and co-authors illustrated a positive correlation between ROS and  $\Delta\psi_m$  via a phenomenon named “ROS-induced ROS release” (Zorov, Filburn, Klotz, Zweier, & Sollott, 2000). The authors reported that initial slow rises in ROS levels could further depolarise  $\Delta\psi$ , which could subsequently cause more ROS to be produced.

ERS is a response to the accumulation of misfolded proteins in the ER. The current study shows that SFN activated all three branches of ERS including IRE1, PERK and ATF6 in a ROS-dependent manner. Previous studies reported the induction of ERS by SFN (H. Liu et al., 2017; Zou et al., 2017) but this current study provides the first evidence to present ROS as a cause of this process. The ER is the largest intracellular production site of  $H_2O_2$ , which is generated as

a by-product of the oxidative protein folding process (Bhattacharai et al., 2021). To maintain ER homeostasis, ROS levels are tightly regulated in this organelle. Increased ROS levels have been shown to impair the folding process and disulfide bond formation, both of which can increase the misfolded protein load and effectively trigger the UPR/ERS (Chong, Shastri, & Eri, 2017). Due to the close biochemical and structural connection between the mitochondria and the ER, possible increases in mitochondrial ROS from dysregulated  $\Delta\psi_m$  and collapsed mitochondrial networks could also pose detrimental impacts to the ER (Bhattacharai et al., 2021).

The findings of this study indicate that ROS is responsible for SFN-induced DNA double-strand breaks. One of the most sensitive cellular targets of ROS is nuclear DNA. A prominent mechanism of oxidative DNA damage is via the interaction of  $H_2O_2$  with metal ions on, or near to DNA to produce  $\bullet OH$  radicals. These highly reactive radicals subsequently attack DNA bases, causing base damage of deoxyribose residues to produce strand breaks (Marnett, 2000). In agreement with the current finding, similar observations were also recorded in umbilical vein endothelial cells and oesophageal cancer cells. Experimental conditions capable of preventing ROS formation successfully prevented nuclear DNA damage and DNA damage responses induced by SFN (Sestili et al., 2010; Zheng et al., 2020).

The current study suggests that SFN-induced autophagy in human lens cells is dependent on ROS, which concurs with other work in colon, prostate and oesophageal cancer cells (Naumann et al., 2011; D. Xiao et al., 2009; Zheng et al., 2020). ROS have been extensively reported as an early inducer of autophagy following nutrient deprivation (Filomeni, Desideri, Cardaci, Rotilio, & Ciriolo, 2010). Also, a large amount of data has converged to state that ROS, specifically those originating from mitochondria, are required for autophagy induction (Murphy, 2009; Scherz-Shouval & Elazar, 2007). At least two separate PTM-related

mechanisms can orchestrate the crosstalk between autophagy and oxidative stress (Filomeni, De Zio, & Cecconi, 2015). AMPK is a key energy sensor and a promoter of autophagy. ROS can activate AMPK by causing S-glutathionylation of its cysteine residues to subsequently facilitate autophagosome maturation. In another mechanism, ROS oxidises cysteine residue 81 of autophagy-related gene 4 (Agt4), inactivating its inhibitory effect on LC3 activity.

In summary, the present work is the first to provide compelling evidence that oxidative stress plays a key role in SFN-induced cytotoxicity in human lens cells. By increasing ROS levels, SFN impairs mitochondrial networks, diminishes  $\Delta\psi_m$ , triggers ERS, elevates DNA damage and induces autophagy, which all lead to cellular demise (**Figure 4. 15**). Having established that ROS play a key role in SFN-induced cellular responses, it is important to understand how oxidative stress results.

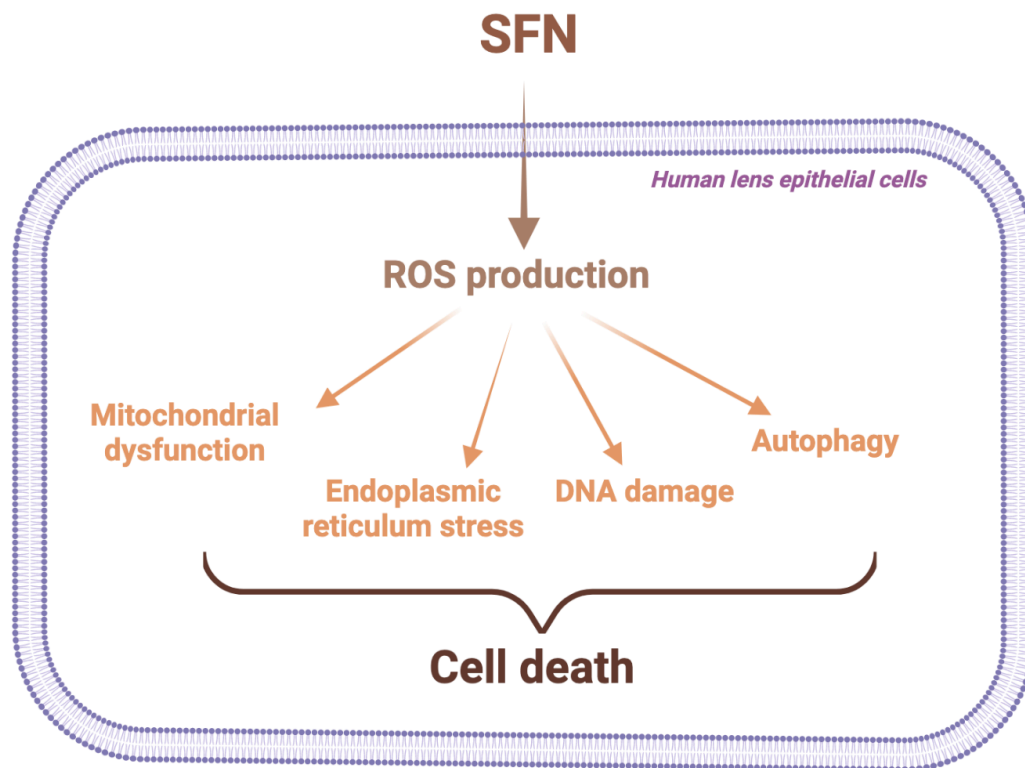


**Figure 4. 15: ROS play a pivotal role in SFN-induced cytotoxicity in human lens epithelial cells.**

# Chapter 5 Impacts of SFN on GSH Homeostasis

---

## 5.1 Introduction

ROS are any free radicals involving oxygen, including  $\bullet\text{OH}$ ,  $\text{O}_2^-$ ,  $\text{H}_2\text{O}_2$ , and  $\text{ONOO}^-$  with  $\bullet\text{OH}$  as the most reactive (Berthoud & Beyer, 2009). ROS in the lens can come from either exogenous or endogenous sources, such as UV exposure, pollution, or cellular respiration. Despite their essential functions in cell signalling, unregulated ROS can lead to oxidative stress, which is associated with metabolic disorders and ageing conditions, such as cataract (Bhatti et al., 2017; Nita & Grzybowski, 2016; Spector, 1995). In the lens, the non-enzymatic and enzymatic antioxidant defence systems help preserve lenticular physiology and lens transparency. Following ROS generation, ROS scavengers remove them, enzymatic antioxidants neutralise them, and the Nrf2-ARE pathway initiates antioxidant transcriptional responses to lessen the oxidative load and restore cellular homeostasis (Kubo, Chhunchha, Singh, Sasaki, & Singh, 2017).

SFN can influence the antioxidant defence systems via a variety of mechanisms. As one of the most potent inducers of the Nrf2-ARE pathway, SFN can indirectly upregulate and increase the activity of phase 2 antioxidant enzymes, such as HO-1, NQO1, glutathione-S-transferase (GST), and glutathione reductase (GR) (Y. Zhang et al., 1992). The redox modulation of SFN also extends to non-enzymatic antioxidants with GSH being one of the major beneficiaries. GSH levels are reported to be increased by SFN in a clinical pilot study (100  $\mu\text{mol}$  encapsulated SFN over 7 days) (Sedlak et al., 2018), in an animal study (0.5, 1.0 and 2.0 mg SFN/kg in rats for over 6 weeks) (Saleh, Mansour, Hashad, & Bakeer, 2019), or in several human cell lines ( $\leq$

5  $\mu$ M SFN) (Dias et al., 2013; Gao, Dinkova-Kostova, & Talalay, 2001; Tarozzi, Morroni, Merlicco, Hrelia, & Angeloni, 2009). On the other hand, high SFN concentrations are shown to deplete GSH levels *in vitro* (Pham, Jacobberger, Schimmer, Cao, & Gronda, 2004; Singh et al., 2005). In human osteosarcoma cells, SFN can also decrease the activity of GR and GPx involved in the GSH system (de Oliveira, Costa, Pedrosa, Pinto, Remdios, et al., 2014).

Glutathione, an anionic tripeptide (L-glutamyl-L-cysteinyl-glycine), is ubiquitously found in all mammalian tissues. This molecule exists in the thiol-reduced form (GSH) and the disulfide-oxidised form (GSSG), with GSH accounting for more than 98% of the total glutathione. In the lens, GSH is the major antioxidant (Giblin, 2000; Reddy, 1990). The concentrations of GSH in the lens are extremely high, ranging from 4 to 6 mM (Lim, Grey, Zahraei, & Donaldson, 2020). The high millimolar concentrations of GSH are sustained by a combination of four pathways: the *de novo* synthesis of GSH, the regeneration of GSH from GSSG, the uptake of GSH from outside the cells, and the GSH turnover (**Figure 5. 1**) (Lv et al., 2019). The *de novo* synthesis consists of two ATP-dependent enzymatic reactions. In the first, also rate-determining step, glutamate-cysteine ligase (GCL) catalyses the formation of gamma-glutamylcysteine (GGC) from L-glutamate and cysteine; in the second step, glutathione synthetase promotes the formation of glutathione of both forms by coupling GGC to glycine. On the other hand, the regeneration of GSH from GSSG is a one-step reaction catalysed by GR. GR restores intracellular GSH by reducing GSSG at the expense of NADPH. GSH can be quenched from the aqueous humour via Na<sup>+</sup> dependent/independent transporters or from the vitreous humour by passive transport, at least as reported in animal studies (Kannan, Yi, Zlokovic, & Kaplowitz, 1995; B. Li, Li, Donaldson, & Lim, 2010; Mackic et al., 1996; Whitson, Sell, Goodman, Monnier, & Fan, 2016). GSH export is also important for the intracellular GSH pool. Following its efflux into the extracellular space, GSH is degraded into its three constituent

amino acids by gamma-glutamyl transpeptidase (GGT) located on the apical plasma membrane of lens epithelial cells to ensure GSH turnover. Glycine, cysteine, and L-glutamate from the breakdown reaction can be then taken up and recycled to increase intracellular GSH levels via the *de novo* synthesis (Lim et al., 2020).

With such an unusually high concentration, GSH is important for maintaining the lens physiology. Multiple functions of GSH include antioxidant defence, maintenance of redox potential, detoxification of xenobiotics by forming conjugates, regulation of cell cycle progression, apoptosis, and a reservoir of cysteine (Lu, 2014). SFN is an isothiocyanate (ITC) xenobiotic, and as other ITCs, upon cellular entry by diffusion, SFN rapidly conjugates via their -N=C=S group with intracellular thiols, mainly GSH, which is the most abundant non-protein thiol (Y. Zhang, 2012). This reaction catalysed by GST marks the first step of the SFN metabolism via the mercapturic acid pathway. Subsequently, SFN-GSH is enzymatically converted to SFN-cysteine-glycine (SFN-Cys-Gly), SFN-cysteine (SFN-Cys), and ultimately SFN-NAC. The immediate interaction of SFN with GSH explains the rapid depletion of intracellular GSH levels following exposure of cells to high concentrations of SFN or other ITCs.

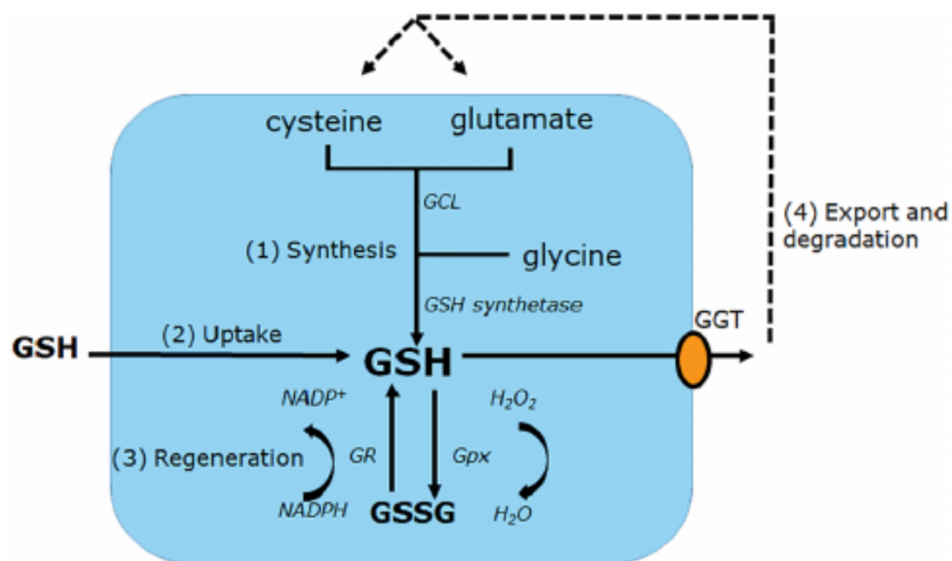


**Figure 5. 1: Maintenance of intracellular GSH levels.**

High cellular levels of GSH are maintained by a dynamic balance between four distinct pathways. **(1)** *De novo* synthesis. **(2)** Direct uptake of GSH via GSH uptake transporters. **(3)** Regeneration of GSH from oxidised glutathione (GSSG) by glutathione reductase (GR). **(4)** GSH turnover. Reprinted from “Age-dependent changes in glutathione metabolism pathways in the lens: New insights into therapeutic strategies to prevent cataract formation—A review” by JC. Lim and co-authors , 2020, *Clinical & Experimental Ophthalmology*, 48, p.1033. Copyright 2020 Royal Australian and New Zealand College of Ophthalmologists.

## 5.2 Aims

As described in the previous chapter, ROS play a key role in SFN-induced cytotoxicity in human lens cells. This prompts a question about how ROS manage to escape the tight regulation of antioxidant defence systems following SFN treatment. The antioxidant defence systems might have been overwhelmed or weakened for ROS to rampage and attack various cellular components. GSH is the major antioxidant molecule in the lens, and high concentrations of SFN has been reported to have adverse effects on GSH homeostasis. This study, therefore, aims to explore the influence of SFN on the GSH system in human lens cells and identify possible mechanisms leading to changes in this system. The hypothesis to be tested is that **SFN depletes the intracellular GSH levels.**

## 5.3 Results

### 5.3.1 SFN depletes the intracellular GSH pool in FHL124 cells.

SFN has been reported to deplete GSH in several experimental models (de Oliveira, Costa, Pedrosa, Pinto, Remdios, et al., 2014; B. R. Kim et al., 2003; Y. Zhang, 2000). The GSH/GSSG ratio was measured to investigate the impacts of SFN on GSH in human lens cells. FHL124 cells were treated with different concentrations (0 – 50  $\mu\text{M}$ ) of SFN for different durations (0 – 24 hours; **Figure 5. 2**). The absolute ratio of GSH/GSSG in the control (t=0, without SFN) was 25.3:1 (n=3), and this was converted to 100%, which serves as the baseline level. SFN treatment decreased the GSH/GSSG ratio in a concentration-dependent manner, with drastic results visible as early as 30 minutes. At the endpoint, the GSH/GSSG values in cells treated with 0 – 5  $\mu\text{M}$  SFN were comparable to the baseline level. Whereas, those in cells treated with 10 or 50  $\mu\text{M}$  remained significantly different from the control, and the treatment of 50  $\mu\text{M}$  kept the GSH/GSSG level below 10% compared to the baseline level ( $4.8 \pm 3.5\%$ ).

Moreover, also at the endpoint, the impacts of different concentrations of SFN on total glutathione, GSH and GSSG levels exhibited a unimodal pattern, with peaks or troughs around 2  $\mu\text{M}$ , although only 50  $\mu\text{M}$  SFN caused significant changes. In terms of total glutathione, GSH and GSSH levels, 50  $\mu\text{M}$  SFN caused significant reductions in total glutathione and GSH levels,  $25.9 \pm 1.9\%$  and  $5.7 \pm 4.3\%$ , respectively, and a significant increase in GSSG levels,  $168.7 \pm 36.5\%$ , relative to the control (**Figure 5. 3**).

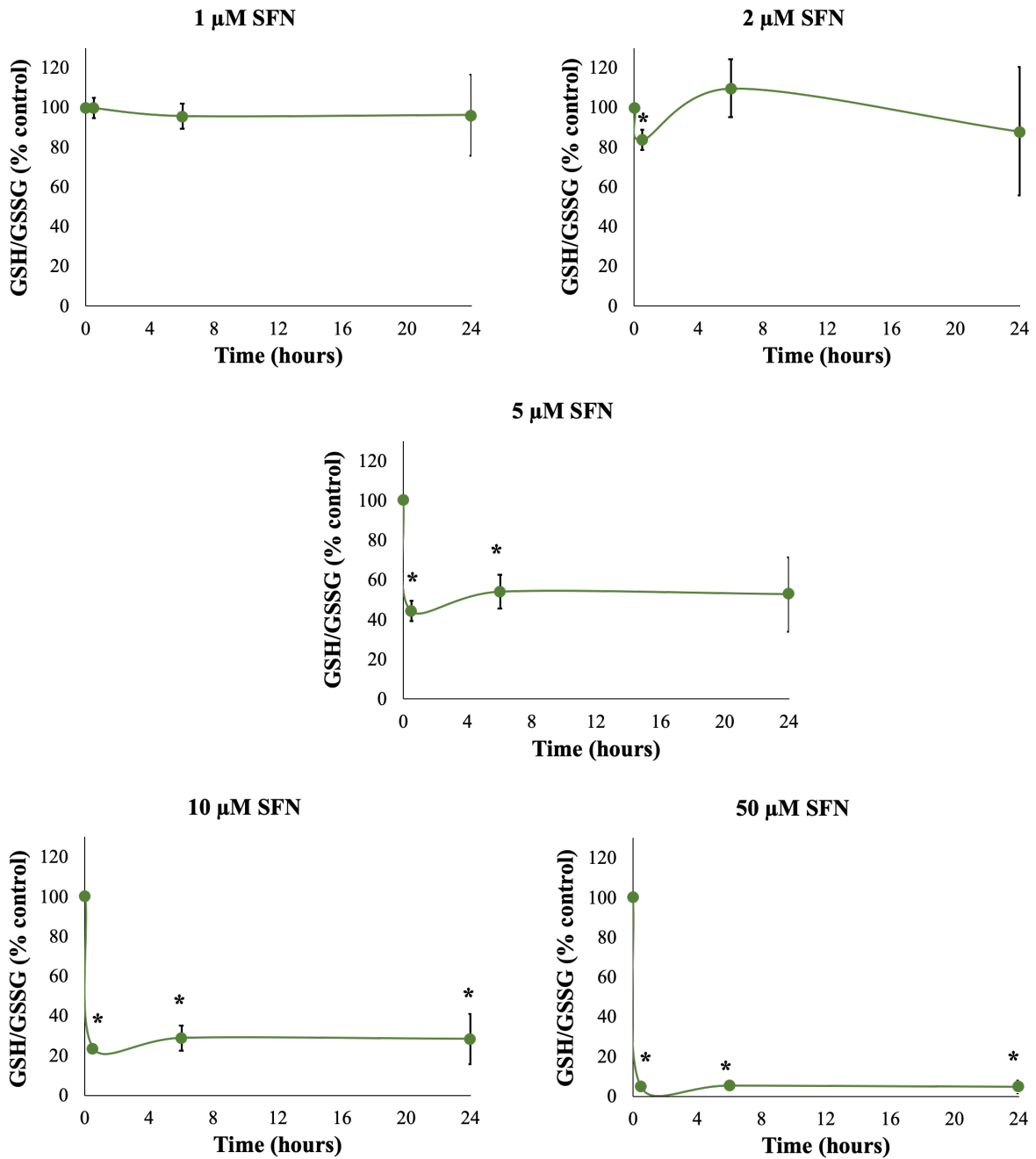


**Figure 5. 2: SFN impairs intracellular GSH/GSSG ratios in FHL124 cells.**

FHL124 cells were treated with different concentrations of SFN (0 – 50 μM) for different durations (0 – 24 hours). GSH homeostasis was measured as GSH/GSSG using a GSH/GSSG luminescent assay. Quantitative data are shown as mean ± SEM (n = 3). An asterisk indicates a significant difference between the treated group and the untreated control at t=0 ( $p \leq 0.05$ ; ANOVA with Dunnett's post hoc).

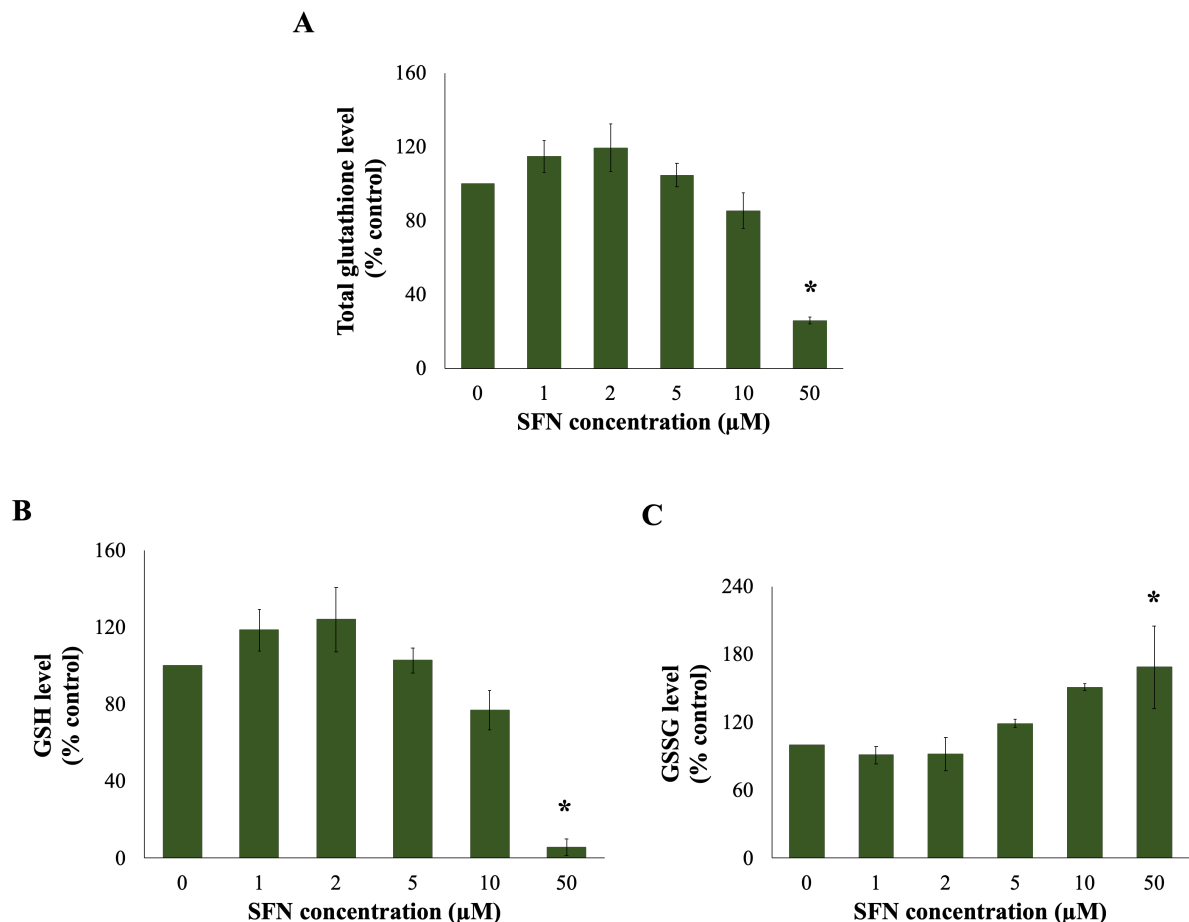


**Figure 5. 3: Impacts of different concentrations of SFN on total glutathione, GSH and GSSG levels in FHL124 cells.**

FHL124 cells were treated with different concentrations of SFN (0 – 50 µM) for 24 hours. Total glutathione and GSSG levels were measured using a GSH/GSSG luminescent assay. GSH levels were calculated based on the detected total glutathione and GSSG levels. A) Total glutathione, B) GSH and C) GSSG. Quantitative data are shown as mean ± SEM (n = 3). An asterisk indicates a significant difference between the treated group and the untreated control ( $p \leq 0.05$ ; ANOVA with Dunnett's post hoc).

### 5.3.2 Impacts of NAC treatment on SFN-induced GSH depletion.

FHL124 cells were either maintained in serum-free (control) EMEM or EMEM supplemented with 1mM NAC. Following a period of 1 hour, half the preparations were treated with SFN (final concentration 50 µM) while the other half did not receive SFN treatment. Cells were incubated in experimental conditions for different durations (4 or 24 hours). In comparison to the baseline level, NAC treatment alone quickly significantly doubled the GSH pool after 4 hours ( $184.6 \pm 44.0\%$ ) (**Figure 5. 4A**), and its level remained high after 24 hours ( $178.1 \pm$

17.2%) (**Figure 5. 4B**). After 24 hours, SFN treatment significantly reduced the GSH/GSSG ratio compared to the baseline. However, in cells treated with NAC + SFN, there was no significant changes, although the GSH/GSSG ratio was 14 times higher than in cells only treated with SFN and half as the baseline level ( $52.3 \pm 17.2\%$ ).

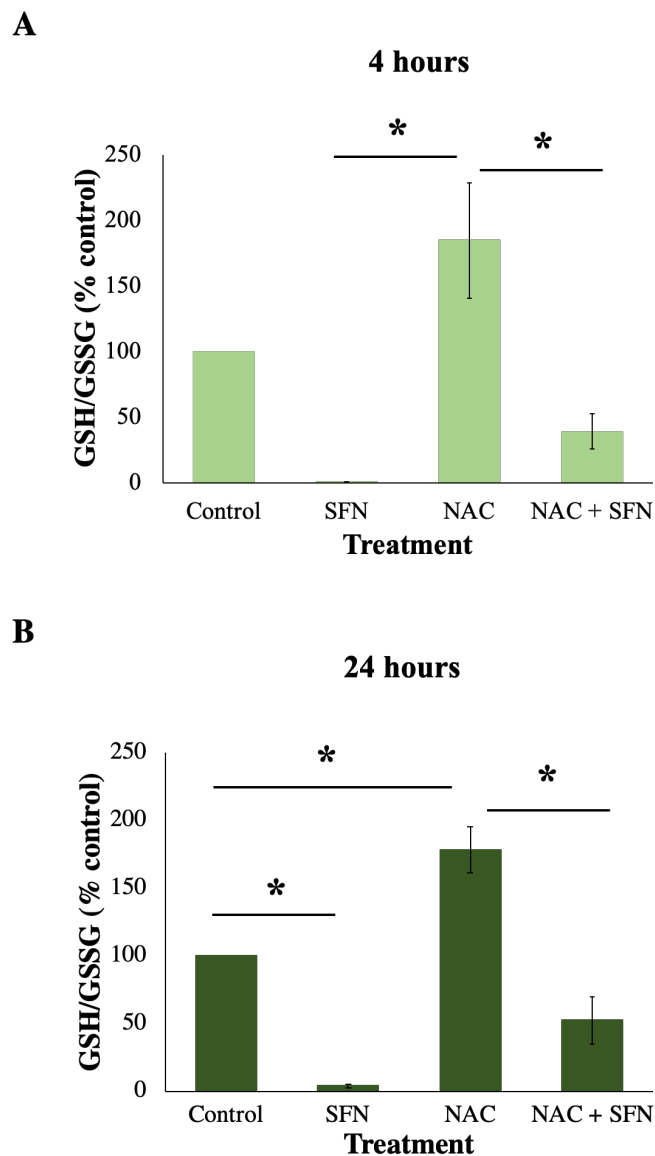


**Figure 5. 4: NAC prevents the GSH depletion by SFN but fails to fully restore the GSH levels.** FHL124 cells were either maintained in serum-free (control) EMEM or EMEM supplemented with 1 mM NAC. Following a period of 1 hour, half the preparations were treated with SFN (final concentration 50  $\mu$ M) while the other half did not receive SFN treatment. Cells were incubated in experimental conditions for different durations. GSH levels were measured as GSH/GSSG using a GSH/GSSG luminescent assay after A) 4 hours or B) 24 hours. Quantitative data are shown as mean  $\pm$  SEM (n=3). An asterisk indicates a significant difference between two groups ( $p \leq 0.05$ ; ANOVA with Tukey's post-hoc).

### 5.3.3 Analysis of intracellular SFN metabolites in FHL124 cells.

It was of interest to investigate what might drive SFN-induced GSH depletion. One possible mechanism was the direct conjugation of SFN with GSH. To investigate this, LC-MS/MS analysis was used to measure different metabolites of SFN in FHL124 cells: SFN, SFN-GSH, SFN-Gly-Cys, SFN-Cys and SFN-NAC. After 1 hour, SFN-GSH was the dominant intracellular metabolite ( $0.94 \pm 0.29$  nmol / $10^6$  cells), fourfold more than SFN, which was the second most abundant ( $0.24 \pm 0.08$  nmol / $10^6$  cells) (**Figure 5. 5**). Only SFN-NAC was not detected.

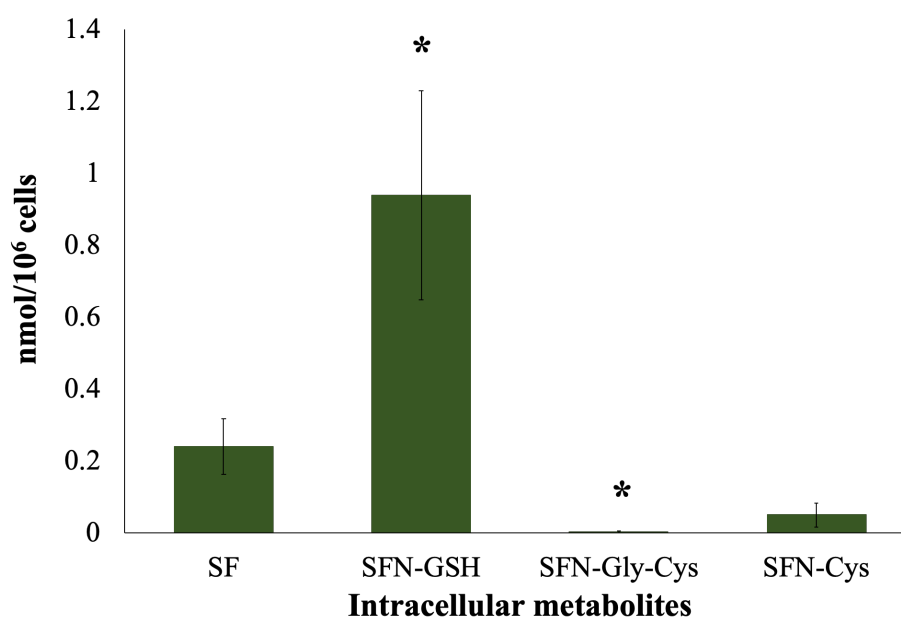


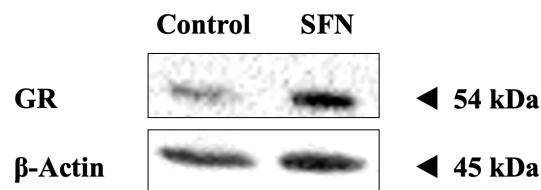
**Figure 5. 5: Analysis of intracellular SFN metabolites in FHL124 cells.**

FHL124 cells were treated with 50  $\mu$ M SFN for 1 hour and extracted for A) extracellular metabolites and B) intracellular metabolite analyses using LC-MS/MS. Quantitative data are shown as mean  $\pm$  SEM (n=3). An asterisk indicates a significant difference between other metabolites against SFN ( $p \leq 0.05$ ; ANOVA with Dunnett's post hoc).

### 5.3.4 SFN increases GR protein levels but decreases its activity in FHL124 cells.

GR is the enzyme that catalyses the conversion of GSSG back to GSH and its activity helps maintain the intrinsically high GSH/GSSG level. After 18 hours, SFN significantly increased GR protein levels by  $265.4 \pm 65.3\%$  (**Figure 5. 6**). Nevertheless, after 2 hours, SFN significantly reduced GR activity to  $66.9 \pm 5.6 \%$  (**Figure 5. 7A**); the reduction continued further, such that after 18 hours the activity reached  $40.6 \pm 10.1 \%$  of the untreated control (**Figure 5. 7B**)

**A**



**B**

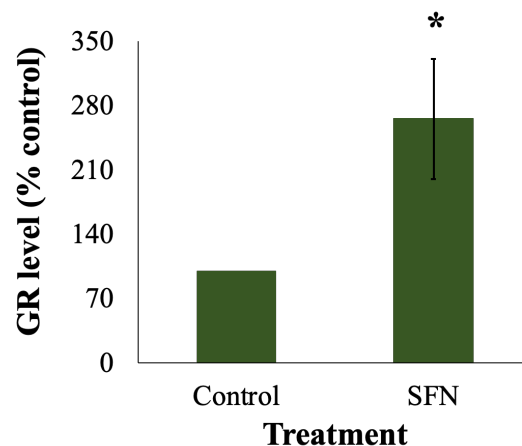


**Figure 5. 6: SFN increases the GR protein level in FHL124 cells.**

Cells were treated with  $50 \mu\text{M}$  SFN for 18 hours and the GR protein level was measured using Western blot. A) Representative blot of GR and B) quantification of Western blot. Quantitative data are shown as mean  $\pm$  SEM ( $n=4$ ). An asterisk indicates a significant difference between the treated group and untreated controls ( $p \leq 0.05$ ; independent Student's *t*-test).

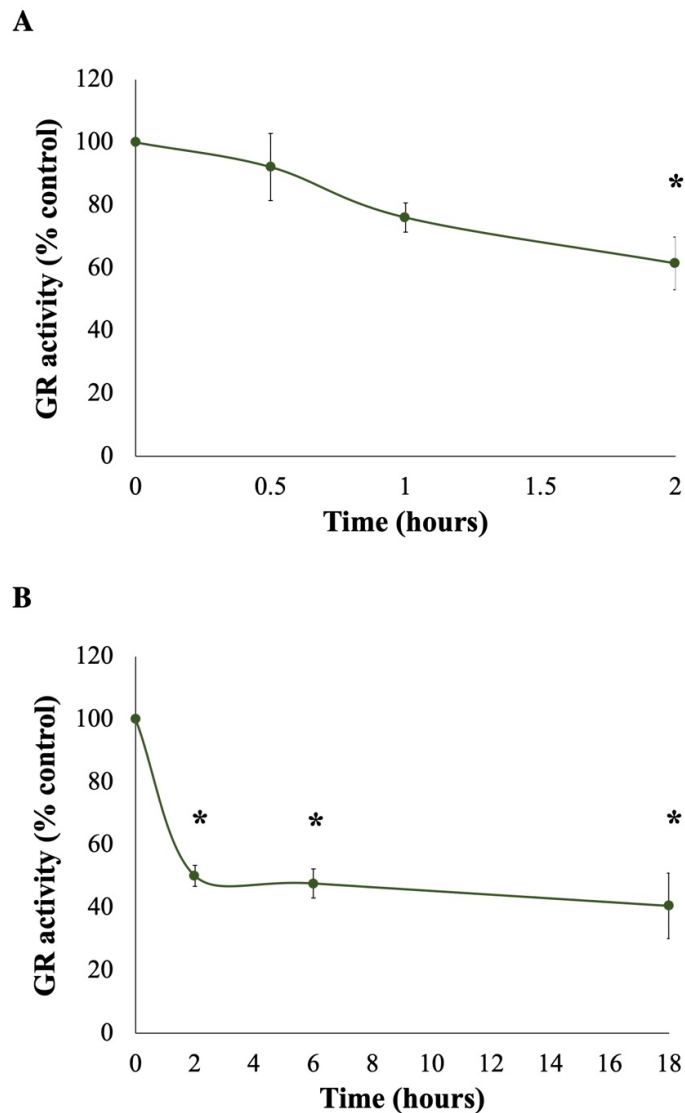


**Figure 5. 7: SFN decreases GR activity.**

Cells were treated with 50  $\mu$ M SFN for different durations over a duration of A) 2 hours or B) 18 hours and GR activity was measured using a GR activity assay. Quantitative data are shown as mean  $\pm$  SEM (n=4). An asterisk indicates a significant difference between the treated group and the untreated control at t=0 ( $p \leq 0.05$ ; ANOVA with Dunnett's post hoc).

### 5.3.5 SFN depletes the intracellular GSH pool in human lens epithelium.

In human lens epithelium, the absolute ratio of GSH/GSSG in the control was 13.9:1 (n=3), and this was converted to 100%, serving as the baseline level. SFN treatment at 50  $\mu$ M depleted the GSH/GSSG ratio to  $12.1 \pm 2.3\%$  compared to the control after 4 hours (**Figure 5. 8**). In more detail, SFN had no impact on total glutathione levels, but significantly decreased GSH

levels by  $60.7 \pm 6.9\%$  and significantly increased GSSG levels by  $541.8 \pm 122.3\%$  compared to the control (**Figure 5. 9**).

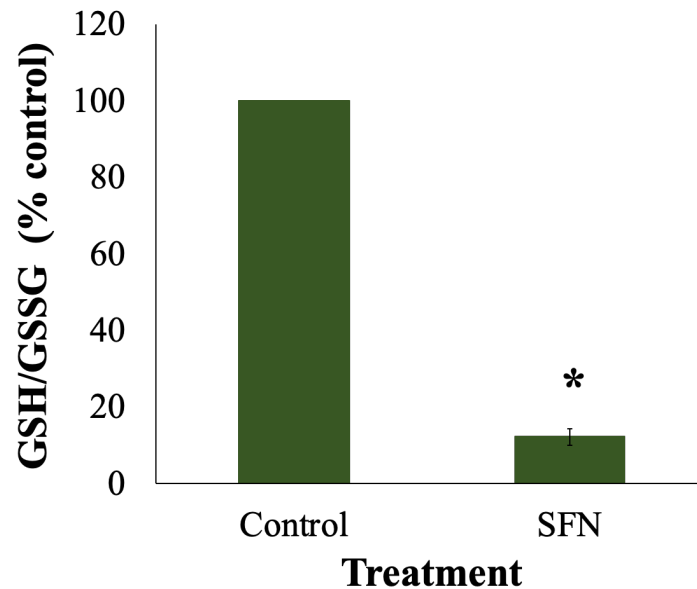


**Figure 5. 8: SFN impairs intracellular GSH levels in human lens epithelium.**

Match-paired capsulorhexis samples were treated with  $50 \mu\text{M}$  SFN for 4 hours. The GSH level was measured as GSH/GSSG using a GSH/GSSG luminescent assay. Quantitative data are pooled from four match-paired human epithelium tissues. Data are presented as mean  $\pm$  SEM. An asterisk indicates a significant difference between the treated group and the untreated control ( $p \leq 0.05$ ; paired Student's *t-test*).

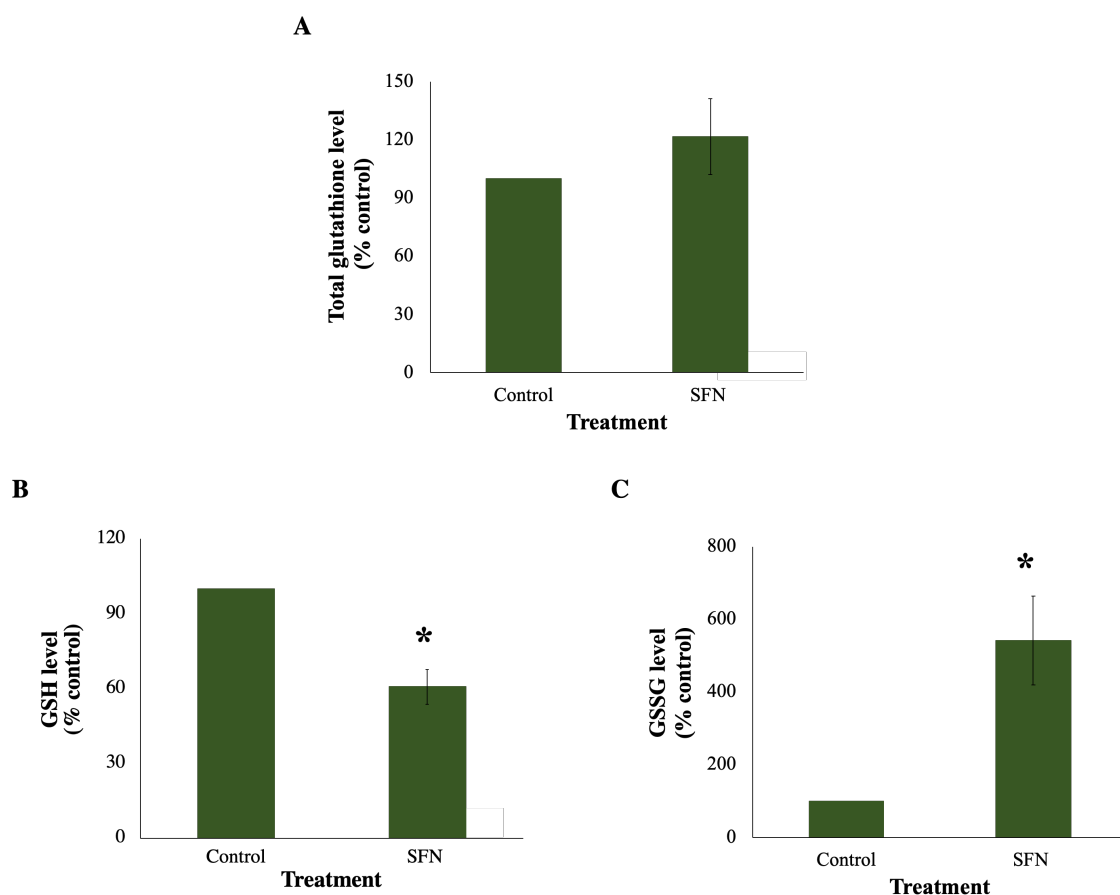


**Figure 5. 9: Impacts of 50  $\mu$ M SFN on total glutathione, GSH and GSSG levels in human lens epithelium.**

Match-paired capsulorhexis samples were treated with 50  $\mu$ M SFN for 4 hours. Total glutathione and GSSG levels were measured using a GSH/GSSG luminescent assay. GSH levels were calculated based on the detected total glutathione and GSSG levels. A) Total glutathione, B) GSH and C) GSSG. Quantitative data are pooled from four match-paired human epithelium tissues. Data are presented as mean  $\pm$  SEM. An asterisk indicates a significant difference between the treated group and the untreated control ( $p \leq 0.05$ ; paired Student's *t*-test).

## 5.4 Discussion

The current study reveals the deleterious impacts of SFN on the GSH system in human lens cells. Through conjugating with GSH via GST and debilitating GR activity, SFN rapidly and markedly depleted the intracellular GSH pool in human lens epithelial cells. This effect of SFN likely increased the oxidative potential and induced oxidative stress in the experimental models.

The GSH/GSSG ratio is often used to assess cellular redox status. Under the action of glutathione peroxidase (GPx), two GSH molecules are converted to one GSSG molecule. In a resting cell, the GSH/GSSG is high since GSH is the dominant form of intracellular glutathione. However, following oxidative stress, this ratio can be significantly reduced, even to 1:1 (Brennan & Kantorow, 2009; Kosower & Kosower, 1978; Townsend, Tew, & Tapiero, 2003). The current study reported that SFN decreased the GSH/GSSG ratio in a concentration-dependent manner, and at 50  $\mu$ M SFN, the GSH/GSSG ratio was decreased to below 10% compared to the baseline level after 30 minutes and did not recover at the endpoint. The persistence of extremely low GSH/GSSG ratios suggests chronic oxidative stress in human lens epithelial cells in the presence of high concentrations of SFN.

In contrast, in bovine aortic endothelial cells, GSH levels recovered to normal levels after 12 hours after having decreased by more than half during the first 30 minutes of 25  $\mu$ M SFN treatment (Y. C. Liu et al., 2008). Such transient decreases in GSH levels and the ability of cells to recover their GSH levels observed in aortic endothelial cells or human liver cancer cells (B. R. Kim et al., 2003) might be attributed to low SFN concentrations (25  $\mu$ M vs 50  $\mu$ M), which resulted in lower drops in GSH levels. A similar observation was also recorded in the current study with low concentrations of SFN. A possible explanation is that low drops in GSH levels resulting from low SFN concentrations are within the cellular capacity to replenish the GSH levels and to restore the redox balance. Whereas, deeper reductions in GSH levels surpass the cellular replenishing capacity.

Moreover, there was a clear distinction in GSH/GSSG ratios between non-cytotoxic concentrations and cytotoxic concentrations. Low concentrations of SFN (1 and 2  $\mu$ M), previously shown to be non-cytotoxic (H. Liu et al., 2013), maintained the decreased

GSH/GSSG ratios above 80%, whereas high, supranutritional concentration (50  $\mu$ M), previously shown to be cytotoxic, decreased the ratios to below 10% against the baseline. This indicates a possible correlation between SFN-induced GSH depletion and cytotoxicity. The intracellular GSH levels were previously reported to determine a cell's fate. In rabbit lens epithelial cells, small reductions in GSH levels by buthionine sulfoximine (BSO) or 1-chloro-2,4-dinitrobenzene (CDNB) did not cause any tragic harm, but a drop in GSH levels to 35% was considered "a life-death threshold" for cells (Giblin, 2000). In the current study, the GSH level in cells treated with 50  $\mu$ M was less than 10%, well surpassing the aforementioned "life-death threshold". On the other hand, in a study using rabbit lens epithelial cells, major drops in GSH content (>75%) induced by BSO, a GSH synthesis inhibitor, did not trigger cell death (Shang *et al.*, 2003). However, assuming that the experimental models of the current study and the Shang *et al.* study are comparable, there is a discrepancy between the remaining GSH levels, 10% vs 25%. Therefore, these findings suggest that SFN-induced cell death may be mediated by the rapid depletion of GSH.

NAC is one of the most widely used antioxidants. The antioxidative agency of NAC is possibly constituted by three mechanisms. The first mechanism is that NAC scavenges oxidants directly through its thiol group, but this is unlikely due to its low kinetic reactions with  $\text{H}_2\text{O}_2$  and  $\text{O}_2^{\cdot-}$ . The second one, also the most accepted one, is that NAC can serve as a source of cysteine for increased GSH biosynthesis. The third mechanism, which was just recently discovered, is that NAC provides cytoprotection via generating direct ROS scavengers  $\text{H}_2\text{S}$  and sulfane sulfur (Ezerina *et al.*, 2018). Therefore, the pro-GSH properties of NAC can account for the double increases in GSH/GSSG ratios following the treatment with 1 mM NAC alone. Similarly, a study in human cancer cells showed that o-phenanthroline - an established antioxidant with no affiliation with GSH synthesis, and mitochondrial complex inhibitors could abrogate ROS

production and DNA damage caused by SFN but had no impact on the dramatic reduction of GSH (Sestili et al., 2010). More importantly, NAC did not fully restore GSH levels following SFN treatment. After 24 hours, the GSH/GSSG ratios in cells pre-treated with NAC before SFN only reached approximately 50% of the control group. This suggests that ROS involvement is downstream of GSH depletion and cytoprotection provided by NAC is also independent of GSH, likely via the generation of H<sub>2</sub>S and sulfane sulfur.

GSH depletion was found to be caused by two different mechanisms. The primary cause is the direct conjugation of SFN and GSH, as demonstrated by the LC-MS/MS analysis, which showed SFN-GSH as the predominant intracellular SFN metabolite and the second most abundant extracellular metabolite. This finding aligns with the current literature, whereby upon entry into mammalian cells, SFN quickly conjugates with GSH as the initial step of its metabolism via the mercapturic acid pathway (Clarke et al., 2011; Kassahun, Davis, Hu, Martin, & Baillie, 1997; Kolm, Danielson, Zhang, Talalay, & Mannervik, 1995). Intracellular GSH is resistant to degradation because there is no intracellular enzyme capable of hydrolysing the gamma-carboxyl group arising from the condensation of glutamate and cysteine residues. Conjugation with endogenous and xenobiotic compounds, such as SFN, is the primary mode of degradation-resistant GSH depletion (Aoyama & Nakaki, 2012; Baudouin-Cornu, Lagniel, Kumar, Huang, & Labarre, 2012; Y. Zhang, Kolm, Mannervik, & Talalay, 1995).

The secondary cause is decreased GR activity: despite doubled protein levels, GR activity dropped by nearly 40%. The decreased GR activity is likely due to irreversible modifications caused by direct SFN-GR interactions (Y. Hu et al., 2007), while the increased quantity implies a compensatory effort. The GR-dependent GSH regeneration is important for maintaining high GSH levels, therefore the activity deficiency caused by SFN might directly exacerbate the

already low GSH levels. Regarding the contrast effects of SFN on GR, scientists should take caution when evaluating the anti- or pro-oxidant properties of SFN. Future studies should investigate how SFN affects other GSH maintenance pathways, such as the *de novo* synthesis from precursor amino acids, and direct GSH uptake from surrounding ocular tissues following synthesis impairment found in animal models (Fan, Monnier, & Whitson, 2017; Lim et al., 2020).

There was no SFN-NAC detected using LC-MS/MS. SFN-NAC is converted from SFN-Cys by arylamine N-Acetyltransferase (NAT), and the formation of SFN-NAC is the final step in the metabolism mercapturic pathway of SFN and SFN-NAC (Juge et al., 2007). The metabolite panel was analysed after 1 hour of SFN addition, and this could have been too early for the metabolism pathway to reach the production of SFN-NAC, or for the amount of SFN-NAC to reach the detectable threshold. Moreover, human NAT was reported to be rapidly inactivated by physiological concentrations of H<sub>2</sub>O<sub>2</sub> and GSH could reverse this inactivation (Atmane, Dairou, Paul, Dupret, & Rodrigues-Lima, 2003). In light of the rapid depletion of GSH within 30 minutes of 50 µM SFN, NAT was possibly disabled, resulting in the inefficient conversion of SFN-Cys to SFN-NAC.

The findings of SFN's detrimental impacts on GSH homeostasis not only provide a better understanding of how SFN affects the antioxidant defence systems, but also present SFN as a promising agent for studying conditions associated with GSH imbalance. For example, in the lens, the high concentrations allow GSH to carry out multiple functions that are essential for the normal physiology of the lens (Fan et al., 2017; Reddy, 1990). However, the *de novo* synthesis, the GR recycling machinery, and the uptake route all diminish with age in this tissue, leading to an age-dependent loss of GSH and gain of GSSG (Brennan et al., 2012; Kubo et al.,

2017; Michael & Bron, 2011). Deprived of GSH, the ageing lens is extremely vulnerable to oxidative stress, and consequently becomes increasingly susceptible to opacity or cataract development. (Fan et al., 2017; Lim et al., 2020). With the ability to deplete GSH in human lens epithelial cells, SFN can certainly be applied to lens epithelial cells to mirror changes in GSH levels in an ageing lens epithelium, establishing a new model to study lens physiology in ageing. Moreover, the current study shows that SFN depletes GSH levels in a concentration-manner, so with the demonstrated knowledge, scientists can easily manipulate the degree of GSH depletion and examine the corresponding outcomes. What distinguishes SFN from other tools to deplete GSH levels in the lens, such as BSO – the GSH synthesis inhibitor, is that SFN can not only rapidly deplete the GSH pool via fast conjugation catalysed by GST but also inhibit regeneration of GSH by GR. With this powerful ability to diminish the GSH pool, at least duo-faceted as evidenced in this study, SFN emerges as a new model to study GSH imbalance in lens ageing and cataract development.

In summary, high supranutritional SFN concentrations debilitate the antioxidant defence system via rapidly depleting GSH (**Figure 5. 10**). The major mechanism causing the depletion appears to be via SFN-GSH conjugation upon cellular entry. The regeneration of GSH is also hampered by the SFN-induced deficiency in GR activity, limiting the recovery of GSH levels. As a consequence, human lens epithelial cells become quickly deprived of the GSH system, its major antioxidant defence, and challenged with oxidative stress, evidenced by critically low GSH/GSSG ratios. With deleterious effects inflicted on the antioxidant defence systems by SFN, it would be interesting to inspect the relationship between GSH depletion and other ROS-dependent cellular events induced by SFN.

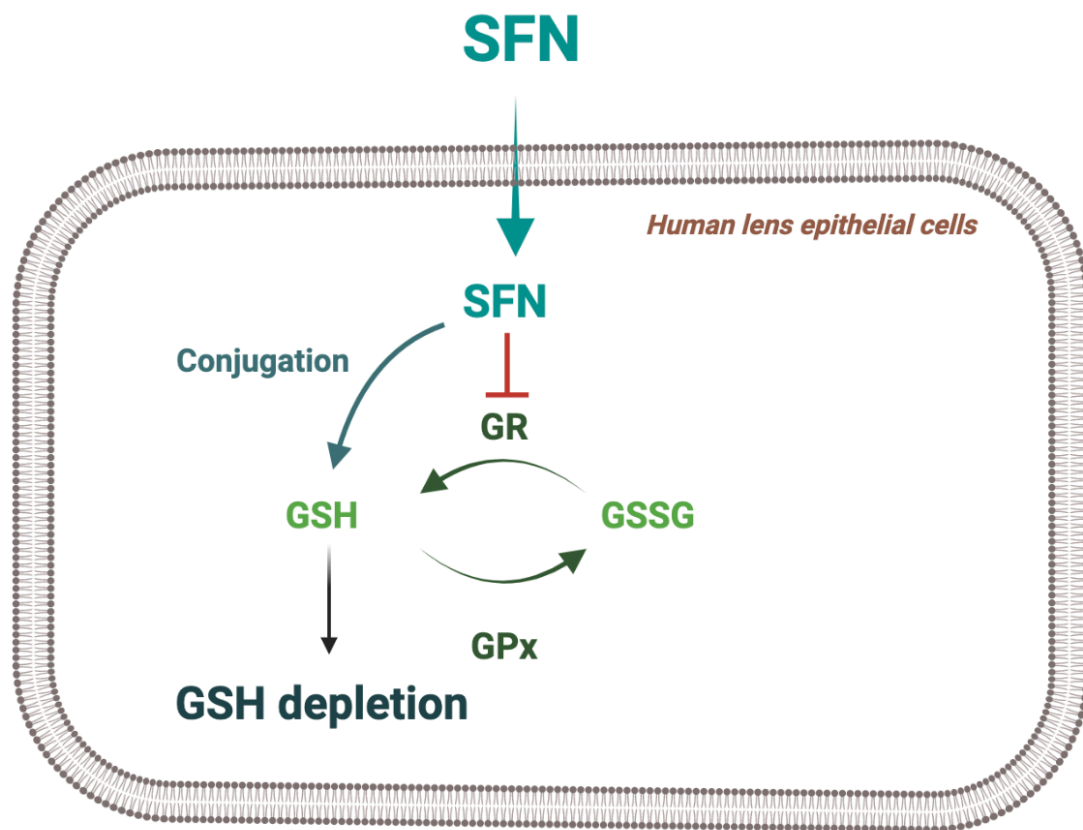


**Figure 5. 10: SFN causes GSH depletion via conjugation and inhibition of GSH regeneration in human lens epithelial cells.**

# Chapter 6 SFN-Induced GSH Depletion Triggers

## Stress and Death

---

### 6.1 Introduction

As previously discussed in **Chapter 5**, GSH is present at high concentrations in the lens. GSH levels are maintained by *de novo* synthesis, regeneration, turnover and direct uptake. Since only metabolically active epithelial and cortical fibre cells are capable of synthesising GSH, there is a decreasing gradient of GSH concentration across this organ towards the mature fibre cells of the lens nucleus. At the site of production, GSH synthesis is further restricted to the cytosol. Approximately 80 – 85% of GSH is found in the cytosol. The remainder is distributed to other cellular organelles (Srinivas, 2014). Due to the lack of GSH *de novo* synthesis machinery, cellular organelles rely on the uptake of cytosolic GSH (cGSH) across their membranes and the salvage of GSSG by glutathione reductase (GR) to maintain their GSH pools (Franco & Cidlowski, 2009). Approximately 10 – 15% of cGSH is distributed to mitochondria, and the rest resides in other organelles, such as the ER, peroxisomes, the nucleus (Montero, Tachibana, Rahr Winther, & Appenzeller-Herzog, 2013). Due to the small volumes of these organelles, their GSH concentrations are still high; the mitochondrial GSH (mGSH) concentration is particularly comparable to that of cGSH. On the contrary, ER has so much more GSSG than any other organelles, since the oxidant environment is essential for the correct folding and secretory pathways of proteins.

The high concentrations of GSH allow GSH to carry out multiple functions that are essential for the normal physiology of the lens and other tissues (Fan et al., 2017; Reddy, 1990).

Amongst these functions, the most important are detoxification of endogenous and exogenous compounds, and protection against free radicals. As a nucleophile, GSH can bind to various endogenous and xenobiotic molecules of an electrophilic nature to prevent them from targeting other cellular molecules and accelerate their elimination from a cell (Lim et al., 2020). On the other hand, the thiol moiety of GSH allows the molecule to act as a direct scavenger that quenches ROS, reactive nitrogen species (RNS) and other species, such as  $O_2^-$ ,  $\bullet OH$ , and  $ONOO^-$  (Aquilano, Baldelli, & Ciriolo, 2014). GSH can also act as a co-factor to support glutathione peroxidase (GPx) to detoxify  $H_2O_2$  and organic peroxides (Lushchak, 2012). The antioxidant properties of GSH also stem from the involvement of GSH in protein S-glutathionylation (Aquilano et al., 2014). Protein S-glutathionylation is an essential, reversible PTM through which disulfide bonds are formed between protein cysteines and GSH cysteines. This process protects cysteine residues in proteins from irreversible oxidation, and also acts as a redox signal transducer by changing the structure and function of the target protein. For example, S-glutathionylation of cysteine residue 294 of the  $\alpha$  subunit of ATP synthase protects this ATP-producing enzyme from irreversible oxidative-mediated PTM to  $SO_2H$  or  $SO_3H$  (Mailloux & Willmore, 2014; S. B. Wang et al., 2011), which was discussed in **Chapter 4**.

Deficiency in GSH levels can variably affect cellular homeostasis and may contribute to the aetiology and/or progression of various degenerative disorders and age-related health conditions (Lushchak, 2012). GSH depletion has been demonstrated as a common feature in dying cells induced by a wide range of stimuli, such as GSH export caused by cytokine withdrawal, oxidation to GSSG caused by ROS elevation, or conjugation with xenobiotics (Beaver & Waring, 1995; Franco & Cidlowski, 2006; Franco, Schoneveld, Pappa, & Panayiotidis, 2007; Ghibelli et al., 1998). Early research suggested that the loss of GSH was a by-product of oxidative stress during cell death. However, recent findings indicate that GSH

depletion and protein S-glutathionylation are important regulators of cell death, especially apoptosis. Nevertheless, the cellular events and molecular mechanisms involved in this process have yet to be linked together (Franco & Cidlowski, 2009; Kalinina & Gavriliuk, 2020).

SFN, an isothiocyanate (ITC), is the hydrolysis product of a glucosinolate found in cruciferous vegetables, such as broccoli and kale. The small, lipophilic SFN can easily diffuse across the lipid bilayer plasma membrane. Upon cellular entry, SFN as an electrophile is rapidly conjugated to GSH as a nucleophile by glutathione-S-transferase (GST), as part of the metabolic mercapturic acid pathway (Janobi et al., 2006; Kassahun et al., 1997; Y. Zhang, 2012). This conjugation step is necessary to prevent free SFN roaming in the cytosol and modifying other molecules, such as nuclear factor kappa-light-chain-enhancer of activated B cells (NF- $\kappa$ B), Keap-1, and microRNAs (Biswas & Rahman, 2013; C. Hu, Eggler, Mesecar, & Breemen, 2011; Sayeed et al., 2017). Nevertheless, via conjugation, high concentrations of SFN can quickly deplete intracellular GSH levels. In human liver cancer cells, such decreases in GSH levels were shown to be essential for the induction of ARE-mediated phase 2 detoxification genes, which subsequently restored the GSH pool (B. R. Kim et al., 2003). However, that only occurred at the established suboptimal concentrations of SFN, such as 25  $\mu$ M. On the contrary, higher concentrations of SFN, such as 50  $\mu$ M, activated JNK-mediated apoptosis instead of the ARE-mediated responses. The prevention of apoptosis by the addition of 1 mM exogenous GSH implies GSH depletion was required for SFN – induced cellular demise. In FHL124 cells, 50  $\mu$ M SFN also dramatically and chronically depleted GSH levels, as shown in **Chapter 5**. However, it remains to be seen whether GSH depletion is a prerequisite for SFN-induced cell death in this cell line.

## 6.2 Aims

So far, it has been demonstrated that in human lens epithelial cells, SFN mediates cytotoxicity in a ROS-dependent manner and severely diminishes GSH levels. ROS and GSH are two sides of the cellular redox homeostasis, and following SFN treatment, cells appear to be challenged by oxidative stress. Whether GSH depletion contributes to SFN-induced cytotoxicity is unknown. GSH depletion has also been suggested as an important regulator of cell death (Franco & Cidlowski, 2009). Therefore, this study aims to investigate the contribution of GSH depletion to SFN-induced cytotoxicity. The hypothesis to be tested is that **GSH depletion plays a pivotal role in stress responses and death triggered by SFN in human lens epithelial cells**. The methodological approach taken will evaluate the protection of GSH addition against cell death, mitochondrial dysfunction, ERS, DNA damage, and autophagy in FHL124 cells and human lens epithelium.

## 6.3 Results

### 6.3.1 Evaluating the effect of GSH supplementation on cell viability following SFN treatment in FHL124 cells.

FHL124 cells were either maintained in serum-free (control) EMEM or EMEM supplemented with different concentrations (0.1 – 10 mM) of GSH. Following a period of 1 hour, half the preparations were treated with SFN (final concentration 50  $\mu$ M) while the other half did not receive SFN treatment. The addition of GSH was intended to increase the intracellular GSH pool. After 18 hours, the effect of GSH on cell viability following SFN treatment was assessed using the Cell-TitreGlo assay (**Figure 6. 1**). GSH had no impact on the SFN-induced loss of cell viability at 0.1 mM, but at 0.5 – 10 mM, GSH significantly prevented the loss of cell viability induced by SFN.

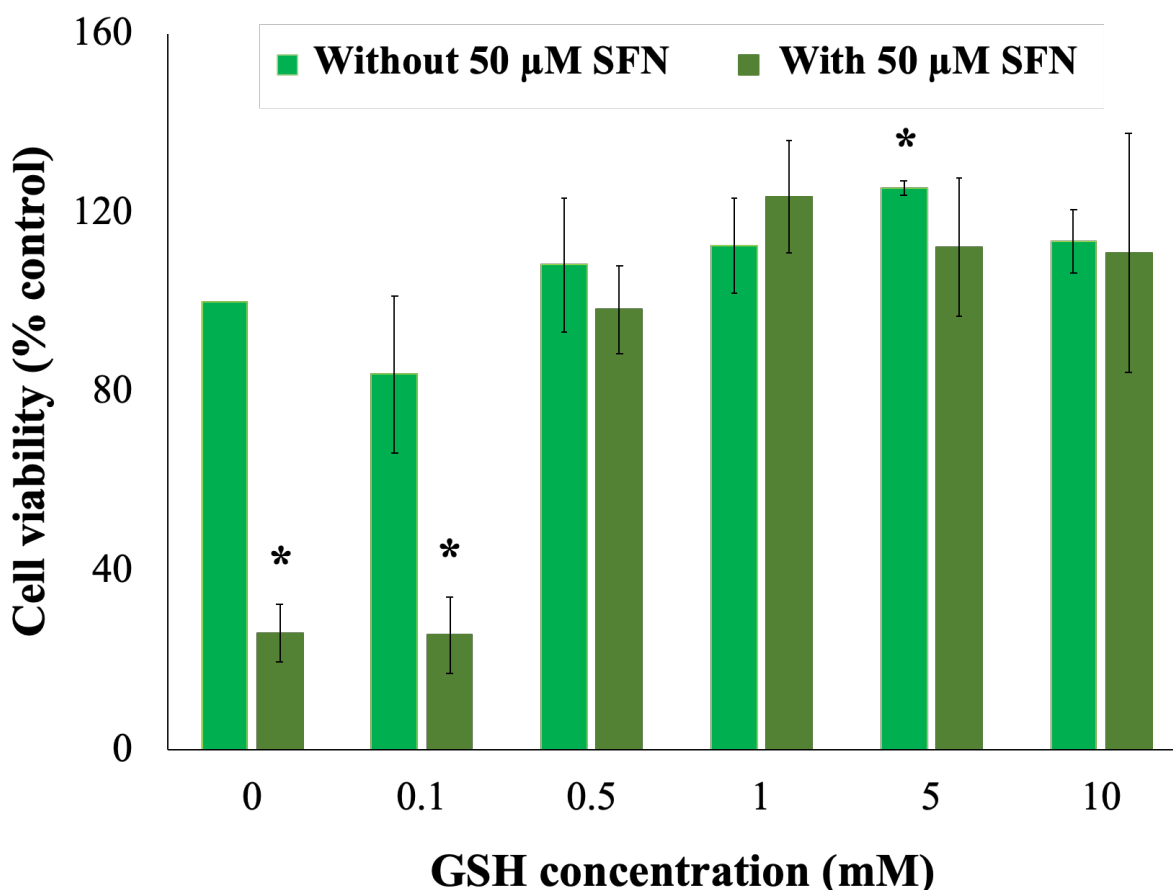


**Figure 6. 1: Effects of different GSH concentrations on cell viability following SFN treatment in FHL124 cells.**

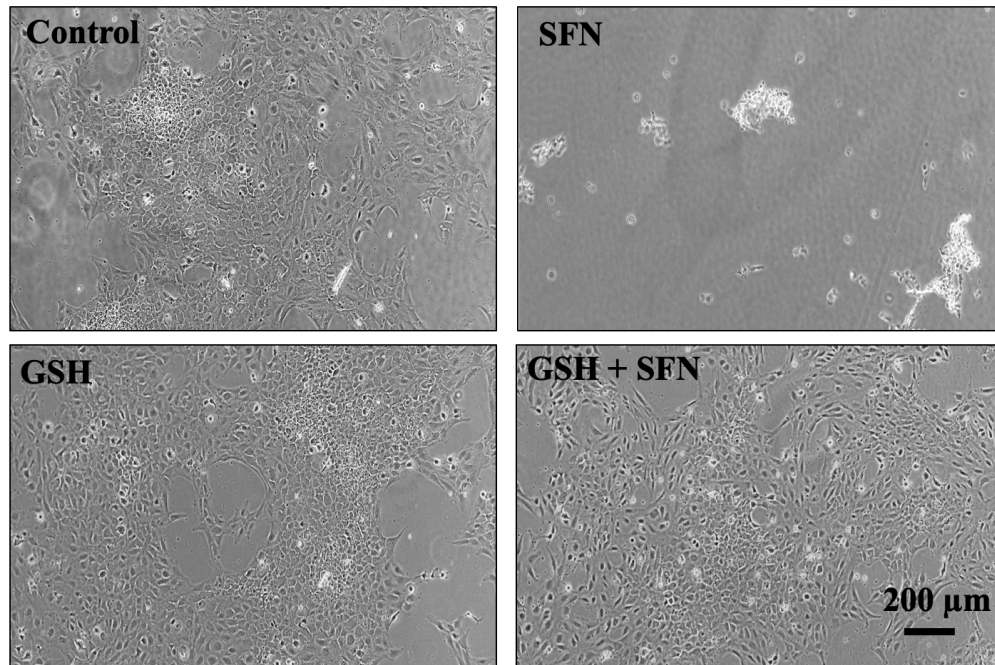
FHL124 cells were either maintained in serum-free (control) EMEM or EMEM supplemented with different concentrations (0.1 – 10 mM) of GSH. Following a period of 1 hour, half the preparations were treated with SFN (final concentration 50  $\mu$ M) while the other half did not receive SFN treatment. Cell viability was measured after 18 hours treated with SFN using a Cell-TitreGlo Luminescent assay. Quantitative data are shown as mean  $\pm$  SEM (n=3). An asterisk indicates a significant difference between the treated group and the untreated group ( $p \leq 0.05$ ; ANOVA with Dunnett's post hoc test).

### 6.3.2 GSH protects FHL124 cells from SFN-induced cytotoxicity.

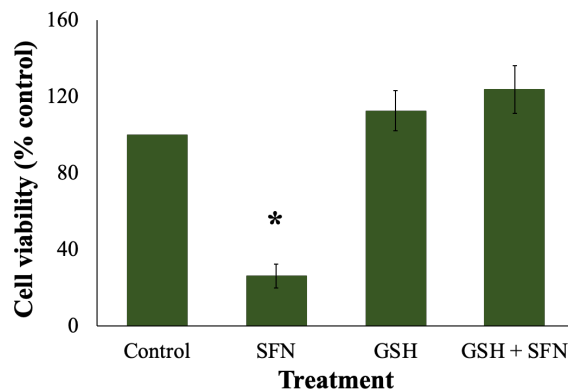
FHL124 cells were either maintained in serum-free (control) EMEM or EMEM supplemented with 1 mM GSH. Following a period of 1 hour, half the preparations were treated with SFN (final concentration 50  $\mu$ M) while the other half did not receive SFN treatment. After 18 hours, FHL124 cells displayed morphological changes, such as detachment, cytoplasmic shrinkage, and nuclear condensation, compared to controls with a typical healthy phenotype, as visualised by phase-contrast microscopy (**Figure 6. 2A**). Biological assays showed that 50  $\mu$ M SFN reduced cell viability to  $26.1 \pm 6.3\%$  while increasing LDH secretion to  $170.7 \pm 10.8\%$

compared to the baseline (**Figure 6. 2B & C**). The treatment with 1 mM GSH successfully prevented the morphological effects and cell damage caused by SFN.

**A**



**B**



**C**

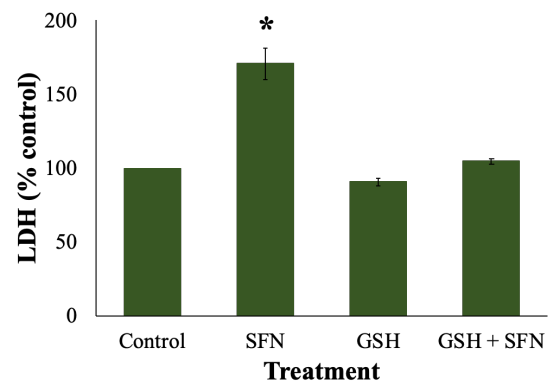


**Figure 6. 2: GSH protects cells from cell death induced by SFN in FHL124 cells.**

FHL124 cells were either maintained in serum-free (control) EMEM or EMEM supplemented with 1 mM NAC. Following a period of 1 hour, half the preparations were treated with SFN (final concentration 50  $\mu$ M) while the other half did not receive SFN treatment. Cells were treated for 18 hours after the addition of SFN. A) Cell morphology was observed using phase-contrast microscopy; B) Cell viability was assessed using a CellTitre-Glo assay (n=3); C) Cytotoxicity was assessed using an LDH assay (n=4). Data are shown as mean  $\pm$  SEM. An asterisk indicates a significant difference between the treated group and all other groups ( $p \leq 0.05$ ; ANOVA with Tukey's post hoc test).

### **6.3.3 GSH protects against collapse of mitochondrial networks caused by SFN in FHL124 cells.**

Mitochondrial networks in both live cells and fixed cells were observed using different microscopes. Mito-GFP cells were co-labelled with MitoTracker Red and the live cells were observed using a Zeiss Observer 7 microscope. Over the course of 75 minutes, SFN interrupted the mitochondrial networks, but GSH prevented that. It was noticed that the mitochondrial networks in the control, GSH, and GSH + SFN samples shrank over time as well, but the degree of shrinkage was negligible in comparison to the SFN sample (**Figure 6. 3**).

In the fixed cell experiment, mitochondria in FHL124 cells were stained with MitoTracker CMXRos red and treated with 50  $\mu$ M SFN for 4 hours. Control groups exhibited a distinct distribution of mitochondria as a mixture of small rods and branched networks of different sizes, which were distributed both near the nucleus and sparsely in the cytoplasm. In accordance with the previous observation, after SFN treatment, most mitochondria were observed to be smaller, more condensed and localised around the nucleus (**Figure 6. 4A**). Derived from the ImageJ analysis, SFN decreased the network size to approximately a third of the control ( $33.1 \pm 4.0\%$ ). GSH treatment restored the mitochondrial network morphology and size to baseline levels (**Figure 6. 4B**).

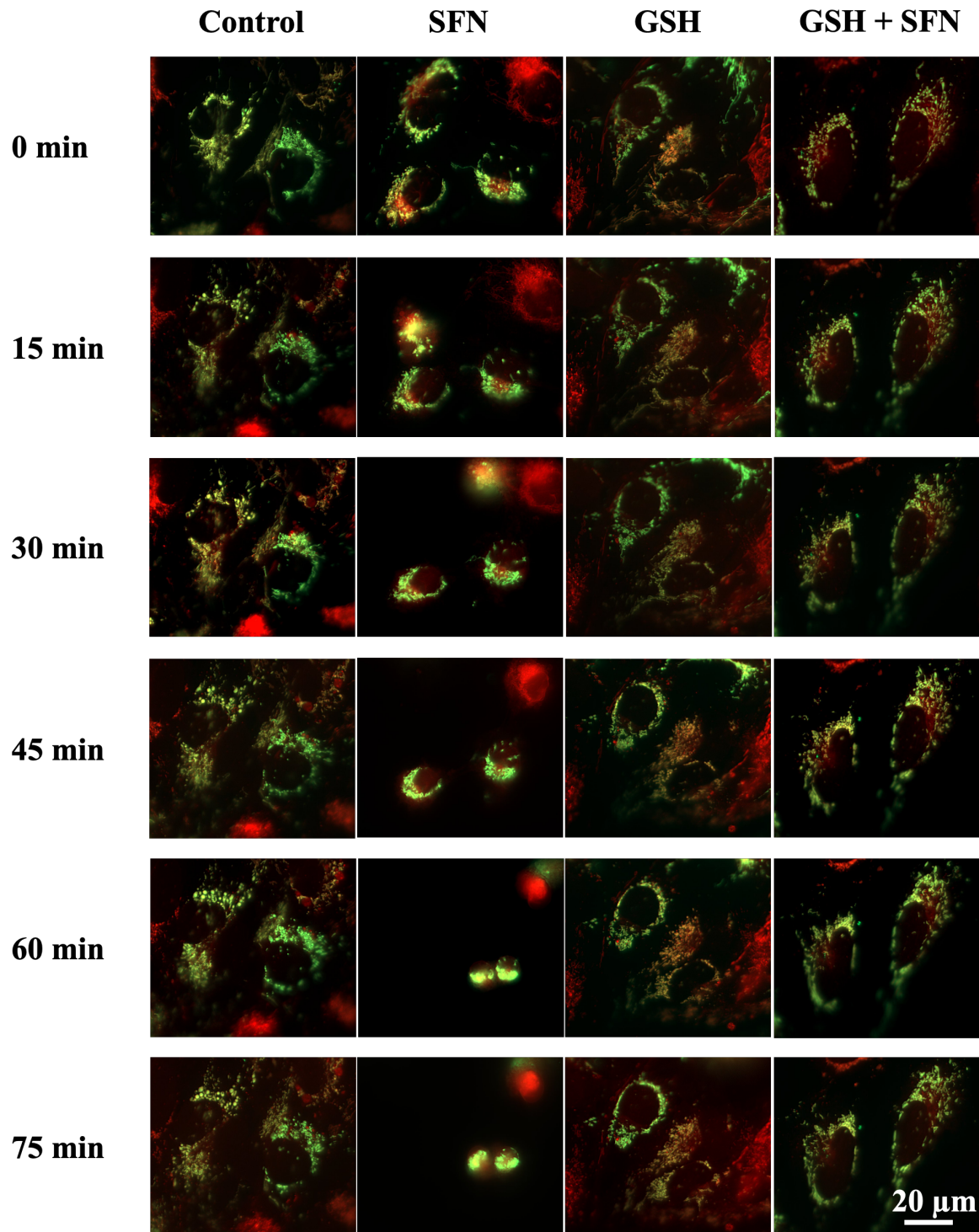


**Figure 6. 3: GSH protects against SFN-induced mitochondrial network shrinkage over time.**

Mitochondria in FHL124 cells were labelled with GFP (green) by transfection and MitoTracker Red CMXRos (red) by direct staining. FHL124 cells were either maintained in serum-free (control) EMEM or EMEM supplemented with 1 mM GSH. Following a period of 1 hour, half the preparations were treated with SFN (final concentration 50  $\mu$ M) while the other half did not receive SFN treatment. Their mitochondria were visualised using widefield microscopy over a duration of 75 minutes after the addition of SFN.

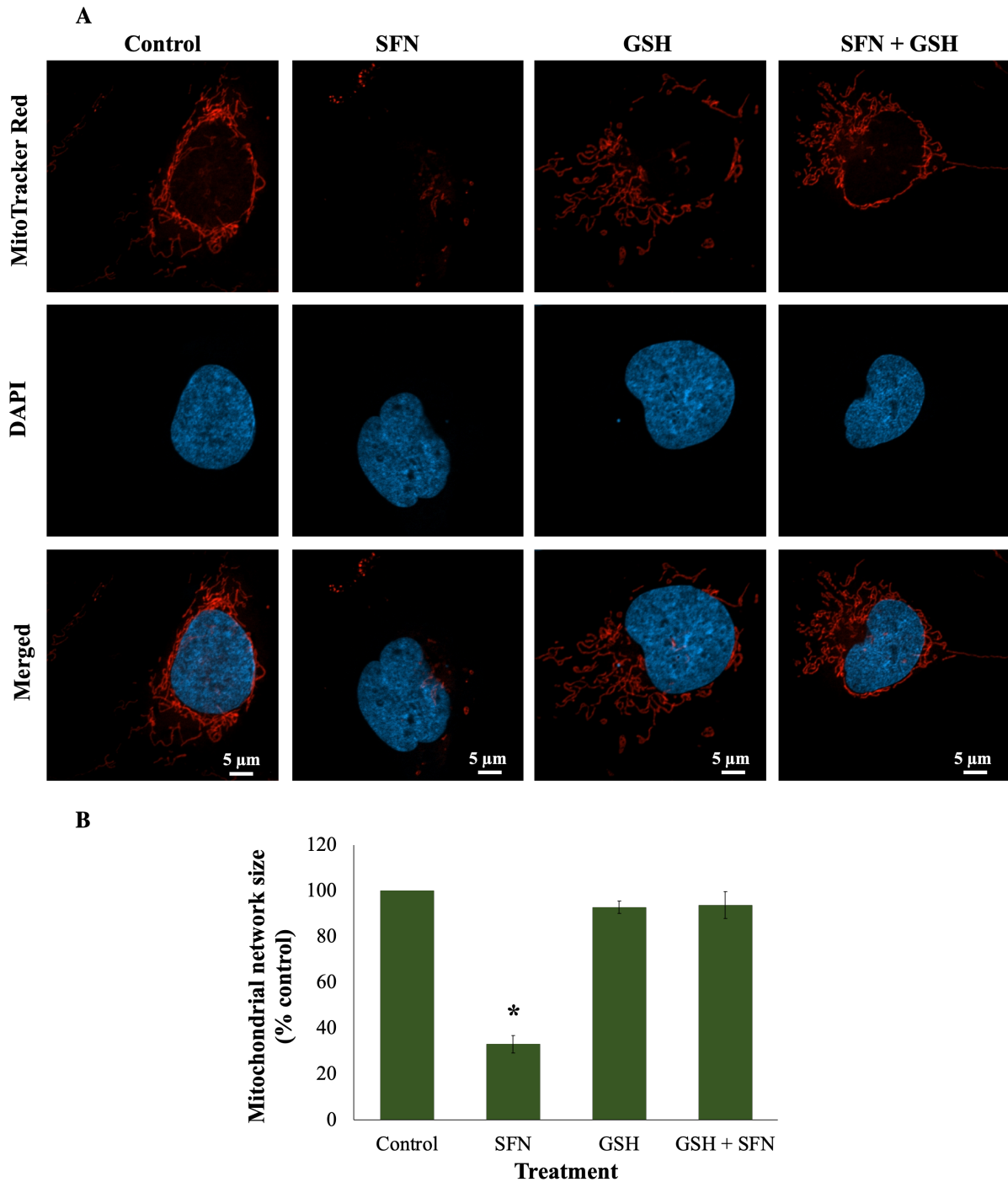


**Figure 6. 4: GSH protects against mitochondrial network shrinkage caused by SFN in FHL124 cells.**

FHL124 cells were either maintained in serum-free (control) EMEM or EMEM supplemented with 1 mM GSH. Following a period of 1 hour, half the preparations were treated with SFN (final concentration 50  $\mu$ M) while the other half did not receive SFN treatment. Cells were treated for 4 hours after the addition of SFN. Mitochondrial networks were labelled with 100 nM MitoTracker CMXRos and imaged using confocal microscopy. A) Representative images (red – MitoTracker, blue – DAPI, merged – MitoTracker and DAPI) and B) quantitative data pooled from 3 separate experiments shown as mean  $\pm$  SEM (20 cells/experiment). An asterisk indicates a significant difference between the treated group and all other groups ( $p \leq 0.05$ ; ANOVA with Tukey's post hoc test).

#### **6.3.4 GSH prevents SFN-induced ERS responses in FHL124 cells.**

After 18 hours, ERS was assessed using qRT-PCR and Western blot. SFN significantly increased expression of several ERS gene markers, including *HSPA5*, encoding the master regulator BiP, by  $135.5 \pm 10.7\%$ , *DDIT3* by  $457.9 \pm 40.0\%$ , and *ERN1* by  $384.7 \pm 34.5\%$ , compared to the baseline levels (**Figure 6. 5**). The protein levels of two ERS markers: P-eiF2 $\alpha$  and XBP-1 were also elevated by approximately fivefold,  $558.3 \pm 92.9\%$  and  $499.4 \pm 167.9\%$ , respectively, against the control levels (**Figure 6. 6**). All SFN-induced changes in levels of ERS gene and protein markers were significantly inhibited by 1 mM GSH treatment.

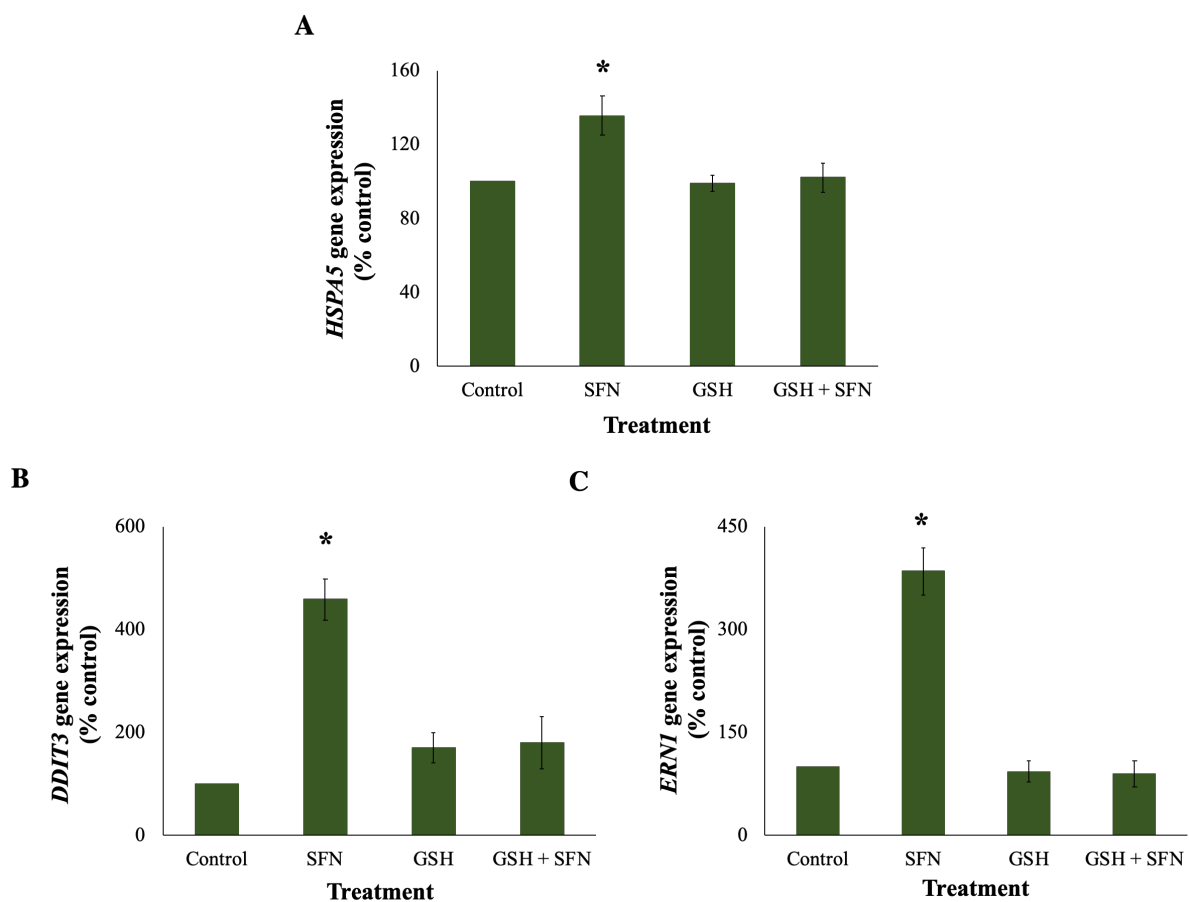


**Figure 6. 5: GSH prevents upregulation of ERS gene markers by SFN in FHL124 cells.**

FHL124 cells were either maintained in serum-free (control) EMEM or EMEM supplemented with 1 mM GSH. Following a period of 1 hour, half the preparations were treated with SFN (final concentration 50  $\mu$ M) while the other half did not receive SFN treatment. After 18 hours, gene expression was measured using Taqman qRT-PCR. A) Gene expression of *HSPA5*, encoding BiP, B) gene expression of *DDIT3*, encoding CHOP, and C) gene expression of *ERN1*, encoding IRE1. Quantitative data are shown as mean  $\pm$  SEM (n=4). An asterisk indicates a significant difference between the treated group and all other groups ( $p \leq 0.05$ ; ANOVA with Tukey's post hoc test).

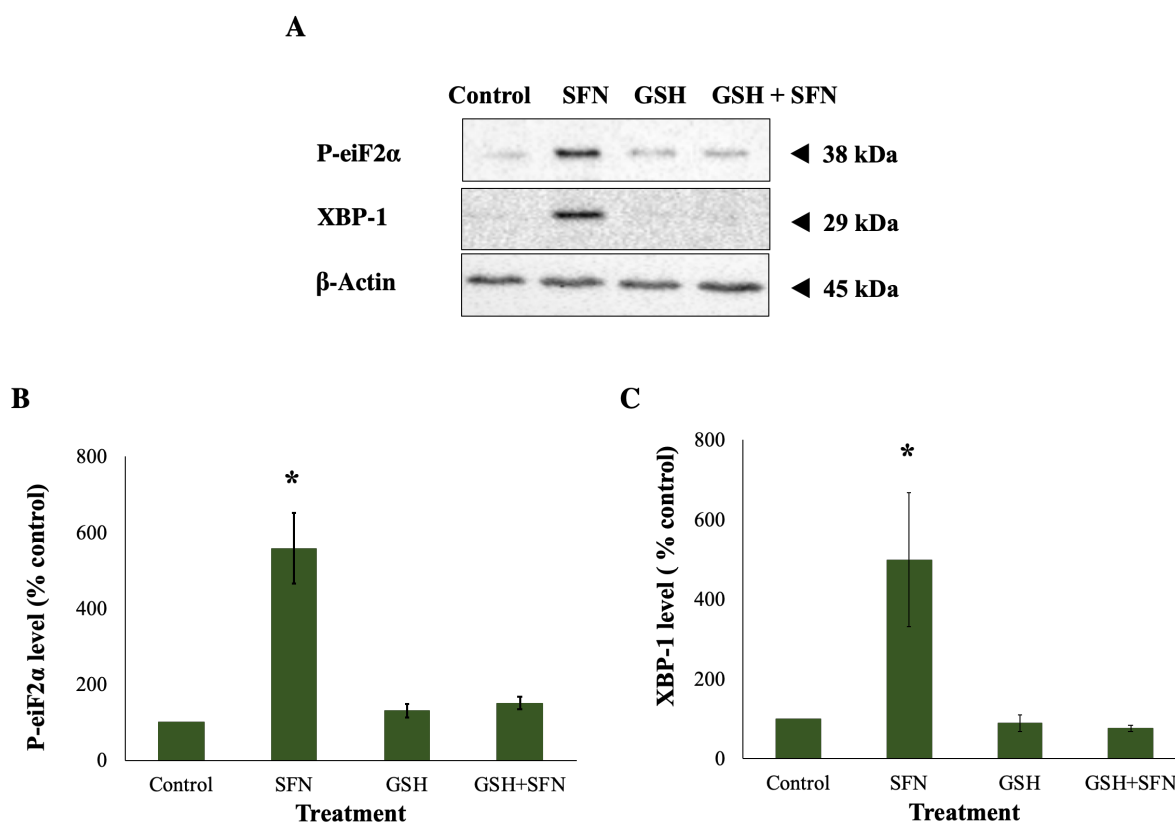


**Figure 6. 6: GSH prevents elevation of ERS protein markers by SFN in FHL124 cells.**

FHL124 cells were either maintained in serum-free (control) EMEM or EMEM supplemented with 1 mM GSH. Following a period of 1 hour, half the preparations were treated with SFN (final concentration 50  $\mu$ M) while the other half did not receive SFN treatment. After 18 hours, protein level was measured using Western blot. A) Protein levels of P-eIF2 $\alpha$  and XBP-1 were assessed via Western blot; B) Quantification of Western blot data of P-eIF2 $\alpha$  normalised against  $\beta$ -Actin using ImageJ; C) Quantification of Western blot data of XBP-1 normalised against  $\beta$ -Actin using ImageJ. Quantitative data are shown as mean  $\pm$  SEM (n=3). An asterisk indicates a significant difference between the treated group and all other groups ( $p \leq 0.05$ ; ANOVA with Tukey's post hoc test).

### 6.3.5 GSH prevents DNA damage induced by SFN in FHL124 cells.

FHL124 cells were treated for 6 hours with 50  $\mu$ M SFN and stained for  $\gamma$ -H2AX foci and DAPI (Figure 6. 7). Following a 6-hour treatment with 50  $\mu$ M SFN, the number of  $\gamma$ -H2AX foci increased by more than  $928.7 \pm 337.1\%$  relative to the control levels. Treatment with 1 mM GSH reduced this dramatically but did not fully restore the foci number to baseline levels,  $228.9 \pm 60.5\%$  relative to the baseline. There was no significant difference between the control and GSH + SFN samples.

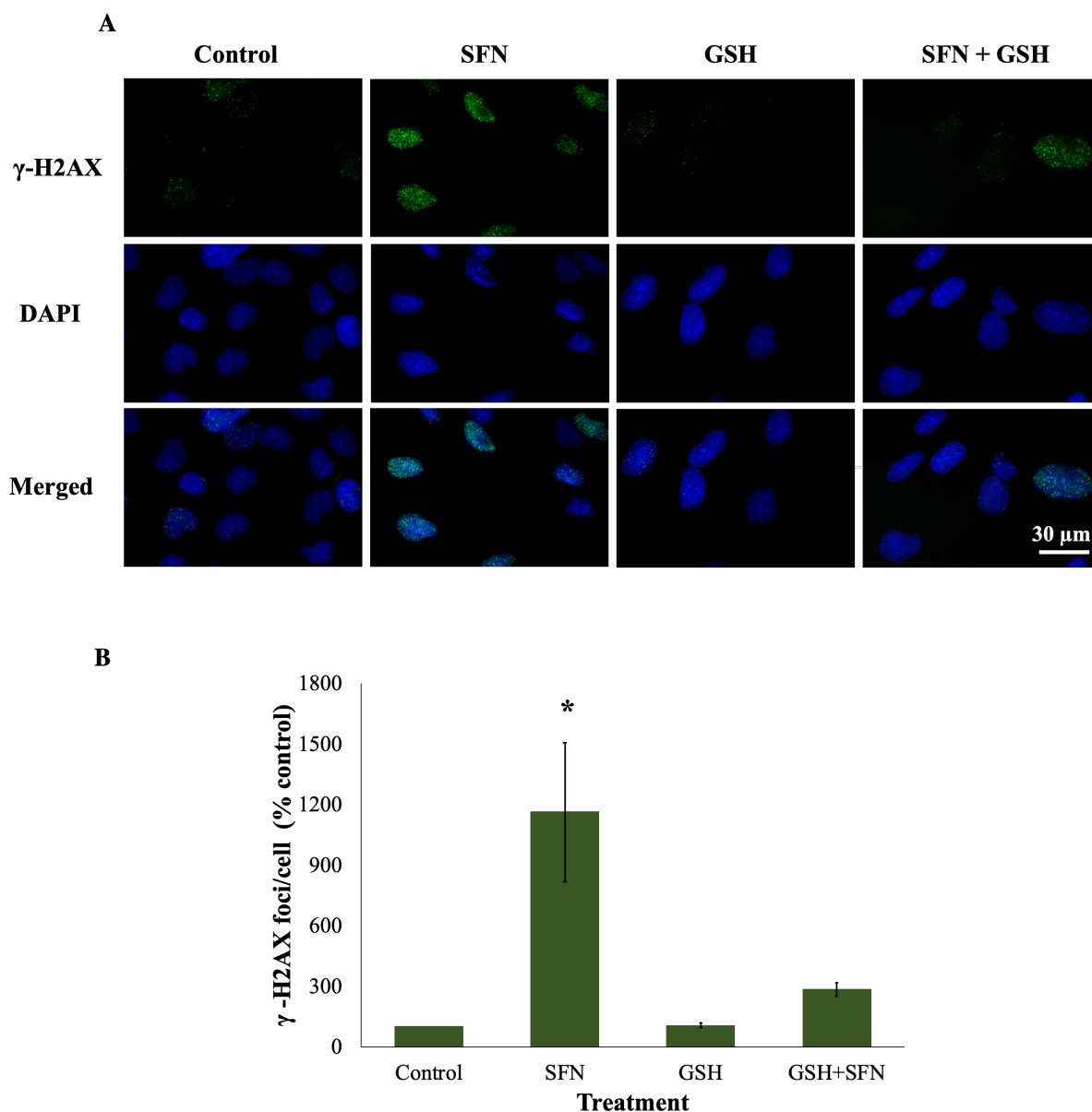
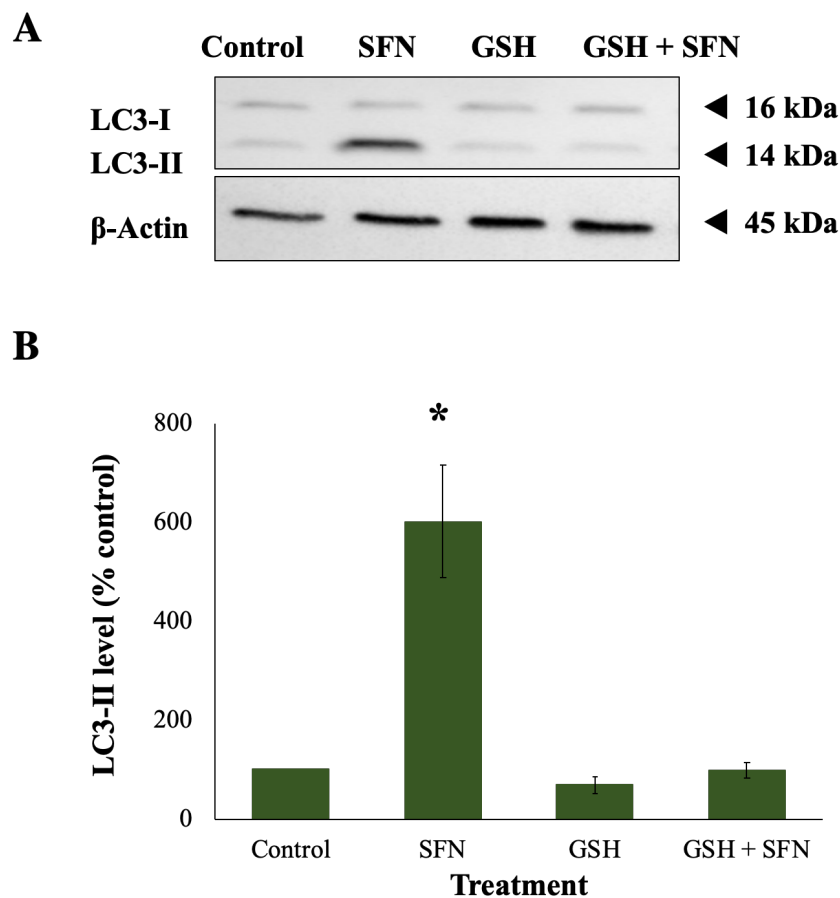


**Figure 6. 7: GSH prevents DNA double-strand breaks induced by SFN in FHL124 cells.**

FHL124 cells were either maintained in serum-free (control) EMEM or EMEM supplemented with 1 mM GSH. Following a period of 1 hour, half the preparations were treated with SFN (final concentration 50  $\mu$ M) while the other half did not receive SFN treatment. After 6 hours,  $\gamma$ -H2AX foci were measured using wide-field microscopy. (A) Representative images (green –  $\gamma$ -H2AX, blue – DAPI, merged –  $\gamma$ -H2AX and DAPI) and (B) quantitative data are shown as mean  $\pm$  SEM (n=4). An asterisk indicates a significant difference between the treated group and all other groups ( $p \leq 0.05$ ; ANOVA with Tukey's post hoc test).

### 6.3.6 GSH prevents autophagy induced by SFN in FHL124 cells.

To investigate autophagy in FHL124 cells, immunoblotting of LC3 was used (**Figure 6. 8**). After 18 hours of SFN treatment, there was no change in LC3-I, but the level of LC3-II increased by  $601.1 \pm 114.5\%$  in FHL124 cells, suggesting elevated autophagy. Treatment with 1 mM GSH significantly prevented this rise.

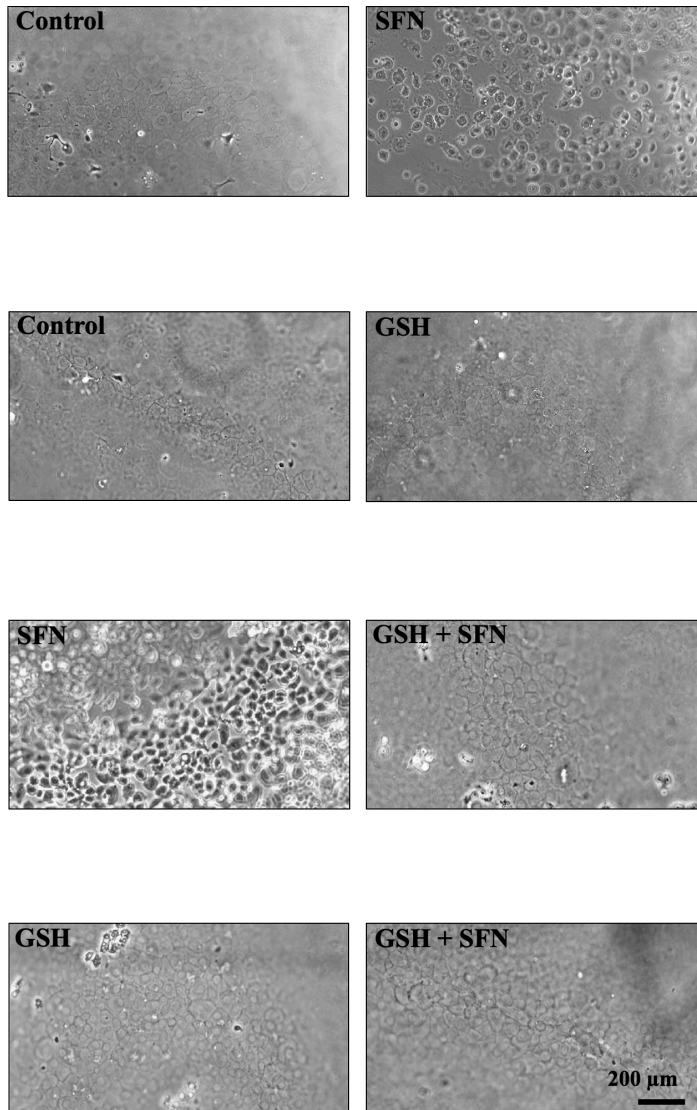
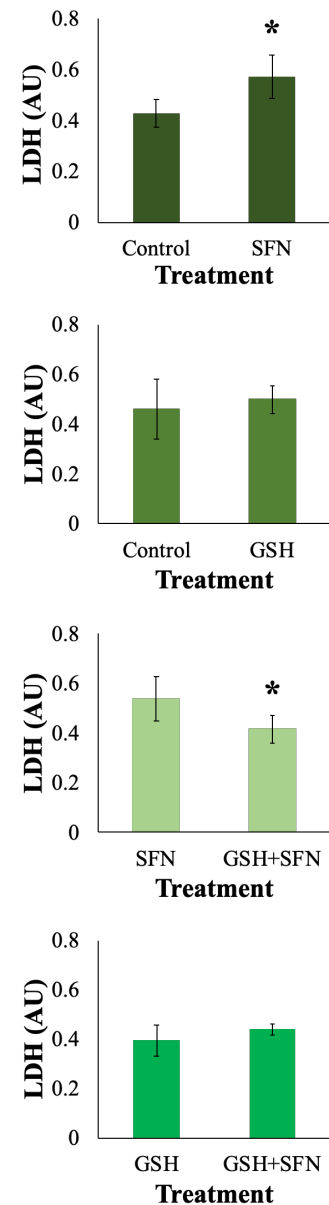


**Figure 6. 8: GSH protects cells from autophagy induced by SFN in FHL124 cells.**

FHL124 cells were either maintained in serum-free (control) EMEM or EMEM supplemented with 1 mM GSH. Following a period of 1 hour, half the preparations were treated with SFN (final concentration 50  $\mu$ M) while the other half did not receive SFN treatment. After 18 hours, LC3-I and LC3-II protein levels were measured using Western blot. A) Representative blot and B) Quantitative data of LC3-II normalised against  $\beta$ -Actin using ImageJ. Quantitative data are pooled from four separate experiments for FHL124 cells. Data are presented as mean  $\pm$  SEM (n = 4). An asterisk indicates a significant difference between the treated group and all other groups ( $p \leq 0.05$ ; ANOVA with Tukey's post hoc test).

### **6.3.7 GSH protects human lens epithelium from SFN-induced cytotoxicity.**

Whole capsulorhexis samples were either maintained in serum-free (control) EMEM or EMEM supplemented with 1 mM GSH. Following a period of 1 hour, half the preparations were treated with SFN (final concentration 50  $\mu$ M) while the other half did not receive SFN treatment. Tissue samples were then incubated for 24 hours. Human epithelium samples also exhibited comparable patterns induced by 50  $\mu$ M SFN as in FHL124 cells: from a single layer of cuboidal epithelial cells positioned next to each other to enlarged, round cells (**Figure 6. 9A**). SFN also increased LDH secretion by nearly 130% in the human lens epithelium relative to the control level (**Figure 6. 9B**). GSH treatment prevented all these detrimental effects induced by SFN in the human lens epithelium.

**A****B**

**Figure 6. 9: GSH protects cells from cell death induced by SFN in human lens epithelium.**

Whole capsulorhexis samples were either maintained in serum-free (control) EMEM or EMEM supplemented with 1 mM GSH. Following a period of 1 hour, half the preparations were treated with SFN (final concentration 50  $\mu$ M) while the other half did not receive SFN treatment. Tissue samples were treated for 24 hours after the addition of SFN. A) Cell morphology was observed using phase-contrast microscopy; B) Cytotoxicity was assessed using an LDH assay. Quantitative data are pooled from four match-paired human epithelium tissues. Data are shown as mean  $\pm$  SEM. AU stands for arbitrary unit. An asterisk indicates a significant difference between the second group and the first group for each pair of treatments ( $p \leq 0.05$ ; paired Student's *t*-test).

### **6.3.8 GSH prevents autophagy induced by SFN in human lens epithelium.**

Western blot of LC3 was also used to examine autophagy in human lens epithelium (**Figure 6. 10A**). After 24 hours, 100  $\mu$ M SFN significantly increased LC3-II protein levels in human lens epithelium and 1 mM GSH prevented LC3-II protein levels from increasing (**Figure 6. 10B**).

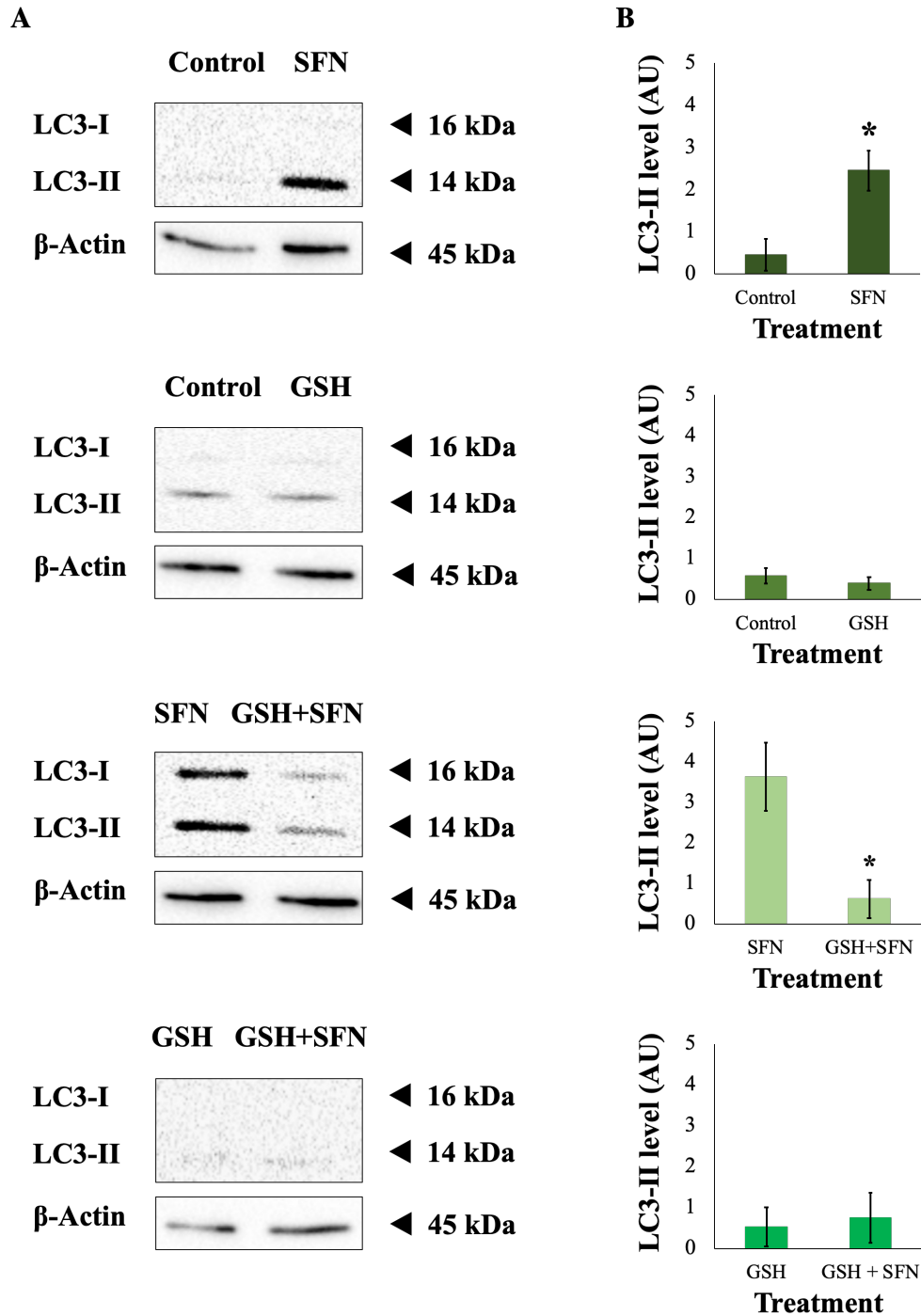


**Figure 6. 10: GSH protects cells from autophagy induced by SFN in human lens epithelium.**

Whole capsulorhexis samples were either maintained in serum-free (control) EMEM or EMEM supplemented with 1 mM GSH. Following a period of 1 hour, half the preparations were treated with SFN (final concentration 100  $\mu$ M) while the other half did not receive SFN treatment. After 24 hours, LC3-I and LC3-II levels were detected using Western blot. A) Representative blots and B) Quantitative data of LC3-II normalised against  $\beta$ -Actin using ImageJ. Quantitative data are pooled from four match-paired human epithelium tissues. Data are presented as mean  $\pm$  SEM. An asterisk indicates a significant difference between the second group and the first group for each pair of treatments ( $p \leq 0.05$ ; paired Student's *t*-test).

## 6.4 Discussion

In **Chapter 5**, 50  $\mu\text{M}$  SFN depleted the intracellular GSH levels rapidly in human lens experimental models, potentially via direct conjugation and inhibition of its recycling. Treating human lens cell and tissue models with exogenous GSH before SFN protected both models from cell death and various downstream stress responses. The findings presented in the study confirm the hypothesis and demonstrate that SFN-induced GSH depletion is a key trigger of SFN-induced cytotoxicity.

In agreement with the key finding presented here, GSH depletion has also been reported as an early hallmark in the progression of cell death in response to different apoptotic stimuli (Franco & Cidlowski, 2009; Mani, Swargiary, & Singh, 2020). The oxidation of GSH to GSSG by free radicals, such as ROS or reactive nitrogen species (RNS), produced by chemotherapeutics and xenobiotics, and the formation of GSH conjugates with highly reactive compounds, for example, 3-Bromopyruvate and isothiocyanates, have been found to drive apoptosis . Decreases in GSH levels due to impairments in GSH synthesis can also lead to cell death. The enzyme glutamate-cysteine ligase (GCL) is one of the key players in *de novo* GSH synthesis. GCL knockout mice die from massive apoptotic cell death (Dalton, Chen, Schneider, Nebert, & Shertzer, 2004) and GCL knockdown neuron cells suffer from apoptosis (Diaz-Hernandez, Almeida, Delgado-Estaban, Fernandez, & Bolanos, 2005). Inhibition of cysteine uptake by uptake inhibitors, such as erastin and sorafenib, can also impair GSH synthesis and induce apoptosis, as reported in retinal pigment epithelial cells (Amstrong, Whiteman, Yang, Jones, & Sternberg, 2004). Replenishing intracellular GSH levels by providing cells with cysteine or GSH precursors, or overexpressing GCL, has been shown to protect against apoptosis (Franco & Cidlowski, 2009).

The important role of GSH depletion in cell death can be attributable to consequent changes in the redox environment and S-glutathionylation. The depletion of GSH might increase cellular oxidative potential and promote ROS formation, which together lead to oxidative stress-mediated apoptosis. Possible mechanisms of oxidative stress-mediated phenomena have been discussed in **Chapter 4**. On the other hand, depletion of GSH in response to xenobiotic conjugation, and consequently, a decrease in the GSH/GSSG ratio, can also amplify protein S-glutathionylation. This type of PTM has been shown to trigger and regulate apoptosis via JNK activation, caspase activation, and inaction of anti-apoptotic signals (Franco & Cidlowski, 2009).

Before cell death, SFN-induced GSH depletion impairs mitochondrial networks, increases ERS, causes DNA double-strand breaks, and elevates autophagy. This could ensue from the subsequent oxidative stress following the fall of GSH antioxidant defence. Ample literature has established that GSH has a key role in protecting cells and their organelles from various stress stimuli, including ROS. The deficiency of GSH due to SFN treatment highly likely increased oxidative stress potential and rendered cellular organelles increasingly vulnerable to oxidative stress. The key role of ROS in these stress events induced by SFN was previously illustrated and discussed in **Chapter 4**. In **Chapter 5**, the intracellular GSH/GSSG ratio was reported to drop below 10% after 4 hours of 50  $\mu$ M SFN. This represents an overview of the GSH homeostasis of the whole cell, cGSH and GSH in other organelles. Therefore, it could be interpreted that SFN also severely depleted the global GSH content.

Mitochondria are a major source of ROS, predominantly  $O_2^-$ . Within the mitochondrial matrix,  $O_2^-$  is converted to  $H_2O_2$ . Due to the absence of catalase, the mGSH system, alongside the thioredoxin (Trx) and peroxiredoxin (Prx) systems, is one of the major  $H_2O_2$  metabolism

pathways in the mitochondria. mGSH is also the primary defence against oxidative damage to mitochondrial membranes through the actions of mitochondrial GST enzymes (Mari, Morales, Colell, Garcia-Ruiz, & Fernandez-Checa, 2009). Therefore, under the potential chronic mGSH depletion induced by SFN, mitochondria likely become significantly susceptible to H<sub>2</sub>O<sub>2</sub> accumulation and its accompanying detrimental oxidative damage, such as mitochondrial network collapse. The link between mGSH and mitochondrial network integrity has been previously reported (Booty et al., 2019). In a study published in the Cell journal, Booty and co-authors reported that the selective disruption of mitochondrial thiol homeostasis afforded by mitoCDNB was sufficient to rapidly induce significant mitochondrial fragmentation in C2C12 myoblast mouse cells. Disruption of S-glutathionylation signalling cascades, as a consequence of GSH depletion, can also damage mitochondrial proteins and eventually impair mitochondrial functions (Mailloux & Willmore, 2014).

In the ER, the GSH/GSSG is relatively low compared to the cytosol or mitochondria (Montero et al., 2013). The oxidising environment created by high GSSG levels is necessary for accurate protein folding in the ER. Similar to mitochondria, the ER needs to import GSH from the cytosol. However, different from mitochondria, the ER does not have GR enzymes to convert GSSG to GSH, making the ER completely dependent on the cGSH pool (Ponsero et al., 2017). Therefore, in this study, the ER-GSH pool likely suffered from the cGSH depletion induced by SFN, which might have led to protein misfolding, and consequently ERS. This finding is supported by a biochemical study where the authors reported that depletion of GSH by BSO treatment increased the formation of non-native disulfide bonds, instead of native ones that are essential for protein folding and maturation (Chakravarthi & Bulleid, 2004).

The supplementation with GSH protects FHL124 cells against SFN-induced double-strand breaks. A possible explanation for this phenomenon might be that GSH has an important role in DNA repair, despite its minimal concentration in the nucleus (Lv et al., 2019). There was an accumulation of DNA damage in the organs of mice that had a defect in GSH metabolism (Rojas, Valverde, Kala, Kaga, & Lieberman, 2000). The thiol group in GSH was specifically found to participate in repairing radical-induced damaged DNA in cancer cells treated with ROS (Alvarez-Idaboy & Galano, 2012). The noticeable feature of this process is the speed, which was fast enough to repair the damage before replication and therefore, to prevent the retention of DNA damage. In cells challenged with ionising radiation, GSH was evidenced to help repair both single-strand breaks and double-strand breaks (Ghoshal et al., 2017; Revesz & Edgren, 1984).

GSH also protects lens cells from SFN-induced autophagy. Compared to the knowledge about the role of ROS in autophagy regulation, the mechanism and interplay between GSH and the initiation and promotion of autophagy are less understood (Lv et al., 2019). Nevertheless, mounting evidence suggests that intracellular GSH levels can drive autophagy at multiple levels. Low levels of GSH, which are slightly under the basal level, appear to initiate autophagy as an adaptive stress response. When severe GSH depletion occurs, caused by nutrient starvation, GSH synthesis inhibition or conjugation with GSH or GSH efflux, excessive ROS generation results and autophagic cell death follows (Desideri, Filomeni, & Ciriolo, 2012; Guo et al., 2011). Replenishment of intracellular GSH levels has been shown to abolish the formation of autophagosomes and prevent autophagy in several experimental models (Lai et al., 2008; Scherz-Shouval et al., 2007; Yuan et al., 2009). The ability of GSH levels to influence autophagy can also be attributable to S-glutathionylation. AMPK is one of the major autophagy

regulators and has been proposed to be activated through this PTM mode (Filomeni et al., 2015; Zmijewski et al., 2010).

Regarding the experimental design, there may be a debate about the merits of GSH supplementation. Human lens epithelial cells were supplemented with GSH 1 hour before the addition of SFN, which is similar to previous studies using ROS scavengers. The purpose of this approach was to increase the intracellular GSH pool prior to SFN treatment and replenish GSH levels following depletion induced by SFN. This objective could be achieved via direct uptake and by degradation and uptake of its constituent amino acids followed by GSH synthesis. It has been reported that intact GSH can be taken up by mouse lenses, human and rat intestinal epithelial cells regardless of how much GSH is already present in the cytosol (Kovacs-Nolan et al., 2014), suggesting no gradient barrier preventing cells from transporting GSH. As a nucleophile, GSH can directly bind to electrophilic SFN without GST (Kolm et al., 1995). The possibility of such spontaneous reactions may raise a potential argument that the addition of exogenous GSH could prevent SFN from accumulating in the cytosol by forming conjugates with SFN in the medium, and for that reason, the absence of SFN-induced cytotoxicity was rather due to the absence of SFN. Nevertheless, extracellular conjugation should be negligible. The evidence comes from a study investigating how NAC prevents SFN uptake (Mi et al., 2010), that has been discussed in **Chapter 4**. GSH has weaker nucleophilicity than NAC (Zhitkovich, 2019). Hence, if the application of 1 mM NAC has negligible impacts on SFN uptake, the use of 1 mM GSH should not interfere with SFN cellular uptake.

Intracellular GSH depletion is established as an early hallmark in the progression of cell death caused by various stress insults. However, the exact mechanisms through which GSH regulates cell death remain elusive. The current study presents a possible mechanism whereby SFN-

induced GSH depletion regulates cell death via triggering diverse stress responses and targeting different cellular organelles (

Figure 6. 11).

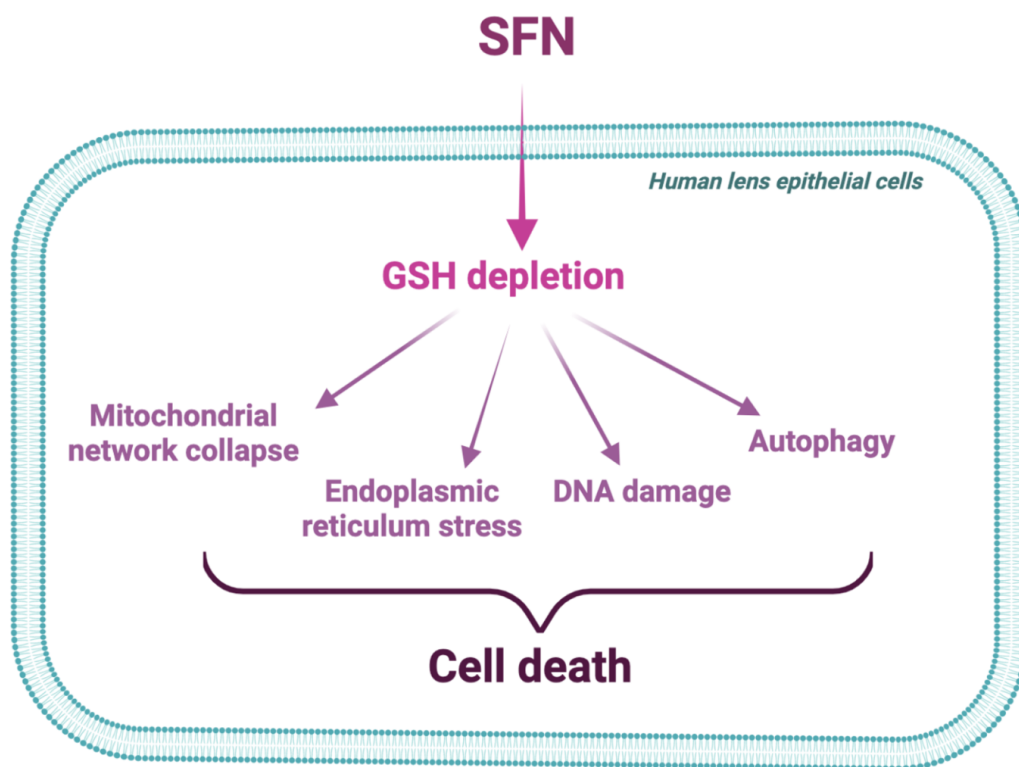


Figure 6. 11: GSH depletion mediates stress and death induced by SFN in human lens epithelial cells.

## **Chapter 7 General Discussion**

---

### **7.1 Summary of results and future work**

PCO remains an important and common complication of cataract surgery. Cataract is highly associated with ageing. As population ageing is a global phenomenon, the number of people undergoing cataract surgery increases. As a result, there is a greater need for better management of PCO. Some improved features in IOL designs have helped slow PCO progression, however, the problem is far from resolved. A combination of improved IOL designs and pharmacological treatment is likely to offer the best outcome to patients after cataract surgery (Wormstone et al., 2021). On the other hand, SFN, an isothiocyanate from cruciferous vegetables, is an emerging therapeutic phytochemical agent for many health conditions, mostly cancer. Recently, SFN-induced cytotoxicity has been shown to have potential to prevent PCO (H. Liu et al.,

2017). However, to reinforce such a promising therapeutic application of SFN, it is pivotal to grasp the mechanisms behind SFN-induced cytotoxicity in the human lens.

Since the first isolation of SFN from broccoli in the early 1990s, thousands of publications have described its efficacy in animal disease models and over 50 clinical trials have examined disease mitigation offered by this agent. SFN is an intriguing molecule that can elicit a range of cellular responses in different organelles (Yagishita et al., 2019). The effects of SFN are often multifaceted, and even contradictory, depending on its concentrations and experimental models. Nevertheless, little is known about how SFN affects human lens cells. Liu and co-authors have reported that SFN triggers cell death in a concentration-dependent manner (H. Liu et al., 2013), and that SFN at 100  $\mu$ M can also increase ROS, trigger ERS and elevate autophagy in foetal human lens epithelial FHL124 cells (H. Liu et al., 2017). In addition, using a different human lens epithelial cell model, Chhunchha and collaborators suggest that cell death caused by this agent is dependent upon ROS generation following the activation of non-canonical Nrf2 signalling (Chhunchha et al., 2019). However, no study has elucidated the complete interplay and sequence of events contributing to SFN-induced cytotoxicity. Therefore, this thesis aims to elucidate key processes and mechanisms linking SFN treatment to cell death in the human lens. Gathered from four result chapters, it is now demonstrated that oxidative stress arising from GSH depletion and ROS formation mediates SFN-induced cytotoxicity in human lens epithelial cells.

In the first result chapter, SFN was reported to not only increase ERS and cause cell death but also damage mitochondrial networks, impair mitochondrial function and trigger DNA damage responses. Two overlapping elements with the previous study are ERS and loss of cell viability. While both studies employ similar biochemical assays to investigate cell populations, the

current study relies on a different method to detect ERS. Instead of measuring expression levels of ERS gene and protein markers, the transcriptional activity of ATF6, one of three pathways in the unfolded protein responses, was assessed. The advantage of this approach is the ability to provide knowledge about the dynamics of ERS. ATF6 cannot regulate gene expression unless a series of ERS signalling events have already taken place: release of ATF6 from BiP – the central regulator of ERS, ATF6 activation in the Golgi apparatus via proteolytic cleavage, and ATF6 translocation into the nucleus. This approach also complements those focusing on gene and protein levels, because together they paint a complete picture of ERS in response to SFN, starting from transcriptional activity, to gene expression and, subsequently, protein levels.

Another highlight of **Chapter 3** is the work on mitochondria. Mitochondria are responsible for numerous physiological cellular events and are also accountable for various pathological conditions (Bhatti et al., 2017; Shadel & Horvath, 2015). Therefore, it is of great interest to examine how mitochondria respond to SFN. This phytochemical has been reported to induce deleterious impacts of SFN to mitochondrial membrane potential ( $\Delta\psi_m$ ) (W. Y. Choi et al., 2008; Rhoden et al., 2021), which provides the essential charge gradient for normal mitochondrial activities. Using a fluorescent dye that is sensitive to  $\Delta\psi_m$ , the study confirmed that SFN also caused loss of  $\Delta\psi_m$  in human lens epithelial cells. There are also other key elements that mediate mitochondrial functions, for example, the integrity of mitochondrial networks. However, there has been little research on the impacts of SFN on mitochondrial networks, and especially, none has been done in the human lens. Therefore, various strategies were introduced to support the investigation of this aspect in human lens epithelial cells. The mitochondrial networks were labelled in two different ways, including cells transfected with GFP signals localising at mitochondria and cells stained with a MitoTracker dye, and were visualised using two different methods, either live imaging or fixed cell imaging. Regardless

of labelling and imaging approaches, SFN was consistently reported to induce irreversible mitochondrial network shrinkage and loss of normal dynamic features, strongly suggesting that SFN can cause dire consequences to mitochondrial networks.

Not only did the current study visualise mitochondrial networks following SFN treatment, but it also developed a workflow to quantify changes in mitochondrial networks. The quantification method was carefully modified from one introduced by the Stuart group (Valente et al., 2017). This resulted in a simpler and easier-to-adopt method, allowing maximising the use of information provided by images acquired from confocal microscopy and overcoming intrinsic limitations of current imaging facilities. Consequently, the extent of mitochondrial network shrinkage observed in images was calculated: SFN significantly shrunk the mitochondrial network size to 30% of the relative baseline size. These technical developments effectively helped demonstrate the detrimental influence of SFN on mitochondrial functions, and now can provide future studies with a selection of robust tools to assess the health of cellular powerhouses. Nevertheless, the current study did not examine the molecular biology involved in the dynamic of mitochondrial networks, which is tightly regulated by the fission/fusion pathways. Accordingly, future research should aim to understand how SFN influences relevant molecules, leading to the collapse of mitochondrial networks.

Additionally, time-response studies in **Chapter 3** provide insight into how early these events can be initiated and how they progress over time following SFN exposure, especially when they may not unidirectionally change. It is exemplified in the measurement of cell viability, where cell viability exhibited a significant surge before depletion, and in mitochondrial networks, where hyperfusion was observed before the networks collapsed. These phenomena suggest that under early stress challenges induced by SFN, human lens cells endeavour to

restore homeostasis, for example, by raising ATP production to provide for energy-consuming adaptive responses or by fusing mitochondrial networks to minimise stress load. It may also imply a small window that “life-death” molecular switches have not been activated and cells can be rescued during this period of time. Taken together, **Chapter 3** successfully confirms some key aspects that have been investigated by Liu and co-authors and expands the repertoire of cellular events to establish a robust platform for subsequent studies.

With a comprehensive portfolio of cellular events induced by SFN, the study then aimed to identify a common mediator of those events. Previously, both Liu et al and Chhunchha et al studies have shown ROS upregulation following SFN (Chhunchha et al., 2019; H. Liu et al., 2017), therefore it was hypothesised that ROS was the common mediator. The treatment of ROS scavengers, NAC or sodium pyruvate, was reported to completely prevent cell death caused by SFN in human lens epithelial cells. The treatment of NAC completely protected lens cells from all cellular events, including mitochondrial dysfunction, ERS, DNA damage, and autophagy. The findings in **Chapter 4** imply that oxidative stress arising from SFN-induced ROS elevation triggers various stress responses and eventually cell death in human lens cells.

In addition to the direct impacts of oxidative stress on each cellular event, there may be crosstalk between them. Mitochondria and the ER closely interact with each other, both physically and functionally. Approximately 5-20% of the mitochondrial surface is directly in contact with the ER via highly dynamic structures called mitochondria-associated membranes (MAMs) to allow functional transit of metabolites and signalling molecules, such as  $\text{Ca}^{2+}$  and ROS (Gorlach, Bertram, Hudecova, & Krizanova, 2015). The ER is the main intracellular reservoir for  $\text{Ca}^{2+}$  (J. Li, Zhang, Brundel, & Wiersma, 2019; Rizzuto et al., 1998). The  $\text{Ca}^{2+}$  released via inositol 1,4,5-trisphosphate receptors ( $\text{IP}_3\text{R}$ ) located on the ER membrane is taken

up by mitochondria for mitochondrial respiration and bioenergetics. Mitochondria provide ATP in return and help buffer the  $\text{Ca}^{2+}$  levels in the ER, which are all crucial for the protein folding machinery in this organelle.

As a result, perturbations in the ER homeostasis can have direct impacts on mitochondria, and vice versa (**Figure 7. 1**). ERS can induce  $\text{Ca}^{2+}$ -dependent detrimental changes in mitochondria, such as loss of  $\Delta\psi_m$ , matrix swelling, mitochondrial permeability transition pore opening, and other mitochondria-mediated apoptotic features, such as cytochrome C release (Deniaud et al., 2008). A feed-forward loop is subsequently formed: with a small amount of cytochrome C being released, more ER  $\text{Ca}^{2+}$  will flow into mitochondria, amplifying the apoptotic signal (Boehning et al., 2003). MAMs also play a role in coordinating ER and mitochondria shape and dynamics. Several proteins involved in mitochondrial fission and fusion are associated with MAMs, including Mfn2 and Fis1 (J. Li et al., 2019). On the other hand, mitochondrial-derived ROS derived from mitochondrial dysfunction can activate ERS by activating the Nrf2 and ATF4 signalling pathways (Bjorkman & Pereira, 2021). Drops in cellular ATP levels following mitochondrial dysfunction reduce the energy-dependent protein-folding machinery in the ER, also leading to ERS (Bravo et al., 2013).

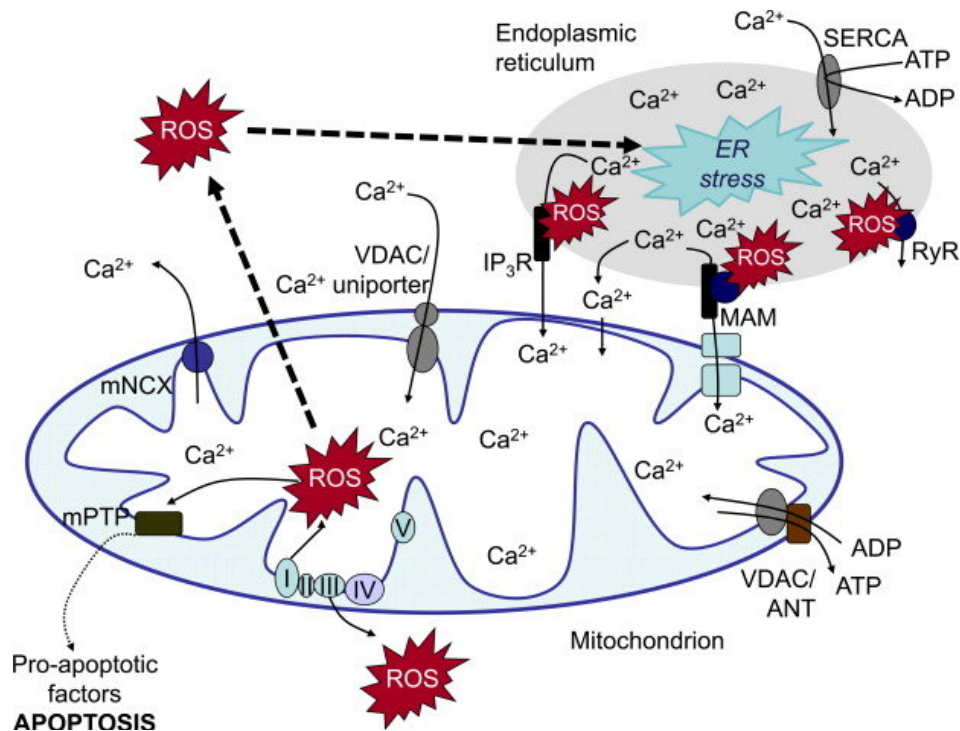


**Figure 7. 1:  $\text{Ca}^{2+}$  and ROS crosstalk between endoplasmic reticulum and mitochondria.**

$\text{Ca}^{2+}$  from ER cisternae flows mainly through  $\text{IP}_3\text{R}$ . These channels are accumulated in MAMs.  $\text{Ca}^{2+}$  from the cytoplasm enter the mitochondrion through voltage-dependent anion channels (VDAC) or  $\text{Ca}^{2+}$  uniporter. High levels of calcium stimulate respiratory chain activity leading to higher amounts of ROS. ROS can further target ER-based  $\text{Ca}^{2+}$  channels leading to increased release of  $\text{Ca}^{2+}$  and further increased ROS levels. Increased ROS and  $\text{Ca}^{2+}$  load can open the mitochondrial permeability transition pore resulting in the release of pro-apoptotic factors. Reprinted from “Calcium and ROS: A mutual interplay” by A. Gorch and co-authors, 2015, *Redox Biology*, 6, 262. Copyright 2015 by the Authors and Elsevier B.V.

Mitochondria and the ER can also influence DNA integrity in the nucleus. Following the collapse of mitochondrial networks, loss of  $\Delta\psi_m$ , and ERS, it is possible that ROS levels increase and ROS leak out of these two major ROS production sites into the cytosol and other organelles, such as the nucleus. Under GSH depletion,  $\text{H}_2\text{O}_2$  is potentially converted to  $\bullet\text{OH}$  in iron-dependent Haber-Weiss Fenton reactions, instead of being detoxified to water. DNA is generally susceptible to ROS, but guanine and thymine are particularly sensitive to oxidative damage produced by  $\bullet\text{OH}$ , resulting in DNA lesions, such as 8-oxo-7,8-dihydroguanine (8-Oxoguanine) and thymine glycol, respectively (Saki & Prakash, 2017). Other effects of ROS on DNA damage have also been discussed in previous chapters. In relation to SFN, inhibition of mitochondrial ROS production has been reported to prevent DNA damage caused by this

agent (Sestili et al., 2010). Furthermore, the results from time-response studies in **Chapter 3** imply that DNA damage is a late event compared to other changes in mitochondria and the ER. Therefore, the sequence of events may go as follows: mitochondrial dysfunction and ERS, then DNA damage.

In response to damaged mitochondria, accumulation of misfolded or unfolded proteins under ERS, and DNA damage, autophagy has been known to be activated as a pro-survival pathway. Autophagy targets and breaks down misfolded proteins to recycle the constituent materials; whereas mitophagy, a selective form of autophagy, helps degrade damaged and superfluous mitochondria to maintain mitochondrial quality. Concerning the current study, accumulating evidence has shown that autophagy can also be triggered by DNA damage response to double-strand breaks (Eliopoulos, Havaki, & Gorgoulis, 2016). Ataxia-telangiectasia mutated (ATM) enzymes are kinases that become activated in response to double-strand breaks and play a major role in H2AX phosphorylation, the key step in DNA damage response. Notably, activated ATM can also activate AMPK, one of the key autophagy inducers, and promote autophagosome formation, connecting DNA damage response to the induction of autophagy (Alexander, Kim, & Walker, 2010). On the whole, the combination of findings in this current study and the literature suggests a possible sequence of events mediated by SFN-induced ROS elevation as well as possible crosstalk between these events, as shown in **Figure 7. 2**.

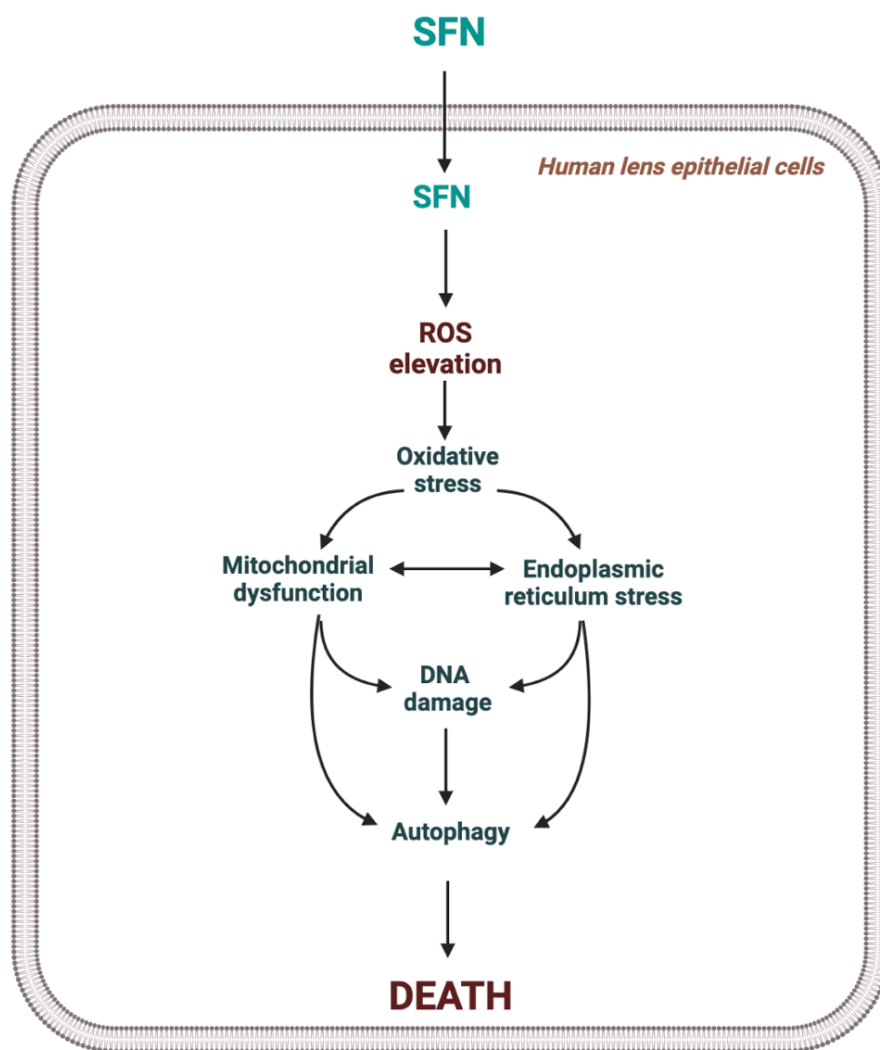


**Figure 7. 2: A relationship between events mediated by SFN-induced ROS elevation in human lens epithelial cells.**

From the findings presented in **Chapter 4**, the key role of ROS in SFN-induced cell death led to an inquiry into how ROS levels became dysregulated under the presence of SFN. In human lens cells, ROS are tightly regulated by multi-layered antioxidant defence systems made of enzymatic and non-enzymatic antioxidants. To maintain a normal redox status, antioxidants with the ability to scavenge ROS are responsible for removing ROS, while enzymatic antioxidants convert ROS into less reactive or harmless molecules. Some examples of enzymatic antioxidants include glutathione reductase (GR), glutathione peroxidase (GPx), catalase, and superoxide dismutase (SOD). On the other hand, some examples of non-

enzymatic antioxidants are GSH, vitamin C, and vitamin E. Among these antioxidants, GSH is the key factor in the maintenance of redox homeostasis in the lens. Therefore, to address the question of how oxidative stress arose following SFN treatment, the study then aimed to assess GSH homeostasis.

The first feature of the GSH homeostasis under investigation in **Chapter 5** was the GSH levels. GSH is the dominant intracellular glutathione form and exists at very high concentrations that can reach up to 6 mM in the lens (Lim et al., 2020). Being abundant in quantity allows GSH to participate in many cellular and molecular events. GSH can directly scavenge ROS and RNS or act as a co-factor for GPx to neutralise H<sub>2</sub>O<sub>2</sub> and organic peroxides. In addition to antioxidant activities, GSH can detoxify xenobiotics and their metabolites, provide cysteine, regulate the cell cycle and mediate cell death (Lu, 2014). At the organelle level, GSH is also the primary defence against oxidative damage to mitochondrial membranes, facilitates proper protein folding in the ER, and is actively involved in DNA repair in the nucleus (Alvarez-Idaboy & Galano, 2012; Ghoshal et al., 2017). Therefore, high GSH levels are crucial for both the antioxidant defence systems and other cellular functions.

Using a luminescent assay, it was reported that 50 µM SFN both rapidly and chronically depleted the GSH levels. Intracellular GSH is resistant to degradation because the gamma-carboxyl group in GSH cannot be hydrolysed by any intracellular enzymes (Baudouin-Cornu et al., 2012). Therefore, it was of great curiosity and interest to identify possible causes of SFN-induced GSH depletion. Mounting evidence has indicated that the primary mode of GSH depletion is conjugation with endogenous or xenobiotic compounds (Aoyama & Nakaki, 2012; Baudouin-Cornu et al., 2012; Y. Zhang et al., 1995). This led to a proposal that conjugation between SFN and GSH was the driving force of GSH depletion. Subsequently, the data from

mass spectrometry confirmed this speculation by showing that SFN-GSH was the major intracellular SFN metabolite. The finding was also strongly supported by many studies on SFN in other cell lines, where within 30 minutes of addition, SFN-GSH has been shown to dominate all SFN metabolites (Janobi et al., 2006; Kassahun et al., 1997; B. R. Kim et al., 2003; Y. Zhang, 2012).

Cells utilise four different pathways to maintain high intracellular GSH levels, including the *de novo* synthesis of GSH from constituent amino acids, the GR route, the uptake of GSH from outside the cells, and the GSH turnover (Lv et al., 2019). Organelles have fewer options due to the absence of the synthesis machinery, so they rely on GSH uptake from the cytosol and GR-dependent GSH recycling (Franco & Cidlowski, 2009; Mari et al., 2009). **Chapter 5** further discovered that SFN interfered with one of those mechanisms to disturb the GSH homeostasis. Using a biochemical assay, SFN was found to retard GR activity over time, and the remarkable damage could be detected as early as 2 hours. By attacking the GSH regeneration route, SFN can effectively extend its deleterious impacts on the GSH homeostasis and exacerbate the deficiency of GSH levels. Nevertheless, since the study was limited to GR activity, future studies should aim to investigate how SFN influences other pathways relevant to the GSH system, such as the *de novo* synthesis. Additionally, in light of SFN-induced ROS formation, it would be interesting to examine GPx that removes H<sub>2</sub>O<sub>2</sub> at the expense of GSH.

Then, how does oxidative stress manifest following SFN treatment? In light of the rapid negative impacts of SFN on the GSH homeostasis, it is likely that GSH depletion preceded ROS elevation and was the primary trigger of oxidative stress. Human lens epithelial cells, just like others, continuously generate ROS regardless of SFN, and the multi-layered antioxidant defence systems ensure that ROS are appropriately dealt with. However, if these cells are

quickly deprived of GSH, their key antioxidant, it is inevitable that cells will become less efficient at regulating ROS, even when ROS are at physiological levels. To prevent redox imbalance and restore redox homeostasis, cells can activate different pathways, such as the Nrf2-ARE signalling pathway, *de novo* synthesis, salvage of GSSG by GR. **Chapter 5** reported that cells treated with low concentrations of SFN could recover GSH levels from depletion in the long term, and sometimes, the GSH levels at the endpoint were even higher than the baseline level, suggesting the existence of a counter-attack mechanism. However, the absence of GSH recovery in cells treated with supranutritional concentrations of SFN indicated the limited capacity of those protective pathways. Therefore, when stress insults overwhelm the defence capacity, the redox homeostasis cannot be restored, ROS become dysregulated, and oxidative stress results. An oxidative vicious cycle can also emerge as follows: dysregulated ROS further exhaust the GSH pool since GSH can act as a direct ROS scavenger or a co-factor for other antioxidant enzymes.

With GSH depletion as the upstream event of ROS, it was logical to ascertain the role of GSH depletion in stress responses induced by SFN. In consideration of the multifaceted roles that GSH undertakes, the rapid and sustained deficiency of GSH induced by SFN likely interferes and interrupts many normal cellular activities. Therefore, **Chapter 6** aimed to evaluate whether the provision of GSH through supplementation could be adequate to overcome all previously reported oxidative damage. From a series of experiments employing the established techniques, GSH treatment was found to completely protect human lens epithelial lens cells against cellular damage, mitochondrial network collapse, ERS, DNA damage, autophagy, and cell death. Considering the data as a whole, it is possible to construct a model that illustrates the interplay that links SFN-induced GSH depletion to SFN-induced cytotoxicity, as shown in **Figure 7. 3**.

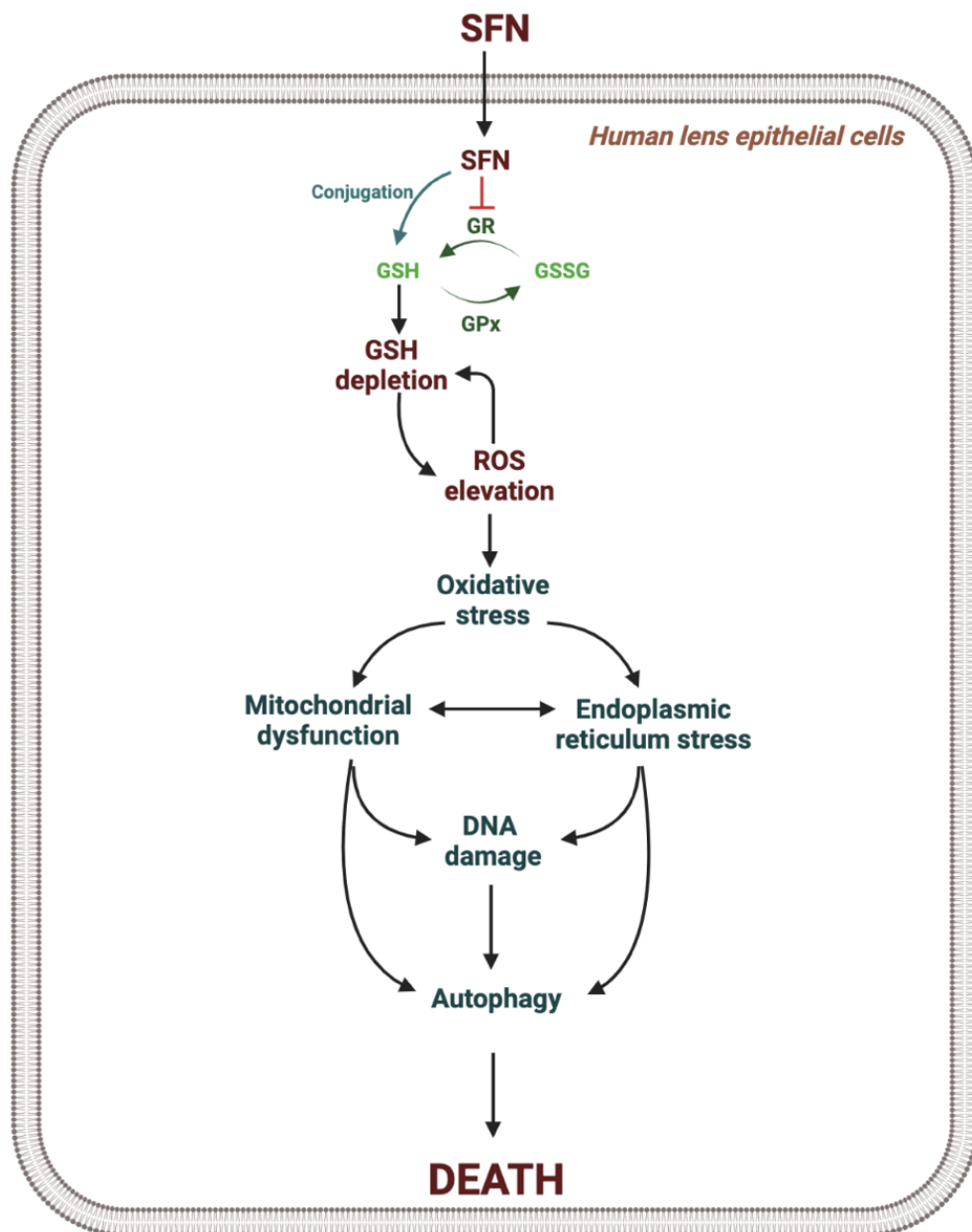


**Figure 7. 3: A proposed mechanism of SFN-induced cytotoxicity in human lens epithelial cells.** Upon cellular entry, high supranutritional SFN concentrations rapidly deplete GSH via direct conjugation. The recovery of GSH levels is further impeded by the SFN-induced deficiency of GR activity, which is responsible for regenerating GSH from GSSG. Cells become quickly deprived of the major antioxidant defence. Consequently, ROS levels increase, and oxidative stress results. ROS generation further exhausts the antioxidant defence system and leads to a vicious oxidative loop.

Simultaneously, oxidative stress causes mitochondrial dysfunction, represented by mitochondrial network shrinkage and loss of mitochondrial membrane potential, and endoplasmic reticulum stress. The crosstalk between mitochondria and the endoplasmic reticulum can further amplify these stress responses. ROS released from these two organelles subsequently attack DNA and cause DNA damage. In response to damaged organelles, accumulation of misfolded and unfolded proteins, and DNA damage, autophagy is induced to restore homeostasis as a pro-survival pathway. However, as the GSH level is severely and chronically depleted, oxidative stress persists. These adaptive responses eventually switch to their pro-apoptotic mode and cell death arises. (SFN: sulforaphane, GSH: reduced glutathione, GSSG: oxidised glutathione, GR: glutathione reductase, GPx: glutathione peroxidase, ROS: reactive oxygen species).

## **7.2 Concluding remarks**

SFN has been reported to induce a wide range of cellular stress responses, including mitochondrial dysfunction, ERS, DNA damage, autophagy and death, in various studies using different experimental models, but mostly cancer studies (W. Y. Choi et al., 2008; de Oliveira, Costa, Pedrosa, Pinto, Remdios, et al., 2014; Singh et al., 2005; D. Xiao et al., 2009; Zheng et al., 2020). The current study is the first to unify this wide range of cellular responses induced by SFN in a human non-cancer, non-virally transformed lens cell line. Consequently, this establishes a robust platform to understand the mechanisms of action of SFN to explore therapeutic potential of this phytochemical not only in the lens but also in other non-cancer disorders, such as inflammatory conditions, metabolic conditions and neurodegenerative diseases (Davidson et al. 2013; Napoli et al. 2021; Houghton 2019).

Furthermore, this current study successfully establishes a complete model showing the interplay between redox status and physiological stress responses leading to SFN induced cell death. SFN depletes GSH levels in lens cells through conjugation and inhibition of GR activity. This leads to increased ROS and oxidative stress that triggers mitochondrial dysfunction, ERS, autophagy and DNA damage leading to cell death. Building on Liu's fundamental work evidencing the therapeutic use of SFN to prevent PCO (H. Liu et al., 2017), the elucidation of its cytotoxicity in this study provides mechanistic understanding to significantly advance the pharmaceutical applications of SFN to manage this condition. Lastly, this study also highlights

SFN as a promising agent to investigate a wide range of pathological conditions and ageing associated with GSH imbalance (Ballatori et al., 2009).

## Reference

---

- Abbaoui, B., Telu, K. H., Lucas, C. R., Thomas-Ahner, J. M., Schwartz, S. J., Clinton, S. K., ... Mortazavi, A. (2017). The Impact of Cruciferous Vegetable Isothiocyanates on Histone Acetylation and Histone Phosphorylation in Bladder Cancer. *J Proteomics*, *156*, 94–103.
- Abdelkader, H., Alany, R. G., & Pierscionek, B. (2014). Age-related cataract and drug therapy: opportunities and challenges for topical and antioxidant delivery to the lens. *J Pharm Pharmacol*, *67*, 537–550.
- Abouzeid, H., & Ferrini, W. (2014). Femtosecond-laser assisted cataract surgery: a review. *Acta Ophthalmol*, *92*, 597–603.
- Aguilera, A., & Gómez-González, B. (2008). Genome instability: a mechanistic view of its causes and consequences. *Nat Rev Genet*, *9*, 204–217.
- Alberts, B., Johnson, A., Lewis, J., Raff, M., Roberts, K., & Walter, P. (2014). *Molecular biology of the cell* (6th ed.). New York: Garland Science.
- Ales, C., & Ruth, A. P. (2014). The cellular and molecular mechanisms of vertebrate lens development. *Development*, *141*, 4432–4447.
- Alexander, A., Kim, J., & Walker, C. L. (2010). ATM engages the TSC2/mTORC1 signaling node to regulate autophagy. *Autophagy*, *6*, 672–673.
- Alvarez-Idaboy, J. R., & Galano, A. (2012). On the Chemical Repair of DNA Radicals by Glutathione: Hydrogen vs Electron Transfer. *J Phys Chem B*, *116*(31), 9316–9325.
- Armstrong, J. S., Whiteman, M., Yang, H., Jones, D. P., & Sternberg, J. P. (2004). Cysteine starvation activates the redox-dependent mitochondrial permeability transition in retinal pigment epithelial cells. *Invest Ophthalmol Vis Sci*, *45*, 4183–4189.
- Andley, U. P., Song, Z., Wawrousek, E. F., Fleming, T. P., & Bassnett, S. (2000). Differential protective activity of alpha A- and alphaB-crystallin in lens epithelial cell. *J Biol Chem*, *275*, 36823–36831.
- Aoyama, K., & Nakaki, T. (2012). Inhibition of GTRAP3-18 may increase neuroprotective glutathione (GSH) synthesis. *In J Mol Sci*, *13*, 12017–12035. <https://doi.org/10.3390/ijms130912017>
- Aquilano, K., Baldelli, S., & Ciriolo, M. R. (2014). Glutathione: new roles in redox signaling for an old antioxidant. *Front Pharmacol*, *5*, 196.
- Atmane, N., Dairou, J., Paul, A., Dupret, J. M., & Rodrigues-Lima, F. (2003). Redox Regulation of the Human Xenobiotic Metabolizing Enzyme Arylamine N-Acetyltransferase 1 (NAT1): Reversible inactivation by hydrogen peroxide. *J Biol Chem*, *278*(37), 35086–35992. <https://doi.org/https://doi.org/10.1074/jbc.M303813200>
- Atwell, L. L., Beaver, L. M., Shannon, J., Williams, D. E., Dashwood, R. H., & Ho, E.

- (2016). Epigenetic Regulation by Sulforaphane: Opportunities for Breast and Prostate Cancer Chemoprevention. *Curr Pharmacol Rep*, 1(2), 102–111.
- Atwell, L. L., Hsu, A., Wong, C. P., Stevens, J. F., Bella, D., Yu, T., ... Ho, E. (2015). Absorption and chemopreventive targets of sulforaphane in humans following consumption of broccoli sprouts or a myrosinase-treated broccoli sprout extract. *Mol Nutr Food Res*, 59(3), 424–433.
- Balaban, R. S., Nemoto, S., & Finkel, T. (2005). Mitochondria, Oxidants, and Aging. *Cell*, 120(4), 483–495.
- Ballatori, N., Krance, S. M., Notenboom, S., Shi, S., Tieu, K., & Hammond, C. (2009). Glutathione dysregulation and the etiology and progression of human diseases. *Biol Chem*, 390(3), 191–214. <https://doi.org/10.1515/BC.2009.033>
- Bansal, M., Singh, N., Pal, S., Dev, I., & Ansari, K. M. (2018). Chemopreventive Role of Dietary Phytochemicals in Colorectal Cancer. In J. Fishbein & J. Heilman (Eds.), *Advances in Molecular Toxicology* (pp. 69–121). Elsevier.
- Bassett, S. A., & Garnett, M. P. G. (2014). The Role of Dietary Histone Deacetylases (HDACs) Inhibitors in Health and Disease. *Nutrients*, 6(10), 4273–4301.
- Bassnett, S., Shi, Y., & Vrensen, G. (2011). Biological glass: structural determinants of eye lens transparency. *Philos Trans R Soc Lond B Biol Sci*, 366, 1250–1264.
- Batliwala, S., Xavier, C., Liu, Y., Wu, H., & Pang, I. (2017). Involvement of Nrf2 in ocular disease. *Oxid Med Cell Longev*, 2017, 1703810.
- Baudouin-Cornu, P., Lagniel, G., Kumar, C., Huang, M. E., & Labarre, J. (2012). Glutathione degradation is a key determinant of glutathione homeostasis. *J Biol Chem*, 287(7), 4552–4561. <https://doi.org/10.1074/jbc.M111.315705>
- Beaver, J. P., & Waring, P. (1995). A decrease in intracellular glutathione concentration precedes the onset of apoptosis in murine thymocytes. *Eur J Cell Biol*, 68(1), 47–54.
- Berthoud, V. M., & Beyer, E. C. (2009). Oxidative stress, lens gap junctions and cataracts. *Antioxid Redox Signal*, 11(2), 339–353.
- Bhattarai, K. R., Riaz, T. A., Kim, H. R., & Chae, H. J. (2021). The aftermath of the interplay between the endoplasmic reticulum stress response and redox signaling. *Exp Mol Med*, 53, 151–167.
- Bhatti, J. S., Bhatti, G. K., & Reddy, P. H. (2017). Mitochondrial dysfunction and oxidative stress in metabolic disorders — A step towards mitochondria based therapeutic strategies. *BBA Mol Basis Dis*, 1863(5), 1066–1077.
- Binkhorst, C. D., & Gobin, M. H. (1964). Injuries to the eye with lens opacity in young children. *Ophthalmologica*, 148, 169–183.
- Biswas, S., & Rahman, I. (2013). Dietary Bioactive Functional Polyphenols in Chronic Lung Diseases. In R. Watson & V. Preedy (Eds.), *Bioactive Food as Dietary Interventions for Liver and Gastrointestinal Disease* (pp. 513–525). Academic Press.
- Bjorkman, S. H., & Pereira, R. O. (2021). The Interplay Between Mitochondrial Reactive Oxygen Species, Endoplasmic Reticulum Stress, and Nrf2 Signaling in Cardiometabolic Health. *Antioxid Redox Signal*, 35(4), 252–269.
- Boehning, D., Patterson, R. L., Sedaghat, L., Glebova, N. O., Kurosaki, T., & Snyder, S. H. (2003). Cytochrome c binds to inositol (1, 4, 5) trisphosphate receptors, amplifying calcium-dependent apoptosis. *Nat Cell Biol*, 5(12), 1051–1061.
- Booty, L. M., Gawel, J. M., Cvetko, F., Caldwell, S. T., Hall, A. R., Mulvey, J. F., ... Murphy, M. P. (2019). Selective Disruption of Mitochondrial Thiol Redox State in Cells and In Vivo. *Cell Chem Biol*, 26(3), 449–461.
- Bourne, R., Flaxman, S. R., Braithwaite, T., Cicinelli, M. V, Das, A., & Jonas, J. B. (2017). Magnitude, temporal trends, and projections of the global prevalence of blindness and distance and near vision impairment: a systematic review and meta-analysis. *Lancet*

- Glob Health*, 5(9), e888–e897.
- Brand, M. D. (2016). Mitochondrial generation of superoxide and hydrogen peroxide as the source of mitochondrial redox signaling. *Free Radic Biol Med*, 100, 14–31.
- Brandsma, I., & van Gent, D. C. (2012). Pathway choice in DNA double strand break repair: observations of a balancing act. *Genome Integr*, 3(1), 9.
- Bravo, R., Parra, V., Gatica, D., Rodriguez, A. E., Torrealba, N., Paredes, F., ... Jaimovich, E. (2013). Endoplasmic reticulum and the unfolded protein response: Dynamics and metabolic integration. *Int Rev Cell Mol Biol*, 301, 215–290.
- Breckwoldt, M. O., Pfitster, F. M. J., Bradley, P. M., Marinkovic, P., Williams, P. R., Brill, M. S., ... Misgeld, M. (2014). Multiparametric optical analysis of mitochondrial redox signals during neuronal physiology and pathology in vivo. *Nat Med*, 20, 555–560.
- Bremer, M., & Doerge, R. W. (2010). *Statistics at the Bench*. New York: Cold Spring Harbor Laboratory Press.
- Brennan, L. A., & Kantorow, M. (2009). Mitochondrial function and redox control in the aging eye: role of MsrA and other repair systems in cataract and macular degenerations. *Exp Eye Res*, 88(2), 195–203. <https://doi.org/10.1016/j.exer.2008.05.018>
- Brennan, L. A., McGreal, R. S., & Kantorow, M. (2012). Oxidative stress defence and repair systems of the ocular lens. *Front in Biosci*, e4, 141–155.
- Briones-Herrera, A., Eugenio-Perez, D., Reyes-Ocampo, J. G., Rivrea-Mancia, S., & Pedraza-Chaverri, J. (2018). New highlights on the health-improving effects of sulforaphane. *Food Funct*, 9(5), 2589–2606.
- Brown, G. C., Brown, M. M., Lieske, H. B., & Lieske, P. A. (2014). Financial return-on-investment of ophthalmic interventions: a new paradigm. *Curr Opin Ophthalmol*, 25(3), 171–176.
- Budisan, L., Gulei, D., Zanoaga, O. M., Irimie, A. I., Chira, S., Braicu, C., ... Berindan-Neagoe, I. (2017). Dietary intervention by phytochemicals and their role in modulating coding and non-coding genes in cancer. *Int J Mol Sci*, 18(6), 1178. <https://doi.org/10.3390/ijms18061178>
- Candia, O. A. (2004). Electrolyte and fluid transport across corneal, conjunctival and lens epithelia. *Exp Eye Res*, 78, 527–535.
- Chakravarthi, S., & Bulleid, N. (2004). Glutathione Is Required to Regulate the Formation of Native Disulfide Bonds within Proteins Entering the Secretory Pathway. *J Biol Chem*, 279(38), 39872–39879.
- Chhunchha, B., Kubo, E., & Singh, D. P. (2019). Sulforaphane-induced Klf9/Prdx6 axis acts as a molecular switch to control redox signaling and determines fate of cells. *Cells*, 8(10), 1159. <https://doi.org/10.3390/cells8101159>
- Choi, W. Y., Choi, B. T., Lee, H., & Choi, Y. H. (2008). Sulforaphane generates reactive oxygen species leading to mitochondrial perturbation for apoptosis in human leukemia U937 cells. *Biomed Pharmacother*, 62(9), 637–644. <https://doi.org/10.1016/j.biopha.2008.01.001>
- Choi, Y. H. (2018). ROS-mediated activation of AMPK plays a critical role in sulforaphane-induced apoptosis and mitotic arrest in AGS human gastric cancer cells. *Gen Physiol Biophys*, 37(2), 129–140.
- Chong, W. C., Shastri, M. D., & Eri, R. (2017). Endoplasmic Reticulum Stress and Oxidative Stress: A Vicious Nexus Implicated in Bowel Disease Pathophysiology. *Int J Mol Sci*, 18(4), 771.
- Chylack, L. T., Leske, M. C., McCarthy, D., Khu, P., Kashiwagi, T., & Sperduto, R. (1989). Lens opacities classification system II (LOCS II). *Arch Ophthalmol*, 107, 991–997.
- Clarke, J. D., Hsu, A., Williams, D. E., Dashwood, R. H., Stevens, J., Yamamoto, M., & Ho, E. (2011). Metabolism and tissue distribution of sulforaphane in Nrf2 knockout and

- wild-type mice. *Pharm Res*, 28(12), 3171–3179. <https://doi.org/10.1007/s11095-011-0500-z>
- Cvekl, A., & Ashery-Padan, R. (2014). The cellular and molecular mechanisms of vertebrate lens development. *Development*, 141(23), 4432–4447.
- Dalton, T. P., Chen, Y., Schneider, S. N., Nebert, D. W., & Shertzer, H. G. (2004). Genetically altered mice to evaluate glutathione homeostasis in health and disease. *Free Radic Biol Med*, 37, 1511–1526.
- Das, B. N., Thompson, J. R., Patel, R., & Rosenthal, A. R. (1994). The prevalence of eye disease in Leicester: a comparison of adults of Asian and European descent. *Jr Soc Med*, 87, 219–222.
- Davidson, R., Gardner, S., Jupp, O., Bullough, A., Butters, S., Watts, L., ... Clark, I. M. (2017). Isothiocyanates are detected in human synovial fluid following broccoli consumption and can affect the tissues of the knee joint. *Sci Rep*, 7, 3398.
- Davidson, R. K., Jupp, O., de Ferrars, R., Kay, C. D., Culley, K. L., Norton, R., ... Clark, I. M. (2013). Sulforaphane represses matrix-degrading proteases and protects cartilage from destruction in vitro and in vivo. *A & R*, 65(12), 3130–3140. <https://doi.org/10.1002/art.38133>
- de Oliveira, J. M. P. F., Costa, M., Pedrosa, T., Pinto, P., Remdios, C., Oliveria, H., ... Santos, C. (2014). Sulforaphane induces oxidative stress and death by p53-independent mechanism: implication of impaired glutathione recycling. *PLoS ONE*, 9(3), e92980. <https://doi.org/10.1371/journal.pone.0092980>
- de Oliveira, J. M. P. F., Costa, M., Pedrosa, T., Pinto, P., Remedios, C., Oliveira, H., & Santos, C. (2014). Sulforaphane induces oxidative stress and death by p53-independent mechanism: implication of impaired glutathione recycling. *PLoS ONE*, 9, e92980.
- Deniaud, A., Sharaf el dein, O., Maillier, E., Poncet, D., Kroemer, G., Lemaire, C., & Brenner, C. (2008). Endoplasmic reticulum stress induces calcium-dependent permeability transition, mitochondrial outer membrane permeabilization and apoptosis. *Oncogene*, 27, 285–299.
- Desideri, E., Filamenti, G., & Ciriolo, M. R. (2012). Glutathione participates in the modulation of starvation-induced autophagy in carcinoma cells. *Autophagy*, 8(12), 1769–1781.
- Dias, I. H. K., Chapple, I. L. C., Milward, M., Grant, M. M., Hill, E., Brown, J., & Griffiths, H. R. (2013). Sulforaphane Restores Cellular Glutathione Levels and Reduces Chronic Periodontitis Neutrophil Hyperactivity In Vitro. *PLoS ONE*, 8(6), e66407.
- Diaz-Hernandez, J. I., Almeida, A., Delgado-Estaban, M., Fernandez, E., & Bolanos, J. P. (2005). Knockdown of glutamate-cysteine ligase by small hairpin RNA reveals that both catalytic and modulatory subunits are essential for the survival of primary neurons. *J Biol Chem*, 280, 38992–39001.
- Dickey, J. S., Redon, C. E., Nakamura, A. J., Baird, B. J., Sedelnikova, O. A., & Bonner, W. M. (2009). H2AX: functional roles and potential applications. *Chromosoma*, 118(6), 683–692.
- Dinkova-Kostova, A. T., & Kostov, R. V. (2012). Glucosinolates and isothiocyanates in health and disease. *Trends in Mol Med*, 18(6), 337–347. <https://doi.org/10.1016/j.molmed.2012.04.003>
- Doudican, N. A., Wen, S. Y., Mazumder, A., & Orlov, S. J. (2012). Sulforaphane synergistically enhances the cytotoxicity of arsenic trioxide in multiple myeloma cells via stress-mediated pathways. *Oncol Rep*, 28(5), 1851–1858. <https://doi.org/10.3892/or.2012.1977>
- Duncan, G., Wang, L., Neilson, G. J., & Wormstone, I. M. (2007). Lens cell survival after exposure to stress in the closed capsular bag. *Invest Ophthalmol Vis Sci*, 48, 2701–2707.

- <https://doi.org/https://doi.org/10.1167/iovs.06-1345>.
- Eldred, J. A., Dawes, L. J., & Wormstone, I. M. (2011). The lens as a model for fibrotic disease. *Philos Trans R Soc Lond B Biol Sci.*, *366*(1568), 1301–1319. <https://doi.org/10.1098/rstb.2010.0341>
- Eldred, J. A., Zheng, J., Chen, S., & Wormstone, I. M. (2019). An in vitro human lens capsular bag model adopting a graded culture regime to assess putative impact of IOLs on PCO formation. *Invest Ophthalmol Vis Sci.*, *60*(1), 113–122. <https://doi.org/10.1167/iovs.18-25930>
- Eliopoulos, A. G., Havaki, S., & Gorgoulis, V. G. (2016). DNA Damage Response and Autophagy: A Meaningful Partnership. *Front Genet.*, *7*, 204.
- Ezerina, D., Takano, Y., Hanaoka, K., Urano, Y., & Dick, T. P. (2018). N-acetyl cysteine functions as a fast-acting antioxidant by triggering intracellular H<sub>2</sub>S and sulfane sulfur production. *Cell Chem Biol.*, *25*, 447–459.
- Fahey, J. W., Talalay, P., & Kensler, T. W. (2012). Notes from the field: “green” chemoprevention as frugal medicine. *Cancer Prev Res.*, *5*, 179–188.
- Fahey, J. W., Zhang, Y., & Talalay, P. (1997). Broccoli sprouts: an exceptionally rich source of inducers of enzymes that protect against chemical carcinogens Broccoli sprouts: an exceptionally rich source of inducers of enzymes that protect against chemical carcinogens. *Proc Natl Acad Sci U S A.*, *94*(19), 10367–10372.
- Fan, X., Monnier, V. M., & Whitson, J. A. (2017). Lens glutathione homeostasis: Discrepancies and gaps in knowledge standing in the way of novel therapeutic approaches. *Exp Eye Res.*, *156*, 103–111.
- Filomeni, G., De Zio, D., & Cecconi, F. (2015). Oxidative stress and autophagy: the clash between damage and metabolic needs. *Cell Death Differ.*, *22*, 377–388.
- Filomeni, G., Desideri, E., Cardaci, S., Rotilio, G., & Ciriolo, M. R. (2010). Under the ROS. thiol network is the principal suspect for autophagy commitment. *Autophagy.*, *6*, 999–1005.
- Finkel, T. (2012). From sulfenylation to sulfhydration: what a thiolate needs to tolerate. *Sci Signal.*, *5*(215), pe10.
- Forrester, J. V., Dick, A. D., McMenamin, P., & Lee, W. (1995). *The eye: basic sciences in practice* (Saunders, Ed.).
- Francis, P. J., Berry, V., Moore, A. T., & Bhattacharya, S. (1999). Lens biology: development and human cataractogenesis. *Trends Genet.*, *15*, 191–196.
- Franco, R., & Cidlowski, J. A. (2006). SLCO/OATP-like transport of glutathione in FasL-induced apoptosis: glutathione efflux is coupled to an organic anion exchange and is necessary for the progression of the execution phase of apoptosis. *J Biol Chem.*, *281*(40), 29542–29557. <https://doi.org/https://doi.org/10.1074/jbc.M602500200>
- Franco, R., & Cidlowski, J. A. (2009). Apoptosis and glutathione: beyond an antioxidant. *Cell Death Differ.*, *10*, 1303–1314. <https://doi.org/https://doi.org/10.1038/cdd.2009.107>
- Franco, R., Schoneveld, O. J., Pappa, A., & Panayiotidis, M. I. (2007). The central role of glutathione in the pathophysiology of human diseases. *Arch Physiol Biochem.*, *113*(4–5), 234–258.
- Fulda, S., Galluzzi, L., & Kroemer, G. (2010). Targeting mitochondria for cancer therapy. *Nat Rev Drug Dis.*, *9*(6), 447–464.
- Fulda, S., Gorman, A. M., Hori, O., & Samali, A. (2010). Cellular Stress Responses: Cell Survival and Cell Death. *Int J Cell Biol.*, *2010*, 214074.
- Galati, S., Boni, C., Gerra, M. C., Lazzaretti, M., & Buschini, A. (2019). Autophagy: A Player in response to Oxidative Stress and DNA Damage. *Oxid Med Cell Longev.*, *2019*, Article ID 5692958.
- Galluzzi, L., Vitale, L., & Aaronson, S. (2018). Molecular mechanisms of cell death:

- recommendations of the Nomenclature Committee on Cell Death 2018. *Cell Death Differ*, 25, 486–541.
- Gao, X., Dinkova-Kostova, A. T., & Talalay, P. (2001). Powerful and prolonged protection of human retinal pigment epithelial cells, keratinocytes, and mouse leukemia cells against oxidative damage: the indirect antioxidant effects of sulforaphane. *Proc Natl Acad Sci U S A*, 98, 15221–15226.
- Geng, Y., Zhou, Y., Wu, S., Hu, Y., Lin, K., Wang, Y., ... Wu, W. (2017). Sulforaphane Induced Apoptosis via Promotion of Mitochondrial Fusion and ERK1/2-Mediated 26S Proteasome Degradation of Novel Pro-survival Bim and Upregulation of Bax in Human Non-Small Cell Lung Cancer Cells. *J Cancer*, 8(13), 2456–2470.
- Ghibelli, L., Fanelli, C., Rotilio, G., Lafavia, E., Coppola, S., Colussi, C., & Ciriolo, M. R. (1998). Rescue of cells from apoptosis by inhibition of active GSH extrusion. *FASEB J*, 12(6), 479–486. <https://doi.org/10.1096/fasebj.12.6.479>
- Ghoshal, N., Sharma, S., Banerjee, A., Kurkalang, S., Raghavan, S. C., & Chatterjee, A. (2017). Influence of reduced glutathione on end-joining of DNA double-strand breaks: Cytogenetical and molecular approach. *Mutat Res*, 795, 1–9.
- Giblin, F. J. (2000). Glutathione: a vital lens antioxidant. *J Ocul Pharmacol Ther*, 16, 121–135. <https://doi.org/10.1089/jop.2000.16.121>
- Gorlach, A., Bertram, K., Hudecova, S., & Krizanova, O. (2015). Calcium and ROS: A mutual interplay. *Redox Bio*, 6, 260–271.
- Grosswiler, L. J. (1984). Photochemistry of proteins: a review. *Curr Eye Res*, 3, 137–142.
- Guarino, V. A., Oldham, W. M., Loscalzo, J., & Zhang, Y. Y. (2019). Reaction rate of pyruvate and hydrogen peroxide: assessing antioxidant capacity of pyruvate under biological conditions. *Sci Rep*, 9, 19568. <https://doi.org/10.1038/s41598-019-55951-9>
- Guerrero-Beltran, C. E., Calderon-Oliver, M., Martinez-Abundis, E., Tapia, E., Zarco-Marquez, G., Zazueta, C., & Pedraza-Chaverri, J. (2010). Protective effect of sulforaphane against cisplatin-induced mitochondrial alterations and impairment in the activity of NAD(P)H:quinone oxidoreductase 1 and  $\gamma$  glutamyl cysteine ligase: studies in mitochondria isolated from rat kidney and in LLC-PK1 cells. *Toxicol Lett*, 199, 80–92.
- Guo, W., Chao, Y., Zhang, Z., Tan, N., Zhao, F., Ge, C., ... He, X. (2011). Disruption of xCT inhibits cell growth via the ROS/autophagy pathway in hepatocellular carcinoma. *Cancer Lett*, 312(1), 55–61.
- Hac, A., Brokowska, J., Rintz, E., Bartkowski, M., Wegrzyn, G., & Herman-Antosiewicz, A. (2019). Mechanism of selective anticancer activity of isothiocyanates relies on differences in DNA damage repair between cancer and healthy cells. *Eur J Nutr*, 59(4), 1421–1432.
- Hammond, C. (2000). Genetic and environmental factors in age-related nuclear cataracts in monozygotic and dizygotic twins. *N Engl J Med*, 342, 1786–1790.
- Hammond, C. (2001). The heritability of age-related cortical cataract: the twin eye study. *N Engl J Med*, 42, 601–605.
- Han, D., Sen, C. K., Roy, S., Kobayashi, M. S., Tritschler, H. J., & Packer, L. (1997). Protection against glutamate-induced cytotoxicity in C6 glial cells by thiol antioxidants. *Am J Physiol*, 273(5), R1771-1778.
- Harman, D. (1956). Aging: a theory based on free radical and radiation chemistry. *J Gerontol*, 11, 298–300.
- Harper, J. V., & Brooks, G. (2005). The Mammalian Cell Cycle. In T. Humphrey & G. Brooks (Eds.), *Cell Cycle Control: Mechanisms and Protocols* (pp. 113–153). <https://doi.org/10.1385/1-59259-857-9:113>
- Harvey, C. J., Thimmulappa, R. K., Sethi, S., Kong, X., Yarmus, L., Brown, R. H., ...

- Biswal, S. (2011). Targeting Nrf2 signaling improves bacterial clearance by alveolar macrophages in patients with COPD and in a mouse model. *Sci Transl Med*, 3(78), 78ra32.
- Hillary, R. F., & FitzGerald, U. (2018). A lifetime of stress: ATF6 in development and homeostasis. *Journal of Biomedical Science*, 25(1), 48. <https://doi.org/10.1186/s12929-018-0453-1>
- Holst, B., & Williamson, G. (2004). A critical review of the bioavailability of glucosinolates and related compounds. *Nat Prod Rep*, 21(3), 425–447.
- Horwacik, I., Gaik, M., Durbas, M., Boratyn, E., Zajac, G., Szychowska, K., ... Rokita, H. (2015). Inhibition of autophagy by 3-methyladenine potentiates sulforaphane-induced cell death of BE(2)-C human neuroblastoma cells. *Mol Med Rep*, 12(1), 535–542. <https://doi.org/10.3892/mmr.2015.3377>
- Houghton, C. A. (2019). Sulforaphane: its “coming of age” as a clinically relevant nutraceutical in the prevention and treatment of chronic disease. *Oxid Med Cell Longev*, 2019, 2716870. <https://doi.org/10.1155/2019/2716870>
- Hsu, Y. C., Chang, S. J., Wang, M. Y., Chen, Y. L., & Huang, T. Y. (2013). Growth Inhibition and Apoptosis of Neuroblastoma Cells Through ROS-Independent MEK/ERK Activation by Sulforaphane. *Cell Biochem Biophys*, 66, 765–774.
- Hu, C., Egger, A. L., Mesecar, A. D., & Breemen, R. B. (2011). Modification of Keap1 Cysteine Residues by Sulforaphane. *Chem Res Toxicol*, 24(4), 515–521.
- Hu, Y., Urig, S., Koncarevic, S., Wu, X., Fischer, M., Rahlfs, S., ... Beckjer, K. (2007). Glutathione- and thioredoxin-related enzymes are modulated by sulfur-containing chemopreventive agents. *Biol Chem*, 388, 1069–1081. <https://doi.org/10.1515/BC.2007.135>
- Hudecova, S., Markova, J., Simko, V., Csaderova, L., Stracina, T., Sirova, M., ... Krizanova, O. (2016). Sulforaphane-induced apoptosis involves the type 1 IP3 receptor. *Oncotarget*, 7(38), 61403–61418.
- Huertas, P. (2010). DNA resection in eukaryotes: deciding how to fix the break. *Nat Struct Mol Biol*, 17(1), 11–16.
- Hung, C. H. L., Cheng, S. S. Y., Cheung, Y. T., Wuwongse, S., Zhang, N. Q., Ho, Y. S., ... Chang, R. C. C. (2018). A reciprocal relationship between reactive oxygen species and mitochondrial dynamics in neurodegeneration. *Redox Biol*, 14, 7–19.
- Igney, F. H., & Krammer, P. H. (2002). Death and anti-death: tumour resistance to apoptosis. *Nat Rev Cancer*, 2, 277–288.
- Jackson, S. P. (2002). Sensing and repairing DNA double-strand breaks. *Carcinogenesis*, 23(5), 687–696.
- Jackson, S. P., & Bartek, J. (2009). The DNA-damage response in human biology and disease. *Nature*, 461(7267), 1071–1078.
- Janobi, A. A. A., Mithen, R. F., Gasper, A. V., Shaw, P. N., Middleton, R. J., Ortori, C. A., & Barrett, D. (2006). Quantitative measurement of sulforaphane, iberin and their mercapturic acid pathway metabolites in human plasma and urine using liquid chromatography–tandem electrospray ionisation mass spectrometry. *J Chromatography B*, 844(2), 223–234. <https://doi.org/10.1016/j.jchromb.2006.07.007>
- Jeggo, P., & Lobrich, M. (2007). DNA double-strand breaks: their cellular and clinical impact? *Oncogene*, 26, 7717–7719.
- Juge, N., Mithen, R. F., & Traka, M. (2007). Molecular basis for chemoprevention by sulforaphane: a comprehensive review. *Cell Mol Life Sci*, 64, 1105–1127. <https://doi.org/10.1007/s00018-007-6484-5>
- Kaiser, A. E., Baniyadi, M., Giansiracusa, D., Giansiracusa, M., Garcia, M., Fryda, Z., ... Bishayee, A. (2021). Sulforaphane: A Broccoli Bioactive Phytochemical with Cancer

- Preventive Potential. *Cancers*, 13(19), 4796.
- Kalinina, E. V., & Gavriiliuk, L. A. (2020). Glutathione Synthesis in Cancer Cells. *Biochem (Mosc)*, 85, 895–907.
- Kallifatidis, G., Boros, J., Shin, E. H. H., McAvoy, J. W., & Lovicu, F. J. (2011). The fate of dividing cells during lens morphogenesis, differentiation and growth. *Exp Eye Res*, 92, 502–511.
- Kang, R., Zeh, H., Lotze, M., & Tang, D. (2011). The Beclin 1 network regulates autophagy and apoptosis. *Cell Death Differ*, 18, 571–580.
- Kannan, R., Yi, J. R., Zlokovic, B. V., & Kaplowitz, N. (1995). Molecular characterization of a reduced glutathione transporter in the lens. *Invest Ophthalmol Vis Sci*, 36(9), 1785–1792.
- Kansanen, E., Jyrkkanen, H. K., & Levonen, A. L. (2012). Activation of stress signaling pathways by electrophilic oxidized and nitrated lipids. *Free Radic Biol Med*, 52, 973–982.
- Kassahun, K., Davis, M., Hu, P., Martin, B., & Baillie, T. (1997). Biotransformation of the naturally occurring isothiocyanate sulforaphane in the rat: Identification of phase I metabolites and glutathione conjugates. *Chem Res Toxicol*, 10, 1228–1233. <https://doi.org/10.1021/tx970080t>
- Keeffe, J., & Taylor, H. R. (1996). Cataract surgery in Australia 1985-94. *Aust NZ J Ophthalmol*, 24, 313–317.
- Kent State University Libraries. (2017a). SPSS Tutorial: paired sample t test. Retrieved June 18, 2021, from <https://libguides.library.kent.edu/SPSS/PairedSamplestTest>
- Kent State University Libraries. (2017b). SPSS Tutorials: independent samples t test. Retrieved August 3, 2021, from <https://libguides.library.kent.edu/spss/independenttttest#:~:text=The Independent Samples t Test compares the means of two,Independent t Test>
- Kent State University Libraries. (2017c). SPSS Tutorials: one way ANOVA. Retrieved June 18, 2021, from <https://libguides.library.kent.edu/SPSS/OneWayANOVA>
- Khaja, W. A., Verma, M., Shoss, B. L., & Yen, K. G. (2011). Visual axis opacification in children. *Ophthalmol*, 118(1), 224–225.
- Kim, B. R., Hu, R., Keum, W. S., Hebbar, V., Shen, G., Nair, S. S., & Kong, A. N. T. (2003). Antioxidant response element-mediated gene expression and apoptosis elicited by sulforaphane. *Cancer Res*, 63, 7520–7525.
- Kim, S. C., Choi, B., & Kwon, Y. (2017). Thiol-reducing agents prevent sulforaphane-induced growth inhibition in ovarian cancer cells. *Food Nutr Res*, 61(1), 1368321. <https://doi.org/10.1080/16546628.2017.1368321>
- Knight-Nanan, D., O’Keefe, M., & Bowell, R. (1996). Outcome and complications of intraocular lenses in children with cataract. *J Cataract Refract Surg*, 22, 730–736.
- Kolm, R. H., Danielson, U. H., Zhang, Y., Talalay, P., & Mannervik, B. (1995). Isothiocyanates as substrates for human glutathione transferases: Structure-activity studies. *Biochem J*, 311, 453–459. <https://doi.org/10.1042/bj3110453>
- Kosower, N. S., & Kosower, E. M. (1978). The glutathione status of cells. *Int Rev Cytol*, 54, 109–160. [https://doi.org/10.1016/s0074-7696\(08\)60166-7](https://doi.org/10.1016/s0074-7696(08)60166-7)
- Kovacs-Nolan, J., Rupa, P., Matsui, T., Tanaka, M., Konishi, T., Sauchi, Y., ... Mine, Y. (2014). In Vitro and ex Vivo Uptake of Glutathione (GSH) across the Intestinal Epithelium and Fate of Oral GSH after in Vivo Supplementation. *J Agric Food Chem*, 62, 9499–9506.
- Krag, S., & Andreassen, T. T. (2003). Mechanical properties of the human posterior lens capsule. *Invest Ophthalmol Vis Sci*, 44(2), 691–696.
- Kubo, E., Chhunchha, B., Singh, P., Sasaki, H., & Singh, D. P. (2017). Sulforaphane

- reactivates cellular antioxidant defense by inducing Nrf2/ARE/Prdx6 activity during aging and oxidative stress. *Sci Rep*, 7, 14130.
- Kühlbrandt, W. (2015). Structure and function of mitochondrial membrane protein complexes. *BMC Biol*, 13, 89.
- Kuszak, J. R., & Costello, M. J. (2004). The structure of the vertebrate lens. In M. Robinson & F. Lovicu (Eds.), *Development of the ocular lens* (pp. 71–118). Cambridge: Cambridge University Press.
- Kyung, S. Y., Kim, D. Y., Yoon, J. Y., Son, E. S., Kim, Y. J., Park, J. W., & Jeong, S. H. (2018). Sulforaphane attenuates pulmonary fibrosis by inhibiting the epithelial-mesenchymal transition. *BMC Pharmacol Toxicol*, 19, 13. <https://doi.org/10.1186/s40360-018-0204-7>
- Lai, Y., Hickey, R. W., Chen, Y., Bayir, H., Sullivan, M. L., & Chu, C. T. (2008). Autophagy is increased after traumatic brain injury in mice and is partially inhibited by the antioxidant gamma-glutamylcysteinyl ethyl ester. *J Cereb Blood Flow Metab*, 28, 540–550.
- Lam, D., Rao, S. K., Ratra, V., Liu, Y., Mitchell, P., King, J., ... Chang, D. F. (2015). Cataract. *Nat Rev Dis Primers*, 1, 15014.
- Lan, H., Yuan, H., & Lin, C. (2017). Sulforaphane induces p53-deficient SW480 cell apoptosis via the ROS-MAPK signaling pathway. *Mol Med Rep*, 16(5), 7796–7804. <https://doi.org/10.3892/mmr.2017.7558>
- Lane, N., & Martin, W. (2010). The energetics of genome complexity. *Nature*, 467, 929–934.
- Lanhiuhihiu, H., Yuan, H., & Lin, C. (2017). Bug. *Mol Med Rep*, 16(5), 7786–7804.
- Lee, G., Won, H., Lee, Y., Choi, J., Oh, T., & Lim, J. (2016). Oxidative Dimerization of PHD2 is Responsible for its Inactivation and Contributes to Metabolic Reprogramming via HIF-1 $\alpha$  Activation. *Sci Rep*, 6, 18928.
- Lee, Y., Kim, J., Park, K., & Lee, M. S. (2019).  $\beta$ -Cell Autophagy: Mechanism and Role in Beta-Cell Dysfunction. *Mol Metab*, 27, S92–S103.
- Lemasters, J. J. (2019). Molecular mechanisms of cell death. In W. Coleman & G. Tsongalis (Eds.), *Essential concepts in molecular pathology* (2nd ed.). Academic Press.
- Leydolt, C., Schartmuller, D., Schwarzenbacher, L., Roggla, V., Schriefl, S., & Menapace, R. (2020). Posterior capsule opacification with two hydrophobic acrylic intraocular lenses: 3-year results of a randomized trial. *Am J Ophthalmol*, 217, 224–231. <https://doi.org/10.1016/j.ajo.2020.04.011>
- Li, B., Li, L., Donaldson, P. J., & Lim, J. C. (2010). Dynamic regulation of GSH synthesis and uptake pathways in the rat lens epithelium. *Exp Eye Res*, 90(2), 300–307. <https://doi.org/10.1016/j.exer.2009.11.006>
- Li, J., Zhang, D., Brundel, B. J. J. M., & Wiersma, M. (2019). Imbalance of ER and Mitochondria Interactions: Prelude to Cardiac Ageing and Disease? *Cells*, 8(12), 1617.
- Li, Q., & Verma, I. M. (2002). NF-kappaB regulation in the immune system. *Nat Rev Immuno*, 10, 725–734.
- Li, Y., & Ding, Y. (2017). Embryonic Development of the Human Lens. In Y. Liu (Ed.), *Pediatric lens diseases* (pp. 1–10). Singapore: Springer.
- Liang, J., Jahraus, B., Balta, E., Ziegler, J. D., Hübner, K., Blank, N., ... Samstag, Y. (2018). Sulforaphane inhibits inflammatory responses of primary human T-cells by increasing ROS and depleting glutathione. *Front Immunol*, 9, 2584. <https://doi.org/10.3389/fimmu.2018.02584>
- Lim, J. C., Grey, A. C., Zahraei, A., & Donaldson, P. J. (2020). Age-dependent changes in glutathione metabolism pathways in the lens: New insights into therapeutic strategies to prevent cataract formation—A review. *Clin Exp Ophthalmol*, 48, 1031–1042. <https://doi.org/10.1111/ceo.13801>

- Lin, H., Ouyang, H., Zhu, J., Huang, S., Liu, Z., Chen, S., ... Liu, Y. (2016). Lens regeneration using endogenous stem cells with gain of visual function. *Nature*, *531*, 323–328.
- Lin, J. H., Walter, P., & Yen, T. S. B. (2013). Endoplasmic Reticulum Stress in Disease Pathogenesis. *Annu Rev Pathol*, *3*, 399–425.
- Lindahl, T. (1993). Instability and decay of the primary structure of DNA. *Nature*, *362*, 709–715.
- Lindahl, T., & Barnes, D. E. (2000). Repair of endogenous DNA damage. *Cold Spring Harb Symp Quant Biol*, *65*, 127–133.
- Linnola, R., Salonen, J., & Happonen, R. (1999). Intraocular lens bioactivity tested using rabbit corneal tissue cultures. *J Cataract Refract Surg*, *25*, 1480–1485.
- Liu, H., Smith, A. J. O., Ball, S. S. R., Bao, Y., Bowater, R. P., & Wormstone, I. M. (2017). Sulforaphane promotes ER stress, autophagy and cell death: implications for cataract surgery. *J Mol Med*, *95*(5), 553–564. <https://doi.org/10.1007/s00109-016-1502-4>.
- Liu, H., Smith, A. J. O., Lott, M. C., Bao, Y., Bowater, R. P., Reddan, J. R., & Wormstone, I. M. (2013). Sulforaphane can protect lens cells against oxidative stress: implications for cataract prevention. *Invest Ophthalmol Vis Sci*, *54*(8), 5236–5248. <https://doi.org/10.1167/iovs.13-11664>
- Liu, X., Yang, W., Guan, Z., Yu, W., Fan, B., Xu, N., & Liao, D. J. (2018). There are only four basic modes of cell death, although there are many ad-hoc variants adapted to different situations. *Cell Biosci*, *8*, 6.
- Liu, Y. C., Hsieh, C. W., Weng, Y. C., Chuang, S. H., Hsieh, C. Y., & Wung, B. S. (2008). Sulforaphane inhibition of monocyte adhesion via the suppression of ICAM-1 and NF- $\kappa$ B is dependent upon glutathione depletion in endothelial cells. *Vascular Pharm*, *48*(1), 54–61.
- Lou, M. F. (2003). Redox regulation in the lens. *Prog Retin Eye Res*, *22*, 657–682.
- Lu, S. C. (2014). Glutathione Synthesis. *Biochim Biophys Acta*, *1830*(5), 3143–3153.
- Lushchak, V. I. (2012). Glutathione Homeostasis and Functions: Potential Targets for Medical Interventions. *J Amino Acids*, *2012*, Article ID 736837.
- Lv, H., Zhen, C., Liu, J., Yang, P., Hu, L., & Shang, P. (2019). Unraveling the Potential Role of Glutathione in Multiple Forms of Cell Death in Cancer Therapy. *Oxid Med Cell Longev*, *2019*, 3150145.
- Mackic, J. B., Jinagouda, S., McComb, J. G., Kannan, R., Kaplowitz, N., & Zlokovic, B. V. (1996). Transport of circulating reduced glutathione at the basolateral side of the anterior lens epithelium: physiologic importance and manipulations. *Exp Eye Res*, *62*(1), 29–37.
- Mah, L. J., El-Osta, A., & Karagiannis, T. (2010).  $\gamma$ -H2AX: a sensitive molecular marker of DNA damage and repair. *Leukemia*, *24*, 679–686. <https://doi.org/10.1038/leu.2010.6>
- Mailloux, R. J., & Willmore, W. G. (2014). S-glutathionylation reactions in mitochondrial function and disease. *Front Cell Dev Biol*, *2*, 68.
- Makley, L. N., McMenimen, K. A., DeVree, B. T., Goldman, J. W., McGlasson, B. N., Rajagopal, P., ... Gestwicki, J. (2015). Pharmacological chaperone for alpha-crystallin partially restores transparency in cataract models. *Science*, *350*, 674–677.
- Mallet, J. D., & Rochette, P. J. (2011). Ultraviolet light-induced cyclobutane pyrimidine dimers in rabbit eyes. *Photochem Photobiol*, *87*, 1363–1368.
- Mani, S., Swargiary, G., & Singh, K. V. (2020). Natural Agents Targeting Mitochondria in Cancer. *Int J Mol Sci*, *21*(19), 6992–6703.
- Mari, M., Morales, A., Colell, A., Garcia-Ruiz, C., & Fernandez-Checa, J. C. (2009). Mitochondrial Glutathione, a Key Survival Antioxidant. *Antioxid Redox Signal*, *11*(11), 2685–2700.

- Marnett, L. J. (2000). Oxyradicals and DNA damage. *Carcinogenesis*, *21*, 361–370.
- McCarty, C. A., & Taylor, H. R. (2001). The genetics of cataract. *Invest Ophthalmol Vis Sci*, *42*, 1677–1678.
- Meister, A. (1995). Glutathione metabolism. *Methods Enzymol*, *251*, 3.
- Mi, L., Sirajuddin, P., Gan, N., & Wang, X. (2010). A cautionary note on using N-acetylcysteine as an antagonist to assess isothiocyanate induced ROS-mediated apoptosis. *Anal Biochem*, *405*(2), 269–271.
- Michael, R., & Bron, A. J. (2011). The ageing lens and cataract: a model of normal and pathological ageing. *Philos Trans R Soc Lond B Biol Sci*, *366*, 1278–1292.
- Milisav, I. (2011). *Cellular Stress Responses, Advances in Regenerative Medicine* (S. Wislet-Gendebien, Ed.). IntechOpen.
- Mironczuk-Chodakowska, I., Witkowska, A. M., & Zujko, M. E. (2018). Endogenous non-enzymatic antioxidants in the human body. *Adv Med Sci*, *63*, 68–78.
- Mizushima, N., & Komatsu, M. (2011). Autophagy: renovation of cells and tissues. *Cell*, *147*(4), 728–741. <https://doi.org/10.1016/j.cell.2011.10.026>
- Montero, D., Tachibana, C., Rahr Winther, J., & Appenzeller-Herzog, C. (2013). Intracellular glutathione pools are heterogeneously concentrated. *Redox Biol*, *1*(1), 508–513.
- Morishita, H., & Mizushima, N. (2016). Autophagy in the lens. *Exp Eye Res*, *144*, 22–28.
- Moshetiva, L. K. (2008). Cataract. In: Moshetova LK, Nesterov AP & Ugorov EA. In *Clinical ophthalmology guidelines* (pp. 72–83). Moscow: Geotar-Media.
- Murphy, M. P. (2009). How mitochondria produce reactive oxygen species. *Biochem J*, *417*, 1–13.
- Napoli, E., Flores, A., Mansuri, Y., Hagerman, R. J., & Giulivi, C. (2021). Sulforaphane improves mitochondrial metabolism in fibroblasts from patients with fragile X-associated tremor and ataxia syndrome. *Neurobiol*, *157*, 105427.
- Naumann, P., Fortunato, F., Zentgraf, H., Buchler, M. W., Herr, I., & Werner, J. (2011). Autophagy and cell death signaling following dietary sulforaphane act independently of each other and require oxidative stress in pancreatic cancer. *Int J Oncol*, *39*(1), 101–109. <https://doi.org/10.3892/ijo.2011.1025>
- Naumann, P., Liermann, J., Fortunato, F., Schmid, T. E., Weber, K. J., Debus, J., & Combs, S. E. (2017). Sulforaphane enhances irradiation effects in terms of perturbed cell cycle progression and increased DNA damage in pancreatic cancer cells. *PLoS ONE*, *12*(7), e0180940.
- Negrette-Guzman, M., Huerta-Yeppez, S., Tapia, E., & Pedraza-Chaverri, J. (2013). Modulation of mitochondrial functions by the indirect antioxidant sulforaphane: A seemingly contradictory dual role and an integrative hypothesis. *Free Radic Biol Med*, *65*, 1078–1089.
- Nguyen, T., Nioi, P., & Pickett, C. B. (2009). The Nrf2-Antioxidant Response Element Signaling Pathway and Its Activation by Oxidative Stress. *J Biol Chem*, *284*(20), 13291–13295.
- Nibourg, L. M., Gelens, E., Kuijter, R., Hooymans, J. M., van Kooten, T. G., & Koopmans, S. A. (2015). Prevention of posterior capsular opacification. *Exp Eye Res*, *136*, 100–115. <https://doi.org/10.1016/j.exer.2015.03.011>
- Nirmala, J. G., & Lopus, M. (2020). Cell death mechanisms in eukaryotes. *Cell Biol Toxicol*, *36*, 145–164.
- Nishikawa, T., Tsuno, N. H., Okaji, Y., Shuno, Y., Sasaki, K., Hongo, K., ... Nagawa, H. (2010). Inhibition of autophagy potentiates sulforaphane-induced apoptosis in human colon cancer cells. *Ann Surg Oncol*, *17*(2), 592–602. <https://doi.org/10.1245/s10434-009-0696-x>
- Nita, M., & Grzybowski, A. (2016). The Role of the Reactive Oxygen Species and Oxidative

- Stress in the Pathomechanism of the Age-Related Ocular Diseases and Other Pathologies of the Anterior and Posterior Eye Segments in Adults. *Oxid Med Cell Longev*, 2016, 3164734.
- O'Mealey, G. B., Berry, W. L., & Plafker, S. M. (2017). Sulforaphane is a Nrf2-independent inhibitor of mitochondrial fission. *Redox Biol*, 11, 103–110.
- Ofri, R. (2008). Lens. In D. Maggs, R. Ofri, & P. Miller (Eds.), *Slatter's fundamentals of veterinary ophthalmology* (pp. 258–276). Elsevier.
- Oshika, T., Nagata, T., & Ishii, Y. (1998). Adhesion of lens capsule to intraocular lenses of polymethylmethacrylate, silicone, and acrylic foldable materials: an experimental study. *Br J Ophthalmol*, 82, 549–553.
- Parnaud, G., Li, P., Cassar, G., Rouimi, P., Tulliez, J., Combaret, L., & Gamet-Payraastre, L. (2004). Mechanism of sulforaphane-induced cell cycle arrest and apoptosis in human colon cancer cells. *Nutr Cancer*, 48(2), 198–206.
- Pedre, B., Barayeu, U., Ezerina, D., & Dick, T. P. (2021). The mechanism of action of N-acetylcysteine (NAC): The emerging role of H<sub>2</sub>S and sulfane sulfur species. *Pharmacol*, 228, 107916.
- Peoples, J. N., Saraf, A., Ghazal, N., Pham, T. T., & Kwong, J. Q. (2019). Mitochondrial dysfunction and oxidative stress in heart disease. *Exp Mol Med*, 51, 1–13.
- Perez-Vives, C. (2018). Biomaterial influence on intraocular lens performance: an overview. *J Ophthalmol*, 2018, 2687385. <https://doi.org/10.1155/2018/2687385>
- Periyasamy, P., & Shinohara, T. (2017). Age-related cataracts: Role of unfolded protein response, Ca<sup>2+</sup> mobilization, epigenetic DNA modifications, and loss of Nrf2/Keap1 dependent cytoprotection. *Prog Retin Eye Res*, 60, 1–19.
- Pfanner, S. W., Warscheid, B., & Wiedemann, N. (2019). Mitochondrial proteins: from biogenesis to functional networks. *Nat Rev Mol Cell Biol*, 20, 267–284.
- Pham, N. A., Jacobberger, J. W., Schimmer, A. D., Cao, P., & Gronda, M. (2004). The dietary isothiocyanate sulforaphane targets pathways of apoptosis, cell cycle arrest, and oxidative stress in human pancreatic cancer cells and inhibits tumor growth in severe combined immunodeficient mice. *Mol Cancer Ther*, 3, 1239–1248.
- Pilch, D. R., Sedelnikova, O. A., Redon, C. E., Celeste, A., Nussenzweig, A., & Bonner, W. M. (2003). Characteristics of  $\gamma$ -H2AX foci at DNA double-strand break sites. *Biochem Cell Biol*, 81, 123–129.
- Podhorecka, M., Skladanowski, A., & Bozko, P. (2010). H2AX Phosphorylation: Its Role in DNA Damage Response and Cancer Therapy. *J Nuc Acids*, 2010, 920161.
- Podhradsky, D., Drobniča, L., & Kristian, P. (1979). Reactions of cysteine, its derivatives, glutathione, coenzyme A, and dihydrolipoic acid with isothiocyanates. *Experientia*, 35(2), 154–155.
- Poljšak, B., & Milisav, I. (2012). Clinical implications of cellular stress responses. *Bosn J Basic Med Sci*, 12(2), 122–126.
- Ponsero, A. J., Igarria, A., Darch, M. A., Miled, S., Outten, C. E., Winther, J. R., ... Toledano, M. B. (2017). Endoplasmic Reticulum Transport of Glutathione by Sec61 Is Regulated by Ero1 and Bip. *Mol Cell*, 67(6), 962–973.
- Rabsilber, T. M., Limberger, I. J., Reuland, A. J., Holzer, M. P., & Auffarth, G. U. (2007). Long-term results of sealed capsule irrigation using distilled water to prevent posterior capsule opacification: a prospective clinical randomised trial. *Br J Ophthalmol*, 91, 912–915.
- Rajendran, P., Kidane, A. I., Yu, T. W., Dashwood, W. M., Bisson, W. H., & Lohr, C. V. (2013). HDAC turnover, CtIP acetylation and dysregulated DNA damage signaling in colon cancer cells treated with sulforaphane and related dietary isothiocyanates. *Epigenetics*, 8(6), 612–623.

- Rakovic, A., Grunewald, A., Kottwitz, J., Bruggermann, N., Pramstaller, P. P., Lohmann, K., & Klein, C. (2011). Mutations in PINK1 and Parkin impair ubiquitination of Mitofusins in human fibroblasts. *PLoS ONE*, *6*, e16746.
- Reddy, V. N. (1990). Glutathione and its function in the lens - an overview. *Exp Eye Res*, *50*, 771–778.
- Rekas, M., Klus, A., & Kosatka, M. (2013). Sealed-capsule irrigation with distilled deionized water to prevent posterior capsule opacification - prospective, randomized clinical trial. *Curr Eye Res*, *38*(363–370).
- Remington, L. A. (2012). Crystallin lens. In L. Remington (Ed.), *Clinical anatomy and physiology of the visual system* (pp. 95–108). Missouri: Elsevier.
- Revesz, L., & Edgren, M. (1984). Glutathione-dependent yield and repair of single-strand DNA breaks in irradiated cells. *Br J Cancer Suppl*, *6*, 55–60.
- Rhee, S. (2006). H<sub>2</sub>O<sub>2</sub>, a necessary evil for cell signaling. *Cell Sig*, *312*, 1882–1883.
- Rhoden, A., Friedrich, F. W., Brandt, T., Raabe, J., Schweizer, M., Meisterknecht, J., ... Cuello, F. (2021). Sulforaphane exposure impairs contractility and mitochondrial function in three-dimensional engineered heart tissue. *Redox Biol*, *41*, 101951.
- Rizzuto, R., Pinton, P., Carrington, W., Fay, F. S., Fogarty, K. E., Lifshitz, L. M., ... Pozzan, T. (1998). Close contacts with the endoplasmic reticulum as determinants of mitochondrial Ca<sup>2+</sup> responses. *Science*, *280*, 1763–1766.
- Rogakou, E. P., Pilch, D. R., Ivanova, B. S., & Bonner, W. M. (1998). DNA Double-stranded breaks induce histone H2AX phosphorylation on serine 139. *J Biol Chem*, *273*, 5858–5868.
- Rojas, E., Valverde, M., Kala, S. V, Kaga, G., & Lieberman, M. W. (2000). Accumulation of DNA damage in the organs of mice that had a defect in GSH metabolism. *Mutat Res*, *447*(2), 305–316.
- Rudolf, E., & Cervinka, M. (2011). Sulforaphane induces cytotoxicity and lysosome- and mitochondria-dependent cell death in colon cancer cells with deleted p53. *Toxicol in Vitro*, *25*(7), 1302–1309.
- Rudolf, K., Cervinka, M., & Rudolf, E. (2014). Sulforaphane-induced apoptosis involves p53 and p38 in melanoma cells. *Apoptosis*, *19*(4), 734–747.
- Saki, M., & Prakash, A. (2017). DNA Damage Related Crosstalk Between the Nucleus and Mitochondria. *Free Radic Biol Med*, *107*, 216–227.
- Saleh, D. O., Mansour, D. F., Hashad, I. M., & Bakeer, R. M. (2019). Effects of sulforaphane on D-galactose-induced liver aging in rats: Role of keap-1/nrf-2 pathway. *Eur J Pharm*, *855*, 40–49.
- Sayeed, M. A., Bracci, M., Lucarini, G., Lazzarini, R., Di Primio, R., & Santarelli, L. (2017). Regulation of microRNA using promising dietary phytochemicals: possible preventive and treatment option of malignant mesothelioma. *Biomed Pharmacother*, *94*, 1197–1224.
- Scherz-Shouval, R., & Elazar, Z. (2007). ROS, mitochondria and the regulation of autophagy. *Trends Cell Biol*, *17*, 422–427.
- Scherz-Shouval, R., Shvets, E., Fass, E., Shorer, H., Gil, L., & Elazar, Z. (2007). Reactive oxygen species are essential for autophagy and specifically regulate the activity of Atg4. *EMBO J*, *26*, 1749–1760.
- Schieber, M., & Chandel, N. S. (2014). ROS function in redox signaling and oxidative stress. *Curr Biol*, *24*, R453–R462.
- Schumacher, B., Pothof, J., Vijg, J., & Hoeijmakers, J. H. J. (2021). The central role of DNA damage in the ageing process. *Nature*, *592*(695), 703.
- Sedlak, T. W., Nucifora, L. G., Koga, M., Shaffer, L. S., Higgs, C., Tanaka, T., ... Sawa, A. (2018). Sulforaphane augments glutathione and influences brain metabolites in human

- subjects: a clinical pilot study. *Mol Neuropsychiatry*, 3(4), 214–222.
- Sestili, P., & Fimognari, C. (2015). Cytotoxic and antitumor activity of Sulforaphane: the role of reactive oxygen species. *Biomed Res Int*, 2015. <https://doi.org/10.1155/2015/402386>
- Sestili, P., Paolillo, M., Lenzi, M., Colombo, E., Vallorani, L., Casadei, L., ... Fimognari, C. (2010). Sulforaphane induces DNA single strand breaks in cultured human cells. *Mutat Res*, 689, 65–73. <https://doi.org/10.1016/j.mrfmmm.2010.05.003>
- Shadel, G. S., & Horvath, T. L. (2015). Mitochondrial ROS signalling in organismal homeostasis. *Cell*, 163, 560–569.
- Shen, G., Xu, C., Chen, C., Hebbar, V., & Kong, A. T. (2006). p53-independent G1 cell cycle arrest of human colon carcinoma cells HT-29 by sulforaphane is associated with induction of p21CIP1 and inhibition of expression of cyclin D1. *Cancer Chemo Pharm*, 57, 317–327. <https://doi.org/10.1007/s00280-005-0050-3>
- Shi, Y., Barton, K., De Maria, A., Petrash, J. M., Shiels, A., & Bassnett, S. (2009). The stratified syncytium of the vertebrate lens. *J Cell Sci*, 122, 1607–1615.
- Shiels, A., & Hejtmancik, J. F. (2007). Genetic origins of cataract. *Arch Ophthalmol*, 125, 165–173.
- Shimada, K., Crother, T. R., & Arditì, M. (2014). DNA Damage Responses in Atherosclerosis. In *Biological DNA Sensor: The impact of nucleic acids on diseases and vaccinology* (pp. 231–253). Academic Press.
- Sies, H., & Jones, D. P. (2020). Reactive oxygen species (ROS) as pleiotropic physiological signalling agents. *Nat Rev Mol Cell Biol*, 21, 363–383.
- Singh, S. V., Srivastava, S. K., Choi, S., Lew, K. L., Antosiewicz, J., Xiao, D., ... Herman-Antosiewicz, A. (2005). Sulforaphane-induced cell death in human prostate cancer cells is initiated by reactive oxygen species. *J Biol Chem*, 280, 19911–19924. <https://doi.org/10.1074/jbc.M412443200>
- Sivapalan, T., Melchini, A., Saha, S., Needs, P. W., Traka, M. H., Tapp, H., ... Mithen, R. F. (2018). Bioavailability of Glucoraphanin and Sulforaphane from High-Glucoraphanin Broccoli. *Mol Nutr Food Res*, 62(18), e1700911.
- Slutzky, L., & Kleinmann, G. (2018). Further Enhancement of Intraocular Open-Capsule Devices for Prevention of Posterior Capsule Opacification. *Trans Vis Sci Tech*, 7(1), 21.
- Smith, A. J. O., Eldred, J. A., & Wormstone, I. M. (2019). Resveratrol Inhibits Wound-healing and Lens Fibrosis: A Putative Candidate for Posterior Capsule Opacification Prevention. *Invest Ophthalmol Vis Sci*, 60, 3863–3877.
- Sonoda, E., Hohegger, H., Saberi, A., Taniguchi, Y., & Takeda, S. (2006). Differential usage of non-homologous end-joining and homologous recombination in double strand break repair. *DNA Repair*, 5, 1021–1029.
- Spector, A. (1995). Oxidative stress-induced cataract: mechanism of action. *FASEB J*, 9, 1173–1182.
- Srinivas, M. (2014). Delivery of glutathione to the lens nucleus. *J Ophthalmic Vis Res*, 9(1), 148–149.
- Steven, B. (2014). Cell biology of lens epithelial cells. In S. Saika, L. Werner, & F. Lovicu (Eds.), *Lens epithelium and posterior capsular opacification* (pp. 25–38). Tokyo: Springer Japan.
- Sun, S. Y. (2010). N-acetylcysteine, reactive oxygen species and beyond. *Cancer Biol Ther*, 9, 109–110.
- Tait, S. W. G., & Green, D. R. (2008). Caspase-independent cell death: leaving the set without the final cut. *Oncogene*, 27, 6452–6461.
- Tanaka, T., Huang, X., & Halicka, H. D. (2007). Cytometry of ATM activation and histone H2AX phosphorylation to estimate extent of DNA damage induced by exogenous agents. *Cytometry Part A*, 71(9), 648–661.

- Tarozzi, A., Morroni, F., Merlicco, A., Hrelia, S., & Angeloni, C. (2009). Sulforaphane as an inducer of glutathione prevents oxidative stress-induced cell death in a dopaminergic-like neuroblastoma cell line. *J Neurochem*, *111*, 1161–1171.
- Tooze, S. A., & Yoshimori, T. (2010). The Origin of the Autophagosomal Membrane. *Nat Cell Biol*, *12*, 831–835.
- Townsend, D. M., Tew, K. D., & Tapiero, H. (2003). The importance of glutathione in human disease. *Biomed Pharmacother*, *57*, 145–155. [https://doi.org/10.1016/s0753-3322\(03\)00043-x](https://doi.org/10.1016/s0753-3322(03)00043-x)
- Tsonis, P. A., & Fuentes, E. J. (2006). Focus on Molecules: Pax-6, the Eye Master. *Exp Eye Res*, *83*(2), 233–234.
- Ursell, P. G., Dhariwal, M., O’Boyle, D., Khan, J., & Venerus, A. (2020). 5 year incidence of YAG capsulotomy and PCO after cataract surgery with single-piece monofocal intraocular lenses: a real-world evidence study of 20,763 eyes. *Eye*, *34*, 960–968.
- Valente, A. J., Maddelena, L. A., Robb, E. L., Moradi, F., & Stuart, F. A. (2017). A simple ImageJ macro tool for analyzing mitochondrial network morphology in mammalian cell culture. *Acta Histochemica*, *119*(3), 315–326. <https://doi.org/10.1016/j.acthis.2017.03.001>
- Vanduchova, A., Anzenbacher, P., & Anzenbacherova, A. (2019). Isothiocyanate from Broccoli, Sulforaphane, and Its Properties. *J Med Food*, *22*(2), 121–126. <https://doi.org/10.1089/jmf.2018.0024>
- Varma, S. D., & Hegde, K. R. (2004). Effect of alpha-ketoglutarate against selenite cataract formation. *Exp Eye Res*, *79*(6), 913–918. <https://doi.org/10.1016/j.exer.2004.06.012>
- Wang, L., Eldred, J. A., Sidaway, P., Sandeson, J., Smith, A. J. O., Bowater, R. P., ... Wormstone, I. M. (2012). Sigma 1 receptor stimulation protects against oxidative damage through suppression of the ER stress responses in the human lens. *Mech Ageing Dev*, *133*(11–12), 665–674. <https://doi.org/10.1016/j.mad.2012.09.005>
- Wang, S. B., Foster, D. B., Rucker, J., O’Rourke, B., Kass, D. A., & Van Eyk, J. E. (2011). Redox regulation of mitochondrial ATP synthase: implications for cardiac resynchronization therapy. *Circ Res*, *109*, 750–757.
- Wang, W., Yan, W., Fotis, K., Prasad, N. M., Lansingh, V. C., Taylor, H. R., ... He, M. (2016). Cataract surgical rate and socioeconomics: a global study. *Invest Ophthalmol Vis Sci*, *57*, 5872–5881.
- Wang, X., Perez, E., Liu, R., Yan, L. J., Mallet, R. T., & Yang, S. H. (2007). Pyruvate Protects Mitochondria from Oxidative Stress in Human Neuroblastoma SK-N-SH Cells. *Brain Res*, *1132*(1), 1–9. <https://doi.org/10.1016/j.brainres.2006.11.032>
- Wang, Y., Wu, H., Dong, N., Su, X., Duan, M., Wei, Y., ... Zhao, Y. (2021). Sulforaphane induces S-phase arrest and apoptosis via p53-dependent manner in gastric cancer cells. *Sci Rep*, *11*, 660.
- Wells, O. S., & El-Khamisy, S. F. (2014). Autosomal Recessive Ataxias Due to Defects in DNA Repair. In M. LeDoux (Ed.), *Movement Disorders* (2nd ed.). Elsevier.
- West-Mays, J. A., & Korol, A. (2014). The lens capsule: synthesis, remodeling, and MMPs. In S. Saika, L. Werner, & F. Lovicu (Eds.), *Lens epithelium and posterior capsular opacification* (pp. 39–57). Tokyo: Springer Japan.
- Weyemi, U., Paul, B. D., Snowman, A. M., Jailwala, P., Nussenzweig, A., Bonner, W. M., & Snyder, S. H. (2018). Histone H2AX deficiency causes neurobehavioral deficits and impaired redox homeostasis. *Nat Comm*, *9*, 1526.
- Whitson, J. A., Sell, D. R., Goodman, M. C., Monnier, V. M., & Fan, X. (2016). Evidence of Dual Mechanisms of Glutathione Uptake in the Rodent Lens: A Novel Role for Vitreous Humor in Lens Glutathione Homeostasis. *Invest Ophthalmol Vis Sci*, *57*(8), 3914–3925.
- Willems, P. H. G. M., Rossignol, R., Dieteren, C. E. J., Murphy, M. P., & Koopman, W. J. H.

- (2015). Redox homeostasis and mitochondrial dynamics. *Cell Metab*, 22, 207–218.
- Wormstone, I. M. (2020). The human capsular bag model of posterior capsule opacification. *Eye*, 34(2), 225–231.
- Wormstone, I. M., & Eldred, J. A. (2016). Experimental models for posterior capsule opacification research. *Exp Eye Res*, 142, 2–12.
- Wormstone, I. M., Liu, C. S., Rakic, J. M., Marcantonio, J. M., Vrensen, G. F., & Duncan, G. (1997). Human lens epithelial cell proliferation in a protein-free medium. *Invest Ophthalmol Vis Sci*, 38, 396–404.
- Wormstone, I. M., Tamiya, S., Eldred, J. A., Lazzaridis, K., Chantry, A., Reddan, J. R., ... Duncan, G. (2004). Characterisation of TGF-beta 2 signalling and function in a human lens cell line. *Exp Eye Res*, 78, 705–714. <https://doi.org/10.1016/j.exer.2003.08.006>
- Wormstone, I. M., Wormstone, Y. M., Smith, A. J. O., & Eldred, J. A. (2021). Posterior capsule opacification: What's in the bag? *Prog Retin Eye Res*, 82, 100905. <https://doi.org/10.1016/j.preteyeres.2020.100905>
- Xiao, D., Powolny, A. A., Antosiewicz, J., Hahm, E., & Bommareddy, A. (2009). Cellular responses to cancer chemopreventive agent D,L-sulforaphane in human prostate cancer cells are initiated by mitochondrial reactive oxygen species. *Pharm Res*, 26, 1729–1738. <https://doi.org/10.1007/s11095-009-9883-5>
- Xiao, Q., Ying, J., Xiang, L., & Zhang, C. (2018). The biologic effect of hydrogen sulfide and its function in various diseases. *Medicine (Baltimore)*, 97(44), e13065.
- Xu, C., Bailly-Maitre, B., & Reed, J. C. (2005). Endoplasmic reticulum stress: cell life and death decisions. *J Clin Invest*, 115(10), 2656–2664. <https://doi.org/10.1172/JCI26373>
- Yagishita, Y., Fahey, J. W., Dinkova-Kostova, A. T., & Kensler, T. W. (2019). Broccoli or Sulforaphane: Is It the Source or Dose That Matters? *Molecules*, 24, 3593. <https://doi.org/10.3390/molecules24193593>
- Yonova-Doing, E., Forkin, Z. A., Hysi, P. G., Williams, K. M., Spector, T. D., Gilbert, C. E., & Hammond, C. J. (2016). Genetic and Dietary Factors Influencing the Progression of Nuclear Cataract. *Ophthalmol*, 123(6), 1237–1244.
- Yoo, S., Kim, K., Nam, H., & Lee, D. (2018). Discovering health benefits of phytochemicals with integrated analysis of the molecular network, chemical properties and ethnopharmacological evidence. *Nutrients*, 10(8), 1042. <https://doi.org/10.3390/nu10081042>
- Yoon, S. Y., Kim, E., & Shin, Y. J. (2015). Oxidative stress in lens. In M. Babizhayev, A. Kasus-Jacobi, J. Alio, D. Li, & L. Zoric (Eds.), *Studies on the cornea and lens* (pp. 187–208). New York: Springer.
- Yu, L., McPhee, C. K., Zheng, L., Mardones, G. A., Rong, Y., Peng, J., ... Lenardo, M. J. (2010). Autophagy termination and lysosome reformation regulated by mTOR. *Nature*, 465(7300), 942–946.
- Yu, X., Zheng, H., Chan, M. T. V., & Wu, W. K. K. (2017). MicroRNAs: new players in cataract. *Am J Transl Res*, 9(9), 3890–3903.
- Yuan, H., Perry, C. N., Huang, C., Iwai-Kanai, E., Carreira, R. S., & Glembotski, C. C. (2009). LPS-induced autophagy is mediated by oxidative signaling in cardiomyocytes and is associated with cytoprotection. *Am J Physiol Heart Circ Physiol*, 296, 470–479.
- Yun, H. R., Jo, Y. H., Kim, J., Shin, Y., Kim, S. S., & Choi, T. G. (2020). Roles of Autophagy in Oxidative Stress. *Int J Mol Sci*, 21(9), 3289.
- Zamaraeva, M. V., Sabirov, R. Z., Maeno, E., Ando-Akatsuka, Y., Bessonova, S. V., & Okada, Y. (2005). Cells die with increased cytosolic ATP during apoptosis: a bioluminescence study with intracellular luciferase. *Cell Death Differ*, 12, 1390–1397.
- Zamponi, N., Zamponi, E., & Cannas, S. A. (2018). Mitochondrial network complexity emerges from fission/fusion dynamics. *Sci Rep*, 8, 363.

- Zhang, B., Wu, X., Liu, J., Song, L., Song, Q., Wang, L., ... Wu, Z. (2019).  $\beta$ -Actin: Not a Suitable Internal Control of Hepatic Fibrosis Caused by *Schistosoma japonicum*. *Front Microbiol*, *10*, 66–78.
- Zhang, Y. (2000). Effects of glutathione on antioxidant response element-mediated gene expression and apoptosis elicited by sulforaphane. *Carcinogenesis*, *21*(6), 1175–1182.
- Zhang, Y. (2012). The molecular basis that unifies the metabolism, cellular uptake and chemopreventive activities of dietary isothiocyanates. *Carcinogenesis*, *33*(1), 2–9.
- Zhang, Y., Kolm, R. H., Mannervik, B., & Talalay, P. (1995). Reversible conjugation of isothiocyanates with glutathione catalyzed by human glutathione transferases. *Biochem Biophys Res Commun*, *206*, 748–755.
- Zhang, Y., Talalay, P., Cho, C. G., & Posner, G. H. (1992). A major inducer of anticarcinogenic protective enzymes from broccoli: isolation and elucidation of structure. *Proc Natl Acad Sci U S A*, *89*(6), 2399–2403.
- Zhang, Y., Tan, L., Li, C., Wu, H., Ran, D., & Zhang, Z. (2020). Sulforaphane alter the microbiota and mitigate colitis severity on mice ulcerative colitis induced by DSS. *AMB Express*, *10*, 119.
- Zhao, L., Chen, X. J., Zhu, J., Xi, Y. B., Yang, X., Hu, L. D., ... Zhang, K. (2015). Lanosterol reverses protein aggregation in cataracts. *Nature*, *523*(607–611).
- Zheng, K., Ma, J., Wang, Y., He, Z., & Deng, K. (2020). Sulforaphane inhibits autophagy and induces exosome-mediated paracrine senescence via regulating MTOR/TFE3. *Mol Nutr Food Res*, *64*(14), e1901231. <https://doi.org/10.1002/mnfr.201901231>
- Zhitkovich, A. (2019). N-Acetylcysteine: Antioxidant, Aldehyde Scavenger, and More. *Chem Res Toxicol*, *32*, 1318–1319.
- Zhou, M., Leiberman, J., Xu, J., & Lavker, R. M. (2006). A hierarchy of proliferative cells exists in mouse lens epithelium: implications for lens maintenance. *Invest Ophthalmol Vis Sci*, *47*, 2997–3003.
- Ziada, A. S., Smith, M. S. R., & Côté, H. C. F. (2020). Updating the Free Radical Theory of Aging. *Front Cell Dev Biol*, *8*(575645).
- Zmijewski, J. W., Banerjee, S., Bae, H., Friggeri, A., Lazarowski, E. R., & Abraham, E. (2010). Exposure to hydrogen peroxide induces oxidation and activation of AMP-activated protein kinase. *J Biol Chem*, *285*, 34154–33164.
- Zoratti, M., & Szabo, I. (1995). The mitochondrial permeability transition. *Biochimica et Biophysica Acta*, *1241*(2), 139–176.
- Zoric, L., Miric, D., Novakovic, T., Pavlovic, A., Videnovic, G., & Trajkovic, G. (2008). Age-related cataract and serum albumin concentration. *Curr Eye Res*, *3*(7), 587–590.
- Zorov, D. B., Filburn, C. R., Klotz, L. O., Zweier, J. L., & Sollott, S. J. (2000). Reactive oxygen species (ROS)-induced ROS release: a new phenomenon accompanying induction of the mitochondrial permeability transition in cardiac myocytes. *J Exp Med*, *192*, 1001–1014.
- Zorova, L. D., Popkov, V. A., Silachev, D. N., Plotnikov, E. Y., Pevzner, I. B., Jankauskas, S. S., ... Zorov, D. (2018). Mitochondrial membrane potential. *Anal Biochem*, *552*, 50–59.
- Zou, X., Qu, Z., Fang, Y., Shi, X., & Ji, Y. (2017). Endoplasmic reticulum stress mediates sulforaphane-induced apoptosis of HepG2 human hepatocellular carcinoma cells. *Mol Med Rep*, *15*, 331–338. <https://doi.org/10.3892/mmr.2016.6016>
- Zucker, S. N., Fink, E. E., Bagati, A., Kaminski, N., Segal, B. H., & Nikiforov, M. A. (2014). Nrf2 amplifies oxidative stress via induction of Klf9. *Mol Cell*, *53*(6), 916–928.
- Zukin, L. M., Pedler, M. G., Groman-Lupa, S., Pantcheva, M. B., Ammar, D. A., & Petrash, J. M. (2018). Aldose Reductase Inhibition Prevents Development of Posterior Capsular Opacification in an In Vivo Model of Cataract Surgery. *Invest Ophthalmol Vis Sci*, *59*(8),

## Appendix

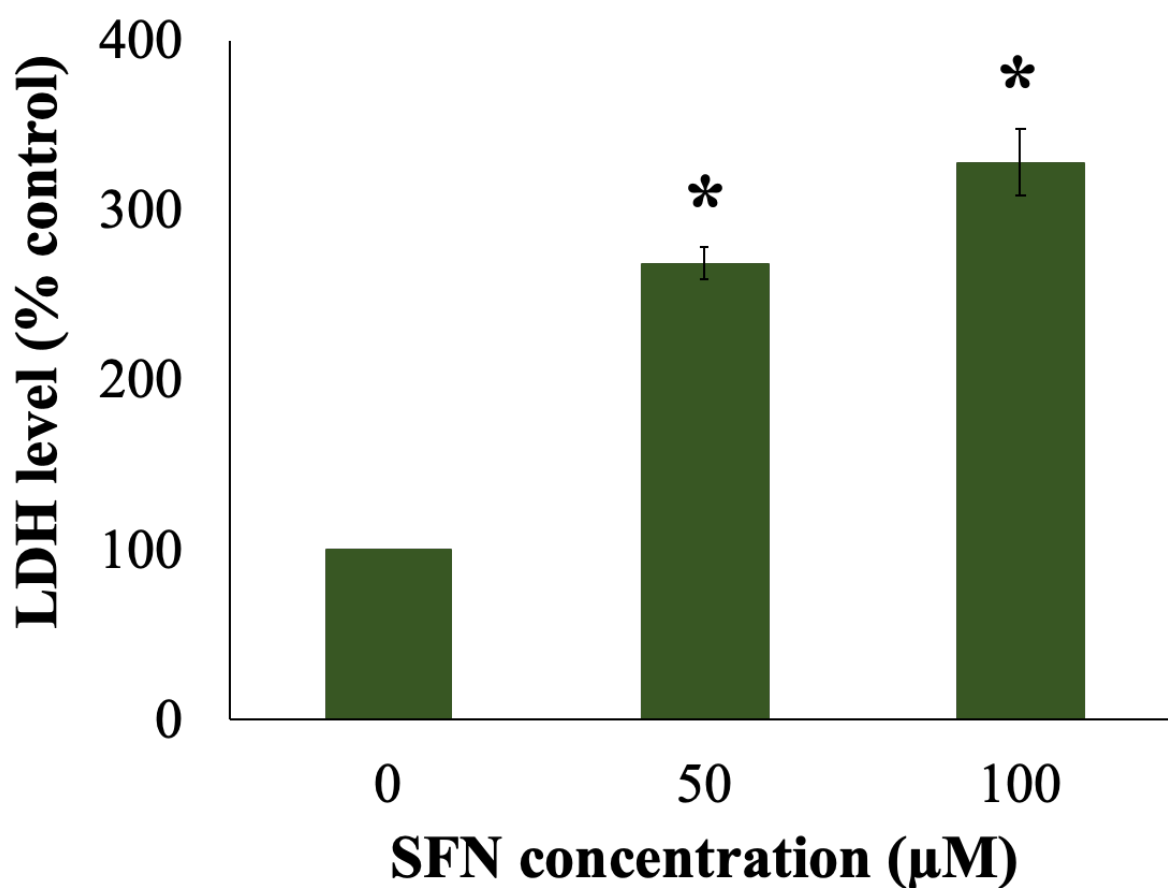


**Figure A. 1: The impacts of different concentrations of SFN on secreted LDH in FHL124 cells.** FHL124 cells were treated with 0 – 100 µM SFN for 18 hours and cellular damage was assessed using the LDH assay. Quantitative data are shown as mean  $\pm$  SEM ( $n = 3$ ). An asterisk indicates a significant difference between the treated group and the untreated control ( $p \leq 0.05$ ; ANOVA with Dunnett's post hoc test).